

Entwicklung und Charakterisierung von gefriergetrockneten Tabletten mittels Lyoc® Technologie

Dissertation
der Mathematisch-Naturwissenschaftlichen Fakultät
der Eberhard Karls Universität Tübingen
zur Erlangung des Grades eines
Doktors der Naturwissenschaften
(Dr. rer. nat.)

vorgelegt von
Faustine Hernandez
aus Colmar/Frankreich

Tübingen
2018

Gedruckt mit Genehmigung der Mathematisch-Naturwissenschaftlichen Fakultät der
Eberhard Karls Universität Tübingen.

Tag der mündlichen Qualifikation: 23.04.2019
Dekan: Prof. Dr. Wolfgang Rosenstiel
1. Berichterstatter: Prof. Dr. Rolf Daniels
2. Berichterstatter: Prof. Dr. Stephan Reichl

Acknowledgements

The realization of the present dissertation could become true thanks to Prof. Dr. Rolf Daniels.

Before beginning my dissertation, I would like to offer my sincere appreciation and gratitude to Prof. Dr. Rolf Daniels, who accepted me in his team, and allowed me to achieve and complete my PhD at the University of Tübingen, in collaboration with TEVA. I am deeply grateful for his support and his constructive comments, which enabled the progress of my work.

I am also thankful to Prof. Dr. Martin A. Wahl who accepted to be the co-rapporter of my dissertation.

This collaboration with TEVA could not happen without the help of Dr. Dieter Swatschek, Head of Formulation Development Department at TEVA and of my supervisor Dr. Michael Rottke, Formulation scientist, who offered me the chance to perform my PhD within TEVA. I am also thankful to my supervisor, Dr. Michael Rottke, who gave me all the tools to understand the aspects of lyophilization and for his exemplary guidance, monitoring and constant encouragement throughout the course of the project I was assigned to. It has been a rewarding experience to work with him and to learn the galenic environment on his side. I also thank Dr. Tanja Westphal-Mirzad who supported me for the achievement of my PhD.

A special thank goes to Dr. Dominique J. Lunter, Klaus Weyhing and Irina Eck who kindly contributed to my work and helped me by the diverse measurements at the University of Tübingen.

I also would like to thank all the staff members of TEVA who also helped me during my experimental work.

To finish, I would like to particularly thank my family who unconditionally supported me during this whole years.

Table of Contents

1	Introduction and Goal	1
2	Theory and Scientific Knowledge	2
2.1	Orally Disintegrating Tablets	2
2.1.1	Definition, Advantages and Drawbacks of ODTs	2
2.1.2	System of Action of ODTs	4
2.1.2.1	Absorption.....	4
2.1.2.2	Distribution.....	6
2.1.2.3	Metabolism.....	7
2.1.2.4	Excretion	7
2.1.3	Manufacturing Technologies of ODTs	7
2.1.3.1	Zydis® Technology.....	9
2.1.3.2	Lyoc® Technology.....	10
2.1.3.3	QuickSolv® Technology.....	12
2.1.3.4	Zydis® vs. Lyoc®	12
2.2	Freeze-drying in ODTs	13
2.2.1	Generalities (Jennings, 2008d).....	13
2.2.2	Lyophilization Cycle.....	13
2.2.2.1	Freezing step	14
2.2.2.2	Primary Drying (P.D).....	21
2.2.2.3	Secondary Drying (S.D)	26
2.2.3	Equipment Presentation (AzbilTelstar, 2015; Jennings, 2008c).....	28
2.2.3.1	Drying Chamber	28
2.2.3.2	Condenser Chamber	29
2.2.3.3	Vacuum Pump	29
2.2.3.4	Sensors	29
2.2.4	Product Formulation	29
2.2.4.1	Formulation Development.....	30
2.2.4.2	Suspension.....	32
3	Materials and Methods.....	35
3.1	Materials	35
3.1.1	Fillers Used	35
3.1.2	Hardness Builders	35

3.1.3 APIs.....	36
3.1.4 Other Excipients.....	36
3.2 Equipments and Software	36
3.2.1 Manufacturing Process Flow Chart	38
3.2.2 Manufacture of the Suspension.....	38
3.2.3 IPC on the Suspension	39
3.2.3.1 Determination of the Critical Temperature	39
3.2.3.2 Viscosity Measurement.....	39
3.2.3.3 Degree of Sedimentation.....	40
3.2.4 Lyocs® Manufacture	40
3.2.5 In Process Control on Lyocs®	42
3.2.5.1 Visual Aspect	42
3.2.5.2 Weight, Dimension and Resistance to Crushing (Hardness)	42
3.2.5.3 Disintegration Time.....	42
3.2.5.4 Moisture Content.....	42
3.2.5.5 Scanning Electron Microscopy (SEM)	43
3.2.5.6 Solid State Determination	43
3.2.5.7 Raman Microscopy	44
3.2.5.8 Porosity.....	45
3.2.5.9 API Release – Paracetamol Lyocs®	46
3.2.5.10 Uniformity of Dosage Form – Paracetamol Lyocs®	46
3.2.5.11 Statistical Analysis	47
4 Results and Discussion	49
4.1 Excipient Screening	49
4.1.1 Study on Diluents.....	49
4.1.1.1 Substance Description.....	49
4.1.1.2 Suspension Characterization	51
4.1.2 Study on Binders.....	53
4.1.2.1 Substance Description.....	54
4.1.2.2 Suspension Characterization	56
4.1.3 Pre-formulation of Lyocs®	56
4.1.3.1 Test on Mannitol	57
4.1.3.2 Type of Mannitol.....	62

4.1.4 Conclusion	78
4.2 Influence of Binder on Suspension and Lyoc® (DoE).....	78
4.2.1 DoE Mannitol/Hypromellose.....	79
4.2.1.1 Definition of Formulation Factors and Responses	79
4.2.1.2 DoE Trial.....	79
4.2.1.3 Statistical Analysis	80
4.2.2 DoE Mannitol/Dextran.....	87
4.2.2.1 Definition of Formulation Factors and Responses	87
4.2.2.2 DoE Trial.....	87
4.2.2.3 Statistical Analysis	88
4.3 Influence of water soluble and limited-water soluble APIs on Lyocs®.....	96
4.3.1 Study on Water-Soluble APIs.....	96
4.3.1.1 Metoclopramide HCl Lyocs®	96
4.3.1.2 Metamizol Sodium Lyocs®	105
4.3.2 Study on Less-Water Soluble APIs.....	111
4.3.2.1 Paracetamol Lyocs®	111
4.3.2.2 Sildenafil Citrate Lyocs®.....	114
4.3.3 Microscopic Characteristics.....	117
4.3.4 Conclusion	121
4.4 Case Study: Development of Paracetamol 100 mg Lyocs®	121
4.4.1 Influence of Mannitol Grade.....	121
4.4.1.1 Tested Formulations.....	121
4.4.1.2 API Release	127
4.4.1.3 Content of Uniformity	130
4.4.1.4 Study of Sedimentation Within The Pipette.....	132
4.4.1.5 Study of Sedimentation Within The Suspension Placed in The Blister Cavity	134
4.4.1.6 Conclusion.....	136
4.4.2 Process Optimization	136
4.4.2.1 Initial Process	136
4.4.2.2 Optimization 1	140
4.4.2.3 Optimization 2.....	142
4.4.2.4 Final Process Optimization	143
4.4.2.5 Conclusion.....	145

5	Summary	146
6	Annex	149
6.1	DSC Measurements	149
6.1.1	DSC Measurements of Diluent/Water Suspensions	149
6.1.2	DSC Measurements of Mannitol/Binder Suspensions	152
6.2	TGA Measurements.....	153
6.2.1	Metoclopramide HCl	153
6.2.2	Metamizol Na.....	153
6.3	API Release	154
6.3.1	Measurement	154
6.3.2	Dissolution Profile Comparison	155
6.4	Content of Uniformity	155
6.4.1	Measurement conditions	155
6.4.2	Statistical Analysis.....	157
6.5	Sedimentation Study.....	158
6.5.1	Sedimentation Within The Pipette.....	158
6.5.2	Sedimentation Within The Lyocs®	158
7	Bibliography	159

List Of Abbreviations

Abbreviation	Meaning
A	Absorbance
API	Active Pharmaceutical Ingredient
DoE	Design of Experiment
DSC	Differential Scanning Calorimetry
D.T	Disintegration Time
ECF	Extra Cellular Fluid
F	Degree of Sedimentation
f ₁	Difference Factor
f ₂	Similarity Factor
FD	Freeze-Dryer
GF	Glass Filter
GIT	Gastro-Intestinal Tract
H	Hardness
IPC	In Process Control
λ	Wavelength
LADME	Liberation, Absorption, Distribution, Metabolism, and Excretion
LoD	Loss on Drying
η	Viscosity
ODT	Orally Disintegrating Tablet
P	Pressure
P _c	Pressure in the Chamber
ρ	Density of the Lyoc®
Ph. Eur.	European Pharmacopeia
P.D	Primary Drying
S.D	Secondary Drying
SEM	Scanning Electron Microscopy
T	Temperature
T _c	Collapse Temperature
T _{cc}	Condenser Chamber Temperature
T _E	Eutectic Temperature
T _{g'}	Glass Transition Temperature of the Maximally Freeze-Concentrated Amorphous Phase
T _F	Freezing Point
T _N	Nucleation Temperature
T _p	Product Temperature
T _s	Shelf Temperature
TGA	Thermogravimetric analysis
XRPD	X-Ray Powder Diffraction

1 Introduction and Goal

Patients much prefer the oral medication, offering an ease of use of the medication and a non-invasive treatment unlike parenteral injectable for instance. Indeed, the oral solid dosage form represents ca. 60 % of the market (Wright, 2015). Nevertheless, conventional tablets or capsules are raising an important problem among patients: difficulty of swallowing. That is why the development of orally disintegrating tablets (ODTs) continuously increased the past decade (Lipp, 2013; Pfister and Ghosh, 2010a).

ODTs are described as oral solid dosage form that disintegrates within a few seconds in the oral cavity without taking water or without chewing. The disintegrated drug forms a suspension or solution in the mouth which is easy to swallow, providing to the patient an easier drug administration. ODTs are therefore offering patients a more convenient treatment than conventional tablets or capsules, especially when patients present swallowing problems, such as pediatric, geriatric and psychiatric patients (Amar et al., 2015; Pfister and Ghosh, 2010a; Seager, 1998). ODTs do not only offer advantages to the patient's comfort and compliance. In some cases, they also help the drug to act more quickly by delivering the active pharmaceutical ingredient (API) directly in the oral cavity i.e. Seligiline Zydis® (Seager, 1998). In contrary to conventional tablets or capsules, the API in the ODT case is already released from its excipients in the mouth and a fraction of API may be absorbed in the pre-gastric tract, accelerating its onset of action (Seager, 1998). Many different manufacturing techniques of ODTs exist, such as direct compression, molding, melt granulation or freeze-drying (McLaughlin et al., 2009). The work presented in this thesis involved the ODTs manufactured by freeze-drying technology. There are three main technologies using freeze-drying (McLaughlin et al., 2009): Zydis® (Catalent), Lyoc® (TEVA) and Quicksolv® (Janssen). The Lyoc® technology will be deeply studied in this thesis. This technology involves the lyophilisation of an aqueous highly concentrated suspension containing different excipients and at least one API, dispensed in preformed blister cavities.

The aim of this thesis was the formulation and process development of freeze-dried tablets on the basis of the developed Lyoc® technology, in order to enhance the scientific database related to this technology. Indeed, there is only little literature related to the formulation and process development of Lyocs® available. For this purpose, an excipient screening on possible diluents and binders was firstly investigated in order to select the excipients usable in the Lyoc® technology. The influence of the API nature on Lyocs® was also studied, in order to gather more information of the use of water-soluble/less-water soluble APIs in the Lyoc® technology. For this purpose, the Lyoc® quality and the Lyoc® morphology using paracetamol, and sildenafil citrate as less-water soluble APIs, and metoclopramide HCl and metamizol sodium as water-soluble APIs were investigated. Finally, paracetamol was used as model drug in order to study the effect of the diluent nature on the API release and the content of uniformity of the Lyocs®. As a suspension is produced and frozen, the risk of sedimentation during the freezing step is high, resulting in a bad product quality. The Lyocs® were manufactured in a GMP-environment, and characterized according to the European Pharmacopeia (Ph. Eur.).

2 Theory and Scientific Knowledge

2.1 Orally Disintegrating Tablets

Pharmaceutical companies are increasingly adapting their products to the patients' needs and expectations in order to improve their compliance and adherence to the treatment. Between all the existing ways of drug administration in the body such as oral, parenteral, transdermal or pulmonary, the most preferred and common used is the oral one (Felton, 2013; Lipp, 2013). Indeed, in comparison to the other routes of drug administration, the oral one is easier to use, non-invasive and considered as accurate in dosing (Felton, 2013; Lipp, 2013). Nevertheless, it was reported in a survey conducted by Hermes Pharma, that 55% of the population may have difficulties in swallowing capsules or tablets primarily due to their large size (HermesPharma, 2014). To overcome these swallowing issues, some patients are breaking the tablets (32% of the people surveyed), chewing the tablets (9% of the people surveyed) or crushing the tablets (17% of the people surveyed) before administration, which could lead to a modification of API release profile and have an impact on the treatment efficiency. Finally, 8% of the patients surveyed simply stop taking their medication (HermesPharma, 2014). This swallowing issue is also affecting the increasing elderly population, which is often administered multiple medications several times per day. These conventional oral dosage forms can become disturbing for older people, which could have an impact on their compliance and on the treatment acceptance. As shown in the Figure 2-1, the elderly population is globally increasing and is supposed to continue on this rate of extension until 2050 (UnitedNations, 2015).

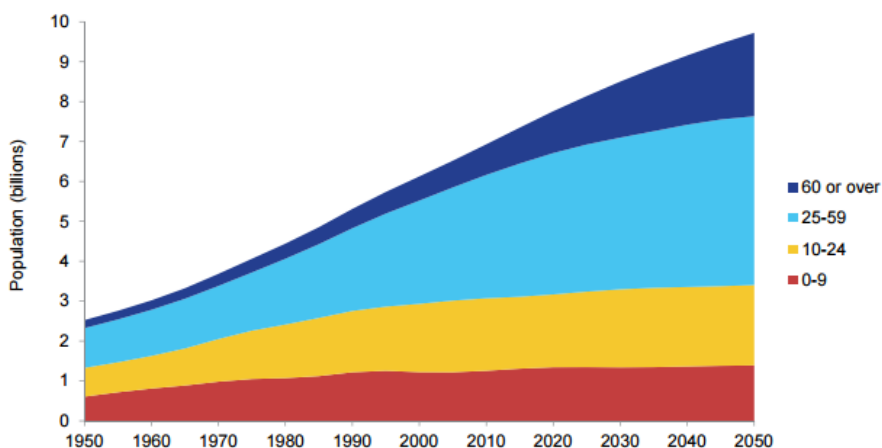


Figure 2-1: Global population by broad age group, 1950-2050 (UnitedNations, 2015).

That is why novel oral drugs have been developed such as ODTs, Orally Disintegrating Granules, or Orally Disintegrating Films, offering to the patients a more convenient therapy and consequently a better adherence to the treatment. In this thesis, only the ODTs will be discussed.

2.1.1 Definition, Advantages and Drawbacks of ODTs

United States Food and Drug Administration defined ODTs as "a solid dosage form containing medicinal substances which disintegrates rapidly, usually within a matter of seconds, when

placed upon the tongue” (CDER, 2008). The Ph. Eur. defines ODTs as “tablets intended to be placed in the mouth where it disperses rapidly before swallowing within 3 minutes” (EDQM, 2014e).

This pharmaceutical dosage form offers plenty of advantages for the patient in comparison to the conventional oral forms (Kumare, 2008; Parkash et al., 2011), such as:

- Simplicity of administration (no need of water for this form),
- Does not leave any residue in the mouth after administration,
- Form adapted for patients who have swallowing difficulties (paediatric, geriatric, and patients suffering from dysphagia),
- Form adapted for psychiatric use,
- Form adapted to patients who do not have an immediate access to water (bedridden, travelling or busy patients),
- Discreet treatment (Kumare, 2008; Parkash et al., 2011).

All these advantages lead to an improvement of the patient’s observance and compliance, helping them to better respect the posology and to take their medication correctly (Parkash et al., 2011).

ODTs also give a marketing strength to the pharmaceutical companies, enabling them to extend their patent protection and their product line by offering an added product value (Pfister and Ghosh, 2010a). Indeed, when a drug patent is about to expire, pharmaceutical companies often improve their dosage form to meet the patients expectations. This marketing launch strategy decreases the costs of research and development in comparison to the one of a novel chemical entity and improves its revenue by extending their portfolio and gaining the customers’ loyalty through the provision of a more convenient treatment (Srivastava et al., 2014). The number of commercial ODTs launched on the combined US, EU and Japanese market was estimated to grow from over 200 products in 2006 (TechnologyCatalysts, 2008) to 450 products in 2009 (TechnologyCatalysts, 2010). This global ODT development growth trend doubled the global revenue of ODT market from 2006 with \$3.8 billion (TechnologyCatalysts, 2008) to 2009 with \$6.4 billion (TechnologyCatalysts, 2010), and was expected to exceed \$13 billion by 2015 (TechnologyCatalysts, 2010).

Despite all those advantages brought by ODTs, some challenges and limitations of this dosage form also have to be highlighted. As a matter of fact, ODTs are very friable and hard to handle. Therefore, ODTs require a special unit of blister packaging, which can increase the manufacturing costs. ODTs are also often hygroscopic, which forces the manufacturer to work in a special environment condition with low relative humidity. Moreover, as the ODT disintegrates in the mouth, the API will be tasted by the patient. In the case of bitter APIs, a taste masking technique will have to be developed in order to improve the mouth feeling. The excipients will also have to be carefully chosen in order to prevent a gritty feeling in the mouth. Finally, due to the tablet size limitation and the taste masking techniques that may be used in the formulation, the dose in ODT is often limited in comparison to conventional tablets (Parkash et al., 2011; Pfister and Ghosh, 2010a; Srivastava et al., 2014). As the dosage form is disintegrating in the mouth, its mode of action should be discussed. Do the ODTs act like a

conventional tablet or capsule, or is the API's bioavailability improved thanks to a pre-gastric absorption? This issue will be discussed in detail in the following section.

2.1.2 System of Action of ODTs

One of the most important characteristics of a drug is its pharmacokinetics, i.e. the fate of the drug in the body. The latter is described through the LADME model (Liberation, Absorption, Distribution, Metabolism, and Excretion). Pharmacokinetics of a drug not only depends on the physicochemical properties of the API (e.g. solubility, permeability, crystallinity, pH, particle size), but also on the pharmaceutical form, on the administration route of a drug and on some patient-related factors such as age, gender, corpulence (Le, 2014d). The ADME model is summarized in Figure 2-2 and will be described in this chapter:

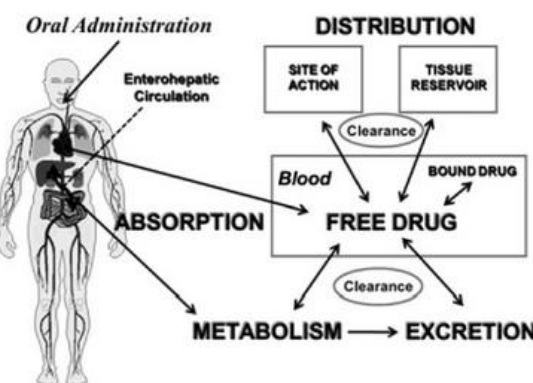


Figure 2-2: Schema of the fate of drugs in the body after oral administration occurring after the liberation of the API (Faqi, 2013).

2.1.2.1 Absorption

Once a drug is administered to a patient, the API has to be released from its pharmaceutical form in order to be dissolved in the biological fluids (Le, 2014a). In our case, the ODT disintegrates instantly in contact with saliva, releasing the API from its matrix in the oral cavity of the patient, i.e. liberation step (Seager, 1998).

The absorption step represents the movement of the API from the site of administration to the blood circulation (Le, 2014a; Sakai, 2008). Two scenarios are possible in our case: the API can either be completely or partly absorbed in the mouth during the tablet disintegration, or it can be absorbed along the gastro-intestinal tract (GIT), like a conventional oral dosage form (Pfister and Ghosh, 2010b; Seager, 1998). The estimated surface areas available for drug absorption in intraoral and GIT, the local pH, the enzymatic activity and the drug absorption capacity are summarized in Table 2-1.

Table 2-1: Characteristics of the Oral Cavity and GIT (Pfister and Ghosh, 2010a).

Absorptive Site	Estimated Surface Area	Local pH	Relative Enzymatic Activity	Relative Drug Absorption Capacity
Oral cavity	100 cm ²	5,8 to 7,6	Moderate	High
Esophagus	-	6 to 7	Low	Low
Stomach	0,1 to 0,2 m ²	1 to 3	High	High
Small intestine	100 m ²	3 to 4	High	High
Large intestine	0,5 to 1 m ²	4 to 6	Moderate	Low
Rectum	200 to 400 cm ²	5 to 6	Low	Low

Despite the small surface area of the oral cavity (100 cm²), the oral mucosa tissue and its rich vascularity gives to the API a high capacity to be absorbed (Pfister and Ghosh, 2010a). When oral absorption occurs, the API goes directly in the systemic circulation, avoiding a hepatic first pass metabolism. Unfortunately, this scenario is pretty rare for ODTs, as the contact of the API with the oral cavity is too short (Le, 2014a). It could nevertheless be observed for the Selegiline Zydis® formulation for example, where the area under curve measured was eight times higher than the one of a conventional tablet, as shown in Figure 2-3 (Seager, 1998).

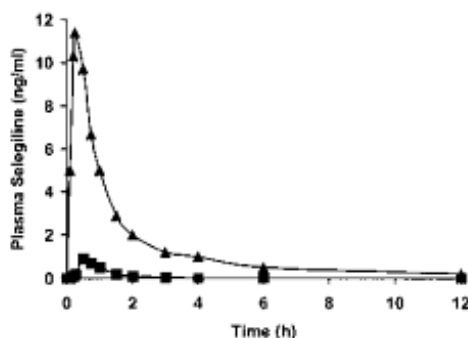


Figure 2-3: Selegiline concentration in plasma following oral administration of tablet (■, 10 mg); Zydis® (▲, 10 mg) (Seager, 1998).

This phenomenon could also be observed for other APIs such as apomorphine, buspirone, midazolam or timolol (Kearney, 2002). It was thus concluded that buccal absorption was observed for APIs having (Kearney, 2002):

- Molecular weight < 500 Da
- High aqueous solubility
- log P at pH 6-7 > 1
- Dose less than 20 mg.

Indeed, it was noticed that for doses smaller than 20 mg, a greater amount of the dissolved drug is retained on the surface of the oral mucosa and can easily be absorbed. On the contrary, larger doses of API will form a mass in the mouth, which will be directly swallowed to go to the stomach (Kearney, 2002).

When any oral absorption is observed, the API will be absorbed like a conventional dosage form, i.e. dissolved in the gastric fluid, spread in the small intestine and absorbed through the intestinal epithelia. Most drug absorption occurs in the small intestine because of its large surface area and of the higher permeable nature of its membrane in comparision to the ones of the stomach (Le, 2014a).

During the passage through the GIT, the API will be exposed to different pH environments as described in the Table 2.1. It will thus have an impact on the API solubility and stability. Moreover, the permeability of the API through the biological membranes also defines the ability of the API to reach the bloodstream. That is why API solubility and permeability both have an impact on absorption (Le, 2014a).

2.1.2.2 Distribution

Distribution is the next step after absorption in the LADME model, determining the transport of the absorbed drug to the body's tissues. Once the API enters the systemic circulation, it is transported in the blood either free (unbound) or bound to plasma proteins (such as albumin or globulin).

As shown in the Figure 2-4, the API molecules will have to diffuse from the blood to the extravascular environment in order to reach the body's tissue (Le, 2014b; Umasankar, 2014). The diffusion process will depend on the size of the API molecule:

- The drug molecules smaller than 50 Da pass directly between the cell membranes, also called the paracellular route.
- The lipophilic molecules cross the cell membranes through passive diffusion,
- The polar or ionized molecules will be actively transported thanks to a carrier.

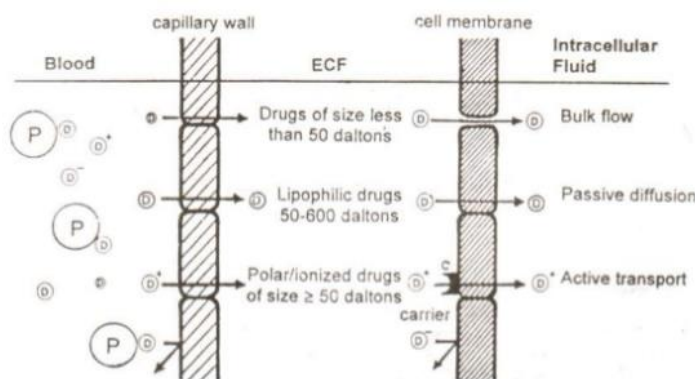


Figure 2-4: Plasma membrane barrier and drug diffusion (ECF = Extra Cellular Fluid) (Umasankar, 2014).

The bound API molecules are too large to diffuse from the blood to the extravascular environment (Umasankar, 2014). That is why only the free API molecules will have a pharmacological activity (Le, 2014b; Umasankar, 2014). Distribution of a drug is not uniform because of the different blood flow rate, permeability and diffusion across the cell membrane. That is why well-perfused organs (i.e. liver, kidney, brain) initially receive more API than the less-perfused ones (i.e. muscle, fat).

2.1.2.3 Metabolism

As soon as the API is ingested and distributed, it will be considered as a foreign substance by the body. Thus, the body will rapidly fight against it to reject it (Pelkonen and Ahokas, 2009). That is why distribution, metabolism and excretion occur quite simultaneously. When the parent drug reaches the liver or the kidneys, the API is biotransformed into metabolites, which can be either less or more toxic molecules. This biotransformation can happen in two kinds of reactions:

- Phase I: The API becomes more polar through reactions of oxidation, reduction or hydrolysis, using metabolic enzymes like cytochrome P450 in order to catalyze the reaction (Pelkonen and Ahokas, 2009; Sakai, 2008).
- Phase II: Reactions of conjugation between the API and another substance like glucuronic acid or sulfuric acid occur, increasing the API solubility and consequently making it more easily excreted by the kidneys (Pelkonen and Ahokas, 2009; Sakai, 2008).

2.1.2.4 Excretion

When a drug is distributed in the organism, the drug and its metabolites have to be removed otherwise the drug concentration will continue to increase after the administration of each successive dose. The organs involved in this step are the kidneys, the biliary system, the lungs, the intestine walls, the salivary glands, the sweat glands and the mammary glands (Sunu, 2013). The kidneys are the principal organs of water-soluble API excretion (Le, 2014c). Indeed, the kidneys are filtering the blood and are creating urine to remove the wastes contained in the blood (Pelkonen and Ahokas, 2009). The limited water-soluble APIs will be reabsorbed in the bloodstream at the end of the filtration, and will recirculate in the whole body again (Sakai, 2008). Biliary system also plays a role in the excretion of large molecules or of lipophilic APIs for example, which are excreted through feces (Pelkonen and Ahokas, 2009). The other excretion ways only play a minimal role in the excretion step.

2.1.3 Manufacturing Technologies of ODTs

The orally disintegrating property of an ODT is not only linked to the judicious selection of highly water-soluble diluents, but also to the highly porous structure present in the tablet. The pores enable the saliva to quickly get inside the tablet, leading to the disintegration of the matrix and the release of the API as a suspension or a solution in the mouth that will be further swallowed. Several ODTs manufacturing techniques have been developed lately and patented and are summarized in Table 2-2.

Table 2-2: ODTs patented technologies, describing their principle, advantages and disadvantages (Amar et al., 2015; Sharma et al., 2010; Srivastava et al., 2014).

Technology	Principle	Advantages (++) / Drawbacks (--)
Freeze-drying <i>ZYDIS®</i> , <i>LYOC®</i> , <i>QUICKSOLV® Technologies</i>	A suspension composed of water, of different excipients and of at least one API is	++ very fast disintegration time.

	lyophilized. The porous structure is given by the sublimated water.	--bad mechanical strength needing appropriated packaging (peel-off blister), costly manufacturing processes, moisture sensitive products requiring low relative humidity manufacturing rooms.
Direct compression <i>WOWTAB® Technology</i>	The API is mixed with a poor compressible saccharide and granulated with a good compressible saccharide. The granulate is then directly compressed.	++ good mechanical strength, low production costs -- moisture sensitive APIs cannot be used, gritty feeling
Floss-based technology <i>COTTON CANDY®, SHEARFORM®, FLASHDOSE® Technologies</i>	Saccharides or polysaccharides are simultaneously flash melted and centrifuged to form the matrix. It is then partially recrystallized to improve the flowability and compressability. The matrix is then milled, mixed to the API and further compressed.	++ good mechanical strength, large drug loading -- high temperature process →temperature sensitive APIs cannot be used
Effervescent with taste masked API <i>ORASOLV®, ORAQUICK® Technologies</i>	The taste of the API is masked using a coating technique. The coated API is then mixed to an effervescent couple composed of a dry acid and a dry base that speeds up the tablet disintegration. The mixture is then directly compressed.	++ bad tastes are covered up. -- low mechanical strength, moisture sensitive products (due to the effervescent couple) requiring low relative humidity manufacturing rooms.

As underlined by Table 2-2, direct compression is the easier and cheaper technique to manufacture ODTs.

Despite the complexity of lyophilization (formulation development and process parameters) and its expensive cost (energy and time costly, low productivity in comparison to tablet press), this process is increasingly used in the pharmaceutical industry because of the different advantages that this technique offers (Siow et al., 2016):

- Preserved API characteristics (minimum physical and chemical changes during the process),
- Highly porous structure obtained through sublimation of ice crystals,
- Faster product dissolution in mouth in comparison to conventional ODTs (Catalent, 2013),
- Better mouth feeling (less sandy than conventional ODTs (Catalent, 2013),

- Precise dosage through a fully automated pipette.

The manufacture of ODTs by means of lyophilization is unfortunately poorly documented in terms of formulation and of process development. The existing patented freeze-drying techniques will be further discussed in this section.

2.1.3.1 Zydis® Technology

Zydis®, developed by R.P. Scherer, was the first marketed fast-dissolving technology of solid oral dosage forms (Kearney, 2002). Those lyophilized products disintegrate in the mouth within a few seconds (3-6 sec), due to the highly porous structure (Pfister and Ghosh, 2010a).

13 Zydis® products are currently globally marketed, as mentioned in Table 2-3.

Table 2-3: Zydis® products present on the global market (Kearney, 2002).

Product	API	Company	First launch
Temesta	Lorazepam	Wyeth	1986
Seresta	Oxazepam	Wyeth	1986
Feldene	Piroxicam	Pfizer	1992
Imodium	Loperamide	Janssen	1993
Pepcid	Famotidine	Merck	1993
Claritin	Loratadine	Schering Plough	1997
Innovace	Enalapril	Merck	1998
Maxalt	Rizatriptan	Merck	1998
Zelapar	Selegiline	Elan	1998
Zofran	Ondansetron	Glaxo Wellcome	1999
Motilium	Domperidone	Janssen	1999
Zyprexa	Olanzapine	Eli Lilly	2000
Semper	Scopolamine/chlorpheniramine	Taisho	2000

Almost all of these products are bio-equivalent to their conventional dosage forms, and are developed as product line extensions, with the aim of improving the patient's compliance. Nevertheless, it was demonstrated for some products like Zelapar for instance, that the bioavailability of the Selegiline was way better than the conventional tablet, due to a pre-gastric absorption. These kinds of products need then a new clinical study in order to determine the toxicity risks and to adapt the dosage (Kearney, 2002; Seager, 1998).

In this technology, the API is suspended in an aqueous solution composed of a water-soluble polymer (mostly gelatin) and a crystalline sugar alcohol (mostly mannitol). The water-soluble polymer provides the strength and resilience of the tablet, whereas the sugar alcohol provides hardness and an elegant structure to the product (Seager, 1998). As shown in Figure 2-5, this solution will be pumped and dosed by weight into preformed blisters with an automated dispensing system to ensure the homogeneity of the samples. The product is frozen within a few minutes through a liquid nitrogen freezing tunnel. This flash freezing set the homogeneity of the substances and creates ice crystal lattice within the product (Kearney, 2002). The blisters will be progressively stored in a refrigerated chamber, to keep the product frozen during the

entire dispensing step. The trays are loaded onto temperature-controlled shelves of the freeze-dryer and the ice crystals will be removed through sublimation, giving this porous structure to the tablet. The gap between the shelves is minimal (see Figure 2-6), in order to maximize the batch size and minimize the drying time, through a higher heat transfer. The typical drying process lasts about 5 hours, allowing the product to reach a final residual moisture of 2% (Kearney, 2002). Once dried, the blisters are directly sealed with an aluminum foil in order to prevent moisture to be reabsorbed into the product (Kearney, 2002; Travers and Grother, 2013).

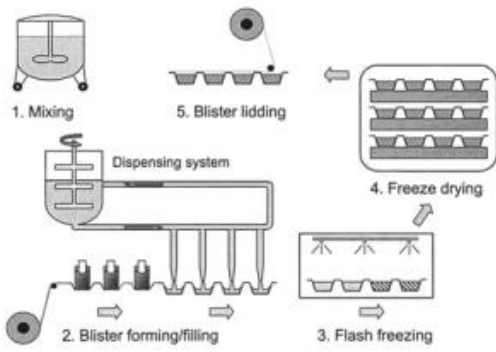


Figure 2-5: Schema of the Zydis® manufacturing process (Kearney, 2002).



Figure 2-6: Bespoke Zydis® freeze-drier, loaded with blister units (Travers and Grother, 2013).

Three main drawbacks can be underlined in this technique. The first one is the use of gelatin, an animal-derived excipient, in the formulation. Indeed, drugs containing gelatin can lead to a non-adherence to the treatment due to religious beliefs (Sattar et al., 2004) or dietary/vegetarian reasons (Vissamsetti et al., 2012).

The second disadvantage of this technique is the limited drug loading of water soluble APIs, set at 60 mg / dose in comparison to 400 mg / dose for non-water soluble APIs (Seager, 1998). This phenomenon can be explained through the fact that water soluble APIs may build up an amorphous structure inside the tablet during the freezing process, leading to collapse of the structure during the primary drying step (Seager, 1998).

The last disadvantage is the very fragile character of the Zydis® products, due to the use a low-concentration matrix in the formulation. Indeed, the more excipients, the less porous structure, and the longer the disintegration of the freeze-dried tablet (Fu et al., 2004; Kearney, 2002). That is why the packaging has to be adapted in order not to break the tablets, by using peel-off blister packaging for instance, which add an extra cost to the Zydis® technique.

2.1.3.2 Lyoc® Technology

The Lyoc® technology was developed by the Lafon Group and differs from the Zydis® technology in several points. Firstly, the Lyoc® formulation is a viscous aqueous matrix mainly composed of a mixture of an undissolved crystalline filler (mannitol or lactose) and a water soluble polymer (dextran). As the Lyoc® technique requires a high-concentrated matrix, the porosity of Lyoc® products is lower than the Zydis® ones, having an impact on its

disintegration time (< 10 sec) and on its hardness. Lyoc® products are denser and more robust than the Zydis® ones (Fu et al., 2004; Kearney, 2002; Pfister and Ghosh, 2010a).

The Lyoc® production process also differs from the Zydis® one. The suspension is dosed by weight with an automated dispensing system in blisters and progressively stored in a freezing chamber at -40°C as shown in Figure 2-7 (Fulzele et al., 2012). The product is frozen within one hour, giving the frozen product larger ice crystals than the Zydis® ones due to the slower freezing rate (Pikal, 2010). The trays are loaded onto the shelves of the freeze-dryer, where the temperature sensors will be connected in order to keep an eye on the product temperature evolution during the drying process. As shown in Figure 2-8, the Lyoc® freeze-dryer configuration is also different than the Zydis® one, as 3 blister tracks are superposed one over the other in order to maximize the batch size and to maximize the production yield. The inter-shelf space is hence bigger in the case of the Lyoc® technology. For more productivity and efficiency, the production team works in three shift work, imposing the whole process to last 8 hours (from the mixing step until the end of drying). The product reaches a final residual moisture of 3% (Kearney, 2002). Once dried, the blisters are directly sealed with an aluminum foil in order to avoid the moisture to be reabsorbed into the product (Kearney, 2002; Travers and Grother, 2013). As the Lyoc® products are robust, they can be packaged in a push-through blister packaging, reducing the packaging costs in comparison to the Zydis® technology (Kearney, 2002).

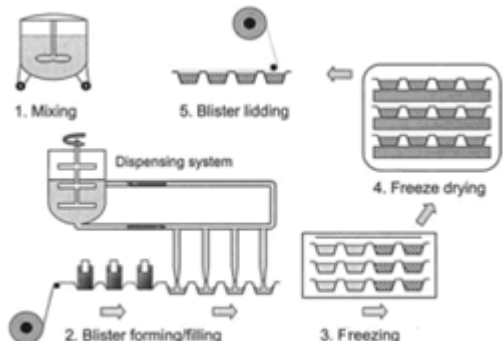


Figure 2-7: Schema of the Lyoc® manufacturing process (Fulzele et al., 2012).



Figure 2-8: Lyoc® freeze-drier, loaded with blister units (Fulzele et al., 2012).

7 Lyoc® products, summarized in Table 2-4, are currently on the market.

Table 2-4: Lyoc® products present on the market (Doctissimo, 2015).

Product	API	Company
Loperamide Lyoc®	Loperamide	Teva Sante
Paralyoc® (250 and 500 mg)	Paracetamol	Teva Sante
Spasfon Lyoc® (80 and 160 mg)	Phloroglucinol	Teva Sante
Vogalene Lyoc®	Metopimazine	Teva Sante
Vogalib®	Metopimazine	Teva Sante

2.1.3.3 QuickSolv® Technology

The QuickSolv® technology was developed by the company Janssen Pharmaceutica (Jeong et al., 2010). The principle of this technique is based on removing a solid frozen solvent from a frozen matrix mixture and is described in the U.S. patent 5,215,756 (Gole et al., 1993). A mixture of a matrix agent, API, secondary components (i.e. sweetening agents, surfactant and flavor agents) and a first solvent (mostly water) is distributed in blisters. The preparation is frozen through a liquid nitrogen freezing tunnel and is then immersed into a second solvent (mostly ethanol) at a temperature below the melting point of the first solvent. The solidified first solvent will thus dissolve into the second solvent and be removed from the tablet. The residual first solvent can be removed using a vacuum chamber under reduced pressure. If the API is soluble in the second solvent, it can dissolve during the immersion step. In this case, a placebo mixture has to be frozen, and the API will be dispersed in a carrier solvent immiscible with the placebo mixture and loaded on the matrix after the immersion step. The QuickSolv® technique is not so used compared to the Zydis® and the Lyoc® one. 2 examples of QuickSolv® products are mentioned in Table 2-5.

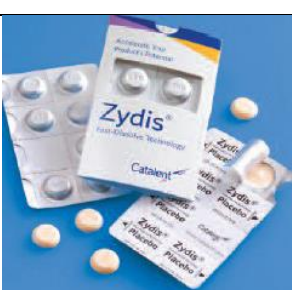
Table 2-5: Example of QuickSolv® products present on the market (McLaughlin et al., 2009).

Product	API
Propulsid QuickSolv®	Cisapride
Risperdal	Risperidon

2.1.3.4 Zydis® vs. Lyoc®

The two most well-known lyophilization techniques for the manufacture of ODTs are Zydis® and Lyoc®. Table 2-6 summarizes the differences between those two techniques.

Table 2-6: Review of Zydis® vs. Lyoc®.

Zydis®	Lyoc®
	
Lyocs® are much bigger tablets than the Zydis® one, allowing larger drug load.	
Disintegration time 3-6 sec	Disintegration time < 10 sec
Freezing-step through a nitrogen tunnel → quick freezing step.	Freezing-step in a freezing room → slower freezing step than Zydis®, leading to larger ice crystals than in Zydis® products.
1 track per shelf, reducing the efficiency.	3 tracks per shelf → bigger productivity than Zydis®.
Product extremely crumbly → peel-off blister	Product quite resilient → normal blister

Hygroscopic product → manufacture in a dry air environment	Hygroscopic product → manufacture in a dry air environment
--	--

2.2 Freeze-drying in ODTs

2.2.1 Generalities (Jennings, 2008d)

Lyophilization is a very gentle stabilizing drying process, where the solvent, in our case water, is removed through sublimation from a frozen liquid sample to provide a dried product. It allows the preservation of the physical and biological characteristics of some heat sensitive products, such as proteins, vaccines or microorganisms. The water removal during the lyophilization process indeed limits the degradation reactions of the product. As the solvent used in the Lyoc® technology is water, the use of the water phase diagram is necessary to understand the sublimation process. Figure 2-9 shows a triple point (Pressure $p=6,11\text{ mbar}$ and Temperature $T=0,01^\circ\text{C}$). At this triple point, the three water phases, i.e. solid, liquid and gas, are simultaneously coexisting. Below this point (at $p = 0,37 \text{ mbar}$ for example), the ice is directly converted from a solid form to a gaseous form by increasing the temperature up to -30°C . If p is higher than $6,11\text{ mbar}$, water passes through all phases by increasing T : solid → liquid → gas. That is why in the lyophilization process, when the freezing step is over, p has to decrease below the triple point before starting the primary drying step in order to preserve the product quality (Jennings, 2008a).

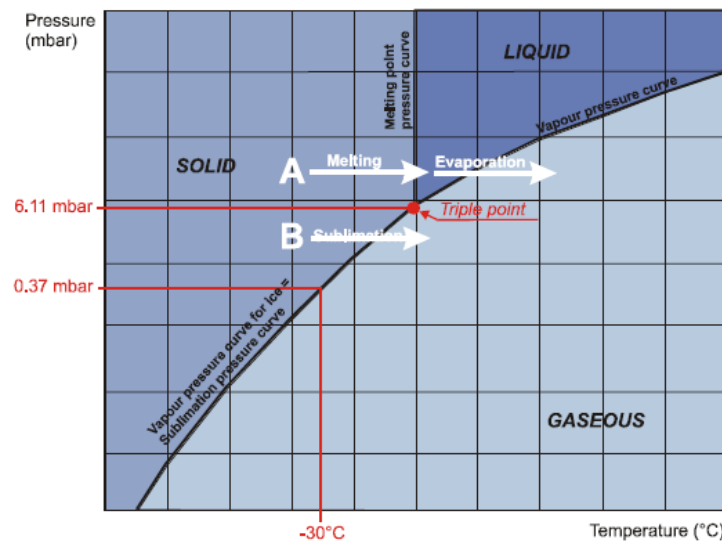


Figure 2-9: Water phase diagram (ChristMartin, 2015), describing the matter change of state: A= from solid to liquid (melting) and from liquid to gas (evaporation), B= from solid to gas (sublimation).

2.2.2 Lyophilization Cycle

The lyophilization cycle is composed of three steps:

- 1) The freezing step consists in freezing the water which is present in the sample, by cooling down the product to a low temperature at atmospheric pressure,

- 2) The primary drying step consists in removing the frozen free water by sublimation under vacuum,
- 3) The secondary drying step consists in removing the bound water remaining in the sample by desorption.

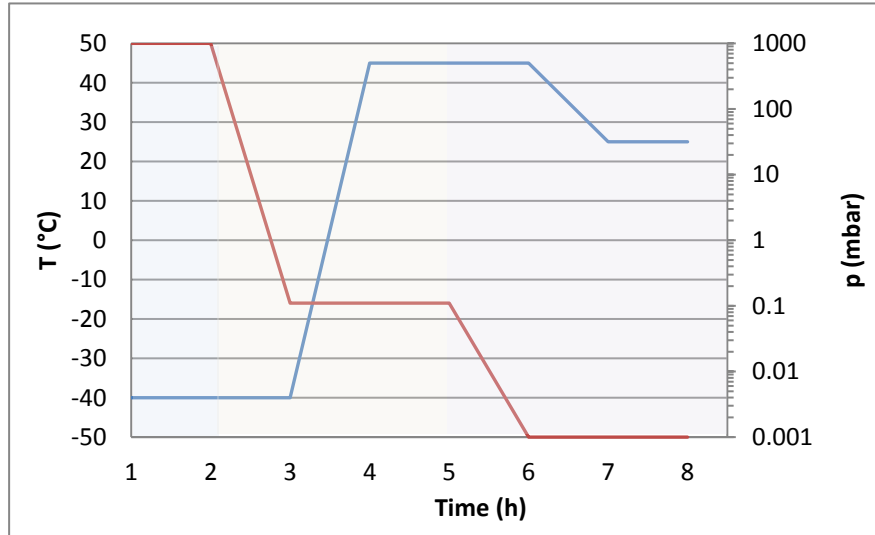


Figure 2-10: Example of a lyophilization cycle. (p: red; T: blue), representing the freezing step (), the primary drying step () and the secondary drying step ()

2.2.2.1 Freezing step

2.2.2.1.1 Structure of Ice

As the product is initially in the liquid state, the product needs firstly to be frozen before sublimation occurs. During this step, the water molecules will build up a particular ice structure within the product.

Ice exists in different crystalline forms, also called polymorphs (Jennings, 2008b). The molecular arrangement differs from one polymorph to the other, having an impact on the free energy of each polymorph and consequently on their thermodynamically stability (Jennings, 2008b). Indeed, the polymorphic structure of lower free energy is thermodynamically more stable (Ronis, 2001). Ordinary ice exists in two different crystal structures: I_h (hexagonal structure), and I_c (cubic structure) (Dutch, 2001; Jennings, 2008b). The I_c structure only exists at P_{atm} at T lower than $-100^{\circ}C$ and transforms into the I_h structure when warmed over $-80^{\circ}C$ (Dutch, 2001; Jennings, 2008b). As shown on Figure 2-11, ice presents many polymorphs. The transition from Ice I to a higher form (II to VII, described in Table 2-7) is only possible at high pressure (over 2 kbar) (Dutch, 2001). As the freezing step of the lyophilization process takes place at P_{atm} and T above $-80^{\circ}C$, the ice will form the I_h structure.

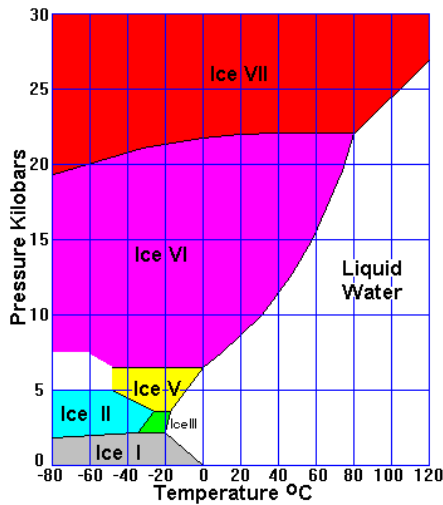


Figure 2-11: Phase diagram of water at high pressure (Dutch, 2001).

Table 2-7: Polymorphic forms of ice (Dutch, 2001).

	Type	Crystal structure
Ordinary Ice	I _h	Hexagonal
	I _c	Cubic
High-Pressure Ice	II	Rhombohedral
	III	Tetragonal
	V	Monoclinic
	VI	Tetragonal
	VII	Cubic

Figure 2-12 represents the lattice hexagonal structure of the I_h form. The red atoms represent oxygen atoms, whereas the solid lines represent hydrogen bonds. The hydrogen atoms are not represented here. As it can be seen in Figure 2-12, each oxygen atom is surrounded by 4 other oxygen atoms, forming a tetrahedral structure. The oxygen-oxygen distance is 2,75 Å and the hydrogen-oxygen distance in the water molecule is 0,99 Å (Jennings, 2008b), which sets the hydrogen-oxygen distance in the hydrogen bond at 1,75 Å. During the freezing step, ice is forming the I_h structure. As the free space between the ice crystals is small, most solutes cannot pass in this crystalline structure, forcing the substances to concentrate in the interstitial region of ice crystal (Jennings, 2008b). However, a separation of solvent-solutes occurs, giving the freeze-dried tablets this porous structure after sublimation.

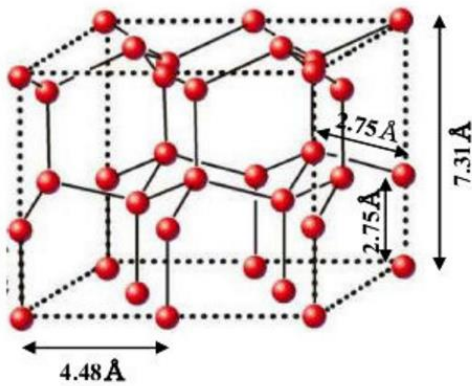


Figure 2-12: Crystalline structure of ice I_h (Hidehisa, 2013).

2.2.2.1.2 Crystal Growth

During the freezing step, crystal nuclei of ice are formed in the sample (nucleation). Those nuclei are the initiator of ice crystals formation (see Figure 2-13). Indeed, crystal growth will occur step by step, until grains are formed (Jennings, 2008a). This nucleation can either be homogenous or heterogeneous (Daniels, 2014). In the first case, the ice nucleation occurs spontaneously involving only the aggregation of pure water molecules (Pikal and Nail, 2014). In the second case, impurity comes into play (such as dirt, sensor, container wall), helping the orientation of molecules to form a stable nucleus (Pikal and Nail, 2014).

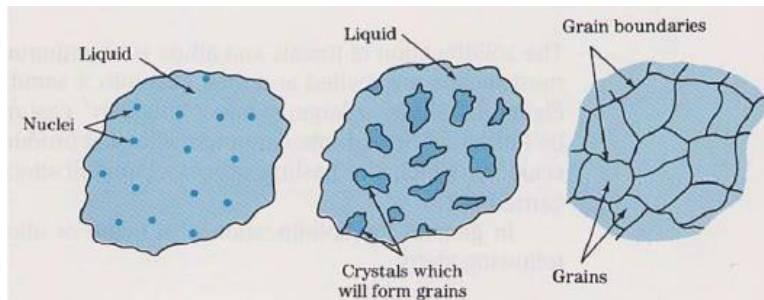


Figure 2-13: Ice nucleation transforming nuclei in crystals through crystal growth (Daniels, 2014).

As explained above, the formation of ice crystal is not spontaneous but it occurs step by step. Firstly, the nuclei are formed at the nucleation temperature (T_N on Figure 2-14), followed by the crystal growth. Nucleation rarely occurs at the thermodynamic solution freezing point (T_F on Figure 2-14), but it often occurs 10-20°C below because of supercooling (Nail et al., 2002; Shon and Mather, 2012). A difference between the nucleation temperature and the freezing point can be observed on Figure 2-14, which is called the degree of supercooling. The increase of temperature from T_N to T_F is due to the heat caused by the sudden ice crystallization (Pikal, 2010). After T_F , the product cools down, converting continuously water into ice.

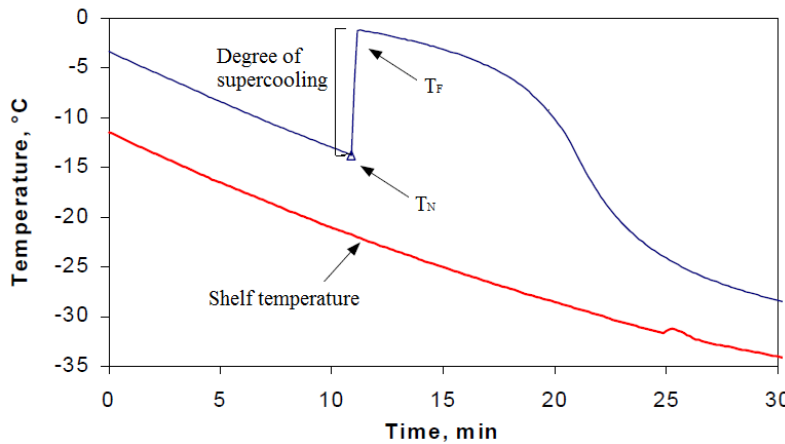


Figure 2-14: Evolution of the product temperature during the freezing step, designating the nucleation temperature (T_N) and the thermodynamic freezing point (T_F) (Pikal and Nail, 2014).

The supercooling is especially dependent on the cooling rate and on the freezing methods used (see Figure 2-15) (Jennings, 2008a; Tang and Pikal, 2004) and will also have an impact on the ice crystal structure and size. As shown on Figure 2-15: high degree of supercooling will occur in case of slow freezing (Awotwe-Otoo and Khan, 2015), resulting in the formation of small ice crystals and so giving small pores to the product during sublimation (Shon and Mather, 2012; Tang and Pikal, 2004). The small pores will impose a bigger resistance to the mass transfer of water vapour during the primary drying, making the sublimation difficult and increasing the primary drying duration (Awotwe-Otoo and Khan, 2015; Shon and Mather, 2012). In the contrary, low degree of supercooling will result in the formation of bigger ice crystals, resulting in bigger pores within the product during sublimation (Shon and Mather, 2012; Tang and Pikal, 2004). The freezing step has hence an impact on the morphological characteristics of the product.

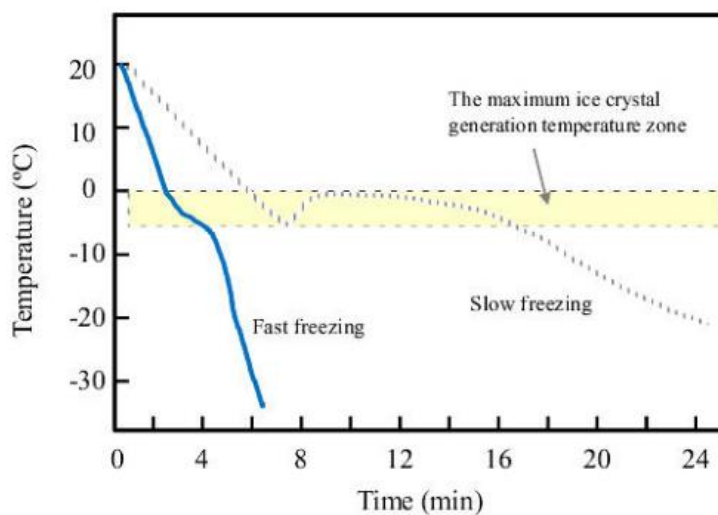


Figure 2-15: Representation of fast and slow freezing (Hidehisa, 2013).

During the ice crystals formation, the solutes (such as the API and the excipients) are forced to be detained in the interstitial region, i.e. between the ice crystals (Jennings, 2008c), and are

concentrating until they also build up either crystallize or a solid amorphous system, according to their freezing behaviour (Milton, 2010). Two phases thus exist in the product, which are ice and freeze-concentrated solution (Daniels, 2014). The physical behaviour of the solutes during the freezing step is summarized below, on the Figure 2-16:

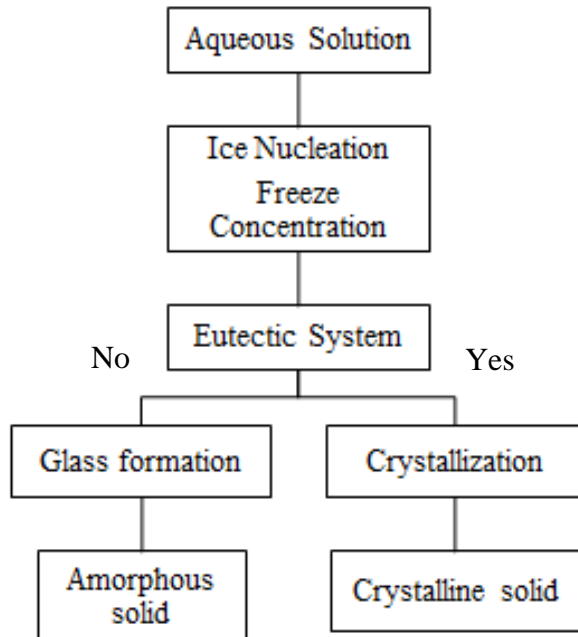


Figure 2-16: Physical behavior of the sample during the freezing step (Daniels, 2014).

2.2.2.1.3 Eutectic System

An eutectic system is defined from the FDA as “a point of a phase diagram where all phases are present and the temperature and composition of the liquid phase cannot be altered without one of the phases disappearing” (FDA, 2014). To describe this system, the phase diagram of Sodium Chloride/Water (see Figure 2-14) in combination with the Gibb’s phase rule can be used:

$$f = C - P + 2$$

where f =number of degrees of freedom (i.e. number of variables that must be fixed to define the system), C =number of components and P =number of phases. The number 2 indicates that T and p can vary.

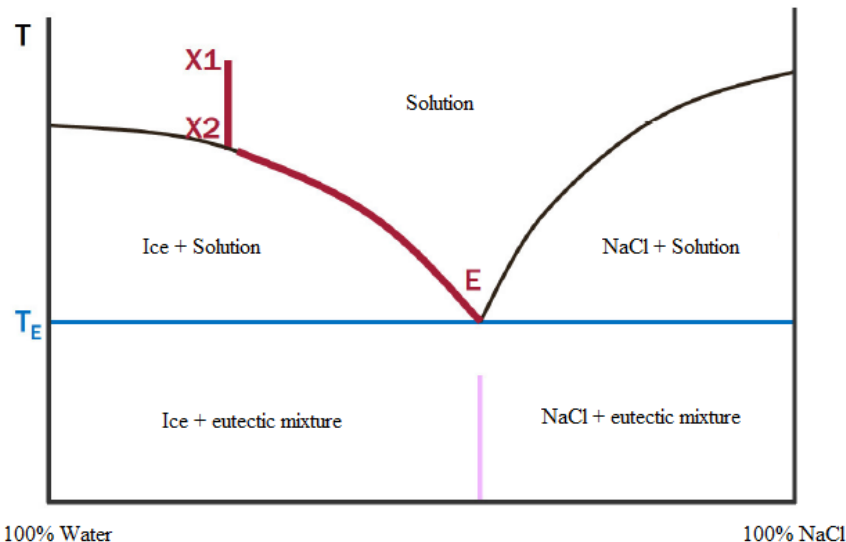


Figure 2-17: Phase diagram of Sodium Chloride/Water (Daniels, 2014).

On Figure 2-17, 2 typical curves can be observed:

- The “liquidus” red line representing the freezing-point depression of water (Phase Diagram Crystallization, 2010) . The addition of a solute in a solvent will result in a decrease of the vapor pressure of water, leading to a freezing point lower than the one of water pure (Jennings, 2008h). The freezing-point depression is hence proportional to the amount of the solute present in the solution (Jennings, 2008h).
- The “solidus” blue line is the separation between the systems Solid and Solution+Solid or Solid and Solution for the point E (Phase Diagram Crystallization, 2010).

Let us consider a NaCl solution with an initially concentration x_1 . During the freezing step, the T decreases until reaching x_2 , where the crystallization of pure water molecules begins. At x_2 , two phases are at the equilibrium, i.e. Solution and Ice. As the temperature keeps decreasing, the water concentration within the sample will decrease, consequently the concentration of NaCl increases in the interstitial region (Jennings, 2008h). That is why the system will follow the red curve x_2E on the Figure 2-17 until reaching the point E. At the equilibrium point E, all the four phases coexist (Jennings, 2008h), i.e. Solution, Ice, NaCl and Eutectic mixture. Therefore at E, $C=2$, $P=4$ and so $f=0$ which means that a change in temperature or in the composition of the solution can only be possible when the number of present phases changes so that $f\neq0$ (Jennings, 2008h). This means that at the eutectic temperature (T_E) the NaCl ions crystallize next to water (Labconco, 2010). Below T_E , the system is separating itself in ice crystals, NaCl crystals and eutectic mixture and the whole system is completely frozen (Labconco, 2010). Above T_E , the system will melt and the system will come back in the Solution state (MillrockTechnology, 2009).

During the primary drying phase, when the product temperature (T_p) exceeds T_E the first few hours, the cake structure will be destroyed due to solutes melting and the visual aspect of the product will not be acceptable (Labconco, 2010). T_E is thus the critical temperature of the process. That is why the product has to be frozen at least 10°C below T_E to give a sufficient energy by rising up the temperature so that the maximum sublimation can occurs before reaching T_E preventing destroying the cake structure (Tang and Pikal, 2004).

2.2.2.1.4 Amorphous System

Lots of sugar and polymer solutions do not crystallize as expected at the eutectic point but solidify like an amorphous glass. Indeed, the solution near the ice crystals is supersaturated. This phenomenon is represented on Figure 2-18:

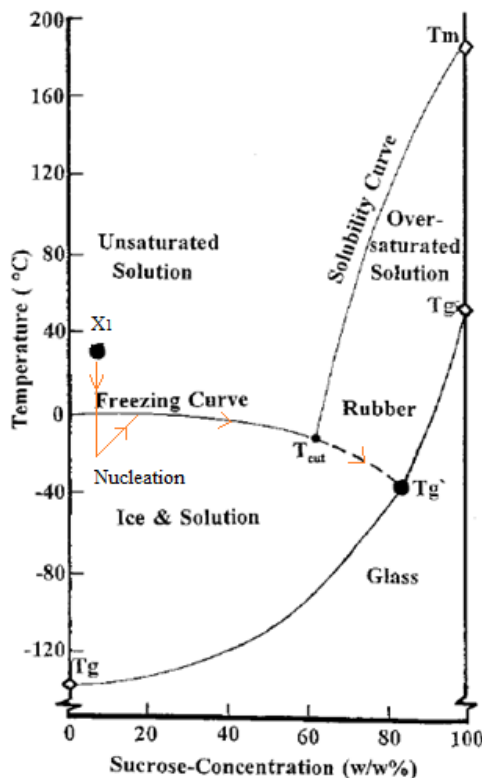


Figure 2-18: Phase diagramm of a Sucrose/Water solution (Tang and Pikal, 2004).

The sucrose solution of concentration x_1 is frozen with the same mechanism explained previously. When T_p goes below T_e , the solution will increasingly concentrate in sucrose. The solute solution will hence become more and more viscous until the glass transition temperature of the maximally freeze-concentrated amorphous phase ($T_{g'}$) is reached. When T_p goes below $T_{g'}$, the crystallization speed is so slow that the system will solidify like a glass, without any complete phase separation (Daniels, 2014; Hatley et al., 1996). The interstitial glassy solute phase contains thus a quantity of non-crystalline water, also called non-frozen water (Daniels, 2014).

During the primary drying step, when $T_{g'}$ is exceeded the viscosity of the amorphous phase will decrease, destroying the porous structure of the cake. This phenomenon is named collapse and occurs at the collapse temperature (T_c), only a few degrees higher than $T_{g'}$ (Jennings, 2008e; Pikal, 2010). $T_{g'}$ is hence the critical temperature of the process.

2.2.2.1.5 In Practice

At the end of the freezing step, all the amount of liquid has to be frozen and T_p needs to be at least at 10°C below T_E (for crystalline solid) or T_g^* (for amorphous solid) of the matrix builder temperature to ensure the complete solidification of the product (Tang and Pikal, 2004). For an optimum process time, the freezing speed rate should be between 0,2 °C/min to 10°C/min (Daniels, 2014). The product is cooled until T_p reaches the shelf temperature (T_s), set up 10°C below the eutectic temperature of the mixture filler/water. This step is made under atmospheric pressure. The freezing duration depends on the thickness of the product pipetted volume. If the volume thickness is less than 1 cm, the freezing step will last one hour. If the volume thickness is bigger than 1 cm, the freezing step will last at least two hours (Tang and Pikal, 2004). As the Lyoc® thickness is around 0,5 cm, the freezing step lasts up to one hour in production.

2.2.2.2 Primary Drying (P.D)

2.2.2.2.1 Energy Transfer

During this step, the frozen water will sublime, transforming itself directly into water vapour (step B on Figure 2-9). The porous nature of the Lyoc® products comes from the place formed by the ice water sublimation (see Figure 2-19).

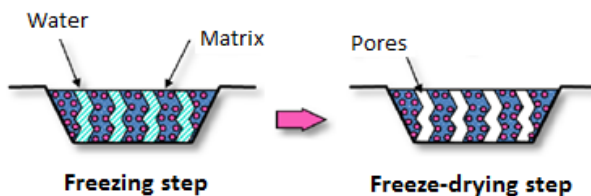


Figure 2-19: Origin of the porous nature of Lyoc® (Schubert, 2014).

The water vapour released by the product will condense and freeze at the surface of the condenser, which is the colder site of the freeze-dryer (between -80 and -90 °C). Sublimation, which is an endothermic phenomenon, requires high amounts of energy (ca. 3800 kJ/kg ice (Daniels, 2014)). This energy will be thermally brought to the product by the increase of T_s (Nail et al., 2002). A difference can nevertheless be observed between the Zydis® technology and the Lyoc® technology. In the Lyoc® technology, the blisters are not in direct contact with the shelves, but positioned on trays. Thermal conduction thus does not happen to a great extent in the Lyoc® technology, reducing considerably the energy input in comparison to other lyophilization techniques. On the same way, convection is also almost irrelevant in our case (Nail et al., 2002), as the distance between the shelves and the blister is too large (ca. 1,5 cm). That is why the heat transfer taking place in the case of the Lyoc® technology is almost exclusively due to **radiation** from the shelves and from the walls of the chamber (see Figure 2-20). It can be seen on Figure 2-20 that sublimation within the Lyoc® products is heterogeneous (Tang and Pikal, 2004). Indeed, the water vapour will begin to evaporate out of the blister from the top surface of the Lyoc® to the bottom of the blister, until the free frozen water is completely removed. This sublimation evolution is called “sublimation front”.

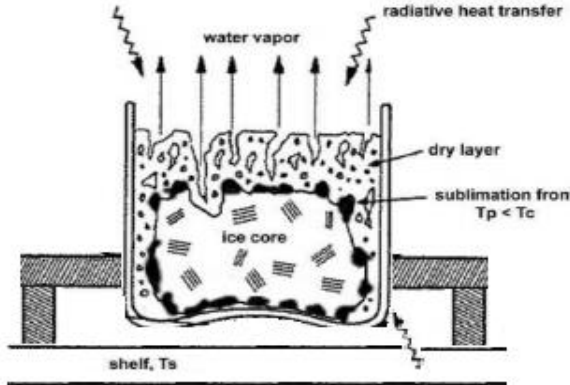


Figure 2-20: Types of heat transfer present in the Lyoc® technology (Daniels, 2014).

2.2.2.2.2 Mass Transfer

As explained in the previous Section, the system needs an energy input in order to sublime. This energy is given by heat, and can be mathematically expressed as (Tang and Pikal, 2004):

$$\frac{dQ}{dt} = \Delta H_s \cdot \frac{dm}{dt}$$

where $\frac{dQ}{dt}$ represents the heat transfer rate, ΔH_s the heat of ice sublimation and $\frac{dm}{dt}$ is the ice sublimation rate. After thermal energy has been applied to the system, the ice will transform in vapour, transferring the vapour out of the product through the pores of the Lyocs®. Once the vapour molecules are in the chamber, they will transfer out of the chamber, following a pressure gradient, in order to be trapped in a frozen state on the condenser that has the colder temperature T_{cc} (Condenser Chamber Temperature) of the system. This mass transfer is possible and accentuated through the use of vacuum (Nail et al., 2002; Tang and Pikal, 2004). Indeed, as expressed in the following equation proposed by Pikal (Pikal and Nail, 2014), the mass transfer depends on the difference between the pressure in the chamber (P_c) and the vapour pressure of ice (P_0) and on the resistance to sublimation of the dry layer (R_c):

$$\frac{dm}{dt} = \frac{P_0 - P_c}{R_c}$$

The difference between P_c and P_0 is obviously the driving force of sublimation (Tang and Pikal, 2004). This means that P_c has to be much lower than P_0 in order to allow a high sublimation rate (mass of ice sublimate per unit of time) and thus to accelerate the P.D step. Nevertheless, too low P_c could lead to large heterogeneity in heat transfer (Tang and Pikal, 2004) and as a consequence cause heterogeneity in T_p within the Lyocs® (Tang and Pikal, 2004). That is why a study on the influence of this ΔP on the sublimation speed was made and summarized by Le Floch (Le Floch, 2008). It was identified that the maximal sublimation speed was observed at $P_c = \frac{P_0}{2}$. The resistance of the dry layer is also an important factor that must be taken into consideration (Tang and Pikal, 2004). Indeed, as mentioned in Section 2.2.3.2.1, the sublimation is heterogeneous, going from the top of the product to the bottom.

Through sublimation, the top of the product is then transformed into a dry layer, which forces the vapour of the bottom layer to sublime. Therefore, the larger the product layer, the more difficult it is to sublime the bottom of the product.

To summarize, sublimation results from:

- a higher shelf temperature
- a low pressure (below the triple point) correlated to the Tcc to increase the diffusion speed rate.

The factors which influence the primary drying speed are:

- The morphology of the frozen suspension: the smaller the pore size is, the more difficult for the vapour water will be able to escape (Pikal, 2010).
- The heating energy brought to the product.
- The vacuum (the deeper down the vacuum goes, the faster the sublimation).
- The transport path to the condenser.

As explained in Section 2.2.3.1, the product can either form an eutectic or an amorphous system. The sublimation mechanism of water can thus differ, according to the system built up during the freezing step. As shown in Figure 2-21, 4 mechanisms are possible:

- When an eutectic system is built up (A), the ice crystals form canals (Jennings, 2008a), allowing the water vapour to diffuse out of the matrix. Those free canals are thus the origin of the porous structure formed in Lyocs®.
- When T_p is higher than T_e and when too many ice crystals are still present in the Lyoc®, the eutectic mixture melt (Tang and Pikal, 2004), as explained in Section 2.2.3.1.1. This phenomenon is called collapse (B). During collapse, the product softens in the surface area and can no longer support its own structure (ChristMartin, 2015). That is why the collapse temperature needs to be known, in order not to exceed it during the beginning of primary drying (Tang and Pikal, 2004). It is usually measured by means of DSC (Jennings, 2008g).
- When an amorphous system is built up (C), ice crystals are immersed in glassy interstitial material (Jennings, 2008a), hampering the flow out of the Lyoc® of water vapour. Indeed, water vapour has first to diffuse through the amorphous matrix. Eutectic mixtures are for this reason easier to sublime than amorphous systems.
- When the resistance of steam diffusion through the amorphous material is too high, cracks from which the steam will be released appear in the amorphous structure (D).

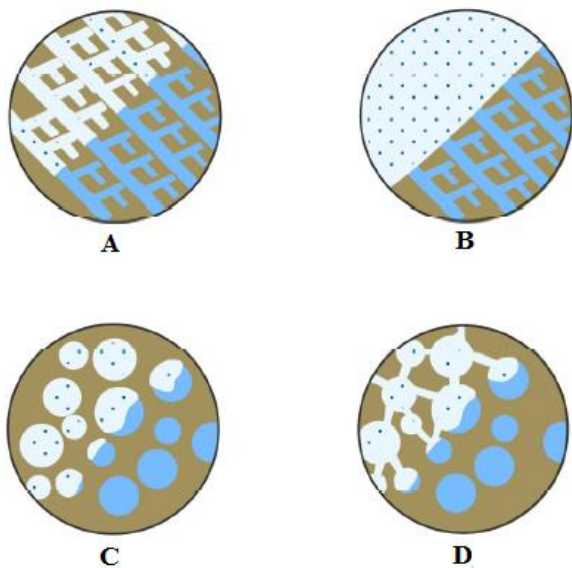


Figure 2-21: Mechanisms of sublimation during P.D of lyophilization. A=Direct sublimation, B=Collapse, C=Diffusion through the matrix, D=Escape through cracking (Daniels, 2014).

2.2.2.1.3 Annealing

As detailed in the previous paragraphs, two main parameters are essential on the P.D step, namely the physical behaviour of the frozen solute (eutectic systems possess higher critical temperature than amorphous systems and thus higher temperature can be applied to the product during the P.D step which reduce the P.D duration) and the size of ice crystals (bigger ice crystals lead to a faster sublimation). The crystallization of an amorphous solute can thus be induced by means of a thermal treatment between the end of the freezing step and the beginning of the P.D step (Abdul-Fattah and Truong, 2010; Wang and Pikal, 2012). This thermal treatment, also called annealing, consists in warming up the product at a temperature above its T_g' without reaching T_c in order to prevent collapse (Barley, 2016; Wang and Pikal, 2012). This temperature is then held during a few hours before being brought again to a lower temperature (Wang and Pikal, 2012). Above T_g' , the mobility of the molecules increases (Wang and Pikal, 2012), allowing crystals to grow through the Ostwald ripening mechanism (Wang and Pikal, 2012). The small crystals will indeed migrate around the bigger ones, offering to the product a good homogeneity and a good visual aspect (Chang and Patro, 2004). This phenomenon will thus lead to the creation of larger ice crystals (Wang and Pikal, 2012), and so reduce the resistance to water vapour during the P.D step due to bigger pores (Chang and Patro, 2004), accelerating the sublimation step. In the case of glycine and mannitol, a conversion of the amorphous proportion into crystalline state could be observed after annealing, increasing the critical temperature of the formulation (see Figure 2-18). The P.D step can thus be performed at higher temperature, decreasing its duration. In our case, annealing is not considered to be an appropriate measure, as it would take too much time in the production step, reducing the productivity. That is why annealing will not be studied further.

2.2.2.2.4 In Practice

In order to avoid reaching the triple point (see Figure 2-9), the pressure in the chamber is firstly decreased under the vapour pressure of ice at T_p , and T_s is then increased by heating the thermal fluid present in the shelves. T_p has to remain 5 to 10°C below the collapse temperature of the product at the beginning of the primary drying to prevent the deformation of the product by collapse. Then, T_s is surprisingly set up around 50°C in order to reduce the cycle time by increasing the energy transfer. This high T_s is specific to the Lyoc® technology, as radiation is the main energy transfer occurring during the P.D step. This step finishes when T_p reaches T_s (Pikal, 2010). In production, this step can last up to 4 hours. All the evolutions of T_p , T_s and P_c are monitored by the use of sensors and can thus be observed in real time. The delimitation between Primary Drying and Secondary Drying can also be done by means of other methods such as:

- Pressure rise test (as shown on figure 2-22) the valve present between the condenser and the chamber is closed during a short time in order to isolate the product, and P_c is observed, in order to check if a rise in pressure can be observed. If the pressure rises, this means that sublimated water vapour accumulates in the chamber and thus the product is not completely dried. That is why the valve is reopened and the primary drying step is prolonged (Fissore et al., 2011). The slower the pressure rises, the drier the product (Reihbandt, 2016).

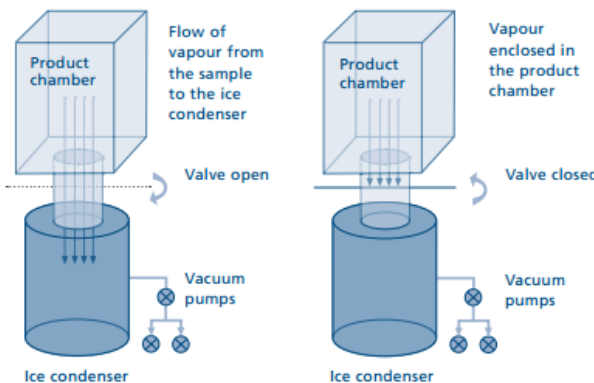


Figure 2-22: Principle of Pressure Rise Test (ChristMartin, 2015).

- Comparative pressure measurement (Pirani vs. Capacitive manometer: P_c is controlled with a capacitive manometer, whereas the Pirani gauge measures the thermal conductivity of the water vapour in the chamber. As soon as the Pirani pressure decreases, the gas composition of the chamber is changing from water vapor to nitrogen, meaning that the sublimation is completed (Bhambere et al., 2015)),
- Decrease of sample weight (by using a microbalance (ChristMartin, 2015))
- Determination of the water vapour in the chamber by means of moisture sensors (the moisture sensor measures the dew point i.e. it can determine the presence of ice or liquid in the sample. The dew point starts decreasing as soon as the sublimation is completed (Reihbandt, 2016)).

The combination between T_p and Pressure rise test is used in this thesis in order to ensure the end of the Primary Drying step.

2.2.2.3 Secondary Drying (S.D)

At the end of the Primary Drying, the entire free water is removed from the product and only bound water (between 10-30% of the total water content (Sadikoglu et al., 2006)) is present in the freeze-dried product (Bhambere et al., 2015). In the case of Lyocs®, the content of remaining water should not exceed 3 %. The nature of bound water present in the product depends on the matrix physical state (Daniels, 2014). In crystalline matrices, the bound water is either adsorbed on the surface of the matrix crystals or is present as water of hydration within the matrix (Daniels, 2014). In amorphous matrices, the bound water is absorbed within the matrix (Daniels, 2014). That is why the rate of water extraction is limited by desorption and evaporation at the surface of the sample in the case of crystalline matrix, whereas it is limited by diffusion of water molecule from the inside of the amorphous matrix through the pore structure (Daniels, 2014; Pikal, 2010). In practice, higher temperature than during Primary Drying is applied to the product at low chamber pressure (down to 1 μ bar) (Bhambere et al., 2015). Bound water requires more energy to be removed than free water, as bound water formed physicochemical interactions with the dried matrix (Galan, 2010). A further study was made by Pikal on the Secondary Drying step regarding the influence of the solid state of the matrix, T and P_c on the rate of Secondary Drying (Pikal, 2010; Pikal and Nail, 2014) and is explained in the following sections.

2.2.2.3.1 Influence of the Matrix Solid State on Secondary Drying

The kinetics of S.D of three different systems (see Figure 2-23), namely Mannitol (crystalline) (Pikal, 2010), Povidone (amorphous) (Pikal, 2010) and Moxalactam di-sodium (amorphous) (Pikal, 2010) were firstly studied. Bound water is therefore being extracted from a crystalline or an amorphous matrix. F represents the fractional attainment of equilibrium (i.e. near zero water) (Pikal, 2010). That is why 1-F represents the normalized water content. It can be noticed on Figure 2-23 that the first hour, the three products lost the maximum amount of water (around 0,2 % for Mannitol, 2 % for Povidone and 4 % for Moxalactam di-sodium), followed by a lower drying rate and finally a plateau at the end of the S.D (around 0,1 % for Mannitol, 1 % for Povidone and 3 % for Moxalactam di-sodium) (Pikal, 2010). The lower plateau observed in the case of Mannitol in comparison to Povidone or Moxalactam di-sodium can be explained by the faster extraction of water in a crystalline matrix than in an amorphous matrix, possibly due to the fact that trapped water in amorphous matrix has to diffuse from the inside of the sample through the pores whereas adsorbed water has to desorb and to evaporate from the surface of the Lyoc® (Pikal, 2010).

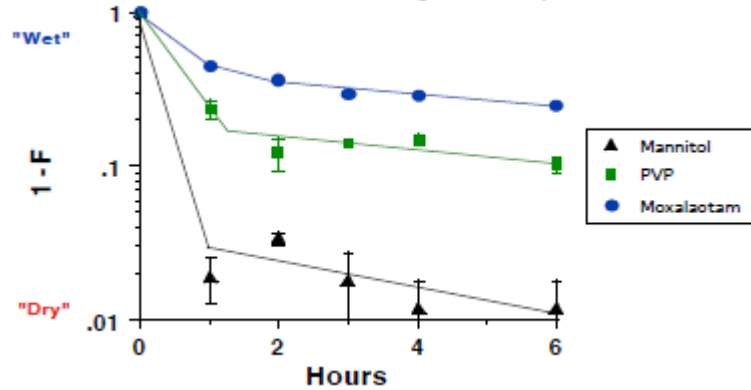


Figure 2-23: Kinetics of S.D. of Mannitol (triangles), Povidone (squares), and Moxalactam di-sodium (circles). Sample preparation: 5 % aqueous solution, 1 cm fill depth, hydration to a uniform moisture of 7 %. S.D conditions: $T_p = 18^\circ\text{C}$, $P_c = 267 \text{ mbar}$ (Pikal, 2010).

2.2.2.3.2 Influence of Temperature on Secondary Drying

S.D was performed on the Moxalactam di-sodium solution of Chapter 2.2.2.3.1 (Pikal and Nail, 2014) with different drying T (see Figure 2-24). It is obviously seen that the drying T has a great influence on the content of water. Indeed, the greater the drying T, the quicker the water is removed and the lower the plateau. This is due to the extra thermal energy brought to the system and helping the trapped water to diffuse more easily through amorphous the matrix.

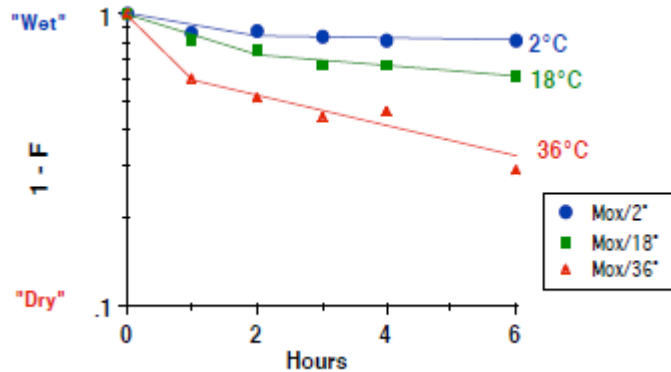


Figure 2-24: Kinetics of S.D. of Moxalactam with a drying T of 36 °C (triangles), 18 °C (squares), and 2 °C (circles). Sample preparation: 5 % aqueous solution, 1 cm fill depth, hydration to an uniform moisture of 7 %. S.D conditions: $P_c = 267 \text{ mbar}$ (Pikal and Nail, 2014).

2.2.2.3.3 Influence of Pressure on Secondary Drying

S.D was performed on the Moxalactam di-sodium and the Povidone solutions of Chapter 2.2.2.3.1 (Pikal and Nail, 2014) with different drying T (see Figure 2-25). Unlike for P.D, P_c does not show any influence on the S.D rate. It can indeed be observed in Figure 2-25, that whatever P_c , the amount of water in the sample is unaltered, meaning that the removal of water in amorphous matrix is limited by the transport, i.e. diffusion in the solid.

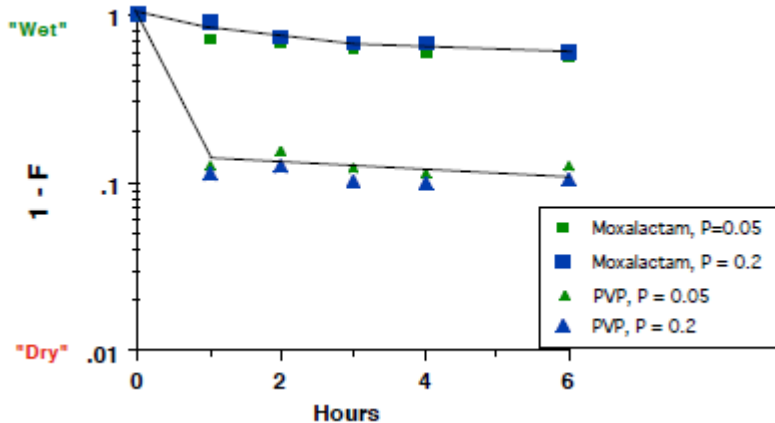


Figure 2-25: Kinetics of S.D. of Moxalactam (squares), and of Povidone (triangles) with different P_c : blue = 0,2 Torr (i.e. 267 mbar) and green = 0,05 Torr (i.e. 67 mbar). Sample preparation: 5 % aqueous solution, 1 cm fill depth, hydration to a uniform moisture of 7 % (Pikal and Nail, 2014).

2.2.3 Equipment Presentation (AzbilTelstar, 2015; Jennings, 2008c)

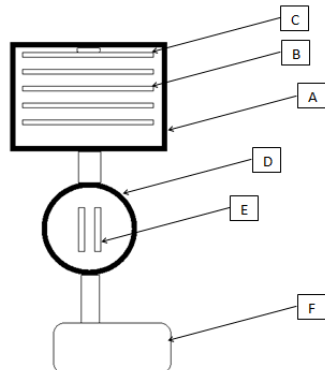


Figure 2-26: Schematic drawing of a freeze-dryer (Jennings, 2008c). A=Drying Chamber, B=Usable shelves, C=Unusable shelf, D=Condenser chamber, E=condenser surfaces, F=Vacuum pump.

2.2.3.1 Drying Chamber

The drying chamber (A on Figure 2-26), which is generally constructed from stainless steel, resists the necessary temperatures and pressures required to the production process. The chamber is closed to the external environment thanks to an acrylic glass or metal door. A gasket is also present in order to allow the vacuum to be correctly set in the chamber. The whole chamber needs to be correctly thermally sealed to prevent thermal conductivity from the environment to the chamber.

The chamber is composed of usable (B on Figure 2-26) and unusable stainless steel shelves (C on Figure 2-26). In the case of the Lyoc® technology, the product is loaded on trays on these usable shelves (see Figure 2-8). The unusable shelf, which is situated at the top of the chamber, helps to protect the products placed on the upper usable shelf from radiation of the drying chamber upper wall. All the usable shelves are bypassed by a heat-transfer fluid (usually silicon oil), which has a double action:

- It removes energy from the product during the freezing step by quickly cooling down the shelves,
- It supplies the product with energy by heating up the shelves for the primary and secondary drying.

T_s can go from -50°C to 80°C, according to the nature of the heat-transfer fluid.

2.2.3.2 Condenser Chamber

The condenser chamber (D on Figure 2-26) contains condenser surfaces (E on Figure 2-26) that capture the water vapour removed from the Lyoc® in the drying chamber. The cooling coils are cooled down to approx. -80°C through refrigerant fluid. The condenser system needs to be efficient, in order to avoid a T_{cc} increase, which could lead to sending back water molecules towards the shelves and compromise the product quality. The condenser chamber is either in the same chamber as the drying chamber, or in a separate one. In the second case, the two chambers are connected by means of a large tube to allow the migration of water molecules. The two chambers are then separated by a valve which allows them to be isolated from each other in order to perform a pressure rise test (mentioned in Section 2.2.2.4).

2.2.3.3 Vacuum Pump

The vacuum pumping system (F on Figure 2-26) regulates the vacuum level during the primary and secondary drying steps. Its role is to decrease the partial pressure of non-condensable gas in order to evacuate the water vapour out of the chamber (ChristMartin, 2015). It has to be able to lower the pressure down to 1 µbar.

2.2.3.4 Sensors

The freeze-dryer also contains different types of sensors to control the evolution of temperature, pressure and the amount of water in the sample during the experiment:

- Temperature sensors (usually PT100 sensors) measure T_p , T_s and T_{cc} ,
- Vacuum gauge measures the pressure in the chamber (Pirani and capacitive vacuum gauge, as explained in section 2.2.2.4),
- LyoRx sensor measures the electrical resistance present in the product, allowing the identification of the solidification and the defrost points.

2.2.4 Product Formulation

Formulation of freeze-dried tablets requires the use of several excipients bringing different properties and characteristics to the product. Indeed, the tablet needs to be hard enough to allow the handling by the patient without breaking, but need also to disintegrate as fast as possible and to have a satisfactory appearance. The viscosity of the suspension needs to be as low as possible in order to be pumped through the long automated dispensing system, but sedimentation has also to be avoided which means that viscosity must not be too low. The physical characteristics of the suspension needed to produce Lyocs® such as viscosity, degree of sedimentation, excipient particle size, API solubility, are thus very important. Excipients

are thus used in order to solve all those challenges, and to give to the product an acceptable visual aspect. The different types and several examples of excipients used in the LyoCs® formulations are listed in Table 2-8.

Table 2-8: Roles of excipients used in LyoCs® (Cephalon, 2009).

Class	Role	Example
Bulking agent / Filler	Component in large amount in the formulation, providing product elegance (Pikal, 2010). Support the cryoprotectant.	Mannitol, Sorbitol, Lactose, Glycine.
Hardness builder / Binding agent	Provides the sufficient hardness to the LyoCs® in order to be pushed out of the blisters without being broken.	Dextran, Hypromellose, Copovidone
Viscosity control	Prevents the suspension to sediment too quickly. Reduce the sedimentation velocity of the suspension.	Xanthan gum
Dispersing agent	Helps the dispersion and the homogenization of the powder in water. Gives a smooth taste in mouth thanks to its surfactant action. Improves the appearance of the LyoCs® surface.	Polysorbate 80, Poloxamer 188, Castor oil, Macrogol 15 hydroxystearate, Docusate sodium.
Sweetening and flavouring agents	Gives flavour and a pleasant taste in mouth.	Sucralose, Aspartame, Acesulfam K, Flavours.
pH buffer	Improves the chemical stability of an API. Plays a role on the API solubility. Optimize the extent of API ionization.	Citric acid, sodium hydroxide.
Solvent	Solvent used to produce the suspension. It will be removed during the lyophilisation process and will give to the freeze-dried tablet a porous nature.	Water.

A closer look will be made on the formulation development, and more specifically on the API, filler and binder requirements.

2.2.4.1 Formulation Development

2.2.4.1.1 API requirements

H. Seager stated in an article (Seager, 1998) that the solubility of the API had a big influence on the freeze-dried product. It was indeed assumed that a non-soluble water APIs build up a crystalline structure during the freezing process (Seager, 1998), whereas water soluble APIs build up an amorphous structure (Seager, 1998). The creation of amorphous structure is leading to difficulties in the drying process due to smaller critical temperature, and is thus more prone to collapse and softening of the structure. H. Seager set limits to the use of non-water soluble APIs at 400 mg / dose in order to keep the desired porous characteristics, and 60 mg / dose for water soluble APIs in order to keep a good cake structure (Seager, 1998). The

use of crystal forming excipients or ion-exchange resins can reduce the solubility of the water soluble API or protect it from collapse (Seager, 1998). Nevertheless, those techniques are bulky for the formulation and lead thus to the manufacture of bigger tablets. H. Seager also proposed another technique in the case of water-soluble APIs (Seager, 1998), which is producing a placebo matrix and spray the mixture API/organic solvent on it. The solvent will then evaporate and the API will be trapped in the pores of the matrix (Seager, 1998). However, this method imposes an additional step and additional costs to the process, which could be inconvenient for the manufacturing of this dosage form already long and expensive. Another characteristic is required on the non-soluble water API particle size in order to prevent sedimentation in the suspension during the process and to avoid a gritty feeling in the mouth during the uptake in mouth of the drug from the patient. For those purposes, the API particle size should not exceed 50 µm (Seager, 1998).

2.2.4.1.2 Filler

Lyoc® suspension is a saturated suspension mainly composed of filler. This dense suspension will give to the final product an elegant visual aspect. As explained in section 2.2.3.1, substances that build up a crystalline structure during the freezing step are preferred. They allow the P.D to be done at higher temperature rates, as those substances have higher critical temperatures than amorphous substances, and also give an elegant aspect to the product (Seager, 1998). Typical fillers used in freeze-dried tablets are Mannitol, Glycine, Sorbitol, Lactose or Maltose (Jennings, 2008f; Seager, 1998) (collapse temperature of Mannitol: -28 °C, Lactose: -28 °C, Sorbitol: -46 °C (Pikal, 2010)). Mannitol is an excipient widely used in the ODTs formulation because of its pleasant taste and its cooling effect in the mouth (Roquette, 2006). Mannitol also confers the specificity of collapse protective agent (Pikal, 2010; Seager, 1998), as it crystallizes during the freeze-drying process, making it the most commonly used filler in freeze-drying applications (Pikal, 2010). Glycine also crystallizes during freeze-drying (Pikal, 2010). It is nevertheless rather used for freeze-dried injectable formulations (Rowe et al., 2009).

2.2.4.1.3 Binding Agent

Binding agents are typically water soluble polymers, that are forming glassy amorphous structures necessary for the strength and the resilience of freeze-dried tablets (Seager, 1998). The entire amount of binding agent is completely dissolved in the solvent, unlike the filler. Those substances are prone to protect the API during the lyophilization and especially during the freezing step, playing the role of cryoprotectant. Povidone and dextran were indeed used as cryoprotectants of living cells (Jennings, 2008f) during the freezing step. The most commonly binders used are gelatin, dextran, povidone, alginates (Pikal, 2010; Seager, 1998). Those polymers also allow increasing the collapse temperature of the formulation due to their high T_g (dextran: -10 °C, povidone: -20 °C, gelatin: -9 °C (Pikal, 2010)). The low T_c of the filler will thus be increased, making the lyophilization cycle more efficient.

2.2.4.2 Suspension

In the Lyoc® technology viscosity plays a fundamental role. In order to develop a viscosity measurement method, each step of the production process has to be considered. The aim of this study is to allow in future a scale-up of the formulation from the laboratory scale to the production scale. In production, the suspension will indeed be pumped from the mixing container until the filling-nozzles through horizontal pipes. Nevertheless, sedimentation has to be prevented for a good quality of the Lyocs®. That is why the suspension has to have an adequate viscosity and consistency in order to flow correctly through the pipes and not to sediment. The flow in the pipes can be roughly described by the Hagen/Poiseuille equation (Mezger, 2012), where the maximum shear rate γ_w is located at the smallest diameter of the whole process, i.e. at the filling nozzle.

$$\gamma_w = \frac{4V}{\pi r^3} \text{ where } r = \text{filling nozzle -radius [m]} \text{ und } V = \text{volume flow rate [m}^3/\text{s}]$$

After taking the parameters and characteristics of the installation used in production into consideration, the shear rate should be as follows $0 \text{ s}^{-1} < \gamma_w < 170 \text{ s}^{-1}$ because of the production parameters summarized in Table 2-9.

Table 2-9: Production scale parameters of the dispensing step.

Production parameters	Value
r [mm]	2,5 mm
Filling time [s]	[0,5 ; 0,65]
V [mL]	[1 ; 1,25]

The mixing step also has to be taken into consideration which is defined to be up to 500 s^{-1} according to the literature (Triantafillopoulos, 1988). The warming up of the suspension in the production scale is not feasible with the equipment present on the site (too long dispensing pipes). That is why the influence of the temperature on the viscosity is not studied.

As previously explained, the viscosity of the suspension needs to be as low as possible to allow the suspension to be pumped, avoiding at the same time sedimentation to occur. Sedimentation and viscosity of a system is however strongly depending on the particle size of the material and the concentration of the suspension. Sedimentation is firstly studied with the help of the Stokes law (Pavlik, 2011). Considering an arbitrary spherical particle in the suspension, this later is subject to three main forces, namely the weight force F_w due to gravity (Pavlik, 2011), the buoyancy force F_b of the immersed particle (Pavlik, 2011) and the drag force F_d corresponding to the resistance of the viscous fluid on the particle (Pavlik, 2011) (see Figure 2-27), with:

$$F_w = \frac{4}{3} \pi r^3 \rho_p g$$

$$F_b = -\frac{4}{3} \pi r^3 \rho_f g$$

$$F_d = -6 \pi \eta r v$$

where ρ_p represents the mass density of the particles, ρ_f represents the mass density of the fluid, g represents the gravitational acceleration, r represents the radius of the particle, η represents the viscosity of the medium and v represents the velocity of the spherical particle (Pavlik, 2011).

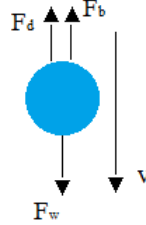


Figure 2-27: Representation of the forces (F_b , F_d , F_w) acting on a spherical particle moving in a fluid at a velocity v (Pavlik, 2011).

At equilibrium, $F_w + F_d + F_b = 0$, which lead to the expression of the velocity of the sphere

$$v = \frac{2(\rho_p - \rho_f)}{9\eta} gr^2$$

showing that the velocity of a spherical particle falling in a fluid, i.e. the settling velocity, increases with the square of the radius of the particle.

Regarding the viscosity, it depends not only on the loading concentration, but also on the particle size of the suspended material (Remmler, 2015). Indeed, the Einstein equation developed for low concentrated suspensions (Remmler, 2015) states that

$$\eta = \eta_0(1 + 2,5 \phi)$$

where η is the viscosity of the suspension, η_0 is the viscosity of the medium, ϕ is the volume fraction of solid in the suspension. According to the Einstein equation, it can be seen that the viscosity is increasing with the concentration of particles in the medium. This relation is valid for $0 \% < \phi < 10 \%$ (Remmler, 2015), as Einstein did not take into consideration the interaction between the particles (Remmler, 2015). That is why Krieger-Dougherty developed a model describing the interaction between particle and fluid according to the concentration of particles suspended (Remmler, 2015). In the case of LyoCs® formulation, the system is loaded up to 65 % of particles, inviting us to take into consideration the following Krieger-Dougherty equation (Remmler, 2015).

$$\eta = \eta_0 \left(1 - \frac{\phi}{\phi_m}\right)^{-[\eta]\phi_m}$$

where ϕ_m represents the maximum volume fraction of solids in suspension and $[\eta]$ represents the intrinsic viscosity (=2,5 for spheres (Remmler, 2015)). This equation reflects the fact that the viscosity is highly dependent on the concentration of particles in the medium as shown on Figure 2-28. At the lower volume fraction of particles (red curve), the system is nearly Newtonian (η is independent on the shear stress and shear rate). By increasing the volume fraction of particles in the medium (blue and green curves), the system becomes shear-thinning

(η decreases as shear rate increases). The increase of particles in the suspension leads to a higher interaction between the particles, leading to an increase in viscosity (Remmler, 2015).

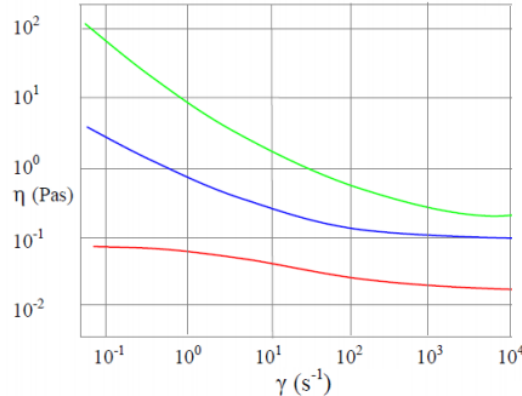


Figure 2-28: Impact of solid loading on viscosity. Red=45 % of particles, Blue=55 % of particles, Green=61 % of particles (Remmler, 2015).

The Krieger-Dougherty equation can also explain the influence of the particle size distribution on the viscosity. The input of different particle size distribution is shown in Figure 2-29. A monodisperse distribution will have a lower ϕ_m than a polydisperse distribution, because of the particle packing (Remmler, 2015). Indeed, a monodisperse distribution will only have one particle size, or rather a uniform particle size, which will give a bigger empty space between the particles in that case. Contrariwise, a polydisperse distribution will contain not only big particles, but also smaller which are able to fill out the empty space between the bigger particles, increasing the ability to load more particles in the medium (Remmler, 2015). Those small particles will play the role of internal lubricant (Remmler, 2015), causing a decrease in the viscosity, as shown in Figure 2-29.

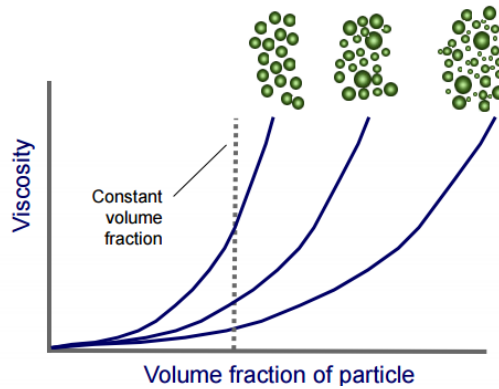


Figure 2-29: Influence of the particle distribution on the viscosity (Remmler, 2015).

The influence of the particle size is also playing an important role on the viscosity (Pahl et al., 1991). Indeed, for a given ϕ , a smaller particle size will increase the number of particles in the medium (Pahl et al., 1991), increasing the interaction between the particles and thus increasing the viscosity (Pahl et al., 1991).

3 Materials and Methods

3.1 Materials

3.1.1 Fillers Used

Table 3-1: Fillers used.

Trade Name	Chemical Name, Ph. Eur.	Producer
Lactose Monohydrate	O- β -D-Galactopyranosyl-(1 \rightarrow 4)- α -D-glucopyranose monohydrate	Alpavit
Maltose Monohydrate	4-O- α -D-Glucopyranosyl- β -D-glucopyranose monohydrate	Merck
Neosorb 70/02 liquid sorbitol	D-Glucitol	ROQUETTE
Neosorb P100T sorbitol		
Parteck SI 150		Merck
Pearlitol® 25 C mannitol	D-Mannitol	ROQUETTE
Pearlitol® 50 C mannitol		
Pearlitol® 110 C mannitol		
Pearlitol® 160 C mannitol		
Pearlitol® 400 DC mannitol		
Pearlitol® 100 SD mannitol		
SweetPearl P90 maltitol	4-O- α -D-Glucopyranosyl-D-glucitol	Merck
Xylisorb 90 xylitol	xylo-Pentane-1,2,3,4,5-pentol	ROQUETTE

3.1.2 Hardness Builders

Table 3-2: Hardness Builders used.

Trade Name	Chemical Name, Ph. Eur.	Producer
Copovidone Kollidon VA 64	Poly(1-vinylpyrrolidone-co-vinyl acetate)	BASF
Dextran 70	Dextran	Pharmacosmos A/S
EMDEX	Dextrates	JRS PHARMA GMBH & CO.KG
Hypromellose 2910, 6 mPa.s	Methyl Hydroxypropyl Cellulose	Samsung Fine Chemicals Co., Ltd.
Lycatab DSH	Maltodextrin	Roquette
Polyvinyl Alcohol	Ethenol, homopolymer	Japan VAM & Poval Co., LTD
Povidone K25	1-Ethenyl-2-pyrrolidinone homopolymer	Ashland Industries Deutschland GmbH

3.1.3 APIs

Table 3-3: APIs used.

Substance	Producer
Metamizol Sodium	Sanofi-Aventis
Metoclopramide Hydrochlorid Monohydrate	AMSA SpA IT-COMO
Sildenafil Citrate	ASSIA CHEMICAL INDUSTRIES LTD
Paracetamol	Aptalis Pharma S.r.l.
Phloroglucinol Anhydrous	DSM Pharma Chemicals

3.1.4 Other Excipients

Table 3-4: Other excipients used

Substance	Role
Purified Water	Solvent

3.2 Equipments and Software

Table 3-5: Equipments and Software used.

Process step	Devices used	Producer
Weighting step	PG5002-S DeltaRange®	Mettler Toledo
Suspension production	Beaker (400 mL)	Duran Group
	Stirrer RW20	IKA
	Dispersion impeller	-
	DSC822e Software: STARe SW 12.00	Mettler Toledo
In Process Control (IPC) on the suspension	Rheometer MCR 301 Plan-Plan Geometry Software: Rheoplus/32 V3.40	Anton Paar
	Graduated cylinder (25 mL)	Duran Group
	IN-PACK Blister machine	Omar
	PVC Foil (250 µm)	-
Blister molding	Aluminum Foil (20 µm)	-
	Multipette M4	Eppendorf
	Freeze-dryer Epsilon 2-6D Software: Martin Christ LPC-32	Christ
IPC on the Lyocs®	MultiCheck	ERWEKA
	ZT72	ERWEKA
	Drying oven Heratherm Oven OMH60	Thermo Scientific

	D8 Advance powder X-ray diffractometer Software: Bruker AXS	Bruker AXS
	SEM Zeiss DSM 940 A Software: Orion Vers. 5.25	Carl Zeiss
	Sputter coater BioRad E 5100	BioRad
	Raman microscope alpha 500	WITec GmbH
	AccuPyc 1330	Micromeritics Instrument Corporation
	DSC822e Software: STArE SW 12.00	Mettler Toledo
	TGA/DSC1 Software: STArE WF DB1	Mettler Toledo
API release	Fully Automated AT70 Smart (UV-Vis spectrophotometer) Software: WinSotax Dissolution System 6.2.3	SOTAX
	Basketstation BS60	SOTAX
	Glass fibre filter GF 1 µm	Gelman
	PE-Lambda 35	Perkin Elmer
	Fraction collector C613/15	SOTAX
	pH-meter	Metrohm
	0,1 cm quartz cell	HELLMA®
Content of uniformity	Photometer Agilent HP 8453 Software: UV-Visible ChemStation	Agilent
	Peristaltic pump	-
	0,01 cm quartz cell	HELLMA®
Statistical study	DoE Software	JMP 11

3.2.1 Manufacturing Process Flow Chart

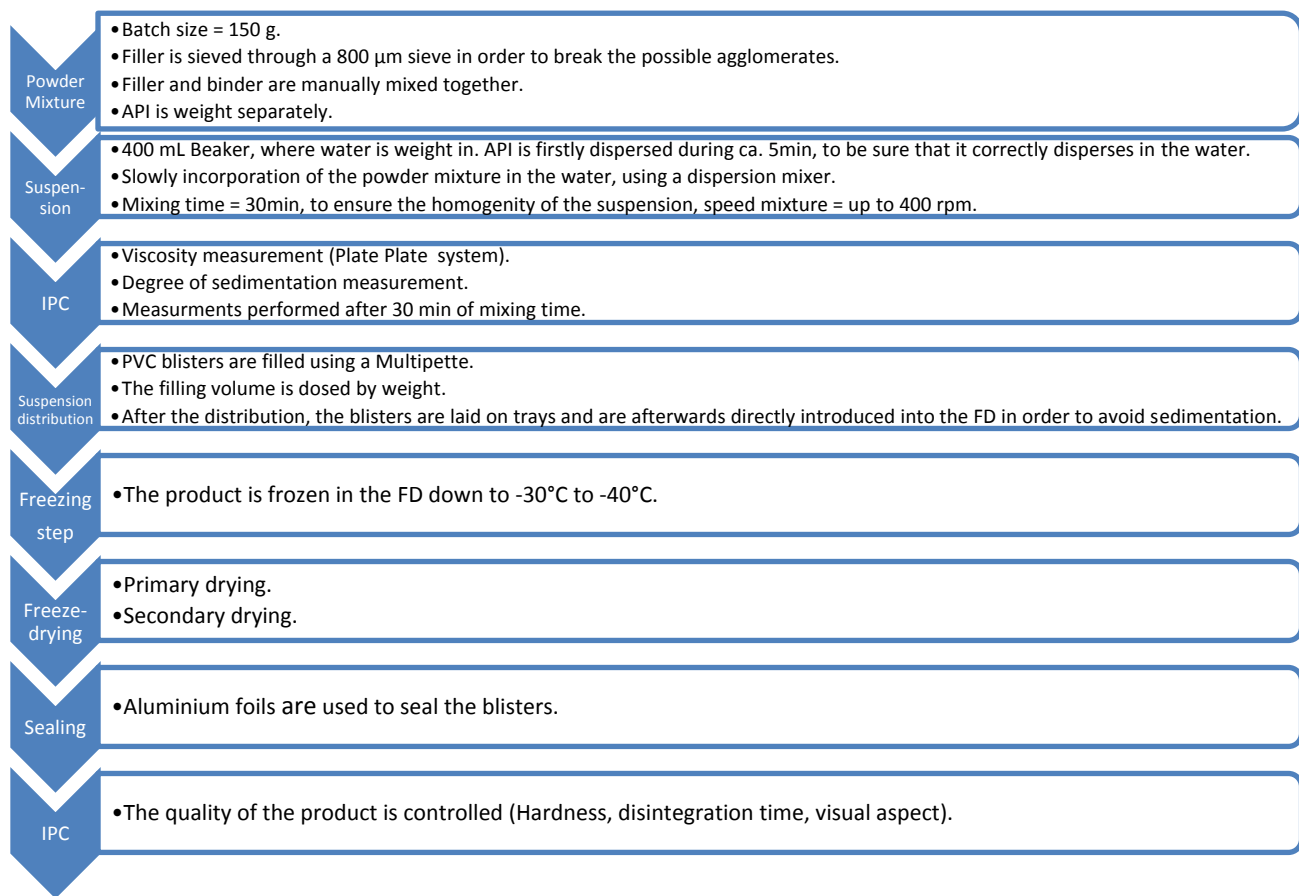


Figure 3-1: Schematic representation of the manufacturing process flow chart.

3.2.2 Manufacture of the Suspension

Figure 3-1 summarizes the entire manufacturing process, from powder mixture to IPC of the Lyocs®. In order to obtain good Lyocs® quality, suspensions containing 50% to 60% of solids (w/w) are freeze-dried. For the development step, 120 Lyocs® of 1 mL are produced per batch. Therefore the batch size of dried substances is set at 150 g. Initially, water is weighed in a 400 mL beaker. If an API is present in the formulation, it is dispersed in water until visual homogeneity is noticed. Filler and binder are then mixed together before being added to the water. A dispersion impeller is used in order to disperse homogeneously the suspended solids in water. The suspension is mixed at 400 rpm for 30 minutes in order to have a homogeneous mixture. PVC blisters (15 mm diameter and 8 mm depth) are molded by using a blistering machine. The suspension is pipetted by means of a Multipette and blisters are filled with 1 mL of suspension.

3.2.3 IPC on the Suspension

3.2.3.1 Determination of the Critical Temperature

3.2.3.1.1 Differential Scanning Calorimetry (DSC)

The critical temperature of the suspension was firstly measured using a DSC DSC822e from Mettler Toledo. This step is primordial in order to optimize the lyophilization process. 10 mg of the suspension are filled into an aluminum crucible and the crucible is then sealed with a perforated aluminum seal. The crucible is then cooled down to -60 °C with a cooling rate of -5 K/min. The sample is held at -60 °C during 10 minutes and is then warmed up to 20 °C with a heating rate of 1 K/min in order to obtain sharp peaks and thus to obtain accurate results. Only the warming-up curve is analyzed.

3.2.3.1.2 Freeze-Dryer For Freezing-Heating Cycle

1 mL of the suspension is filled into a blister cavity and placed in the freeze-dryer using the same freezing conditions as those during the Lyocs® production. The samples are then exposed to the conditions mentioned in Table 3-6:

Table 3-6: Method developed to measure the critical temperature of the suspensions formulated using a FD.

Step	Temperature	Pressure
Pre-cooling of shelves	-40°C	1000 mbar
Freezing of the suspension	-40°C	1000 mbar
FD chamber put under pressure	-40°C	0,1 mbar
Warming up	From -40°C to 20°C with a heating rate of 2 K/min	0,1 mbar

The critical temperature is determined at the temperature at which the Lyocs® present air bubbles on their surface.

3.2.3.2 Viscosity Measurement

Based on Section 2.2.4.2, the suspension viscosity measurement is carried out in the rotational mode for $2 \text{ s}^{-1} < \gamma < 500 \text{ s}^{-1}$. As the suspension contains large particles, a parallel plate measuring system is used. Otherwise, with a cone plate system, the particles could agglomerate at the tip of the cone (AntonPaar). A wet cloth is also set all around the measurement geometry to prevent the suspension from drying out on the edge during the measurement. The measurement method is summarized in Table 3-7:

Table 3-7: Viscosity measurement method.

Measurement time	30 sec	1 min	30 points every 20 sec
Temperature of the bottom plate	20°C	20°C	20°C
Rotation, γ	$\gamma = 5 \text{ s}^{-1}$	$\gamma = 0 \text{ s}^{-1}$	$\gamma = 2-500 \text{ s}^{-1}$
Explanation	These 2 steps are to unify the sample and to remove its history (due to stress caused on the sample during mixing and pipetting).		

The viscosity of the suspension is evaluated at γ_w , i.e. at the filling nozzle where the maximum shear rate is located.

3.2.3.3 Degree of Sedimentation

Sedimentation occurs in a liquid dosage form when the particles are settling under gravitational force. This phenomenon should be avoided during the production of Lyocs®. If it happens, it could indeed impact the quality of the product and on the API repartition within the Lyocs®.

The degree of sedimentation is measured using a 25 mL graduated cylinder:

$$F = \frac{V_{\text{at } t=60 \text{ min}}}{V_{\text{at } t=0 \text{ min}}} \text{ (Swarbrick et al., 2014).}$$

where $V_{\text{at } t=60 \text{ min}}$ represents the equilibrium volume of the sediment after 60 min of standing time in mL and $V_{\text{at } t=0 \text{ min}}$ represents the total volume of the suspension in mL.

The larger F, the better the suspendability.

The sedimentation of the suspension in the FD will then be visually observed and associated to the F value and to the viscosity value.

3.2.4 Lyocs® Manufacture

The Lyocs® are produced the same way as in the production site. On each shelf three racks are superposed on each other. On each rack, two blister foils (20 Lyocs® per blister foil) are placed. The production efficiency is then 120 Lyocs® per shelf. Figure 3-2 represents the FD used during the whole experiments of this dissertation.



Figure 3-2: Filled FD Epsilon 2-6D (3 shelves with 3 racks per shelf)

1 mL of suspension is pipetted in each blister cavity, which corresponds to a product height of ca. 5 mm. The lyophilization process is summarized in Table 3-8:

Table 3-8: Lyophilization manufacturing process of LyoCS®.

Step	Time [hh:mm]	T [°C]	Vacuum [mbar]	T ramp [°C/min]
Loading	00:00	-40	1000	-
Freezing	02:15	-40	1000	-
Primary Drying	00:35	-40	0,2	-
	01:35	45	0,2	0,90
	06:00	45	0,2	-
Secondary Drying	04:00	45	0,2	-
	00:30	25	0,2	0,67
	00:30	25	0,2	-
Total duration	15:25			

During the process, four temperature sensors (PT 100) control the product temperature. The LyoRx sensor monitors the electrical resistance of the product during the whole process. This sensor cannot only determine the freezing point but it can also emit a warning in case of collapse during the primary drying step. In Figure 3-3, an example of a lyophilization cycle is represented, showing both set parameters (such as shelf temperature, set vacuum), and the experiment values obtained during lyophilization (such as product temperature, vacuum in the chamber).

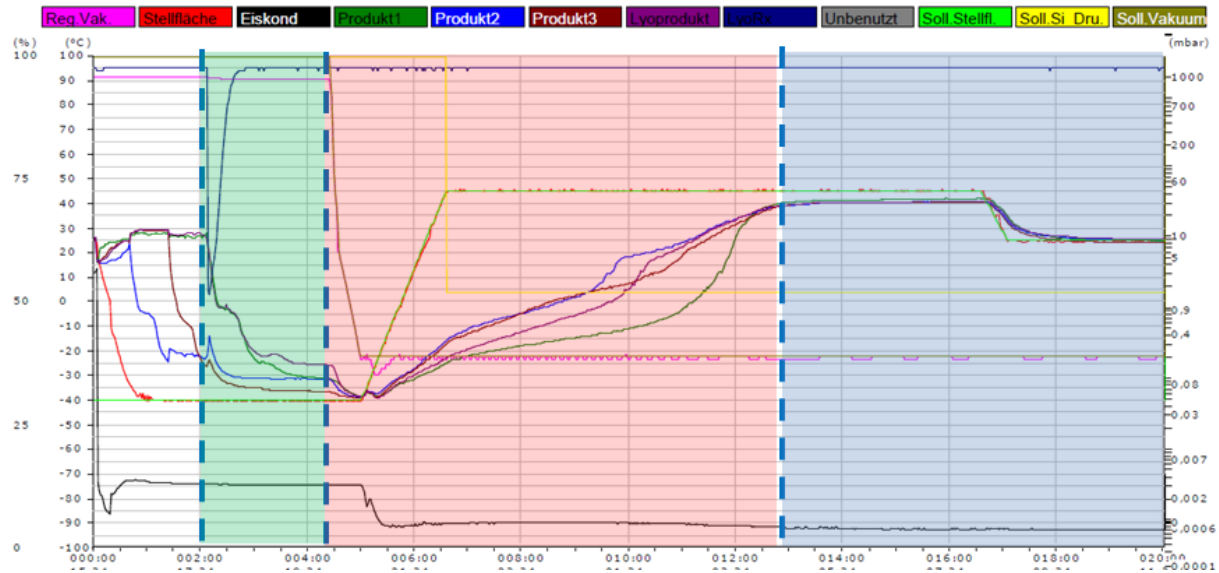


Figure 3-3: Freeze-drying process: Temperature and Pressure evolution as function of time, white=loading step, green=freezing step, red=P.D, blue=S.D. Curves legend is summarized on the top of the graph.

3.2.5 In Process Control on Lyocs®

3.2.5.1 Visual Aspect

The Lyocs® are firstly visually examined at the end of lyophilization cycle. The Lyocs® quality is also observed after unpacking (powdery, presence of cracks or bumps on the surface of the Lyocs®), in order to check if the freeze-dried tablets are resilient enough to de-blistering activities and if the Lyocs® keep a good consistency.

3.2.5.2 Weight, Dimension and Resistance to Crushing (Hardness)

20 Lyocs® ($n=20$) are randomly collected from the whole batch and checked using a MultiCheck apparatus from ERWEKA. The average of the Lyocs® weight, hardness, diameter and height are measured according to the paragraph 2.9.8 of the Ph. Eur. (EDQM, 2014d).

3.2.5.3 Disintegration Time

As the Lyocs® are supposed to disintegrate within 30 seconds in the mouth, the disintegration time is a crucial parameter. In this thesis, the disintegration time is determined according to the paragraph 2.9.1 of the Ph. Eur. (EDQM, 2014a), using an automated disintegration apparatus ZT72 from ERWEKA. The disintegration time (D.T) of 6 Lyocs® ($n=6$) is measured in 700 mL of purified water warmed up at 37°C.

3.2.5.4 Moisture Content

The moisture content contained in Lyocs® is measured using a loss on drying (LoD) method according to the chapter 2.2.32 of the Ph. Eur. (EDQM, 2014b). 10 Lyocs® are carefully milled and 1 g of sample is collected in a glass bottle previously dried. The bottle is placed in an oven at 105°C for 4 hours and cooled down afterwards in a desiccator during 2 hours. The

bottle is then weighed again in order to determine the LoD. Each measurement is made in duplicate ($n=2$).

3.2.5.5 Scanning Electron Microscopy (SEM)

The determination of the morphology of the Lyocs® is made through SEM. The Lyocs® are broken into two pieces (1st step on Figure 3-4), and one piece is glued on the aluminum sample carrier with a conductive paste. The sample is then coated with a thin gold layer under pressure (ca. 0,04 mbar) by means of a sputter coater Biorad E 5100. This sputter coating process is made 4 times during 60 s, with a current of 20 mA and an acceleration voltage of 2,1 kV. The sample is then analyzed with a Zeiss DSM 940 A SEM, applying an acceleration voltage of 5000 V. A general view of the whole Lyoc®, a zoomed view of the upper surface of the Lyoc® and a zoomed view of the middle of the Lyoc® are photographed, as shown on Figure 3-4.

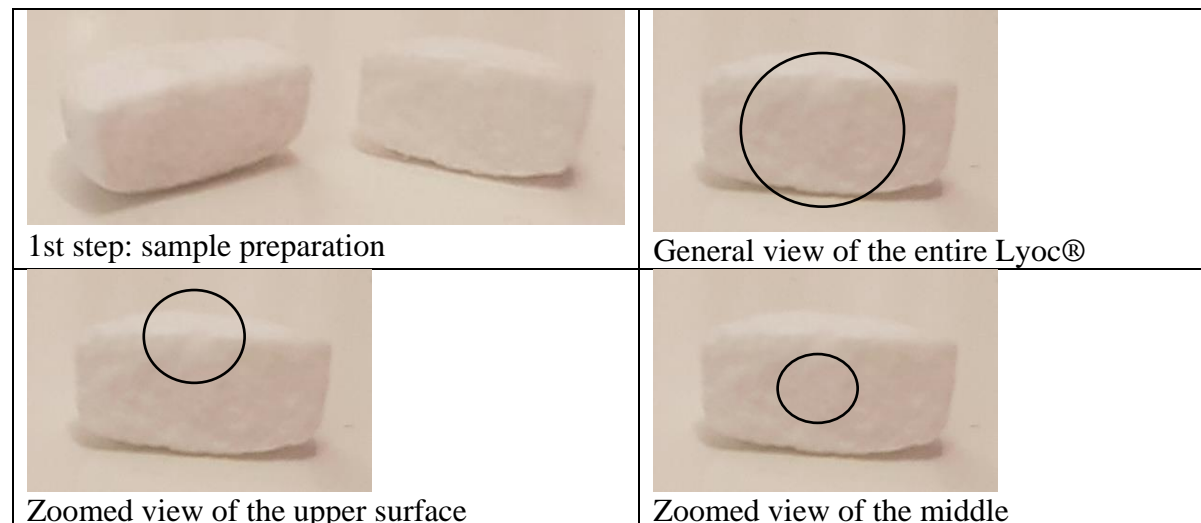


Figure 3-4: Sample preparation and picture sampling point.

3.2.5.6 Solid State Determination

To determine the solid state of the different materials present in the formulation before and after lyophilization, three different techniques were used (namely DSC, Thermogravimetric analysis TGA and X-ray diffraction).

3.2.5.6.1 DSC

5 mg of the powder is filled into an aluminum crucible and the crucible is then sealed with a perforated aluminum seal. The crucible is then warmed up to from room temperature to 300 °C with a heating rate of 10 K/min, using a DSC822e from Mettler Toledo.

3.2.5.6.2 TGA

5 mg of the powder is filled into an aluminum crucible. The crucible is then warmed up to from room temperature to 300 °C with a heating rate of 10 K/min, using a TGA/DSC1 from Mettler Toledo.

3.2.5.6.3 X-Ray Diffraction

The X-ray diffraction of the different raw materials, placebo Lyocs® and drug loaded Lyocs® are conducted with a D8 Advance powder X-ray diffractometer from Bruker AXS. The conditions of the measurement are summarized in Table 3-9:

Table 3-9: Conditions of the X-ray powder diffractometry (XRPD) measurements.

Diffractometer geometry	Reflection mode (Bragg-Brentano geometry)
Radiation	Cu K α 1/ α 2
Source	34 kV / 40 mA
Detector	Vantec-1 (electronic window: 3°)
K β filter	Ni (diffracted beam)
Measuring circle diameter	435 mm
Detector window slit	12 mm
Anti-scatter slit (diffracted beam)	8 mm
Divergence slit	v6.00 (variable)
Soller slit (incident /diffracted beam)	2.5°
2 θ range	2° \leq 2 θ \leq 55°
Step size	0.016
Step time	0.2 s

3.2.5.7 Raman Microscopy

Raman microscopy is used in order to evaluate the API spatial distribution within the Lyocs® and to determine if the lyophilized API exists in a crystalline state, an amorphous state or in a solid solution with a molecularly dispersed API as represented in Figure 3-5. Indeed, during lyophilization, the API could solidify in interaction with one of the excipients by H-bounding for instance (Gryczke, 2012), leading to a solid solution state.

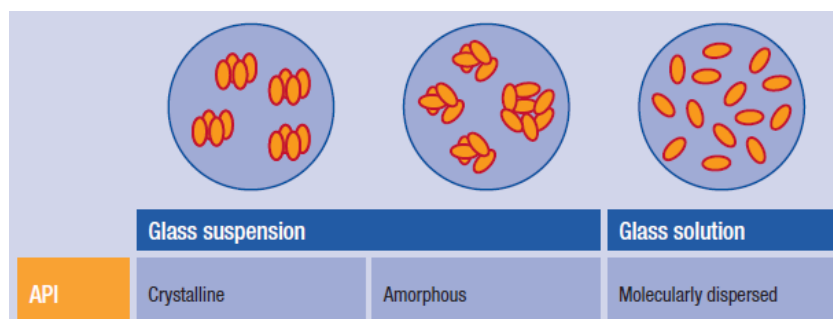


Figure 3-5: Schematic representation of an API in crystalline, amorphous or molecularly dispersed state (Gryczke, 2012)

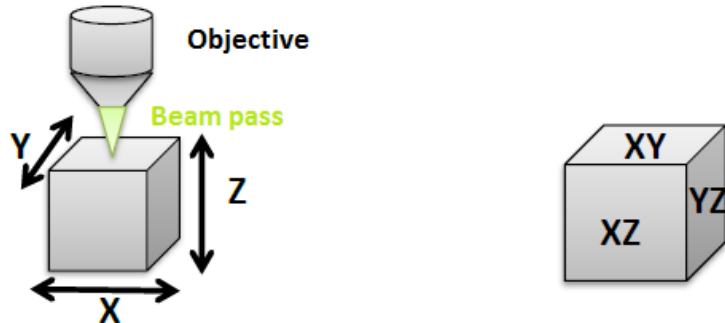


Figure 3-6: Illustration of the spatial mapping (Lunter, 2016).

The XY and XZ orientations (see Figure 3-6) are scanned with the Raman microscope alpha 500, WITec GmbH, using a laser of 532 nm with a power of 20 mW and a radiation time of 0,08 sec.

On the XY plane, two scans are taken with different objective sizes:

- a 500x500 μm area is scanned with a 10x0,25 Numerical Aperture NA objective (Resolution ca. 1,3 μm)
- a 100x100 μm area is scanned with a 40x0,6 NA objective (Resolution ca. 0,8 μm).

On the XZ plane, a 50x25 μm area is scanned with a 40x0,6 NA objective (Resolution ca. 0,8 μm).

Raman Imaging is then conducted by adding a filter to the measured scans. Indeed, a spatial mapping is achievable by adjusting the following equation to each spectrum of the scanned section

$$\vec{S} = \sum_{k=1}^N a_k \vec{B}_k$$

where \vec{B}_k represents the Raman spectrum of the substance k, N represents the number of compounds present in the sample, a_k represents the adjustment factor of the substance proportional to the percentage of substance present in the sample and \vec{S} is the superposition of each spectrum.

Intensity images are calculated for each compound by means of the a_k factor, giving a specific color to each substance.

3.2.5.8 Porosity

The density ρ of Lyocs® is measured by means of a gas pycnometer (AccuPyc 1330, Micromeritics), in order to determine the free volume within the Lyocs® and thus evaluate the porosity of the manufactured products. The porosity of ODTs is indeed an important parameter, allowing the estimation of water penetration into the sample (Ölmez and Vural, 2009).

The sample is firstly purged with helium 10 times with a purge pressure of 134 kPa in order to remove the last molecule of water that could be present in the sample. The sample density is then measured 5 times with a helium equilibration rate of 34 Pa/min. This method is applied

on 5 Lyocs®. After that, the porosity is calculated with the following equations (Ölmez and Vural, 2009):

$$\text{Experimental Porosity [%]} = \left[1 - \left(\frac{m}{\rho \cdot V} \right) \right] \cdot 100$$

The experimental values are compared to the calculated ones, resulting from the following equation established in the U.S. patent 20100080829 A1 (Dulieu et al., 2010):

$$\text{Predicted Porosity [%]} = \frac{\text{Volume of water per Lyoc®}}{\text{Volume pipetted}} \cdot 100$$

3.2.5.9 API Release – Paracetamol Lyocs®

The equipment used to measure the in-vitro API release is constituted of a UV-vis spectrophotometer (SOTAX Fully Automated AT70 Smart) composed of a paddle stirrer apparatus (SOTAX Basketstation BS60), in an initial volume of 900 mL of phosphate buffer (pH 5,8) at a temperature of $37 \pm 0,5$ °C with a stirring speed of 50 rpm. The sampling is automatically performed at 5, 10, 15, 20, 30, 45 and 60 min after providing the Lyoc® to the system. The sample is filtered on a 1 µm glass filter (GF) before reaching the 0,1 cm quartz cell. The API concentration is then determined at a wavelength of 243 nm (see Annex 6.3). The measurement is performed on 6 Lyocs®.

3.2.5.10 Uniformity of Dosage Form – Paracetamol Lyocs®

3.2.5.10.1 Uniformity of Dosage Form on Entire Lyoc®

The uniformity of dosage form of each batch is measured, in order to check the homogeneity of API within the tablets. This test is performed based on the Ph. Eur., paragraph 2.9.40 (EDQM, 2014f). 10 tablets are randomly picked up in the whole batch and each tablet is separately dissolved in 100 mL of solvent. The content of uniformity is measured by means of UV-VIS spectroscopy with a wavelength λ range between 200 and 500 nm (λ_{\max} of paracetamol = 249 nm according to the Ph. Eur. (EDQM, 2014c)) with a 0,1 mm quartz cuvette. The solvent used to dissolve the tablets is [1 mL 85% H₃PO₄ in 1 L H₂O : MeOH (9:1)].

3.2.5.10.2 Uniformity of Dosage Form on Half Lyoc®

API sedimentation within Lyocs® is studied by cutting the Lyoc® in the half horizontal plane and by measuring the API content in each half of Lyoc®. Each half Lyoc® is weighed and dissolved in 50 mL of solvent in order to keep the same measurement parameters as in the chapter 3.2.5.10.1. An absorption measurement is then performed on each sample. The API content per half Lyoc® is calculated by means of the following equation:

$$API \text{ content } [mg/g] = \frac{A_{Tst} C_{Ref} V_{Tst} \bar{m}}{A_{Ref} m_{Tst}}$$

- A_{Tst} = Absorption of the test solution
 C_{Ref} = Concentration [mg/mL] of the reference substance in the reference solution
 V_{Tst} = Volume [mL] of the test solution
 \bar{m} = Average mass [g]
 A_{Ref} = Absorption of the reference
 m_{Tst} = Initial weight [mg] of the test substance

As represented on Figure 3-7:

- the top of the Lyoc® represents the part of the Lyoc® in contact with the Aluminum foil,
- the bottom of the Lyoc® represents the part of the Lyoc® in contact with the bottom of the PVC foil.



Figure 3-7: Representation "Top / Bottom" of the Lyoc®.

3.2.5.11 Statistical Analysis

The statistical software JMP® is used in the frame of the formulation development, in order to work on formulation optimization of Lyocs®.

The “Custom Design Tool” was chosen in the JMP Software, since this tool takes into consideration the different responses, factors and constraints of the system and builds up the associated “Design of Experiment” adapted to the given issue. The factors were defined to be the compounds concentrations (i.e. water, binder, filler) whereas the responses were defined to be the resulting quality attributes (i.e. viscosity, degree of sedimentation, hardness and disintegration time).

The “Factors and Responses” limits were defined and entered in the JMP Software before creating computer-assisted the experimental design of 12 runs with one center point and a 2nd term interactions. Those 12 formulations allow evaluating all responses by varying each factor in the determined range. Each formulation was prepared at a batch size of 120 Lyocs®.

After inserting the experimental response data, each response was analyzed individually in order to determine how well the statistical model fits the response data. To achieve this, the statistical adjustment of each response to the model was checked with the tool “Fit Model”. This tool analyses the possible interactions and the quadratic effects between the factors, and therefore rebuild a better adjusted model if necessary. The model was considered as fitted when the R^2 and $R^2\text{Adj}$ values of the “Actual by predicted Plot” were > 0.990 . A fitted least

squares model was then used to determine the effect of each factor on each response. In a second step, an analysis on the “Sorted Parameter Estimated” table was carried out in order to determine the statistical significant factors and interactions present for each response. Factors with t-values $< 0,05$ were considered as significant, meaning that those factors have an influence on the studied response.

Finally, the determination of the optimized formulation was performed by means of the optimizer tool “Prediction Profiler” available in the JMP Software, by maximizing the desirability function of each response. Once the optimized formulation was estimated, it was experimentally tested in order to measure the responses obtained and to check if the predicted values fitted with the experimental responses.

Statistical difference was evaluated by means of the t-value calculated with the equation (ResearchMethodsKnowledgeBase, 2006):

$$t = \frac{|\bar{x}_1 - \bar{x}_2|}{\sqrt{\frac{s_1^2}{n} + \frac{s_2^2}{n}}}$$

Statistical analysis on the API dissolution profile was performed by means of the evaluation of both difference factor (f_1) and similarity factor (f_2), given by (CDER, 1997; EMEA, 2010):

$$f_1 = \frac{\sum[R(t) - T(t)]}{\sum[R(t)]}$$

$$f_2 = 50 \times \log \left[\frac{100}{\sqrt{1 + \frac{\sum[R(t) - T(t)]^2}{n}}} \right]$$

With n = number of sampling points, R(t) = mean percentage of dissolved API for reference product at time t and T(t) = mean percentage of dissolved API for tested product at time t.

Two dissolution profiles are deemed to be similar or equivalent when $f_1 < 15$ and $f_2 > 50$ (CDER, 1997; EMEA, 2010).

4 Results and Discussion

4.1 Excipient Screening

An excipient screening was carried out, in order to determine which excipients could be used in the Lyoc® technology. In the currently marketed formulations, only two types of matrix builder are used, namely mannitol and lactose, and only dextran is used as hardness builder. This gives the formulator too few choices for the formulation development of a drug. This study was conducted on placebos.

4.1.1 Study on Diluents

Diluent is the main compound present in the Lyocs®. Not only does it give the tablet a homogenous structure, but it also protects and should not interact with the API. As the Lyocs® are disintegrating in the mouth, their organoleptic properties should be pleasant to ensure the patient compliance. Therefore only sweet soluble diluents were taken into consideration. Those six substances listed in Table 4-1 were deeper examined in more details.

Table 4-1: List of investigated diluents and their relative sweetness (Roquette, 2012; Rowe et al., 2009).

Diluent	Sweetness relative to sucrose
Lactose monohydrate (present in marketed products)	0,2
Maltitol	0,9
Maltose monohydrate	0,3
Mannitol (present in marketed products)	0,4
Sorbitol	0,6
Xylitol	ca. 1

4.1.1.1 Substance Description

Lactose monohydrate (Rowe et al., 2009):

Lactose is a disaccharide composed of galactose and glucose units (Figure 4-1). Lactose is a white crystalline powder. A Maillard-reaction can occur between lactose and substances having a primary or secondary amine group, leading to a brown coloration of the finish product. This could impede the visual aspect of the product, leading to possible complaints from the client. Its melting range lies between 201 and 202°C.

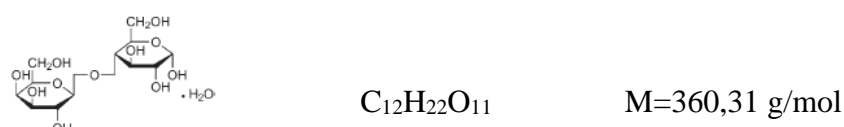


Figure 4-1: Structural formula of lactose monohydrate.

Maltitol (Rowe et al., 2009):

Maltitol is a disaccharide composed of one glucose unit linked with a sorbitol unit (Figure 4-2). Maltitol is a white crystalline powder, having a sweet taste. It is also a non-hygroscopic substance (maximum 1,0 % water), which is an advantage for the Lyoc® technology. Its melting range lies between 148 and 151°C.

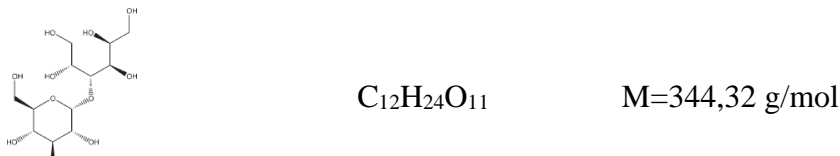


Figure 4-2: Structural formula of maltitol.

Maltose monohydrate (Rowe et al., 2009):

Maltose is a disaccharide of two glucose units (Figure 4-3). Maltose is a white crystalline powder, having a sweet taste. A Maillard-reaction can occur between maltose and substances having a primary amine group, leading to a brown coloration of the product. This could impede the visual aspect of the product, leading to possible complaints from the client. Its melting range lies between 120 and 125°C.

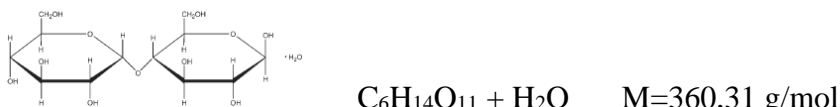


Figure 4-3: Structural formula of maltose monohydrate.

Mannitol (Rowe et al., 2009):

Mannitol is an acyclic sugar alcohol, containing six alcohol groups (Figure 4-4). Mannitol is a white crystalline powder, having a sweet taste and a cooling effect in the mouth. Mannitol is also a non-hygroscopic substance (maximum 0,5 % water), which is an advantage for the Lyoc® technology. Mannitol possesses three polymorphic modifications, namely α , β and δ . The melting range of mannitol lies between 166 and 168°C.

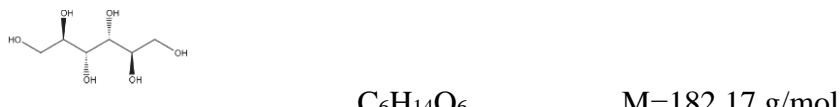


Figure 4-4: Structural formula of mannitol.

Sorbitol (Rowe et al., 2009):

Sorbitol is an isomer of mannitol (Figure 4-5). Sorbitol is a white hygroscopic crystalline powder, having a sweet taste. Sorbitol possesses four crystalline polymorphs and one amorphous form, which leads to different melting points between 93 and 112°C.



Figure 4-5: Structural formula of sorbitol.

Xylitol (Rowe et al., 2009):

Xylitol is an acyclic sugar alcohol, containing five alcohol groups (Figure 4-6). Xylitol is a white crystalline hygroscopic powder, having a sweet taste and a cooling effect in the mouth. Its melting range lies between 92 and 96°C.

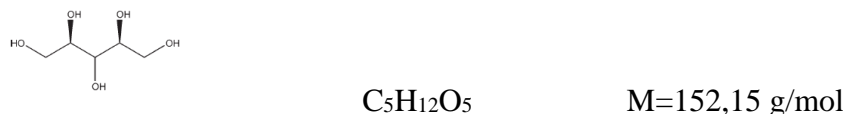


Figure 4-6: Structural formula of xylitol.

4.1.1.2 Suspension Characterization

Lyocs® are produced from a viscous suspension. Indeed, the suspension is saturated in diluent. The diluent is thus not completely dissolved in water, which gives the final product a consistent structure. As explained in the section 2.2.5, the diluent should be a crystallizing excipient due to its higher critical temperature (T_c) in comparison to an amorphous compound ($T_e > T_{g'}$). The use of a crystalline filler will have a huge impact on the process time (since a higher T_c allows faster increase of T and/or higher T_s settings during the sublimation phase) and will also protect the API during the lyophilization cycle. The solid state and the critical temperature of the Diluent/Water suspensions were firstly determined through DSC (see Annex 6.1.1).

The DSC thermograms of lactose, maltose and mannitol suspensions present a sharp exothermic peak, proving that these substances build up a crystalline structure during lyophilization. Moreover, they have a higher T_c than the other substances. The DSC thermograms of sorbitol presented a glass transition (broader peak than the crystalline one) meaning that this substance builds up an amorphous structure with a quite low T_c . Maltitol and xylitol build up both a crystalline and an amorphous structure with a low T_c . Considering the solid state of the maltitol, sorbitol and xylitol suspensions, can those substances be used anyway within the framework of the Lyoc® technology? To answer this question, the FD was used. The suspensions analyzed through DSC were also analyzed with the FD method described in Chapter 3.2.3.1.2. The T_c results obtained with both methods are summarized in Table 4-2.

Table 4-2: Comparison of the different Diluent/Water suspensions T_c , measured by DSC ($n=3$) and with the freeze-dryer ($n=2$).

	Lactose (50% w/w)	Maltitol (60% w/w)	Maltose (50% w/w)	Mannitol Pearlitol® 110 C (50% w/w)	Sorbitol Neosorb 70/02 (70% w/w)	Xylitol (60% w/w)
DSC measurement T_c [°C]	0,49±0,26	-11,76±0,17	-2,45±0,93	-0,25±0,13	-32,90±0,23	-57,30±2,38
Freeze-dryer measurement T_c [°C]	None	-14	-5	None	Could not be frozen	-17

The lactose and mannitol suspensions do not reveal any air bubbles on the surface during the FD test. The frozen water is able to sublime without causing collapse within the Lyocs®. The freezing temperature of the sorbitol suspension is too low to be reached in the FD, meaning that sorbitol cannot be used for the Lyoc® technology. The xylitol and maltitol suspensions have too low critical temperatures. These substances would need a much longer time to be freeze-dried and are therefore non-efficient from a production point of view. The maltose suspension has a higher critical temperature than maltitol, sorbitol and xylitol and could be considered as a new excipient usable in the Lyoc® technology.

One advantage of the T_c measurement with the freeze-dryer is that the evolution of $T_{product}$ can be followed in real time (see Figure 4-7).

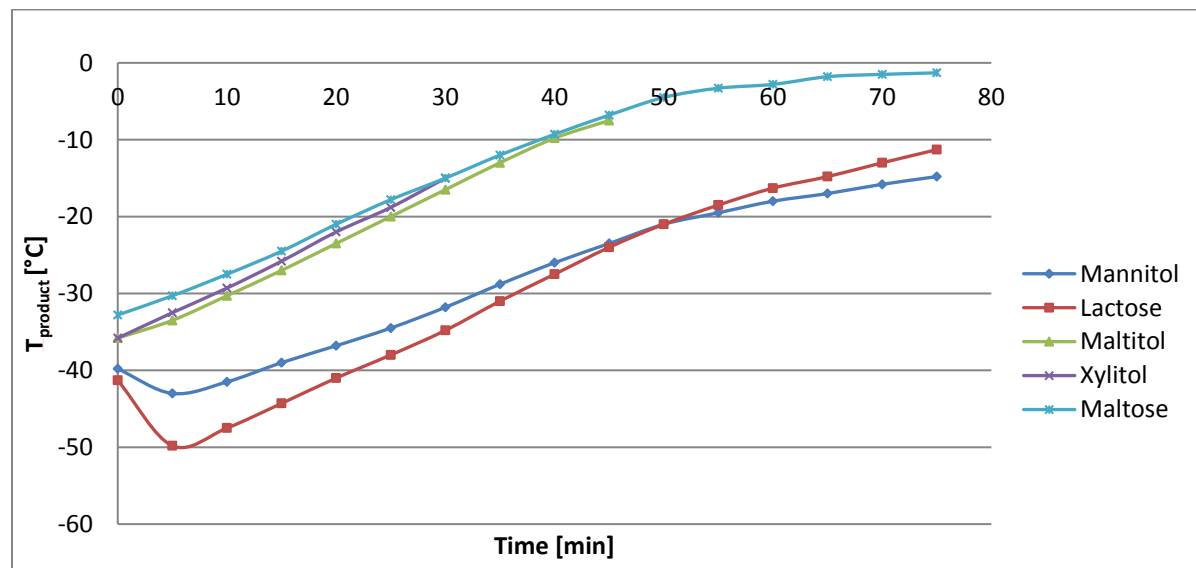


Figure 4-7: Evolution of $T_{product}$ of the various diluents in function of time ($n=2$).

Sublimation is an endothermic process, i.e. the product is absorbing heat energy from the shelves. As shown on Figure 4-7, two different $T_{product}$ evolutions can be observed: the evolution of $T_{product}$ of the lactose and mannitol suspensions is firstly decreasing before increasing again, whereas of the other $T_{product}$ substances are increasing from the beginning. The fact that T_p is decreasing is the sign of a beginning of evaporation within the product,

meaning that the product will be easily sublimated (Le Floch, 2008). It could be explained by a faster onset of sublimation with lactose and mannitol than the other substances, leading to a higher water loss at the beginning of the drying process. During the first 10 min of sublimation, the frozen water may easily sublime for mannitol and lactose, which could explain this evolution of temperature, unlike maltitol, xylitol and maltose. T_p of maltitol, maltose and xylitol are increasing so fast that their T_c is reached too quickly, leading to the collapse of the Lyocs®. The lyophilization process of these latter three substances has to be prolonged to prevent a too fast temperature increase and they are therefore not potential diluents from a production point of view. Indeed, the manufacture of Lyocs® will not be productive enough by using excipients that need a long drying time.

According to the T_c values and to the evolution of T_p as well as considering the solid state of each diluent, mannitol and lactose are the most interesting substances. Nevertheless, lactose may cause an intolerance in some patients, which limits its use as excipient. Lactose is also subjected to the Maillard-reaction and is a hygroscopic substance (content of water \approx 4,5-5,5%). The Maillard-reaction could lead to a bad visual aspect of the product (due to brown coloration), whereas the hygroscopic criteria could lead to product absorbing too much water of the ambient air, impacting the quality of the final product by provoking a decrease of hardness for instance. The other negative point of lactose is that its taste is pretty flavorless unlike mannitol which has a cooling effect. As explained in the chapter 2.1.1, the taste of ODTs is an important criterion for patients. It is easier to mask the taste of an API with a sweet diluent having a cooling effect in mouth than with a tasteless diluent. Therefore, only mannitol will be studied in this thesis.

4.1.2 Study on Binders

Binders are used in Lyocs® formulation to give hardness and robustness to the freeze-dried tablets. This substance has to be a water-soluble polymer (Blonde, 1974). The choice of binders was made after a few investigations in patents (Blonde, 1974; Nguyen, 2011) and in the Handbook of Pharmaceutical Excipients (Rowe et al., 2009). Table 4-3 shows a list of some typical binders with a summary of their main applications.

Table 4-3: List of investigated binders.

Binder	Main application
Copovidone	Used as binder in direct compression and wet granulation or as film forming agent in coated solutions (Rowe et al., 2009).
Dextran	Used as binder agent in lyophilization, as blood volume expander in intravenous solutions, or as lubricant in eye drops (Pharmacosmos, 2016).
Dextrotes	Usually used as diluent in direct compression. Can also be used as binding agent by addition of water (Rowe et al., 2009).
Hypromellose	Used as tablet binder, film forming agent in coated solutions or dissolution enhancer for example (Rowe et al., 2009).
Maltodextrine	Used as binder and diluent in direct compression and wet granulation, such as viscosity increasing agent (Rowe et al., 2009).
Polyvinyl alcohol	Usually used in ophthalmic and topical products. Also used as stabilizing agents for emulsions (Rowe et al., 2009).
Povidone	Used as binder in tableting and wet granulation or as dispersing agent (Rowe et al., 2009).

4.1.2.1 Substance Description

Copovidone (Rowe et al., 2009):

Copovidone is a copolymer of 1-ethenyl-2-pyrrolidinone and ethenyl acetate (Figure 4-8). Copovidone is a white to yellow white amorphous, having a faint taste. It is a hygroscopic powder (less than povidone though). Its melting point stands at 140°C.

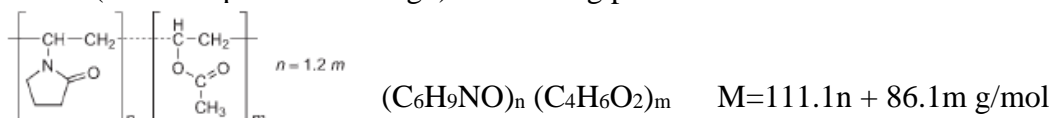


Figure 4-8: Structural formula of copovidone.

Dextran (Mogoșanu and Grumezescu, 2015):

Dextran is a high molecular weight branched polysaccharide of D-glucose monomers (Figure 4-9). It is a white tasteless powder.



Figure 4-9: Structural formula of dextran.

Dextrotes (Rowe et al., 2009):

Dextrotes is a purified mixture of glucose monohydrate and different polysaccharides derived from starch. Dextrotes is composed of 5% oligosaccharide and 95% glucose (w/w). Dextrotes is a white sweet powder. It is slightly hygroscopic. Its melting point stands at 141°C.

Hypromellose (Rowe et al., 2009):

Hypromellose is a mixture of methyl and hydroxypropyl ether of cellulose (Figure 4-10). It is a white tasteless hygroscopic powder. Hypromellose forms a viscous colloidal solution in water. It is available in several grades that vary in viscosity and substitution type. Its melting point range lies between 190 and 200°C.



Figure 4-10: Structural formula of hypromellose.

Maltodextrin (Rowe et al., 2009):

Maltodextrin consists of D-glucose units with a dextrose equivalent (DE) less than 20 (Figure 4-11). The DE value represents the hydrolysis of starch into glucose units. Maltodextrin is a nonsweet white powder. Its solubility and hygroscopicity increase as the DE increases.



Figure 4-11: Structural formula of maltodextrin.

Polyvinyl alcohol (Rowe et al., 2009):

As its name implies, the monomer of polyvinyl alcohol is vinyl alcohol (Figure 4-12). It is a white hygroscopic powder. Its melting point lies between 180 and 190°C.

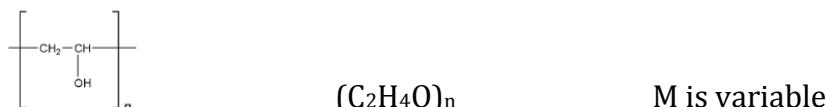


Figure 4-12: Structural formula of polyvinyl alcohol.

Povidone (Rowe et al., 2009):

Povidone has N-vinylpyrrolidone as monomer (Figure 4-13). It is a white hygroscopic amorphous powder. Its melting point stands at 150°C.

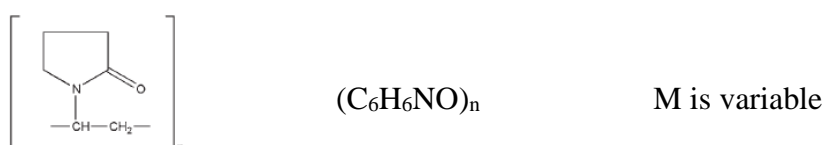


Figure 4-13: Structural formula of povidone.

4.1.2.2 Suspension Characterization

As underlined in the U.S patent 3,855,712 (Blonde, 1974), binders are used in a proportion up to 10 % of the dried mass in lyophilized tablets. Above 10 % of binder, the resulting lyophilized tablet will be too hard because of the cohesion within the particles caused through its binding effect, leading to a disintegration time higher than 30 sec (Blonde, 1974). In order to see if binding agents have an impact on the T_c of mannitol, suspensions of Diluent/Binder (90 %/10 % w/w) were analyzed through DSC (see Annex 6.1.2). As shown in the Table 4-4, there were no significant changes on the T_c of mannitol, as the peaks of all binder types overlapped. This could be due to the too low concentration of binder in the suspension. Dextran seems to be the most appropriate binder, since T_c Diluent/Binder only differs from the T_c Diluent suspension from 0.02°C. Except for dextates where the T_c was approx. 1 degree below the other binders, all other binders seem to be alternative binders for the Lyoc® technology.

Table 4-4: Comparison of the different Diluent/Binder (90 %/10 % w/w) suspensions T_c with the 100 % Diluent suspension, measured by DSC (n=3).

	90 %/10 % (w/w)	100 % diluent
Copovidone	-0,44±0,12	
Dextran	-0,27±0,10	
Dextates	-1,64±0,13	
Hypromellose	-0,72±1,05	
Maltodextrine	-0,69±0,08	
Polyvinyl alcohol	-0,64±0,17	
Povidone	-0,56±0,22	
		-0,25±0,13

4.1.3 Pre-formulation of Lyocs®

The first challenge of the pre-formulation step was to define correctly the range of each compound present in the formulation. In fact:

- the concentration of the binder should not exceed 10 %, otherwise as previously explained, the tablets might be too hard and might not disintegrate within 30 s (Dulieu et al., 2010),
- the amount of diluent depends on the viscosity of the resulting suspension,
- the amount of water present in the formulation is limited by the condenser capacity. In the production, three batches are continuously manufactured each day. After the third batch, the condenser is defrosted. 30 000 blisters of 8 or 10 Lyocs® are produced per batch. The condenser capacity is 600 kg. Considering that 90% of the condenser can efficiently entrap water, the maximal amount of water is established at 750 mg per Lyoc® (see Table 4-5).

Table 4-5: Calculation of the amount of water per Lyoc®.

Blister per batch	30 000	
Lyocs® per blister	8	10
Lyocs® per batch	240 000	300 000
Total condenser capacity	600 kg	
90% of the condenser capacity	540 kg	
Condenser capacity per batch	180 kg	
Maximum amount of water per Lyoc®	750 mg	600 mg

4.1.3.1 Test on Mannitol

4.1.3.1.1 IPCs Range Determination

IPCs are very important for the product quality determination. Lyocs® belong to the ODTs category, which means that they should disintegrate in the mouth within 30 sec. As the Lyocs® are packed in a PVC-blister foil sealed with a 25 µm aluminum foil, they have to be resilient enough to be pushed through this aluminum foil in order to resist the de-blistering step. Another alternative could be the use of peel-off blister. This option would unfortunately increase the production costs, which should be avoided as far as possible. Except the maximum disintegration time, there are no real range values of IPCs for the Lyoc® technology. That is why a pre-test was firstly performed to determine the different IPC ranges. Four marketed Lyocs® were studied in this section (see Table 4-6).

Table 4-6: IPC results of manufactured products±SD.

	Spasfon 80 mg Lyoc®	Spasfon 160 mg Lyoc®	Paralyoc 500 mg Lyoc®	Lopéramide 2 mg Lyoc®
η [mPa.s] <i>Value read at 174 s⁻¹</i>	239	241	Paracetamol micro-encapsulated with cellulose to mask the taste → particle size =380 µm, too high for a viscosity measurement with the Plate-Plate geometry→ η measurement not relevant	Lopéramide is an OEB 3 substance (substance too harmful to be handled by women). The suspension could not be reproduced and so the values of η and F could not be measured.
F <i>Measured with a graduated cylinder after letting the suspension stand 60 min</i>	0,98	0,99	1	
Hardness [N], n=20	44±5	22±3	32±5	79±16
D.T[s], n=6	4±1	71±35	150±30	89±28
Visual aspect	Lyocs® are visually good. Some are sticking to the aluminum foil.	Lyocs® are not hard enough. They become broken when they are pushed through the blisters.	Good quality: They do not stick to the blisters.	Good quality: They do not stick to the blisters.

The disintegration time higher than 30 sec (see Table 4-6) is due to the unsuitable measurement method. The Lyocs® are sticking to the disks of the disintegration apparatus ZT72, distorting the results. The minimum hardness is defined to be between 22 N and 32 N (see Table 4-6). It could nevertheless not be precisely determined. That is why a second test was performed by producing placebos containing mannitol and different percentages of dextran (see Table 4-7). In the marketed formulations, the percentage of dextran is between 1,6 and 5,6 % of the total mass, the percentage of mannitol is between 22 and 55 % of the total mass and water is between 43 and 57 % of the total mass. That is why the percentage of dextran was set under 1,7 % in order to determine the minimum hardness.

Table 4-7: Placebo formulations with different percentages of dextran to determine the minimum hardness.

	%/dose		
	F1	F2	F3
Batch Nr	140268	140269	140270
Mannitol	55,60	55,03	54,46
Dextran	0,57	1,14	1,71
Water	43,83	43,83	43,83

Table 4-8: IPCs results of the formulations F1-F3±SD.

	F1	F2	F3
Hardness [N], n=20	22±3	27±6	37±10
D.T [s], n=6	4±1	5±1	4±2
Visual aspect	The Lyocs® are not hard enough: they become broken when they are pushed through the blister foils. They are powdery and leave a thin layer on the PVC foil.	The Lyocs® are a bit powdery and leave a thin layer on the PVC foil.	The Lyocs® leave a thin layer on the PVC foil.

As shown in Table 4-8, F2 and F3 give good IPC results, unlike F1 where the Lyocs® were too soft. The minimum hardness (H) is therefore set at 27 N.

Regarding the determination of degree sedimentation limits and the viscosity limits, different suspensions presenting different viscosities were produced and frozen in the freeze-dryer. It was noticed that:

- for $\eta < 50 \text{ mPa.s}$, the suspension settles during the freezing step, leading to powdery Lyocs®.
- for $\eta > 600 \text{ mPa.s}$, the suspension is too viscous and cannot be dispensed in the blister foils.

- for $F < 0,85$, the suspension settles during the freezing step, leading to powdery Lyocs®, which cannot be properly de-blistered without breaking.

A summarized table of the IPC ranges is presented in Table 4.9:

Table 4-9: Determination of IPC ranges of Lyocs®.

IPC range	
Viscosity <i>Value read at 174 s⁻¹</i>	$50 < \eta < 600$ mPa.s
Degree of sedimentation <i>Measured with a graduated cylinder after letting the suspension stand 60 min</i>	$0,85 < F < 1$
Hardness	$H > 27$ N
Time of disintegration	$t < 30$ sec

4.1.3.1.2 Influence of Binders on Mannitol Lyocs®

The binders mentioned in the section 4.1.2.1 were combined at different concentration to mannitol and the resulting Lyocs® quality was studied.

The percentage of binder was increased progressively between 1,2 and 6,1 % of the wet mass (i.e. between 2 and 10 % of the dried mass, as mentioned in the U.S patent 3,855,712 (Blonde, 1974)). As soon as the suspension was too viscous to be dispensed in blisters or that the resulting D.T of the Lyocs® was too high, any further increase of the binder concentration was performed. The tested formulations are summarized in Tables 4-10 and 4-11.

Table 4-10: Formulations F1-F20 in %.

		% of substance																		
	Copovidone	Dextran				Dextrates				HPMC		Malto-dextrin		Polyvinyl alcohol		Povidone				
	F1	F2	F3	F4	F5	F6	F7	F8	F9	F10	F11	F12	F13	F14	F15	F16	F17	F18	F19	F20
Mannitol	59,7	57,9	59,7	57,9	56,6	54,8	59,7	57,9	56,6	54,8	59,7	57,9	59,7	57,9	59,7	57,9	59,7	57,9	56,6	54,8
Copovidone	1,2	3,0																		
Dextran			1,2	3,0	4,3	6,1														
Dextrates							1,2	3,0	4,3	6,1										
Hypromellose												1,2	3,0							
Maltodextrine														1,2	3,0					
Polyvinyl alcohol															1,2	3,0				
Povidone																	1,2	3,0	4,3	6,1
Water	39,1	39,1	39,1	39,1	39,1	39,1	39,1	39,1	39,1	39,1	39,1	39,1	39,1	39,1	39,1	39,1	39,1	39,1	39,1	39,1

Table 4-11: Formulations F1-F20 in mg/dose.

		mg / dose																		
	Copovidone	Dextran				Dextrates				HPMC		Malto-dextrin		Polyvinyl alcohol		Povidone				
	F1	F2	F3	F4	F5	F6	F7	F8	F9	F10	F11	F12	F13	F14	F15	F16	F17	F18	F19	F20
Mannitol	686	665	686	665	651	630	686	665	651	630	686	665	686	665	686	665	686	665	651	630
Copovidone	14	35																		
Dextran			14	35	49	70														
Dextrates							14	35	49	70										
Hypromellose												14	35							
Maltodextrine														14	35					
Polyvinyl alcohol															14	35				
Povidone																	14	35	49	70
Water	450	450	450	450	450	450	450	450	450	450	450	450	450	450	450	450	450	450	450	450
Total	1150	1150	1150	1150	1150	1150	1150	1150	1150	1150	1150	1150	1150	1150	1150	1150	1150	1150	1150	1150

IPCs are summarized in the table below (Table 4-12).

Table 4-12: IPCs of formulations F1-F20.

	Copovidone		Dextran				Dextrates				HPMC		Malto-dextrin		Polyvinyl alcohol		Povidone			
	F1	F2	F3	F4	F5	F6	F7	F8	F9	F10	F11	F12	F13	F14	F15	F16	F17	F18	F19	F20
H [N]	35	48	30	35	85	102	26	37	42	49	29	-	32	44	66	148	31	65	54	65
D.T [s]	10	12	12	11	11	18	12	7	3	4	29	-	12	9	13	105	5	9	10	20
Visual aspect	Do not stick to the blister. Smooth surface. Quick disintegration in mouth. Bitter taste due to copovidone.	Material sticks to the aluminum foil. Little bump on the surface. Powdery. Quick disintegration in mouth.	Not powdery. Do not stick to the blister. Little bump on the surface. Quick disintegration in mouth.				Do not stick to the blister. Smooth surface. Quick disintegration in mouth.				Do not stick to the blister. Smooth surface. Quick disintegration in mouth.		Material stays stuck to the aluminum foil. Smooth surface. Quick disintegration in mouth. F12 was too viscous and could not be pipetted.		Do not stick to the blister. Smooth surface. Quick disintegration in mouth.		Do not stick to the blister. Smooth surface. Quick disintegration in mouth.			

Based on the IPC results (H and D.T) and the visual aspect summarized in Table 4-12, dextran, dextrates and povidone are good binders. If an incompatibility can be observed between dextran and the API, dextrates or povidone both present a good alternative as binders. As copovidone gives a bitter taste to the tablets, it is not a suitable binder for the Lyoc® technology. The Lyocs® containing 5 % of polyvinyl alcohol disintegrated too slowly, which is the reason why it will not be further studied. HPMC and maltodextrin gave pipetting problems above 5 % (the resulting suspensions were too viscous). This could be linked to the fact that both substances also play the role of viscosity increasing agent (Rowe et al., 2009).

4.1.3.2 Type of Mannitol

Several types of mannitol exist, depending on its manufacturing process. Among each mannitol type, different grades of mannitol also exist, i.e. particle sizes with more or less fines. The particle size is also an important parameter to take into consideration in the ODTs formulation. Indeed, the larger the particle, the sandier the feeling in the mouth and the more unpleasant the tablet will taste. In our case, as mannitol is the main component in the formulation, its particle size can play also a role in sedimentation during the freezing step according to the Stokes' law. The larger the particle size, the faster the sedimentation. That is why the mannitol type and its particle size are investigated in this section.

4.1.3.2.1 Description of Mannitol Type

Three kinds of mannitol are available in the Roquette® portfolio: Pearlitol® C, Pearlitol® DC and Pearlitol® SD (Roquette, 2016).

Pearlitol® C refers to mannitol crystalline powder (Roquette, 2006). It is only composed of the β -modification of mannitol and is obtained by means of crystallization from water (Roquette, 2006). 4 grades are available: Pearlitol® 25 C ($D_{50} = 25 \mu\text{m}$), Pearlitol® 50 C ($D_{50} = 50 \mu\text{m}$), Pearlitol® 110 C ($D_{50} = 110 \mu\text{m}$) and Pearlitol® 160 C ($D_{50} = 160 \mu\text{m}$) (Roquette, 2016). The grade 110 C is a special grade manufactured for the LyoCS® production.

Pearlitol® DC refers to mannitol used for direct compression (Roquette, 2006). It is only composed of the β -modification of mannitol and it is obtained through a thermal granulation process (Roquette, 2006). It is very condensed and is less porous than Pearlitol® C, which gives it a slow dissolution rate (Roquette, 2006). 3 grades are available: Pearlitol® 300 DC ($D_{50} = 250 \mu\text{m}$), Pearlitol® 400 DC ($D_{50} = 360 \mu\text{m}$) and Pearlitol® 500 DC ($D_{50} = 520 \mu\text{m}$) (Roquette, 2016).

Pearlitol® SD refers to spray-dried mannitol (Roquette, 2006). It is mainly composed of the α -modification of mannitol ($> 50\%$). The remaining fraction is the β -modification of mannitol (Roquette, 2006). 2 grades are available: Pearlitol® 100 SD ($D_{50} = 100 \mu\text{m}$) and Pearlitol® 200 SD ($D_{50} = 180 \mu\text{m}$) (Roquette, 2016).

In Figure 4-14, SEM images of the three types of mannitol are represented (Roquette, 2016). The differences previously described between the different mannitol qualities are distinctly observed:

- The SEM image of Pearlitol® C shows an orthorhombic needles crystalline structure,
- The SEM image of Pearlitol® DC shows granule particles having a porous structure,
- The SEM image of Pearlitol® SD shows typical spray-dried particles. A porous structure is also visible.



Figure 4-14: SEM pictures of Pearlitol® C (left), Pearlitol® DC (middle) and Pearlitol® SD (right) (Roquette, 2016).

4.1.3.2.2 Influence of Mannitol Type on IPC Results

The aim of this study was to compare the IPC results according to the mannitol type. For this, the formulation of the model drug (Spasfon 80) was used to set the quantity of binder (i.e. 25 mg/dose) and of diluent (i.e. 715 mg/dose). The quantity of water for each mannitol type formulation was then determined through viscosity measurements (see Figure 4-15). The purpose was to have similar formulations, i.e. same amount of binder, of water and of diluent, in order to have significant and representative IPC comparisons between the batches. The amount of water was thus adjusted in order to have a viscosity between 50 and 600 mPa.s (as explained in Chapter 4.1.3.1.1) to allow the pipetting step and to prevent suspension sedimentation.

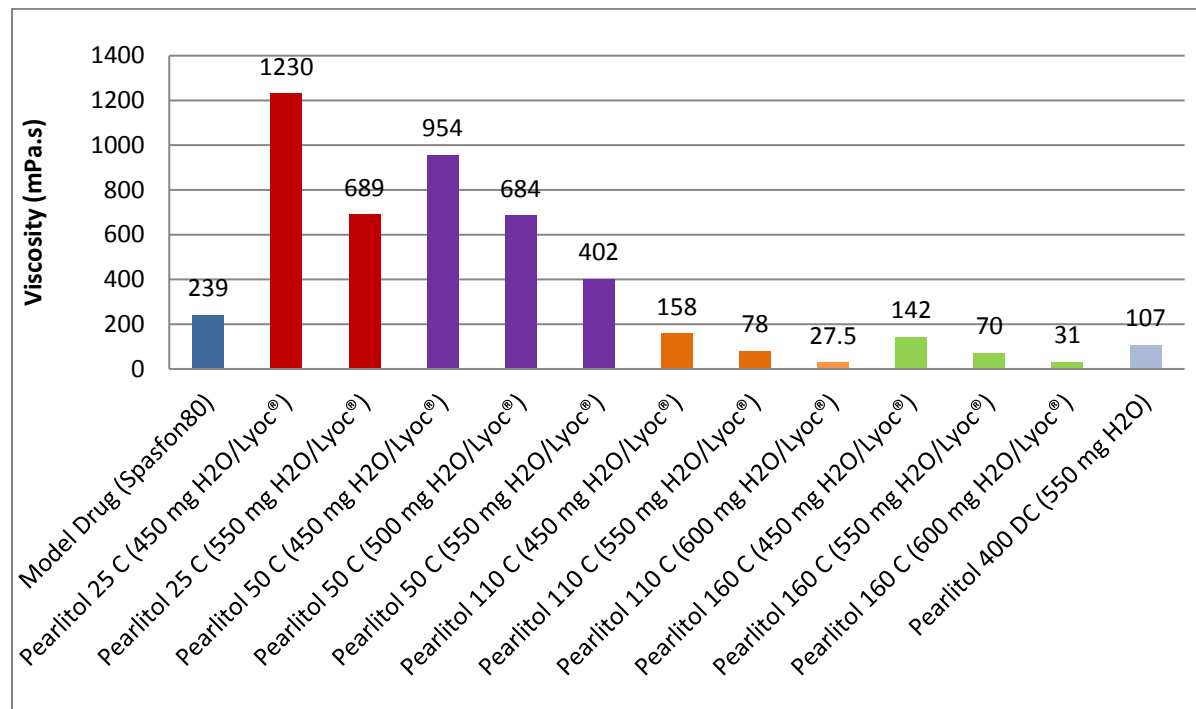


Figure 4-15: Viscosity measurement of suspensions of different mannitol type having different water contents (n=1).

As shown in Figure 4-15, Spasfon 80 Lyoc[®] has a viscosity of 239 mPa.s.

A manufacture problem was encountered with Pearlitol® 100 SD. The resulting suspension was too viscous, even with a water amount going up to 750 mg/dose (which is the maximum

amount of water, see Section 4.1.3), so that it was impossible to pipette this suspension and thus to measure its η . The Pearlitol® SD type is not usable at all for the Lyoc® technology, as the resulting suspension is too viscous to be pipetted.

Pearlitol® 110 C and 160 C Lyoc® can be produced with a water amount up to 550 mg / dose, as their viscosities are beyond 50 mPa.s. For a water amount of 600 mg/dose, the suspensions of Pearlitol® 110 C and 160 C are too liquid ($\eta < 50$ mPa.s) and settle in the FD during the freezing step.

Pearlitol® 400 DC suspension could only be produced from a water content of 550 mg/dose. For a lower water concentration, the suspension presented clusters and was thus not homogeneous.

Pearlitol® 50 C suspension presented problems to be pipetted due to its lower particle size, corresponding to a higher impact on viscosity. Indeed, the formulation needed a water amount beyond 500 mg water/dose to be dispersible and to have an appropriate viscosity to be pipetted. Pearlitol® 25 C suspension also needed a water amount beyond 550 mg / dose. Using Pearlitol® 25 C with 600 mg water / dose would be better in term of viscosity, as η would be lower than 600 mPa.s. Nevertheless, for the other mannitol grades, water amount up to 550 mg / dose resulted in suspensions that were too liquid and that settled in the FD. That is why the water amount was set up at 550 mg/dose for this test. The final formulation set for this test is summarized in Table 4-13.

Table 4-13: Formulation determined for mannitol testing.

Substance	mg / dose
Mannitol	715
Dextran	25
Water	550
Total	1290

4.1.3.2.3 Influence of Mannitol Type

Lyocs® containing Pearlitol® 110 C and Pearlitol® 400 DC as diluents were produced as described in section 3.2 and their properties were compared. The formulations are summarized below, in Table 4-14.

Table 4-14: Formulations of Pearlitol® 110 C, 400 DC and 100 SD Lyocs® in mg/dose.

Substance	mg / dose	
	Pearlitol® 110 C $D_{50} = 110 \mu\text{m}$ SAP-Nr 245445	Pearlitol® 400 DC $D_{50} = 360 \mu\text{m}$ SAP-Nr 15534
Batch Nr	160316	160047
Mannitol	715	715
Dextran SAP-Nr 236561	25	25
Water SAP-Nr 14022	550	550
Total	1290	1290

IPCs are summarized in Table 4-15.

Table 4-15: IPC results of the previous formulations \pm SD.

IPC results		
	Pearlitol® 110 C	Pearlitol® 400 DC
η [mPa.s]	78	107
F	0,98	0,98
Sedimentation in FD	No	No
H [N]	53 \pm 8	51 \pm 17
D.T [s]	5 \pm 1	5 \pm 3
Results	Quick disintegration in mouth, taste good. Good visual aspect. Do not break during unpacking.	Quick disintegration in mouth, sandy feeling in the mouth. Lyocs® powdery on the surface. Do not break during unpacking.

The D.T and H of both formulations were similar. The problem of the Pearlitol® DC type is its high mean particle size. The lowest particle size is 250 μm . Nevertheless, the sandy feeling in the mouth is already discernable from a particle size of 200 μm (Kimura et al., 2015). Since the lowest particle size of Pearlitol® DC is 250 μm , Pearlitol® DC could have been used in combination with Pearlitol® 100 C if it would have brought some formulation advantages. Nevertheless, H and D.T of the Pearlitol® DC formulation are similar to the one of the Pearlitol® C formulation. Moreover, the resulting Lyocs® containing Pearlitol® 400 DC have a powdery structure, which does not bring any advantages to use the DC mannitol type. Therefore only Pearlitol® C will be studied further.

4.1.3.2.4 Influence of Mannitol Grade

In the production, only the Pearlitol® 110 C grade is used for the manufacture of Lyocs®. In this section, all the 4 Pearlitol® C grades will be investigated (see Table 4-16).

Table 4-16: Formulations of Pearlitol® 25 C, 50 C, 110 C and 160 C Lyocs® in mg/dose.

Substance	mg / dose			
	Pearlitol® 25 C $D_{50} = 25 \mu\text{m}$ SAP-Nr 129474	Pearlitol® 50 C $D_{50} = 50 \mu\text{m}$ SAP-Nr 261244	Pearlitol® 110 C $D_{50} = 110 \mu\text{m}$ SAP-Nr 245445	Pearlitol® 160 C $D_{50} = 160 \mu\text{m}$ SAP-Nr 109613
Batch Nr	160036	160037	160316	160317
Mannitol	715	715	715	715
Dextran SAP-Nr 236561	25	25	25	25
Water SAP-Nr 14022	550	550	550	550
Total	1290	1290	1290	1290

Table 4-17: IPC results of the previous formulations.

IPC results				
	Pearlitol® 25 C	Pearlitol® 50 C	Pearlitol® 110 C	Pearlitol® 160 C
η [mPa.s]	689	402	78	70
F	1	1	0,98	0,96
Sedimentation in FD	No	No	No	No
H [N]	50±10	52±13	53±8	44±9
D.T [s]	21±3	16±2	5±1	5±2
Aspect	Quick disintegration in mouth, taste very good (softer and cooler effect than Lyocs® using Pearlitol® 110C). Good visual aspect. Do not break during unpacking.	Quick disintegration in mouth, taste very good (softer and cooler effect than Lyocs® using Pearlitol® 110C). Good visual aspect. Do not break during unpacking.	Quick disintegration in mouth, taste good. Good visual aspect. Do not break during unpacking.	Quick disintegration in mouth, sandy feeling in the mouth. Good visual aspect. Do not break during unpacking.

According to the IPC results summarized in Table 4-17, Pearlitol® 25 C, 50 C and 110 C can be used for the production of Lyocs®. The advantages of both grades 25 C and 50 C is that they give an extra cooling effect in mouth and they present a smaller particle size, which will considerably reduce the risk of sedimentation during the Lyocs® manufacturing. Nevertheless, a higher amount of water is needed for both of those grades to avoid having a too viscous suspension (water amount from 450 mg/dose is usable for Pearlitol® 110 C and Pearlitol® 160 C, as shown in Figure 4-15, vs. 550 mg of water/dose for Pearlitol® 25 C and Pearlitol® 50 C). Indeed, for a constant mass of particles in a suspension, the smaller the particle size, the greater the number of particles is in the system and the more interactions between the particles (Fletcher and Hill). In addition, it can be noticed that the smaller the particle size, the

higher the disintegration time. This phenomenon could be due to the fact that those 2 grades create more cohesion within Lyocs® due to their small particle size. Particles may be able to stick really close together, giving a less porous structure to the Lyocs® unlike Pearlitol® 110 C and Pearlitol® 160 C. Pearlitol® 160 C gave a sandy feeling in the mouth due to the larger particle size of this grade, which is a negative aspect for ODTs. That is why Pearlitol® 160 C is not recommended to be used alone. The best mannitol grade is Pearlitol® 110 C in term of viscosity, and Pearlitol® 25 C and 50 C have an interesting cooling effect in mouth but give the suspension a too high viscosity, which may cause pipetting problems.

A mixture of mannitol grades (Pearlitol® 25 C and 160 C) could overcome both problems of high viscosity and sandy feeling in the mouth. Indeed, the extra cooling and smooth effect of Pearlitol® 25 C could bring an interesting plus in ODTs formulations. Moreover, the use of smaller grade could also overcome the possible API sedimentation due to its smaller particle size. Indeed, Pearlitol® 25 C will thicken the suspension, playing both roles of diluent and viscosity enhancer. That is why a further test was conducted by mixing both grades 25 C and 160 C at different concentrations (see Table 4-18).

Table 4-18: Formulations of Pearlitol® 25 C/160 C (1+1), 25 C/160 C (3+1) and 25 C/160 C (1+3) Lyocs® in mg/dose.

Substance	mg / dose		
	Pearlitol® 25 C/160 C (3+1)	Pearlitol® 25 C/160 C (1+1)	Pearlitol® 25 C/160 C (1+3)
Batch Nr	160296	160295	160297
Pearlitol® 25 C <i>SAP-Nr 129474</i>	476,7	357,5	238,3
Pearlitol® 160C <i>SAP-Nr 109613</i>	238,3	357,5	476,7
Dextran <i>SAP-Nr 236561</i>	25	25	25
Water <i>SAP-Nr 14022</i>	550	550	550
Total	1190	1190	1190

IPCs are summarized in Table 4-19.

Table 4-19: IPC results of the previous formulations \pm SD.

IPC results			
	Pearlitol® 25 C/160 C (3+1)	Pearlitol® 25 C/160 C (1+1)	Pearlitol® 25 C/160 C (1+3)
η [mPa.s]	331	183	143
F	0,98	0,98	0,98
Sedimentation in FD	No	No	No
H [N], n=20	56±13	39±12	70±15
D.T [s], n=6	8±1	10±3	11±2
Results	Quick disintegration in mouth, taste good, not sandy, strong cooling effect in the mouth. Good visual aspect. Do not break during unpacking	Quick disintegration in mouth, taste good, not sandy, strong cooling effect in the mouth. Good visual aspect. Do not break during unpacking	Quick disintegration in mouth, taste good, not sandy, strong cooling effect in the mouth. Good visual aspect. Do not break during unpacking

Table 4-19 clearly shows that $\eta(1+3) < \eta(1+1) < \eta(3+1)$. This is coherent since the amount of Pearlitol® 25 C in the formulation is increasing as following: Pearlitol® 25 C amount (1+3) < Pearlitol® 25 C amount (1+1) < Pearlitol® 25 C amount (3+1). It could be expected that the more Pearlitol® 25 C, the longer D.T, and the harder the tablets, due to a higher amount of particles in the formulation. Nevertheless, this trend could not be observed.

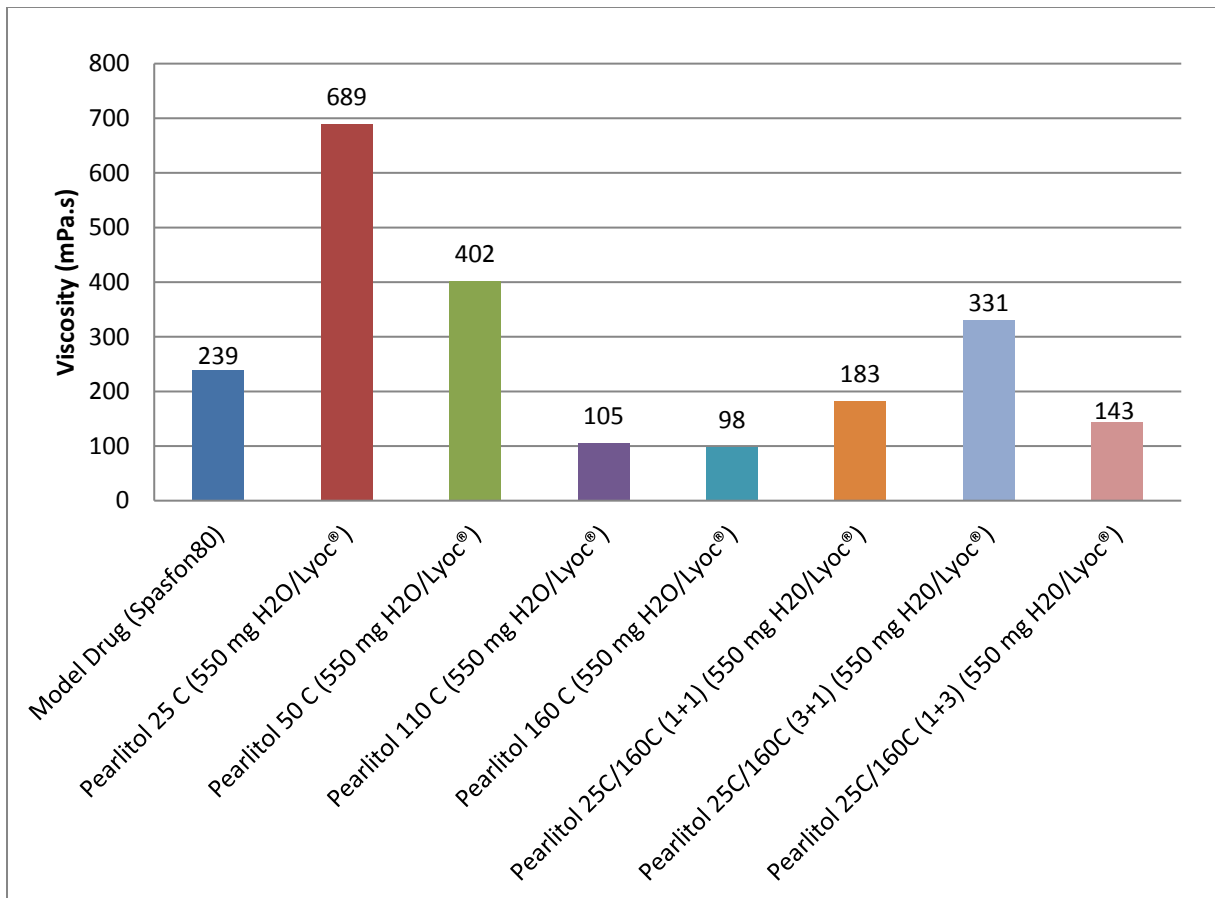


Figure 4-16: Viscosity measurement of suspensions containing different grade of mannitol, with 550 mg water per Lyoc® (n=1).

Figure 4-16 indicates the viscosity values of each Pearlitol® suspension. The combination of Pearlitol® 25 C/160 C gave a good viscosity profile to the suspension ($143 \text{ mPa.s} < \eta < 331 \text{ mPa.s}$) and also better IPC results than the pure grades of Pearlitol® 25 C or Pearlitol® 160 C. Indeed, the cooling effect of Pearlitol® 25 C was present in the 3 formulations presenting combination of 25 C and 160 C, unlike formulations using Pearlitol® 110 C or 160 C alone. The sandy effect of Pearlitol® 160 C disappeared in those formulations due to its reduced amount. D.T of combined Pearlitol® was lower of 10 seconds than the formulation containing Pearlitol® 25 C alone. This mixture of Pearlitol® 25 C and 160 C could then be a good alternative to the usual Pearlitol® 110 C used in marketed products, bringing an interesting cooling feeling in mouth to the ODT product. Between the three formulations composed of combined Pearlitol® grade, Pearlitol® 25 C/160 C (1+1) seems to be the favorite one, as its viscosity value is the nearest one to the one of the model drug (Spasfon 80 mg Lyoc®). Moreover, this formulation has the lower H, meaning that the resulting D.T in mouth should be the lower of the 3 formulations.

4.1.3.2.5 Microscopic Characteristics

The morphology of the Lyocs® was studied through SEM. The manufactured sample Spasfon 80mg Lyoc® collected from the production was used as model for the SEM analysis. Indeed, it is the earliest marketed formulation, composed of dextran, mannitol and phloroglucinol (API). Each sample was broken in two and three SEM-pictures were captured: a general view from the whole Lyoc®, a zoomed view of the upper surface of the Lyoc® and a zoomed view of the middle of the Lyoc®. The SEM pictures of Lyocs® were compared with one SEM picture of a Zydis® product found in the literature (Seager, 1998), in order to compare the two concurrent technologies.

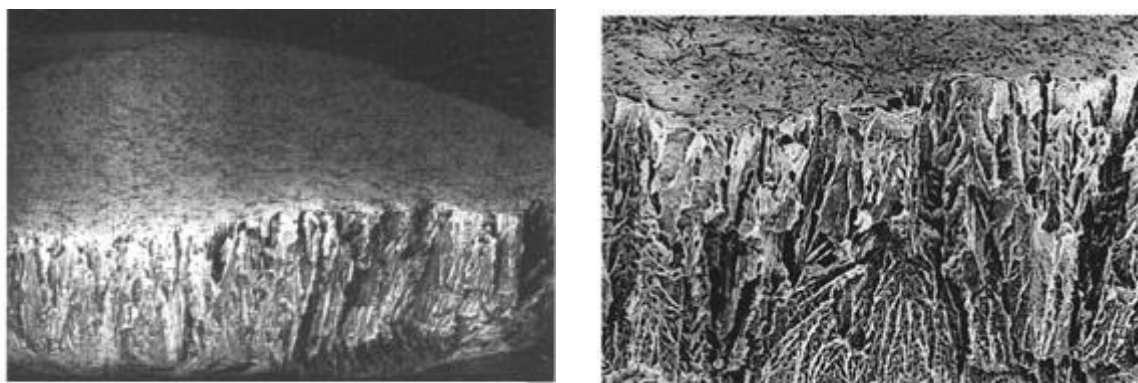


Figure 4-17: SEM pictures of a Zydis® matrix (x50 left, x150 right) (Seager, 1998).

The highly porous structure of the Zydis® product shown in Figure 4-17 is due to the low excipients concentration, giving less dense products than with the Lyoc® technology. Vertical pores are visible in the Zydis® tablet, facilitating the saliva to go through the tablet.

On the first picture of each Lyoc® sample (respectively Figure 4-18, 4-21, 4-24, 4-27, 4-30, 4-33, 4-36, 4-39 and 4-42), their porosity structure is not so evident to be observed, unlike the Zydis® dosage forms. This is due to the high concentration of filler in the formulation of Lyocs®. Nevertheless, on the second picture of each sample (respectively Figure 4-19, 4-22, 4-25, 4-28, 4-31, 4-34, 4-37, 4-40 and 4-43), when a finer zoom (either already visible with x100 in most cases or with x500) is used, the porous structure can be observed on the surface of the Lyocs®. Those pores allow the penetration of saliva in the whole tablet, resulting to the quick disintegration of the Lyoc® in the mouth. The third picture (respectively Figure 4-20, 4-23, 4-26, 4-29, 4-32, 4-35, 4-38, 4-41 and 4-44) shows how porous the Lyocs® are. In general, an inhomogeneity within the tablets can be observed. This phenomenon may be due to the quick freezing rate during the lyophilization process. Indeed, mannitol is crystallizing during lyophilization. Slow freezing rates lead to large and homogenous crystals that have time to grow up, whereas fast freezing rates lead to an inhomogeneous structure of small ice crystals that have no time to be built up and to grow up (Daniels, 2014). As the freezing process for the Lyoc® technology is quite fast ($T_{ramp} = 0,90^{\circ}\text{C}/\text{min}$), mannitol crystals do not have time to grow up properly, giving this microscopic inhomogeneous structure. The needle crystalline structure of pure Pearlitol® C observed in its SEM picture (see Figure 4-14) is also recognizable in the Lyoc® structure. A finer structure and a better homogeneity is observed for Pearlitol® 25 C Lyocs® (see Figure 4-21) than Pearlitol® 50 C (see Figure 4-24), 110 C

(see Figure 4-27) and 160 C Lyocs® (see Figure 4-30). Nevertheless, Pearlitol® 110 C (see Figure 4-29) and 160 C Lyocs® (see Figure 4-32) present more space between the particles than Pearlitol® 25 C (see Figure 4-23) and 50 C Lyocs® (see Figure 4-26), which could explain the faster disintegration time of Pearlitol® 110 and 160 C Lyocs® (D.T respectively 5 s for Pearlitol® 110 and 160 C Lyocs® vs. 21 s for Pearlitol® 25 C Lyocs® and 16 s for 50 C Lyocs®). The space between the particles is indeed represented through the black areas visible between the particles.

For Pearlitol® 400 DC Lyocs®, agglomerates can be observed on the top of Figure 4-33, representing the bottom of the blister cavity. This phenomenon was driven by the sedimentation of the large particle size of Pearlitol® 400 DC ($D_{50} = 360 \mu\text{m}$) during the freezing step.

A further study was performed on the formulations containing a mixture of mannitol grades (25 C and 160 C). On the overall view of the Lyocs® (see Figures 4-36, 4-39 and 4-42), it can be observed that their structures are similar to the one of the Pearlitol® 110 C Lyocs® (see Figure 4-27) with additional coarse particles coming from the Pearlitol® 160 C. On the zoomed view of the Lyocs® (see Figures 4-38, 4-41 and 4-44), the space between the particles is also similar to the one of Pearlitol® 110 C Lyocs® (see Figure 4-29), which could explain their shorter D.T than the formulation containing pure Pearlitol® 25 C.

The microscopic analysis carried out by means of SEM could thus identify the differences between the different mannitol types and grades used. It can be concluded that the formulations Pearlitol® 110 C, 25 C/160 C (1+1), 25 C/160 C (1+3), 25 C/160 C (3+1) Lyocs® are microscopically similar.

In conclusion, even if Pearlitol® 110 C is widely used for the Lyocs® manufacture, a mixture of Pearlitol® 25 C and 160 C could be further investigated and used at larger scale, for its numerous benefits (such as its lower D.T, its innovative cooling taste, and its suitable viscosity).

Combining both SEM and IPC results, the placebo matrix of the Pearlitol® 25/160 C (1+1) formulation seems to be the most appropriate since:

- Its viscosity is high enough to avoid sedimentation of the API during freezing activities,
- Its hardness is quite low, meaning that the D.T in mouth could be reduced in comparison to the remaining formulations.
- Its microscopic structure is very similar to the one of Pearlitol® 110 C Lyocs®.

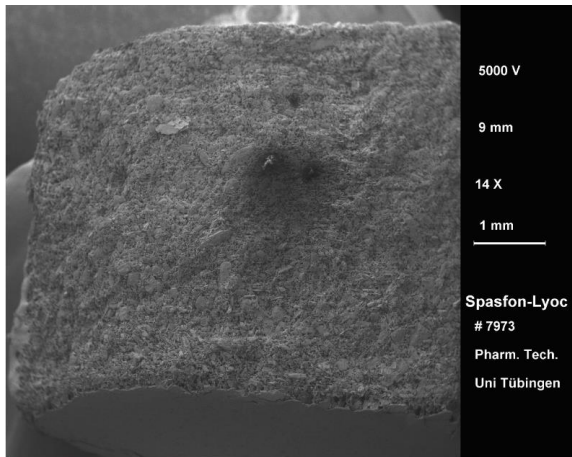


Figure 4-18: SEM picture of Spasfon Lyoc® (Entire structure), 14x magnification.

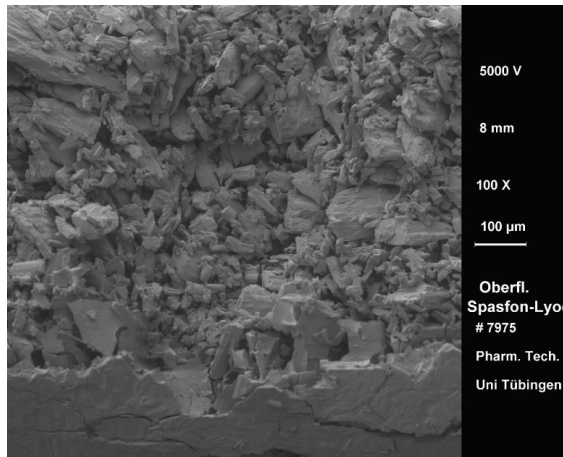


Figure 4-19: SEM picture of Spasfon Lyoc® (Surface), 100x magnification.

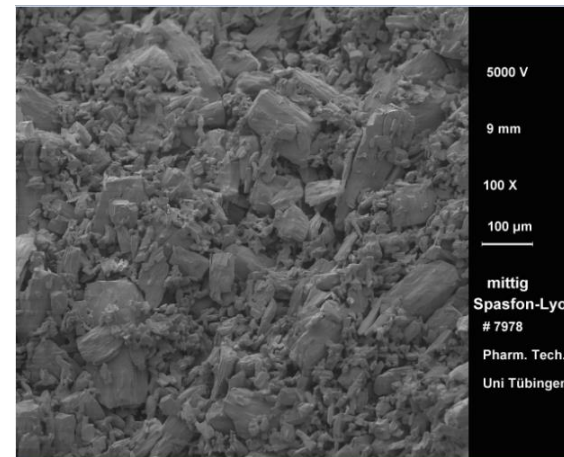


Figure 4-20: SEM picture of Spasfon Lyoc® (Center), 100x magnification.

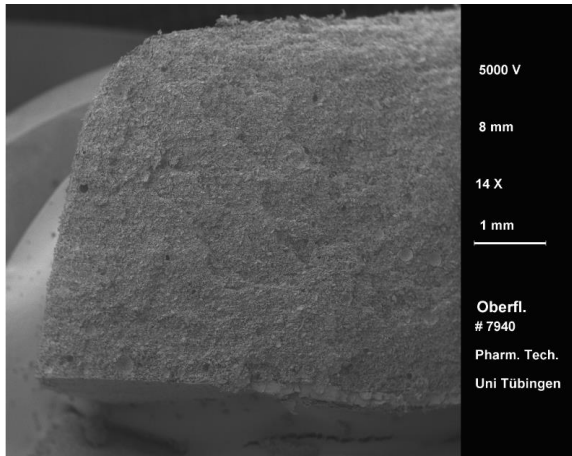


Figure 4-21: SEM picture of Pearlitol® 25 C Lyoc® (Entire structure), 14x magnification.

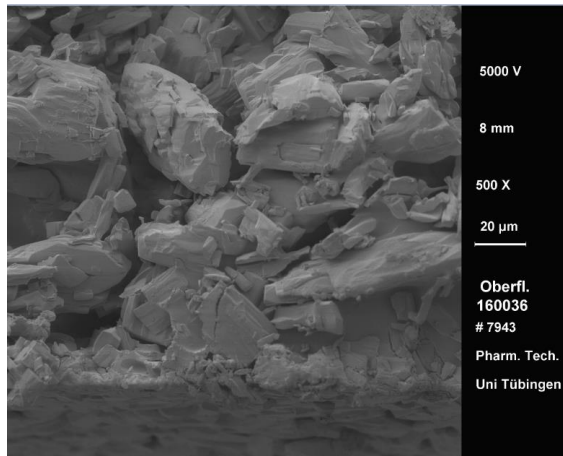


Figure 4-22: SEM picture of Pearlitol® 25 C Lyoc® (Surface), 500x magnification.

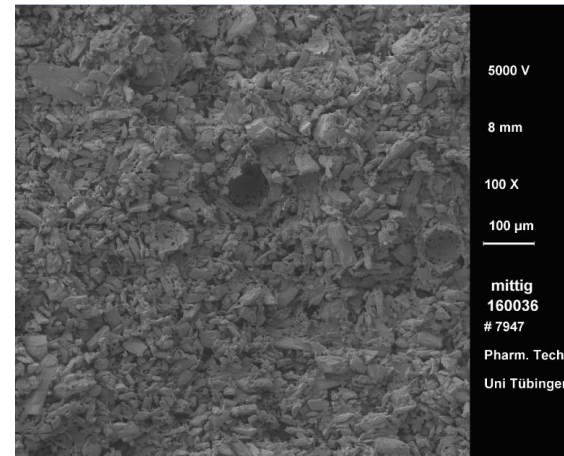


Figure 4-23: SEM picture of Pearlitol® 25 C Lyoc® (Center), 100x magnification.

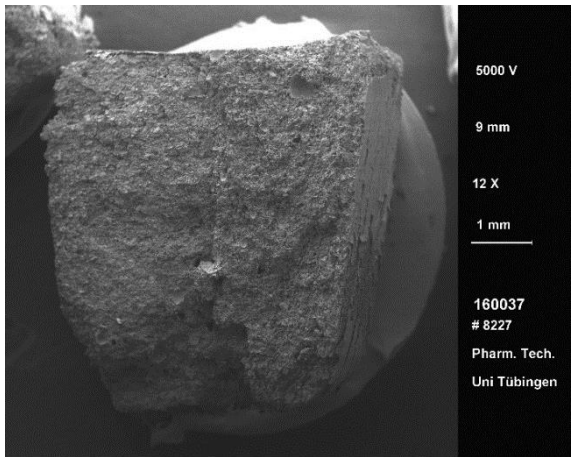


Figure 4-24: SEM picture of Pearlitol® 50 C Lyoc® (Entire structure), 12x magnification.

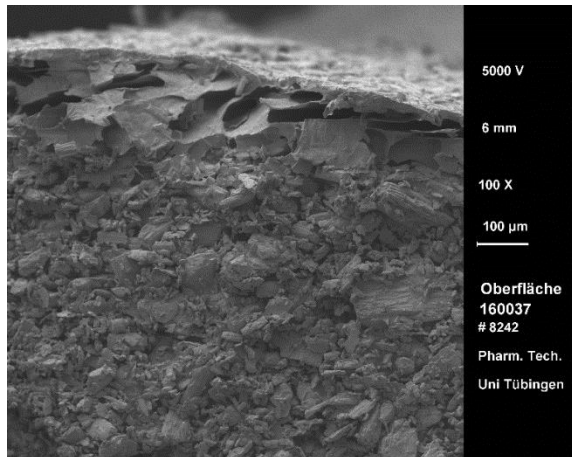


Figure 4-25: SEM picture of Pearlitol® 50 C Lyoc® (Surface), 100x magnification.

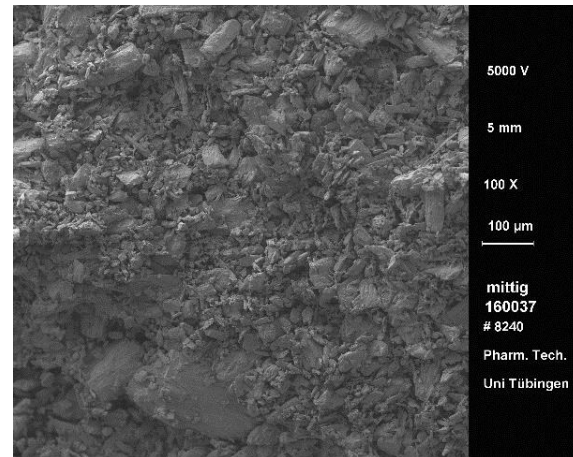


Figure 4-26: SEM picture of Pearlitol® 50 C Lyoc® (Center), 100x magnification.

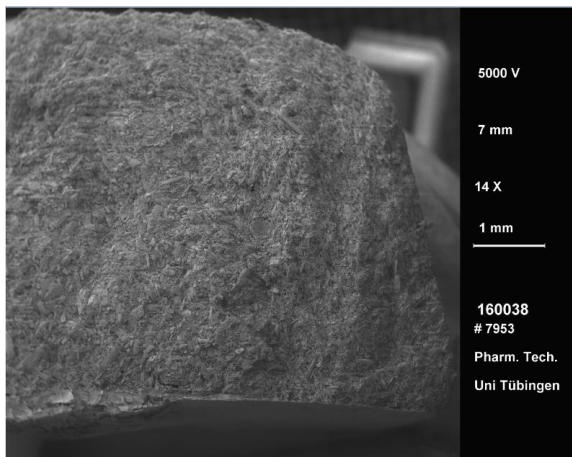


Figure 4-27: SEM picture of Pearlitol® 110 C Lyoc® (Entire structure), 14x magnification.

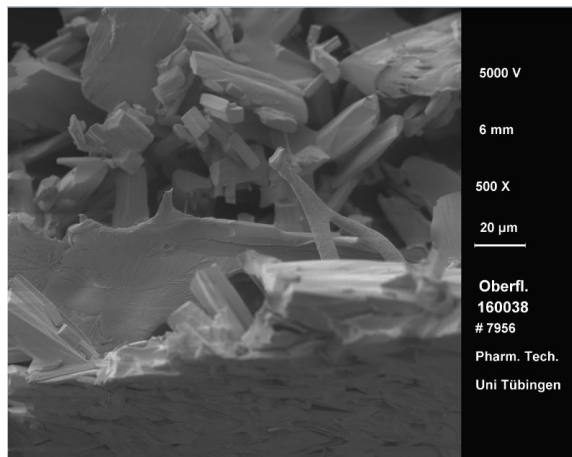


Figure 4-28: SEM picture of Pearlitol® 110 C Lyoc® (Surface), 500x magnification.

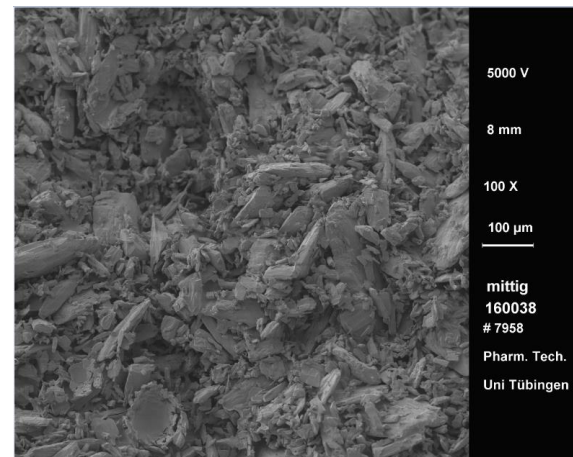


Figure 4-29: SEM picture of Pearlitol® 110 C Lyoc® (Center), 100x magnification.

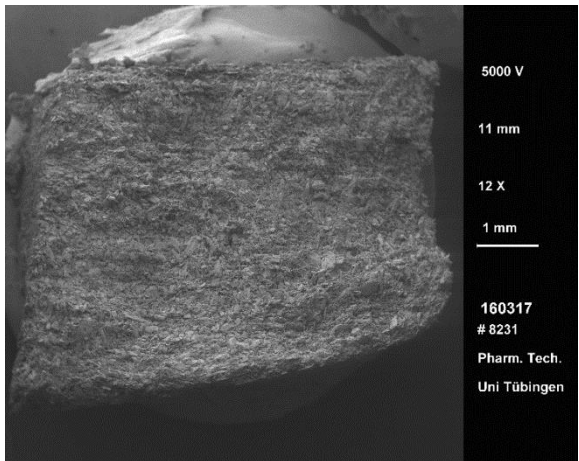


Figure 4-30: SEM picture of Pearlitol® 160 C Lyoc® (Entire structure), 12x magnification.



Figure 4-31: SEM picture of Pearlitol® 160 C Lyoc® (Surface), 100x magnification.

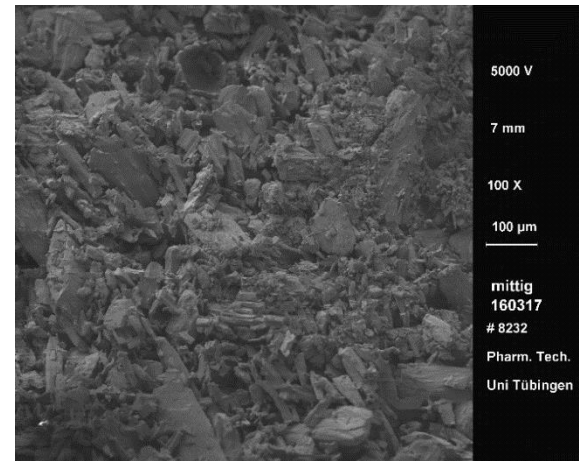


Figure 4-32: SEM picture of Pearlitol® 160 C Lyoc® (Center), 100x magnification.

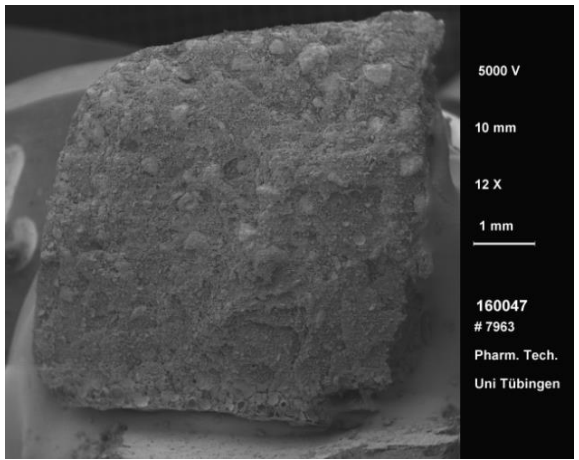


Figure 4-33: SEM picture of Pearlitol® 400 DC Lyoc® (Entire structure), 12x magnification.

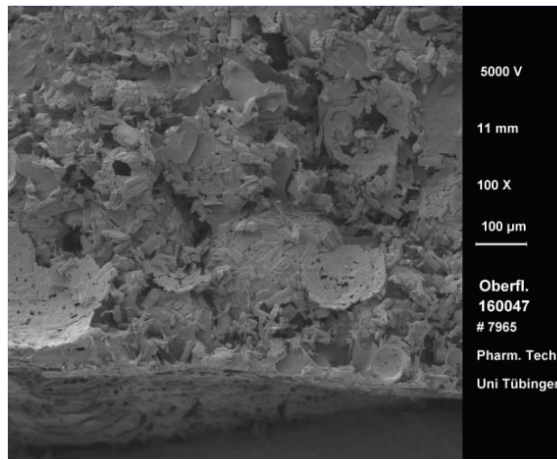


Figure 4-34: SEM picture of Pearlitol® 400 DC Lyoc® (Surface), 100x magnification.

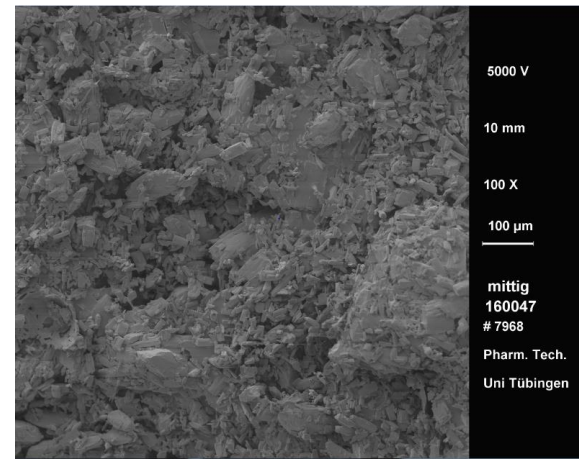


Figure 4-35: SEM picture of Pearlitol® 400 DC Lyoc® (Center), 100x magnification.

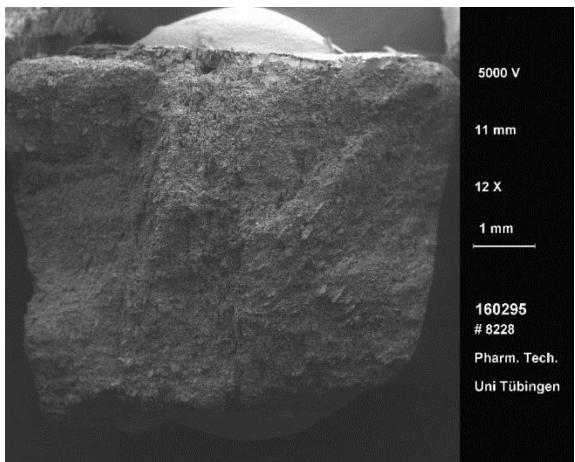


Figure 4-36: SEM picture of Pearlitol® 25/160 C (1+1) Lyoc® (Entire structure), 12x magnification.

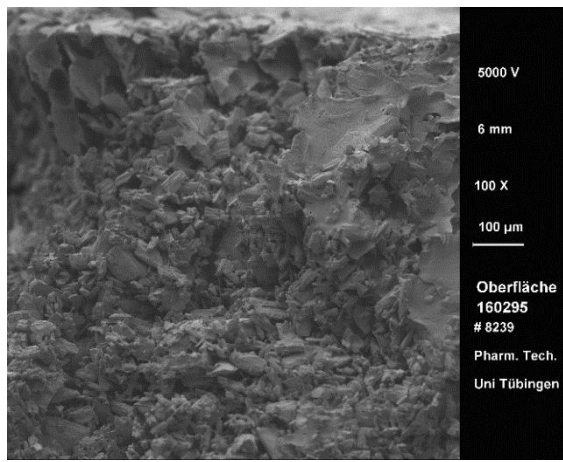


Figure 4-37: SEM picture of Pearlitol® 25/160 C (1+1) Lyoc® (Surface), 100x magnification.

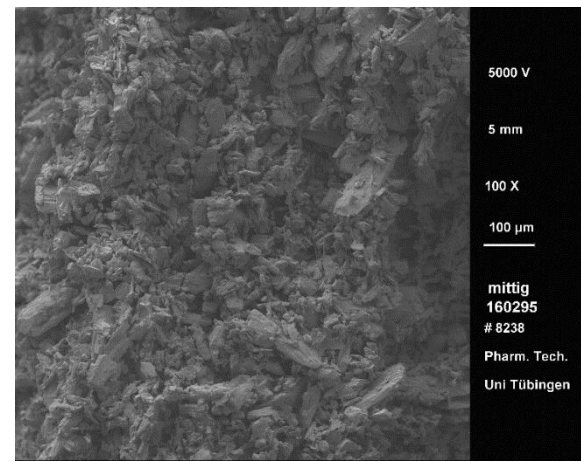


Figure 4-38: SEM picture of Pearlitol® 25/160 C (1+1) Lyoc® (Center), 100x magnification.

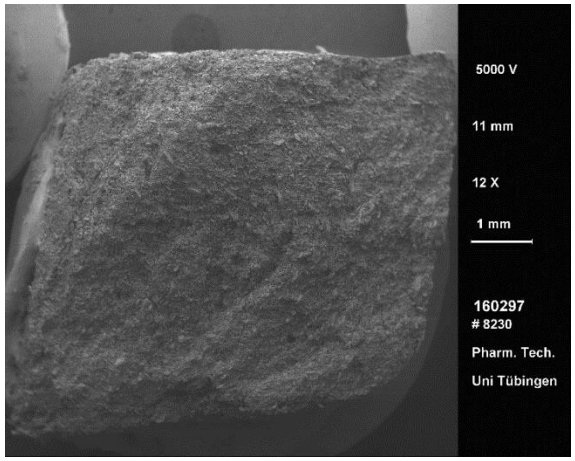


Figure 4-39: SEM picture of Pearlitol® 25/160 C (1+3) Lyoc® (Entire structure), 12x magnification.

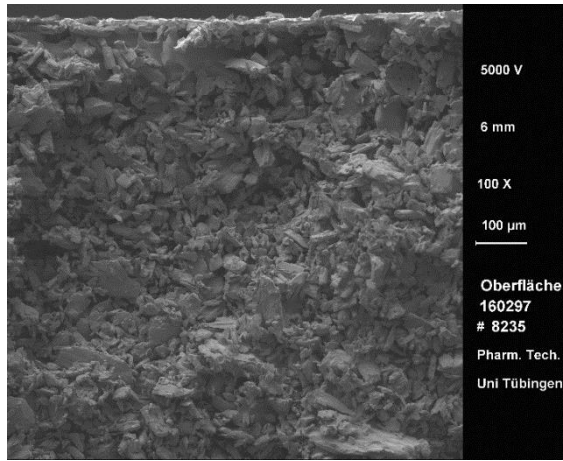


Figure 4-40: SEM picture of Pearlitol® 25/160 C (1+3) Lyoc® (Surface), 100x magnification.

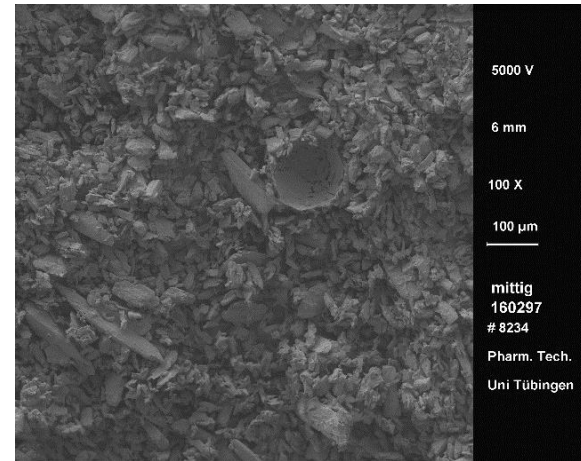


Figure 4-41: SEM picture of Pearlitol® 25/160 C (1+3) Lyoc® (Center), 100x magnification.

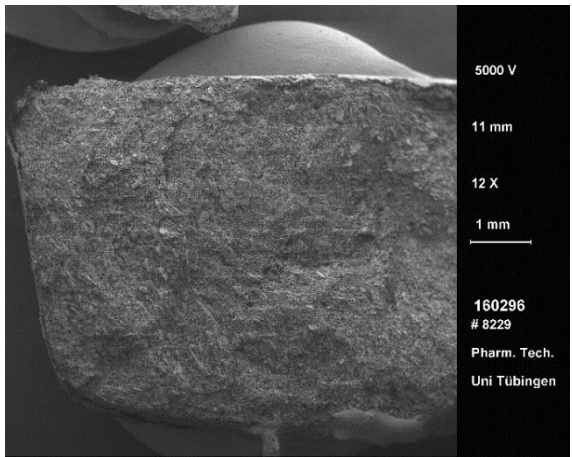


Figure 4-42: SEM picture of Pearlitol® 25/160 C (3+1) Lyoc® (Entire structure), 12x magnification.

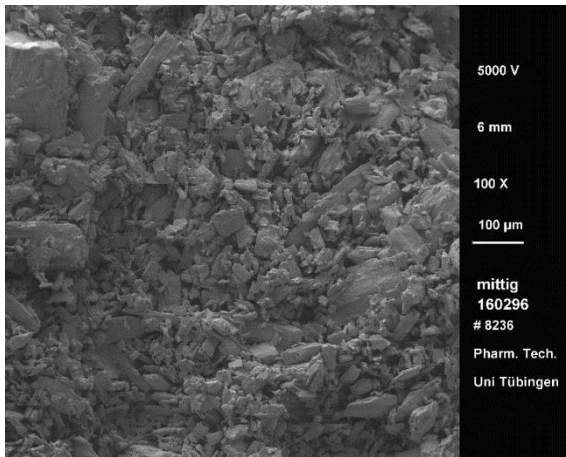


Figure 4-43: SEM picture of Pearlitol® 25/160 C (3+1) Lyoc® (Surface), 100x magnification.

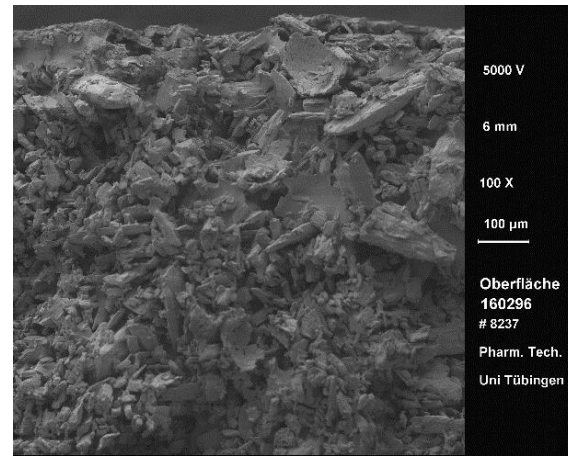


Figure 4-44: SEM picture of Pearlitol® 25/160 C (3+1) Lyoc® (Center), 100x magnification.

4.1.3.2.6 Porosity of Lyocs®

The porosity of the Lyocs® produced in the chapter 4.1.3.2.4 was measured as described in the Section 3.2.5.8 and calculated by means of the equation given in the U.S. patent 20100080829 A1 (Dulieu et al., 2010), as explained in the Section 3.2.5.8:

$$\text{Porosity [%]} = \frac{\text{Volume of water per Lyoc®}}{\text{Volume pipetted}} \cdot 100$$

Indeed, the porosity of the Lyoc® is resulting from the sublimated water, which corresponds to the percentage of water present in the dosage form before lyophilization.

Table 4-20: Porosity measurements of the different Lyocs® (n=5) vs. porosity estimation.

	Porosity measured [%]	Porosity calculated [%]	% error
Spasfon 80 Lyoc®	52,1	53,5	2,7
Pearlitol® 25 C	56,7	55,0	3,0
Pearlitol® 50 C	53,6	55,0	2,6
Pearlitol® 110 C	56,9	55,0	3,3
Pearlitol® 160 C	58,9	55,0	6,6
Pearlitol® 25/160 C (3+1)	58,8	55,0	6,5
Pearlitol® 25/160 C (1+1)	58,4	55,0	5,8
Pearlitol® 25/160 C (1+3)	58,6	55,0	6,1

Table 4-20 summarizes the porosity results of the different Lyoc® formulations. The porosity values vary between 52 % and 59 %, compared to 80 % for the Zydis® technology (Kearney, 2002). This huge difference is due to the structural aspect of the two different products: Zydis® products are composed of a low concentration of diluent, leading to a low intrinsic mechanical strength and a high porosity (Kearney, 2002), unlike Lyoc® products which are produced with a high diluent concentration.

The % error between the measured porosity and the calculated one are lower than 5% for Pearlitol® 25 C Lyocs®, Pearlitol® 50 C Lyocs® and Pearlitol® 110 C Lyocs®.

The % error of the formulations containing Pearlitol® 160 C is in fact higher than 5 %, but the measured porosity is still relatively close to the theoretical one. The formula used to calculate the porosity of Lyocs® seems thus suitable for the estimation of the product porosity once the formulation is determined.

The higher measured porosity of formulations containing Pearlitol® 160 C could result to a lower D.T. Nevertheless, this trend could not be noticed in the D.T tests. This could be due to the fact that during the D.T, some Lyocs® are sticking to the disks, which hinders the Lyocs® to disintegrate properly.

4.1.4 Conclusion

A first selection of excipients and a determination of their range of use could be set through this first study.

It could be concluded that the favorite diluent regarding production efficiency and tolerance was mannitol. Among all the different types of mannitol available on the market (i.e. crystalline, spray-dried and thermal granulated), only the crystalline one is suitable to the Lyoc® technology, with a particle size lower than 160 µm in order to prevent a gritty sensation in mouth during Lyoc® administration. Mixtures of Pearlitol® C grades, and more precisely Pearlitol® 25 C and 160 C, could be successfully processed, bringing several advantages to the formulations:

- it avoided the high viscosity problem encountered for the formulation containing Pearlitol® 25 C alone,
- it gave to the product an extra cooling and smooth effect due to Pearlitol® 25 C,
- it prevented the sandy mouth feeling encountered for the formulation containing Pearlitol® 160 C alone,
- it gave to the resulting suspension a higher viscosity without using an extra viscosity enhancer,
- does not require a special grade but can use two regular commercial grades.

Regarding binders, diverse water-soluble polymers are appropriated for the Lyoc® technology, especially dextran, dextlates and povidone with a proportion Diluent/Binder up to 90 %/10 % w/w of the dried mass in lyophilized tablets. Over 10 %, the resulting lyophilized tablet will be too hard because of the cohesion built up by the binding agent, leading to a high disintegration time (Blonde, 1974). HPMC and maltodextrin can be used up to 5 % because of their viscosity enhancer properties (Rowe et al., 2009).

4.2 Influence of Binder on Suspension and Lyoc® (DoE)

DoE systems are increasingly used in pharmaceutical development, not only for formulation optimization, but also for process optimization, allowing development activities as cheapest as possible. Indeed, all responses are evaluated by varying each factor with as fewer experiments as possible. The goal of carrying out a DoE was to figure out if it is possible to determine an optimized formulation of Lyocs®. Indeed, the IPCs ranges are so broad that it might only be possible to find out the Design Space of a formulation without being able to optimize it. Moreover, the challenges present in formulation development of Lyocs® are very high, since Lyocs® have to be hard enough to be handled by the patient without breaking while at the same time the disintegration time should stay lower than 30 sec; the viscosity of the suspension has to be as low as possible in order to be able to be pumped while at the same time avoiding sedimentation. Two DoEs were performed using mannitol as diluent. In the first DoE, hypromellose was used as binder. Indeed, it was previously noticed that using a too high concentration of hypromellose could cause some pipetting problems because of the high viscosity of the resulting suspensions (see Section 4.1.3.1.2). The second DoE was made with dextran, which is used as binder in the marketed products. The JMP® Software was used to build up the DoEs and to analyze the resulting data. The “Custom Design” function in JMP® was used in order to get a tailor-made design meeting the specific requirements.

4.2.1 DoE Mannitol/Hypromellose

4.2.1.1 Definition of Formulation Factors and Responses

The three variables in the system were the concentration of Pearlitol® 110 C, hypromellose and water. Based on the previous pre-formulation tests (see Section 4.1.3.1.2), the ranges of the factors were firstly determined. The next step was to define which responses could be important and relevant to define and treat correctly this system. Viscosity η , degree of sedimentation F, hardness H and disintegration time D.T were determined as being the determining responses of the system. Table 4-21 summarizes the complete variables and responses of the studied system.

Table 4-21: Definition of the factors and responses of the DoE system Mannitol / Hypromellose / Water.

Factors	Factors level	
	Low	High
Mannitol	36 % \Leftrightarrow 432 mg	61 % \Leftrightarrow 732 mg
Hypromellose	0,5 % \Leftrightarrow 6 mg	3 % \Leftrightarrow 36 mg
Water	36 % \Leftrightarrow 432 mg	61 % \Leftrightarrow 732 mg
Responses	Response Target Range	
Viscosity η [mPa.s]	$50 < \eta < 600$ mPa.s	
Degree of sedimentation F	$0,85 < F < 1$	
Hardness H [N]	$27 < H < 80$ N	
Disintegration time D.T [s]	$D.T < 30$ s	

4.2.1.2 DoE Trial

A total of 12 runs with one center point (F4) and a 2nd term interactions were generated and summarized on Figure 4-45 and 4-46:

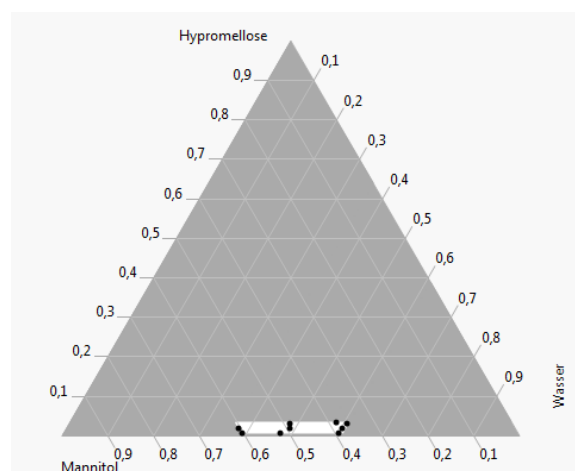


Figure 4-45: Ternary plot of the DoE Mannitol / Hypromellose / Water.

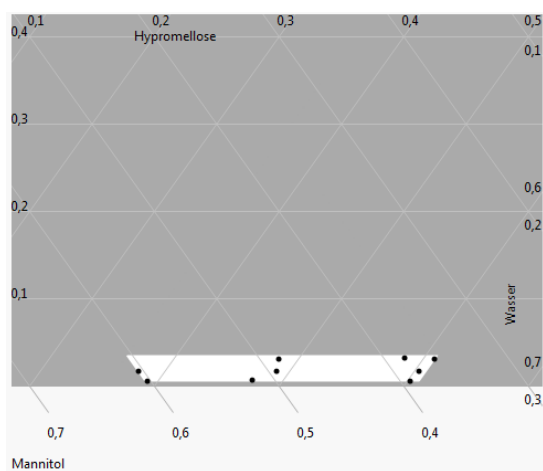


Figure 4-46: Zoom on Figure 4-45.

Table 4-22 represents the 12 formulations of the DoE Mannitol / Hypromellose / Water in mg/dose.

Table 4-22: DoE formulations.

Substance	mg / dose											
	F1	F2	F3	F4	F5	F6	F7	F8	F9	F10	F11	F12
Batch Nr	150447	150448	150449	150450	150451	150452	150453	150454	150455	150456	150457	150458
Mannitol <i>SAP-Nr 245445</i>	582	454,8	470,4	591,6	723,6	732	732	723,6	432	724,8	470,4	432
Hypromellose <i>SAP-Nr 16458</i>	36	20,4	6	20,4	6	36	36	6	36	20,4	6	36
Water <i>SAP-Nr 14022</i>	582	724,8	723,6	588	470,4	432	432	470,4	732	454,8	432	660
Total	1200	1200	1200	1200	1200	1200	1200	1200	1200	1200	908,4	1128

Table 4-23: IPC results from F1-F12, \pm SD.

IPC results												
	F1	F2	F3	F4	F5	F6	F7	F8	F9	F10	F11	F12
η [mPa.s]	225	22	10	68	182	1770	1770	182	52	523	19	64
F	0,96	0,72	0,5	0,94	0,9	1	1	0,92	0,84	0,98	0,86	0,96
Sedimentation in FD	No	Yes	Yes	No	No	-	-	No	Yes	No	Yes	No
H [N], n=20	43 \pm 11	22 \pm 3	10 \pm 4	38 \pm 6	10 \pm 10	-	-	10 \pm 16	48 \pm 10	50 \pm 11	10 \pm 3	48 \pm 5
D.T [s], n=6	16 \pm 8	5 \pm 6	5 \pm 3	16 \pm 5	9 \pm 2	-	-	9 \pm 2	20 \pm 9	51 \pm 24	5 \pm 2	21 \pm 7

120 Lyocs® were produced per batch. This is why the batch size of the dried substances was set up at 150g. The Lyocs® were manufactured and controlled like described in the section 3.2. IPCs are summarized in Table 4-23.

A first approach could be performed before a statistical analysis of the data:

- F6 and F7 were too viscous and could not be handled. It could be conclude that the ratio $\frac{\text{Hypromellose}}{\text{Water}}$ has to stay below 8,3 % in order to have a suitable viscosity. Those two batches were excluded from the DoE as they could not give any experimental results.
- Regarding H values, 6 mg per Lyoc® of hypromellose was defined to be too low to provide the Lyocs® a sufficient hardness.
- When the amount of water is above 660 mg per Lyoc® (F2, F3 and F9), the suspension settles down in the freeze-dryer during the freezing step. It was noticed that when the suspension settles down in the freeze-dryer, the resulting Lyocs® are powdery after unpacking. As a consequence, the sedimentation of the suspension during the freezing step has to be controlled very carefully.
- F2, F3, F9 and F11 gave powdery Lyocs® due to the sedimentation of the suspension in the freeze-dryer. A detailed statistical analysis need to be performed in order to define through which factor sedimentation occurs during the freezing step.
- F1, F4, F5, F8, F10 and F12 had a very good visual aspect.

4.2.1.3 Statistical Analysis

Each response was analyzed individually in order to determine how well the statistical model fits the response data. The model was considered as fitted when the R² and R²Adj values were

near to 1. A fitted least squares model was then used to determine the effect of each factor on each response. Factors with t-values $< 0,05$ were considered as statistically significant.

4.2.1.3.1 Study of the Viscosity Response

The predicted plot of the viscosity (Figure 4-47) shows a very good fitting of the model, since $R^2=0,998$.

After analyzing the Sorted Parameter Estimates table, several statistically significant factors and interactions were observed for the viscosity. Hypromellose (t-value $< 0,0001$) and water (t-value = 0,0005) both have a strong influence on the viscosity unlike mannitol (t-value = 0,7924). The Prediction Profiler plot also confirms this trend: the more hypromellose in the system, the more viscous the suspension is. The less water, the more viscous the suspension is. Those results are coherent since the higher the concentration of hypromellose in water, the more viscous the solution through the formation of a gel-structure. Mannitol does not seem to play an influence on the viscosity, as its plot in the Prediction Profiler shows a horizontal line tendency. Significant interactions between mannitol-water (t-value = 0,0002), mannitol-hypromellose (t-value = 0,0022) and hypromellose-water (t-value = 0,0336) were also observed.

The entire viscosity results meet the specifications for each factors within the ranges studied.

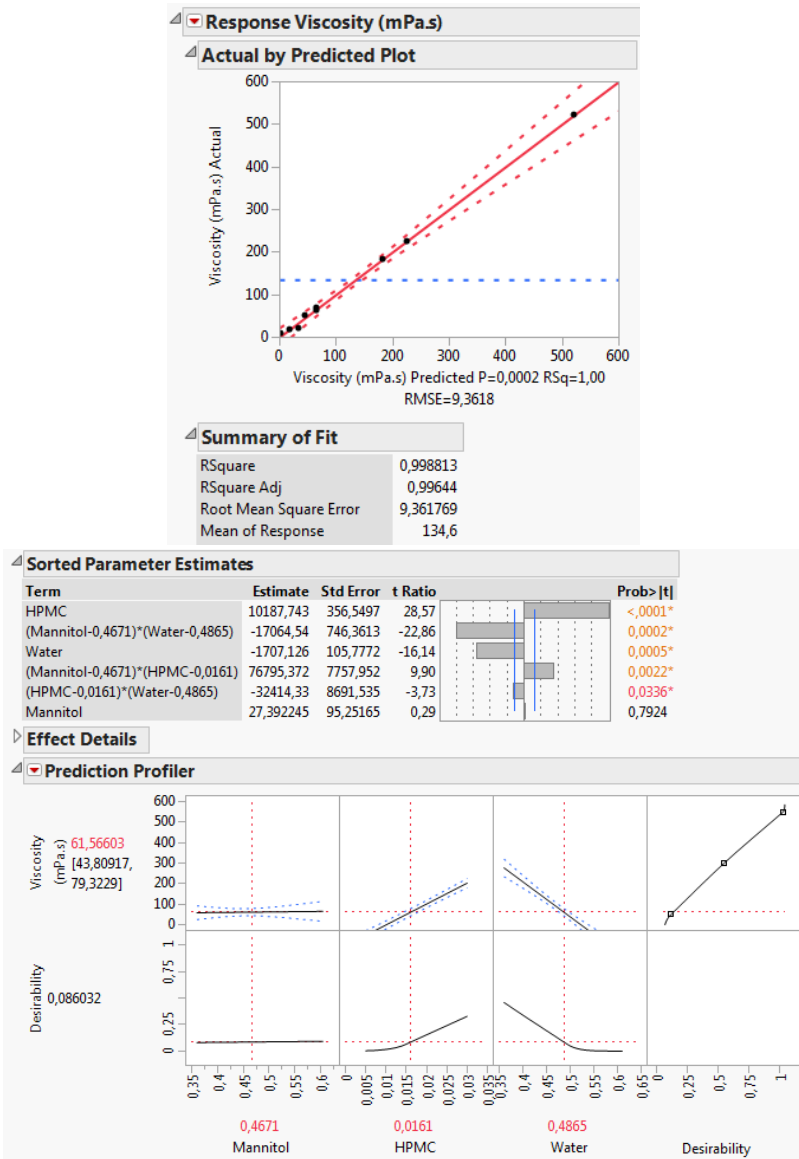
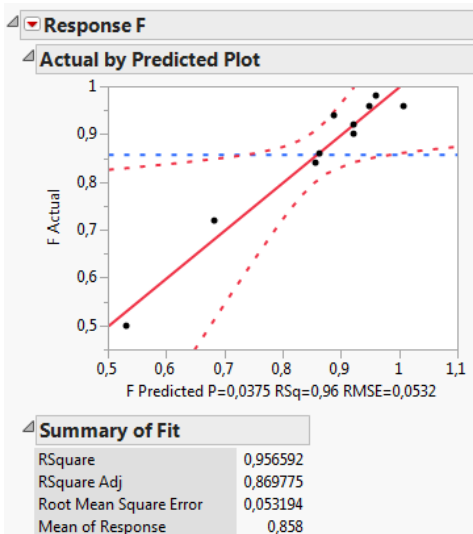


Figure 4-47: Viscosity response parameter estimates.

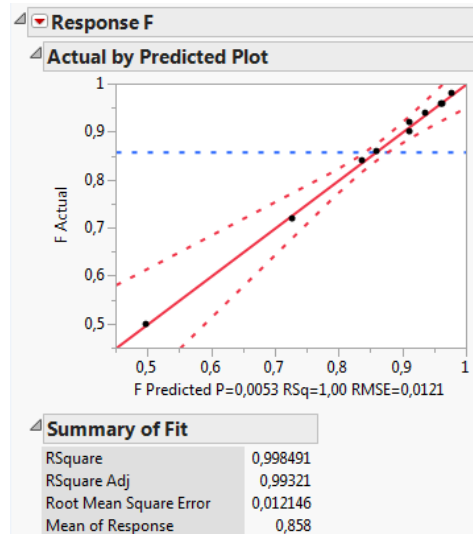
4.2.1.3.2 Study of the F Response

The predicted plot of F (Figure 4-48) shows a proper fitting of the model since $R^2=0.956$. An adjustment of the model through JMP® was still performed (new $R^2=0.998$).

After analyzing the Sorted Parameter Estimates table, several statistically significant factors and interactions were observed for F. Hypromellose ($t\text{-value} = 0,0053$) and water ($t\text{-value} = 0,0067$) seem to have a strong influence on F unlike mannitol ($t\text{-value} = 0,5602$). A significant interaction between hypromellose-water ($t\text{-value} = 0,0143$) was also observed. Quadratic effects of water ($t\text{-value} = 0,0143$) and hypromellose ($t\text{-value} = 0,0225$) on F were also noticed. These results are coherent, since hypromellose builds up a gel structure in water, decreasing the risks of sedimentation. These results are also obviously linked to the one of the viscosity. According to the Prediction Profiler, hypromellose has to stay above 0,6% and water has to stay below 55% in order to stay within the IPCs specifications defined in section 4.2.1.1.



Predicted plot of the response F before fitting the model



Predicted plot of the response F after fitting the model

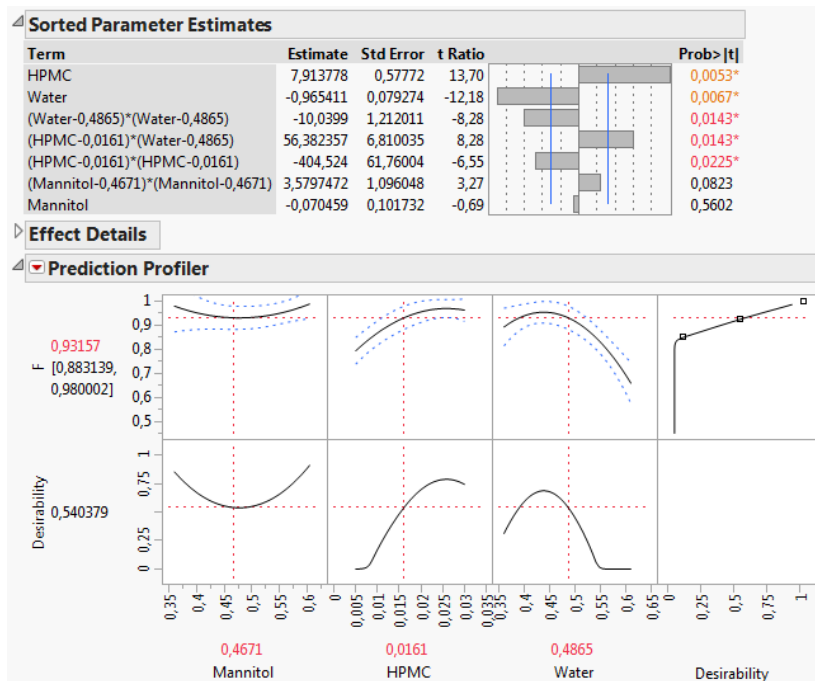
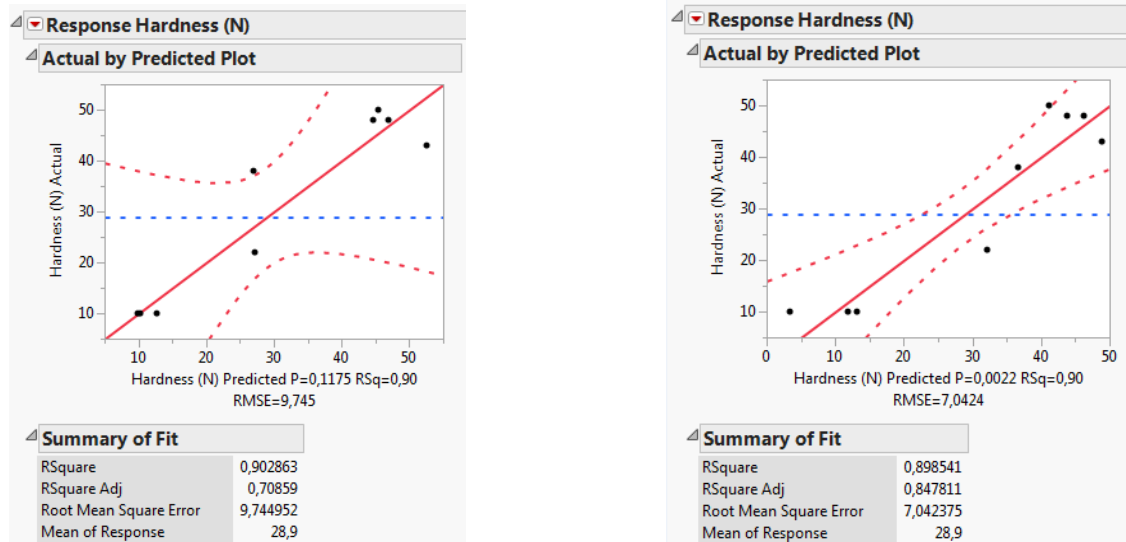


Figure 4-48: F response parameter estimates.

4.2.1.3.3 Study of the Hardness Response

The predicted plot of Hardness (Figure 4-49) shows a correct fitting of the model ($R^2=0,903$). An adjustment of the model through JMP® was possible (new $R^2=0,898$ and R^2_{Adj} improved). After analyzing the Sorted Parameter Estimates table, only hypromellose ($t\text{-value} = 0,0004$) seemed to be statistically significant for the hardness. On the Prediction Profiler plot, it can be detected that the more binder in the formulation, the harder the Lyocs®; and the less water in the formulation, the harder the Lyocs®. Once again, these results are coherent since the less

water in the formulation the less porous are the LyoCS® and the more resilient are the LyoCS®. According to the Prediction Profiler, hypromellose has to stay above 1% in order to have LyoCS® hard enough.



Predicted plot of the response H before fitting the model

Predicted plot of the response H after fitting the model

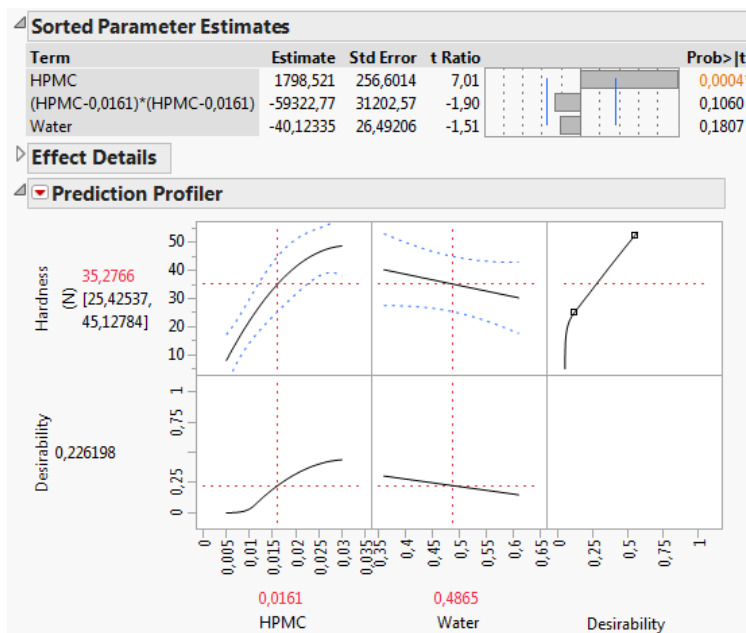
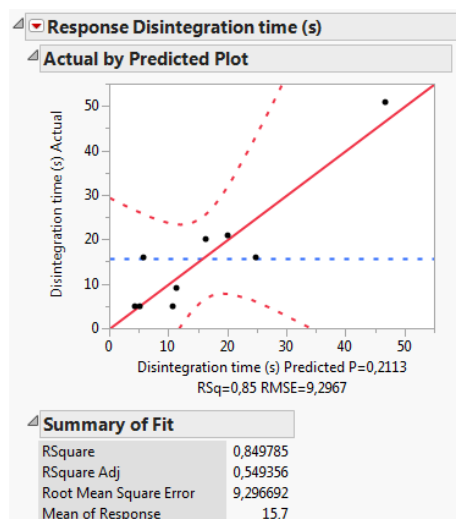


Figure 4-49: H response parameter estimates.

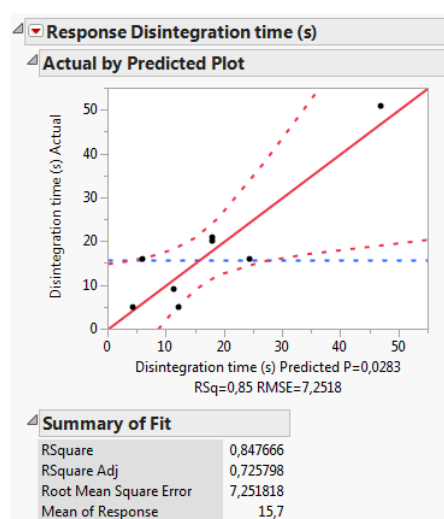
4.2.1.3.4 Study of the Disintegration Time Response

The predicted plot of disintegration time (Figure 4-50) shows a bad fitting of the model ($R^2=0.849$). An adjustment of the model through JMP® was possible (new $R^2=0,847$ and R^2_{Adj} improved).

After analyzing the Sorted Parameter Estimates table, hypromellose (t-value = 0,0058) is significant for the disintegration time. As it is supported in the literature, the Prediction Profiler plot shows that the more binder in the formulation, the slower the disintegration time. Indeed, the binder is bringing cohesion between the particles within the LyoCs®, reinforcing the structure of the LyoCs® and so, increasing the D.T. Mannitol showed to have a quadratic effect (t-value = 0,0214) and mannitol proportion should stay below 58 % in order to have a D.T < 30 sec. An interaction between mannitol-hypromellose (t-value = 0,0226) was also observed. The problem of the technique used for the measurement of the D.T is that the LyoCs® stick sometimes on the disk, which may skew the results. Another quantifying method more appropriate for the ODTs, such as Texture Analyzer, should be used.



Predicted plot of the response D.T before fitting the model



Predicted plot of the response D.T after fitting the model

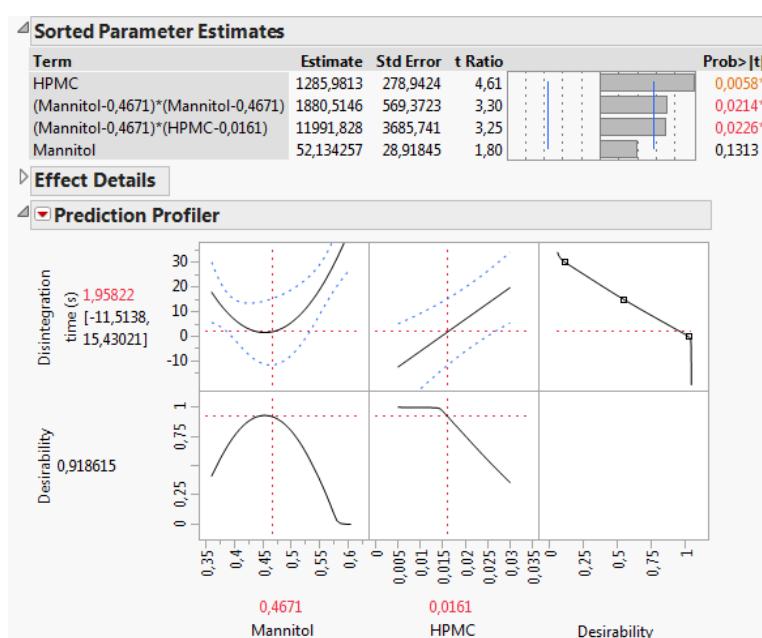


Figure 4-50: D.T response parameter estimates.

After having analyzed the entire statistical results, the Design Space of DoE Mannitol/Hypromellose could be adjusted at: [36 %<Mannitol<58 %], [1 %<HPMC<3 %], [36 %<H₂O<55 %]

4.2.1.3.5 Optimized Formulation

After adjusting individually the model of each response, the tool “Prediction Profiler” of JMP® could calculate the optimized formulation. Figure 4-51 summarizes the prediction values of each response for the optimized formulation, by maximizing the desirability function of each response.

Table 4-24: Optimized formulation converted in mg/dose.

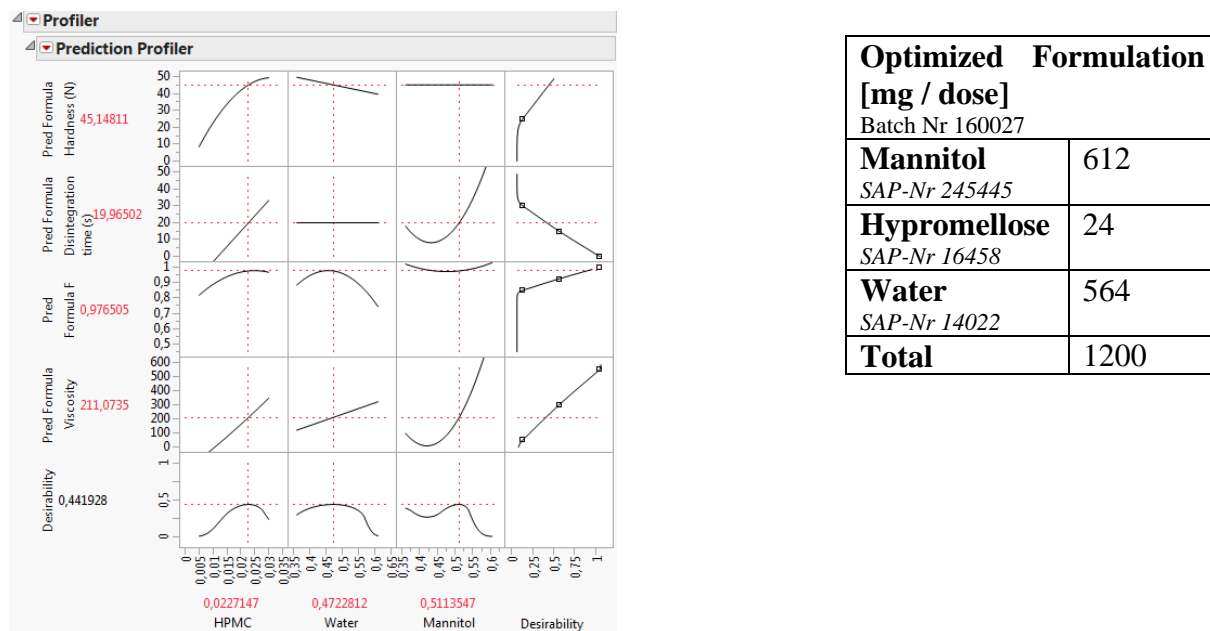


Figure 4-51: Optimized formulation of the DoE Mannitol / Hypromellose / Water in %.

Lyocs® composed with optimized formulation summarized in Table 4-24 were produced to check if the predicted values fitted with the experimental responses. Table 4-25 summarizes the IPC results of the predicted and the actual parameter values.

Table 4-25: IPC results of the optimized formulations, and difference calculated between the experiment results and the predicted results ($\Delta \pm SD$).

IPC results	Predicted	Measured	Difference Δ
Viscosity [mPa.s], n=1	211	209	$\Delta\eta = 2$ mPa.s
F, n=1	0,98	0,96	$\Delta F = 0,02$
Hardness [N], n=20	45	51±10	$\Delta H = 6$ N
D.T [s], n=6	20	25±10	$\Delta t = 5$ s

The differences between the predicted responses and the experimental responses calculated in Table 4-25 are not significant since they are very low, meaning that the model fits very well.

This DoE not only allowed to determine a Design Space of the different factors of the formulation (especially the min and max values of hypromellose and the maximum ratio of

Hypromellose)_{Water}). It also allowed determining successfully its optimized formulation despite the broad ranges of IPCs.

4.2.2 DoE Mannitol/Dextran

An equivalent DoE study was performed with dextran as binder.

4.2.2.1 Definition of Formulation Factors and Responses

The three variables in the system were the concentration of Pearlitol® 110 C, dextran and water. Based on the previous pre-formulation tests (see section 4.1.3.1.2), the ranges of the factors were firstly set. As previously seen in the section 4.2.1.1, viscosity η , F, the hardness H and the disintegration time D.T were defined as responses. Table 4-26 summarizes the complete factors and responses of the studied system.

Table 4-26: Definition of the factors and responses of the DoE system Mannitol / Dextran / Water.

Factors	Factors level [%]	
	Low	High
Mannitol	40 % \Leftrightarrow 480 mg	60 % \Leftrightarrow 720 mg
Dextran	1,5 % \Leftrightarrow 18 mg	10 % \Leftrightarrow 120 mg
Water	30 % \Leftrightarrow 360 mg	50 % \Leftrightarrow 600 mg
Responses	Response Target Range	
Viscosity η [mPa.s]	$50 < \eta < 600$ mPa.s	
Degree of sedimentation F	$0,85 < F < 1$	
Hardness H [N]	$27 < H < 80$ N	
Disintegration time D.T [s]	$D.T < 30$ s	

4.2.2.2 DoE Trial

A total of 12 runs with one center point (F5) and a 2nd term interactions were generated (see Figure 4-52).

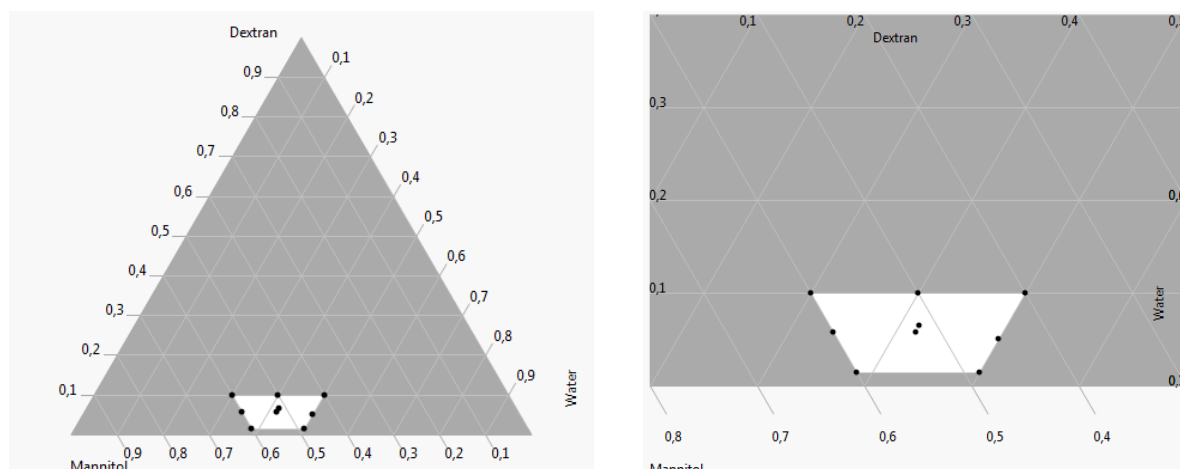


Figure 4-52: Ternary plot of the DoE Mannitol/Dextran / Water and zoomed area.

Table 4-27 represents the 12 formulations of the DoE Mannitol / Dextran / Water in mg/dose.

Table 4-27: DoE formulations.

Substance	mg / dose											
	F1	F2	F3	F4	F5	F6	F7	F8	F9	F10	F11	F12
Batch Nr	160107	160108	160080	160109	160081	160084	160110	160082	160075	160083	160111	160085
Mannitol <i>SAP-Nr 245445</i>	480	720	720	539	629	493	600	720	720	720	582	619
Dextran <i>SAP-Nr 236561</i>	120	69	120	61	69	107	120	120	18	18	18	78
Water <i>SAP-Nr 14022</i>	600	411	360	600	502	600	480	360	462	462	600	503
Total	1200	1200	1200	1200	1200	1200	1200	1200	1200	1200	1200	1200

Table 4-28: IPC results from F1-F12, \pm SD.

IPC results												
	F1	F2	F3	F4	F5	F6	F7	F8	F9	F10	F11	F12
η [mPa.s]	100	1250	2130	56	248	93	594	-	94	226	27	272
F	0,96	1	1	0,98	0,99	0,98	1	-	1	1	0,8	0,99
Sedimentation in FD	No	No	No	No	No	No	No	-	No	No	Yes	No
H [N], n=20,	136 \pm 52	96 \pm 14	179 \pm 27	73 \pm 30	87 \pm 20	64 \pm 19	130 \pm 27	-	45 \pm 8	70 \pm 13	38 \pm 7	120 \pm 25
D.T [s], n=6	19 \pm 2	37 \pm 10	46 \pm 11	5 \pm 2	13 \pm 3	13 \pm 1	27 \pm 10	-	11 \pm 1	7 \pm 4	11 \pm 1	28 \pm 8

120 Lyocs® were produced per batch. This is why the batch size of the dried substances was set up at 150g. The Lyocs® were manufactured and controlled like described in the section 3.2. IPC results are summarized in Table 4-28.

A first approach could be performed before analyzing statistically the data:

- The more dextran, the harder are the Lyocs® which is an advantage for the product handling by the patient, but the longer the disintegration time.
- F3 and F8 were too viscous. Lyocs® could barely be produced for F3 and could not be produced for F8. F8 was thus excluded from the DoE as it could not give any experimental results.
- F11 gave powdery Lyocs® due to the sedimentation of the suspension during the freezing step.
- F1, F2, F3, F4, F5, F6, F7, F9, F10 and F12 had a very good visual aspect.

4.2.2.3 Statistical Analysis

The same statistical analysis was carried on as in the section 4.2.1.3, i.e. a model adjustment before determining the optimized formulation. A fitted least squares model was then used to determine the effect of each factor on each response. Factors with t-values $< 0,05$ were considered as statistically significant.

4.2.2.3.1 Study of the Viscosity Response

The predicted plot of the viscosity (Figure 4-53) shows a very good fitting of the model ($R^2=0,994$).

After analyzing the Sorted Parameter Estimates table, several statistically significant factors, quadratic effects and interactions were observed for the viscosity. Mannitol (t-value = 0,0175) and water (t-value = 0,0196) both have a strong influence on the viscosity unlike dextran (t-value = 0,2514). In the DoE Mannitol/HPMC, the binder HPMC had a strong influence on the viscosity. In this case, dextran does not have a strong influence on the viscosity. This is coherent, since HPMC is a viscosity increasing agent unlike dextran. Quadratic effects of mannitol (t-value = 0,0177) and water (t-value = 0,0193) were also seemed to be statistically significant. This means that mannitol interacts with itself, such as water. Those quadratic effects of mannitol and water are detectable on the Prediction Profiler curves:

Interpretation of the quadratic effect of mannitol: since the prediction profiler curve of mannitol is horizontal, mannitol does not have an influence on viscosity until 47.5 %. Beyond 47.5%, the more mannitol present in the formulation, the more viscous is the suspension. This is coherent, since the viscosity is increasing with the concentration of particles in the medium. Significant interactions between mannitol-dextran (t-value = 0,0188) and dextran-water (t-value = 0,0202) were also observed.

The Prediction Profiler plot shows that an increase of mannitol in the suspension from 47.5% leads to an increase of the viscosity, and a decrease of water in the suspension below 48% also leads to an increase of the viscosity. Therefore, mannitol has to stay below 58% and water has to stay up to 38% in order to meet the viscosity range defined in the section 4.2.2.1.

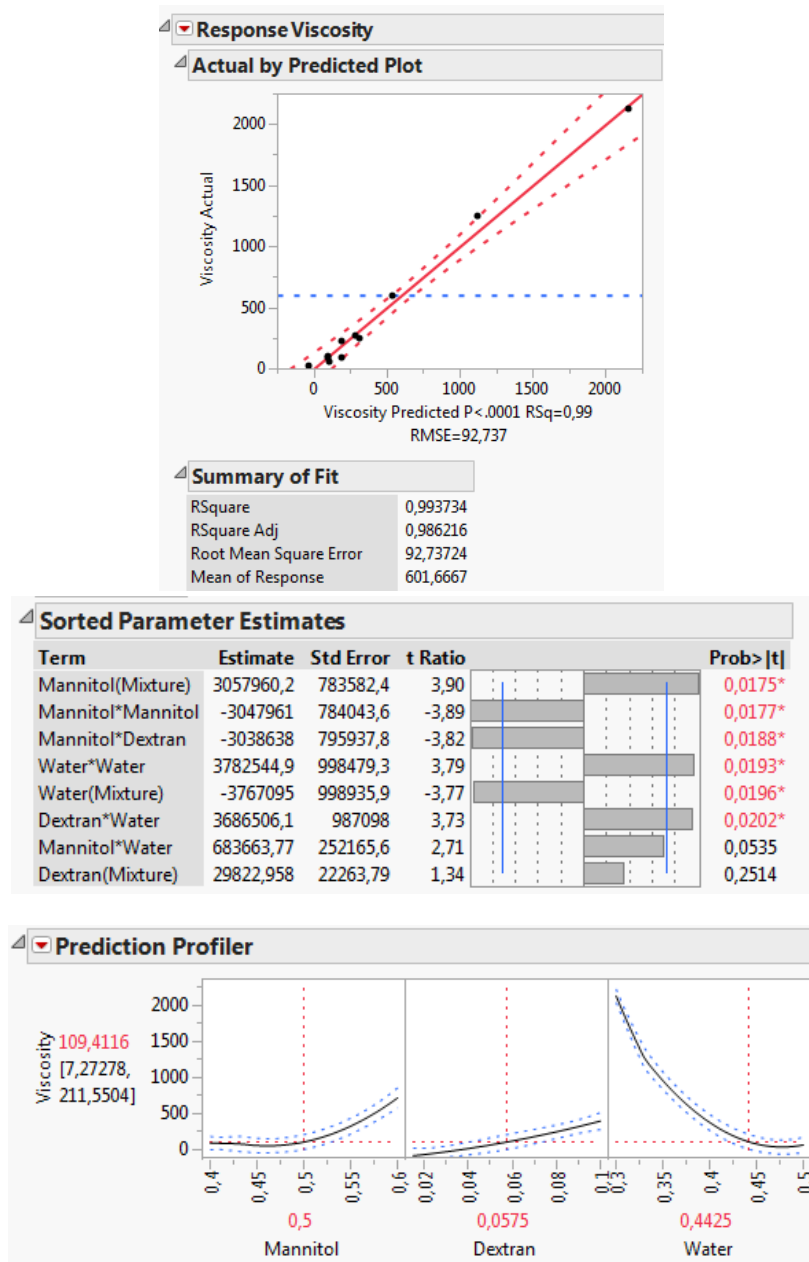
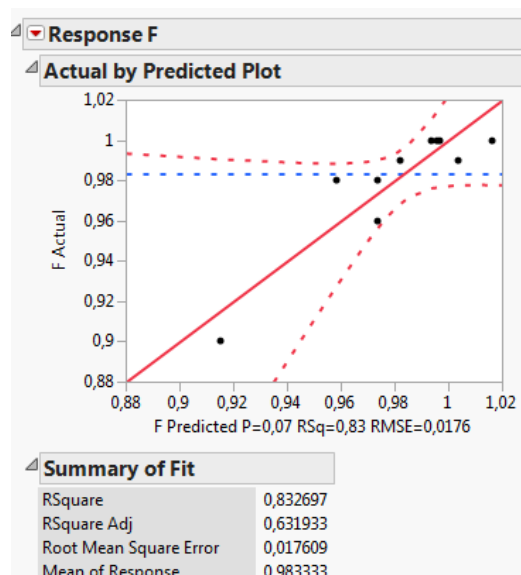


Figure 4-53: Viscosity response parameter estimates.

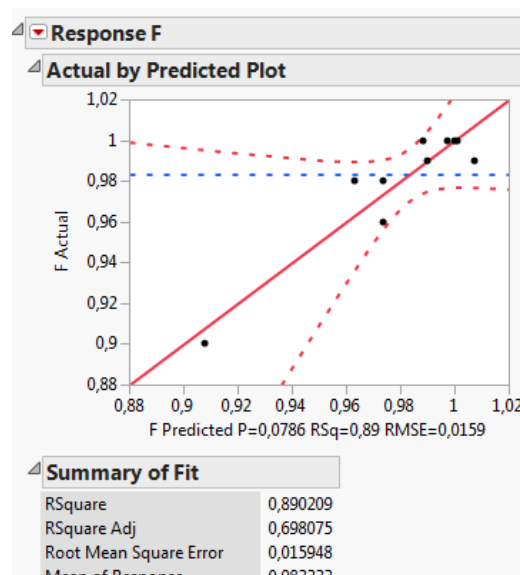
4.2.2.3.2 Study of the F Response

The predicted plot of F (Figure 4-54) shows a bad fitting of the model ($R^2=0.833$). An adjustment of the model through JMP® was possible (new $R^2=0,890$).

After analyzing the Sorted Parameter Estimates table, mannitol (t-value < 0,0001) and water (t-value = 0,0014) seem to have a strong influence on F unlike dextran (t-value = 0,1558). These results are coherent, since dextran does not play any influence on the viscosity of the suspension. The ratio mannitol/water plays here an important role on the viscosity and so on F. The more mannitol is present in the suspension the more viscous is the suspension and the less the suspension settles down. The less water is present in the formulation the more viscous is the suspension and the less the suspension settles down. This trend can also be observed on the Prediction Profiler plot. The results of F and of the viscosity are also linked and match perfectly with the theory. The entire F results met the specifications for each factor within the studied ranges.



Predicted plot of the response F before fitting the model



Predicted plot of the response F after fitting the model

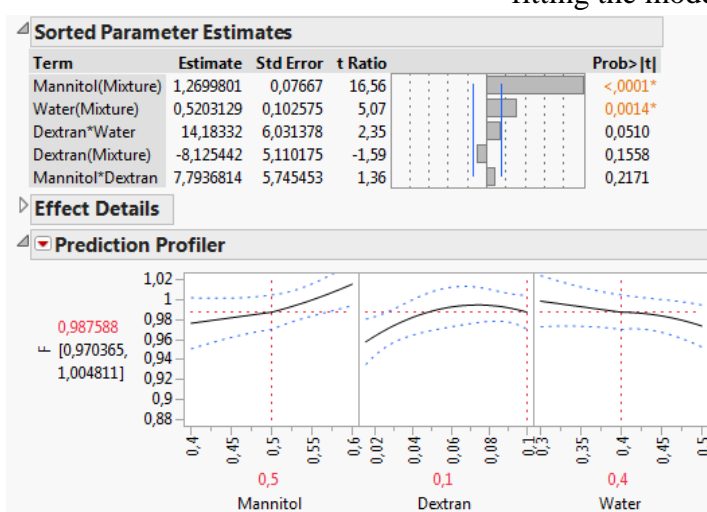
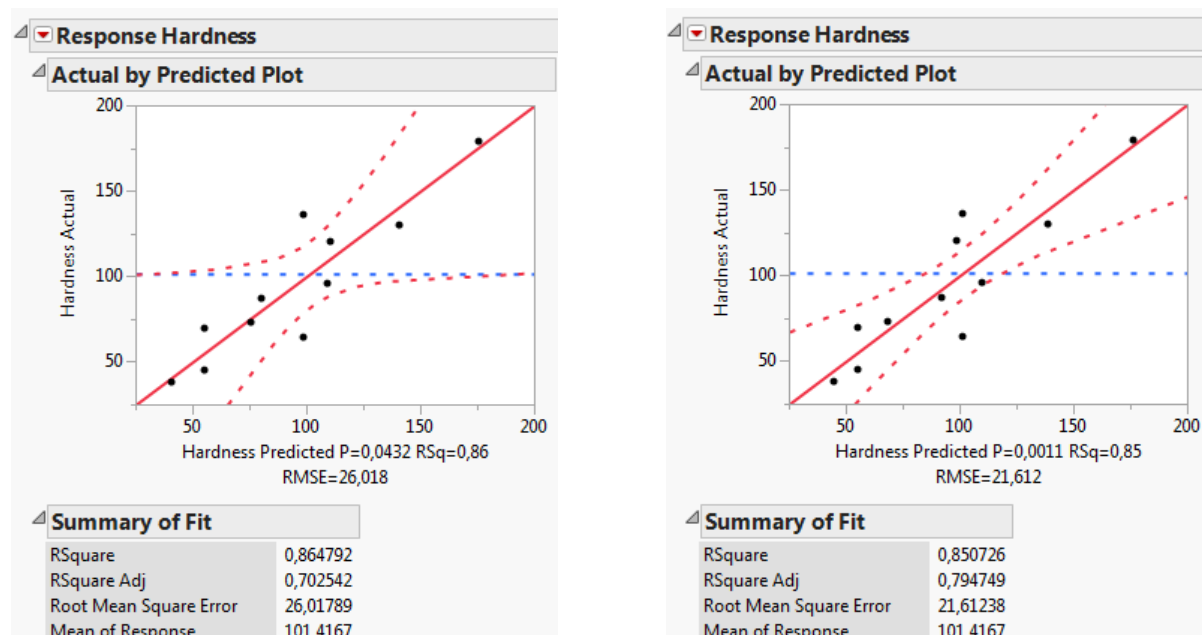


Figure 4-54: F response parameter estimates.

4.2.2.3.3 Study of the Hardness Response

The predicted plot of Hardness (Figure 4-55) shows a bad fitting of the model ($R^2=0.865$). An adjustment of the model through JMP® was possible (new $R^2=0.851$ and $R^2\text{Adj}$ improved). After analyzing the Sorted Parameter Estimates table, only dextran ($t\text{-value} = 0,0009$) and water ($t\text{-value} = 0,0278$) seemed to be statistically significant for the hardness. Once again, these results are coherent. The more binder in the formulation, the harder Lyocs® are. The less water in the formulation the less porous are the Lyocs® and the more resilient are the Lyocs®. This trend can also be seen on the Prediction Profiler plot. The entire hardness results meet the specifications for each factors within the ranges studied.



Predicted plot of the response H before fitting the model

Predicted plot of the response H after fitting the model

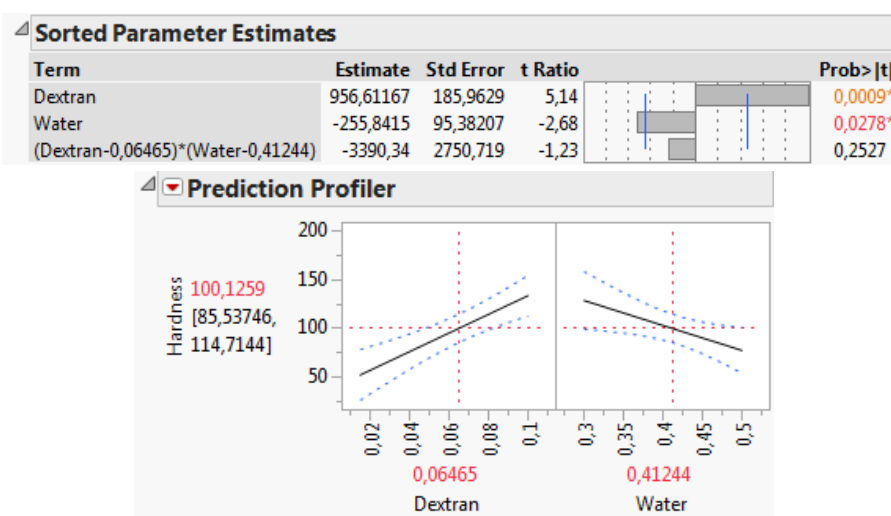


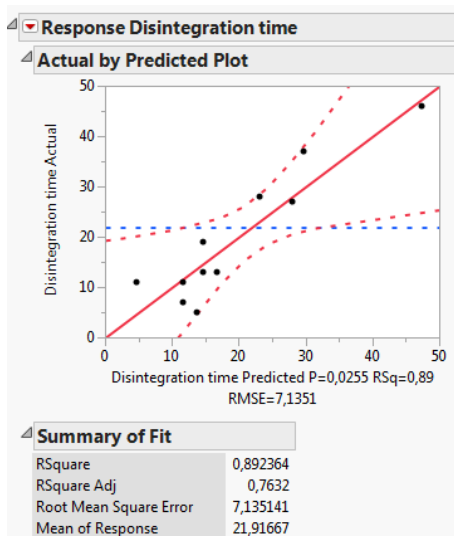
Figure 4-55: H response parameter estimates.

4.2.2.3.4 Study of the Disintegration Time Response

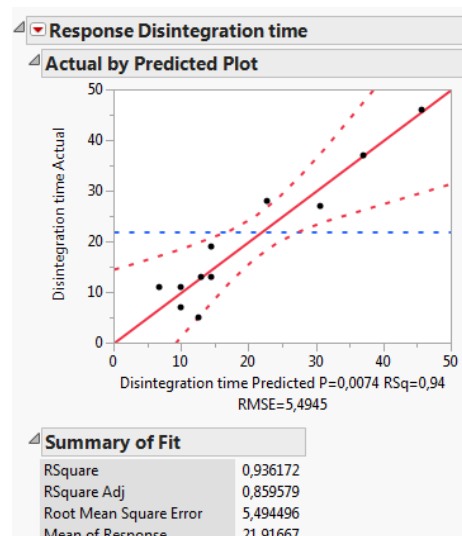
The predicted plot of disintegration time (Figure 4-56) shows a bad fitting of the model ($R^2=0.892$). An adjustment of the model through JMP® was possible (new $R^2=0.936$ and R^2_{Adj} improved).

After analyzing the Sorted Parameter Estimates table, any factors or interactions between factors seemed to be statistically significant for the disintegration time. All the t-values were greater than 0,05. Again, the problem of the disintegration time measurement is that the Lyocs® stick sometimes on the disk, which may skew the results. Another quantifying method more appropriate for the ODTs, such as Texture Analyzer, should be used.

On the Prediction Profiler plot, it can be seen that the less water is present in the formulation, the higher the disintegration time. This again is linked to the porous structure left by the water in the Lyocs® after the drying step. The less water, the less porous Lyocs® are and the most difficult it is for the saliva to penetrate the pores and dissolve the tablet. The more binder and diluent, the slower the disintegration time. Nevertheless, the disintegration time stays within the IPC ranges for the mannitol and dextran studied ranges. Water has to be higher than 33% in order to give enough pores to the Lyocs® and to allow a fast disintegration.



Predicted plot of the response D.T before fitting the model



Predicted plot of the response D.T after fitting the model

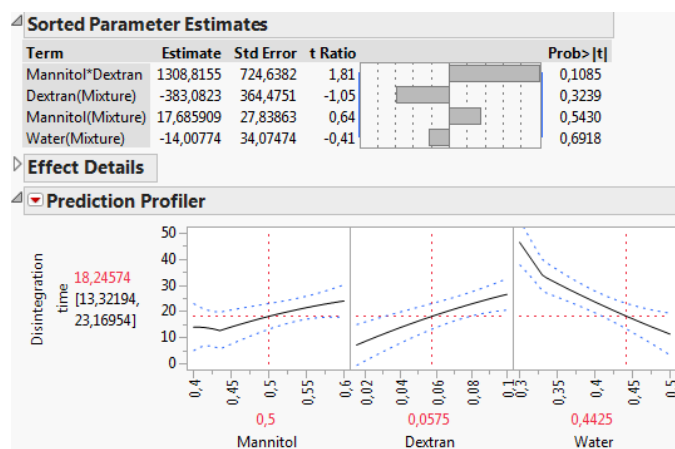


Figure 4-56: D.T response parameter estimates.

After having analyzed the entire statistical results, the Design Space of DoE Mannitol/Dextran could be adjusted at: [40 % < Mannitol < 58 %], [1,5 % < Dextran < 10 %], [38 % < H₂O < 50 %].

4.2.2.3.5 Optimized Formulation

After individually adjusting the model of each response, the tool “Prediction Profiler” of JMP® could calculate the optimized formulation. Figure 4-57 summarizes the prediction values of each response for the optimized formulation, by maximizing the desirability function of each response.

Table 4-29: Optimized formulation converted in mg/dose.

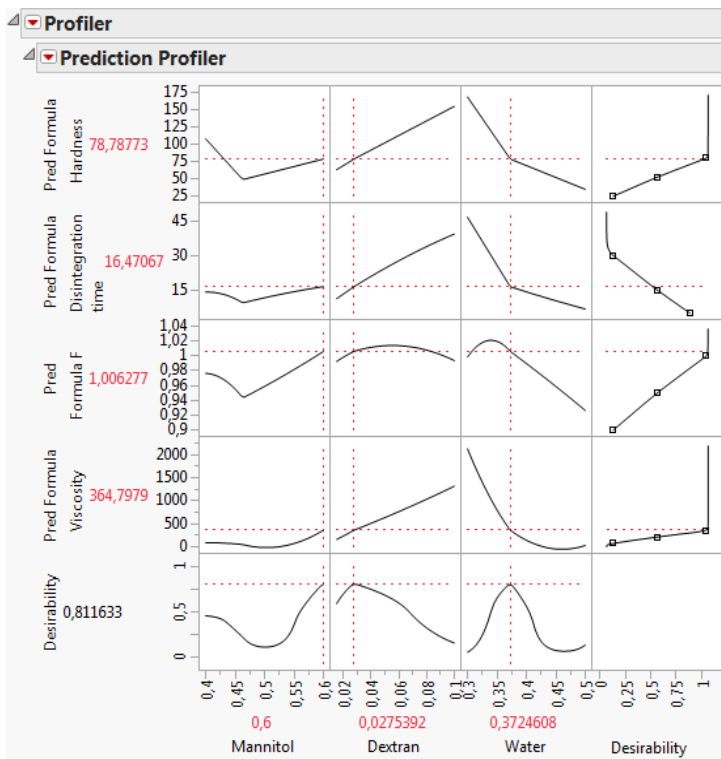


Figure 4-57: Optimized formulation of the DoE Mannitol / Dextran / Water in %.

Lyocs® composed with optimized formulation summarized in Table 4-29 were produced to check if the predicted values fitted with the experimental responses. Table 4-30 summarizes the IPC results of the predicted and the actual parameter values.

Table 4-30: IPC results of the optimized formulations, and difference calculated between the experiment results and the predicted results (Δ , $\pm SD$).

IPC results	Predicted	Measured	Difference Δ
Viscosity [mPa.s], n=1	365	401	$\Delta\eta = 36 \text{ mPa.s}$
F, n=1	1,00	1,00	$\Delta F = 0$
H [N], n=20	79	85 ± 24	$\Delta H = 6 \text{ N}$
D.T [s], n=6	16	10 ± 1	$\Delta t = 6 \text{ s}$

The differences between the predicted responses and the experimental responses calculated in Table 4-30 are not significant since they are very low, which means that the model fits very well. A formulation optimization and a Design Space can also successfully be determined through DoE for the mixture Mannitol/Dextran/Water despite the broad ranges of IPCs.

Optimized Formulation	
[mg/dose]	
Batch Nr 160282	
Mannitol SAP-Nr 245445	720
Dextran SAP-Nr 236561	33
Water SAP-Nr 14022	447
Total	1200

4.3 Influence of water soluble and limited-water soluble APIs on Lyocs®

A question which is raised in the literature is the maximum loading dose of water soluble API in freeze-dried tablets (limit of water-soluble API < 60 mg / dose (Seager, 1998)). It was indeed hypothesized that during the freezing or the drying step of the lyophilization process, water soluble API builds up an amorphous structure within the freeze-dried tablet, which can lead to a damage of the cake structure by collapsing (Seager, 1998). Two water soluble APIs and two limited-water soluble APIs were studied to check this hypothesis (see Table 4-31):

Table 4-31: Water soluble and less-water soluble APIs studied with their respective solubility.

API	According to Ph. Eur. 1.4	Solubility [mg/mL]
Metoclopramide HCl monohydrate <small>SAP-Nr 15372</small>	Very soluble	67 (Selleckchem, 2013)
Metamizol sodium <small>SAP-Nr 17993</small>	Very soluble	500 (Caelo, 2015)
Paracetamol <small>SAP-Nr 251937</small>	Sparingly soluble	14 (TEVA-ratiopharm, 2010)
Sildenafil Citrate <small>SAP-Nr 115199</small>	Slightly soluble	3,5 (TEVA-ratiopharm, 2012)

The problem encountered by using water-soluble API in the formulation is that from a specific amount of API, the Lyocs® are exploding in the freeze-dryer due to a loss of their structure. First of all, the limit dose of water-soluble API was figured out. The resulting Lyocs® having a good quality were then analyzed with X-ray powder diffraction with the method described in Section 3.2.5.6, to determine if the water soluble APIs build up an amorphous structure within Lyocs® during lyophilization.

In this section, only the hardness and the disintegration time were measured for the IPC tests. The formulation of the model drug in terms of amount of excipients was used in this chapter.

4.3.1 Study on Water-Soluble APIs

4.3.1.1 Metoclopramide HCl Lyocs®

The following formulations summarized in Table 4-32 were produced using metoclopramide HCl monohydrate as API, with a batch size of 150 g on dried substance.

Table 4-32: Composition of the tested formulations containing metoclopramide HCl.

Substance	mg / dose						
	Placebo	F1	F2	F3	F4	F5	F6
Batch Nr	150521	150534	150535	150488	150489	150490	150491
Metoclopramide HCl <i>SAP-Nr 15372</i>	0	50	100	110	120	130	140
Mannitol <i>SAP-Nr 245445</i>	715	665	615	605	595	585	575
Dextran <i>SAP-Nr 236561</i>	25	25	25	25	25	25	25
Water <i>SAP-Nr 14022</i>	550	550	550	550	550	550	550
Total	1290	1290	1290	1290	1290	1290	1290

For F1-F6, the API-water mixture was completely transparent, which means that the API was completely solved in water. The Metoclopramide HCl Lyocs® exploded beyond 140 mg API / dose. The maximal API load is thus evaluated at 18 % on the dried mass of Lyocs®. Table 4-33 summarizes the H and D.T of the tested formulations.

Table 4-33: IPC results of the tested formulations, \pm SD.

IPC results							
	Placebo	F1	F2	F3	F4	F5	F6
H [N], n=20	66 \pm 21	109 \pm 24	108 \pm 15	99 \pm 19	109 \pm 15	96 \pm 13	100 \pm 20
D.T [s], n=6	15 \pm 2	4 \pm 2	7 \pm 6	5 \pm 1	3 \pm 0	4 \pm 2	5 \pm 0

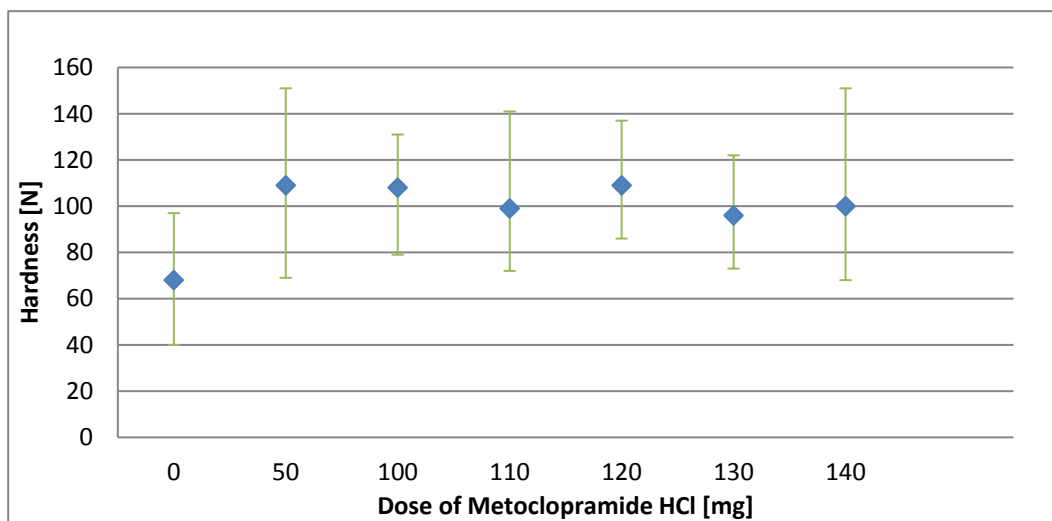


Figure 4-58: Hardness average with min and max values (n=20).

No significant influence of the quantity of metoclopramide HCl in the formulation was noticed on the hardness of the resulting Lyocs® represented on Figure 4-58. This means that the Lyocs® are losing their structure from a certain amount of metoclopramide HCl within the Lyoc®, since a concentration beyond 140 mg of metoclopramide HCl led to a Lyoc® explosion during the sublimation step. The D.T of the Lyocs® is also decreasing as soon as API is present

in the formulation (see Table 4-33), meaning that the API is lowering the cohesion between the substances within the tablets, allowing the Lyocs® to disintegrate faster.

Metoclopramide HCl 100 mg Lyoc® and the respective raw materials of its formulation were firstly analyzed by means of DSC in order to determine the solid state of metoclopramide HCl within Lyocs® after the lyophilization process. Figure 4-59 represents the crystalline structure of Pearlitol® 110 C through the presence of a sharp melting peak at 167,93 °C (n=3). Figure 4-60 represents the crystalline structure of metoclopramide HCl through the presence of a sharp melting peak at 185,83 °C (n=3). The first 3-peak pattern (between ca. 60 °C and 115 °C) could be due to the loss of HCl gas or of water. A TGA analysis of metoclopramide HCl revealed that metoclopramide loses a half molecule of water per mol of metoclopramide (see Annex 6.2.1), meaning that metoclopramide HCl forms a hemihydrate after lyophilization.

Figure 4-61 represents a superposition of the thermograms of Metoclopramide HCl 100 mg Lyoc® (black), mannitol (red), and metoclopramide HCl (green). The thermogram of the Metoclopramide HCl 100 mg Lyoc® only has a crystalline peak similar to the one of the mannitol pattern, with a slight shift probably due to a polymorphic change of mannitol transforming the β form to either α or δ after lyophilization, like already observed by Alexandre Kim (Kim et al., 1998). Indeed, Alexandra Kim brought to light the transformation of mannitol polymorphism as function of freezing rate ($\beta \rightarrow \alpha + \beta$ in the case of slow freezing and $\beta \rightarrow \delta$ for fast freezing). A melting peak of metoclopramide HCl is not notable on the black curve, which could be explained by the fact that metoclopramide HCl is getting amorphous during lyophilization. The solid state of metoclopramide HCl after lyophilization will be further study by XRPD.

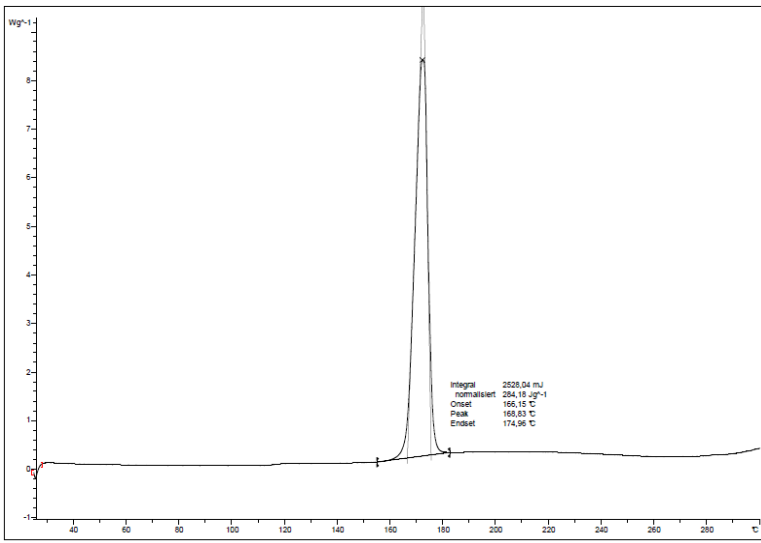


Figure 4-59: DSC thermogram of mannitol.

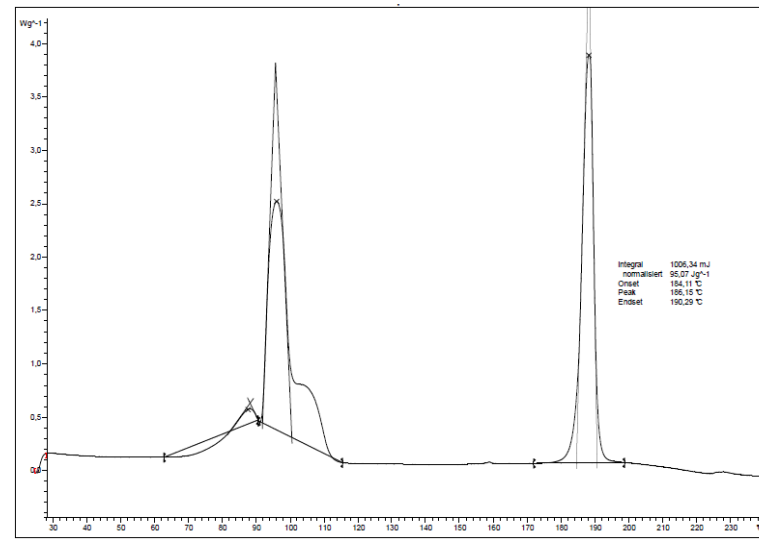


Figure 4-60: DSC thermogram of metoclopramide HCl.

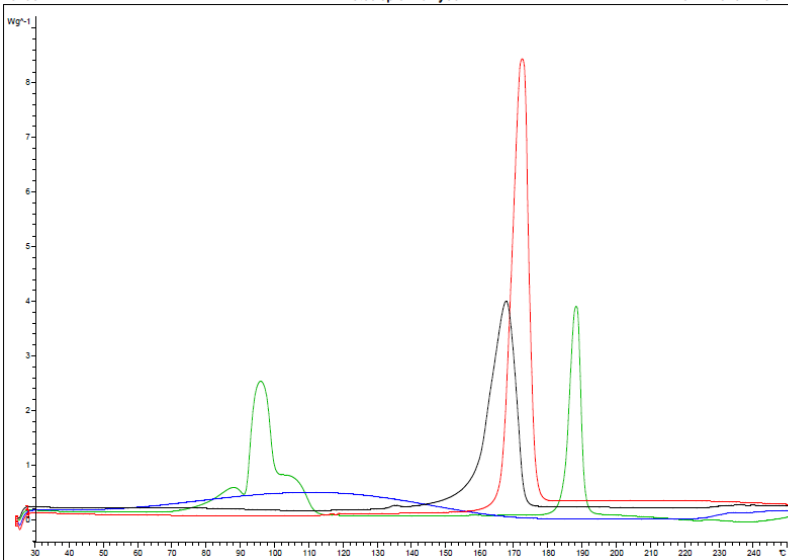


Figure 4-61: DSC thermogram of dextran (blue), mannitol (red), metoclopramide HCl (green) and Metoclopramide HCl 100 mg Lyoc® (black).

Metoclopramide HCl and the Lyocs® formulations (Placebo, F1, F2 and F4) were further analyzed through XRPD (see Figure 4-62) in order to deepen the previous DSC analysis. The freeze-dried tablets were carefully milled and the resulting powder was disposed on the sample carrier.

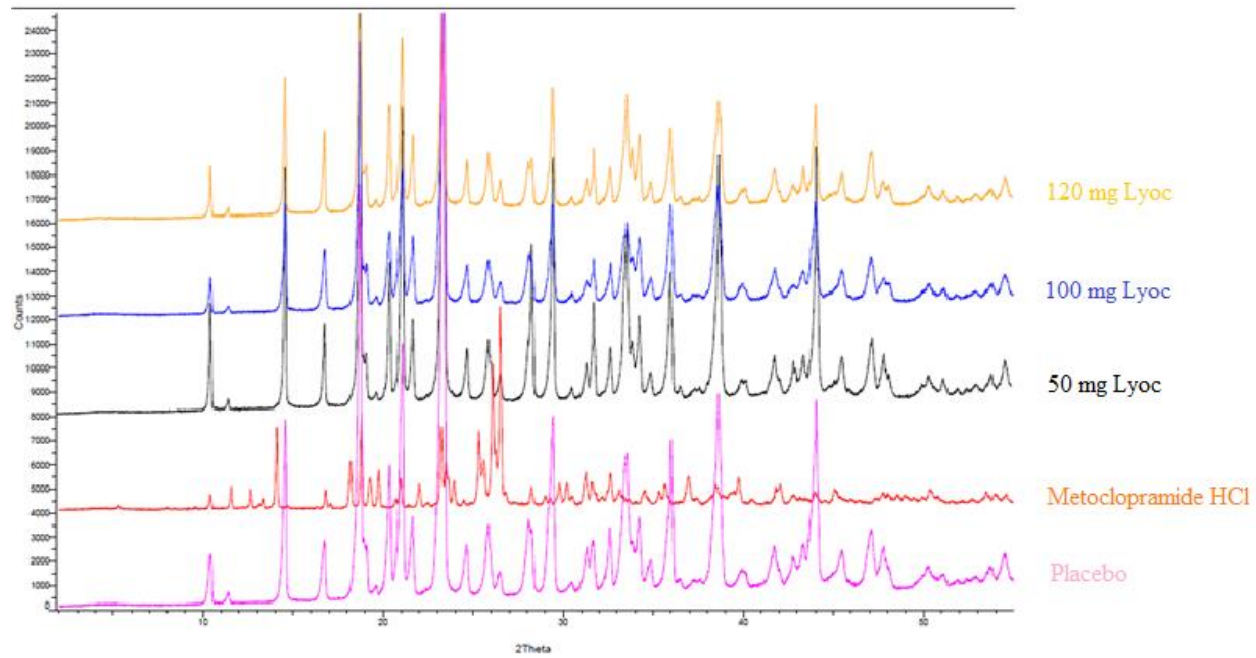


Figure 4-62: X-ray powder diffractogram overlay of metoclopramide HCl and of the freeze-dried formulations.

As shown in the figure 4-62, the diffractograms of Placebo, F1, F2 and F4 are identical regarding peak positions. All the reflexes from F1, F2 and F4 are thus related to the Placebo matrix. Due to the absence of reflexes related to metoclopramide HCl on the diffractograms F1, F2 and F4, metoclopramide HCl could be postulated to get amorphous through the lyophilization process.

The Figure 4-63 shows the Raman spectra of each pure substance measured with the conditions described in the Section 3.2.5.7. Since the Raman spectra of each compound are very different from each other (see Figure 4-63), the API distribution within the Lyocs® should be easily detectable.

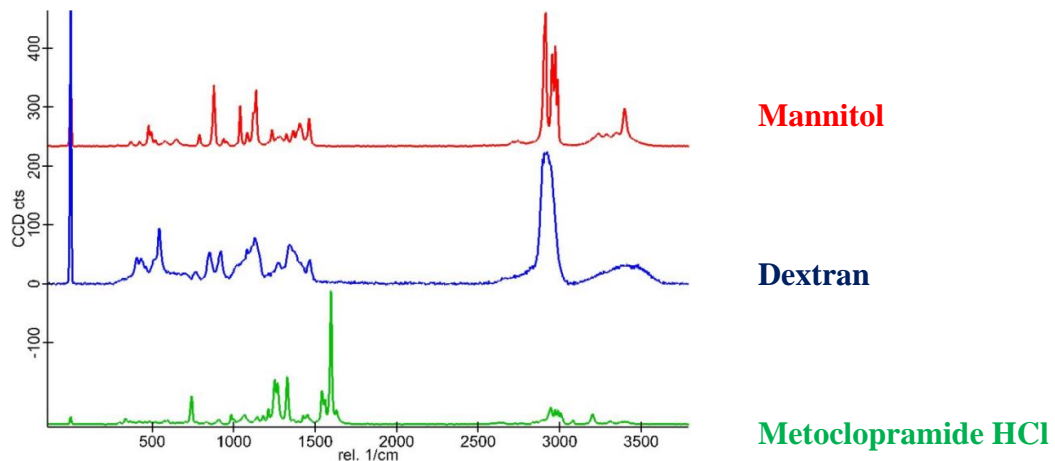


Figure 4-63: Raman spectra of mannitol (red), dextran (blue) and metoclopramide HCl (green).

A horizontal and a vertical scan were conducted and the characteristic peaks of each substance were then registered in order to ascribe a color to each substance and to allow a color mapping representation of the Lyoc® surface. This analysis can thus detect at which position the substances can be localized. With this Raman analysis, it is also possible to determine if the substances solidify separately or together, by further studying the obtained mapping picture and the resulting Raman spectra.

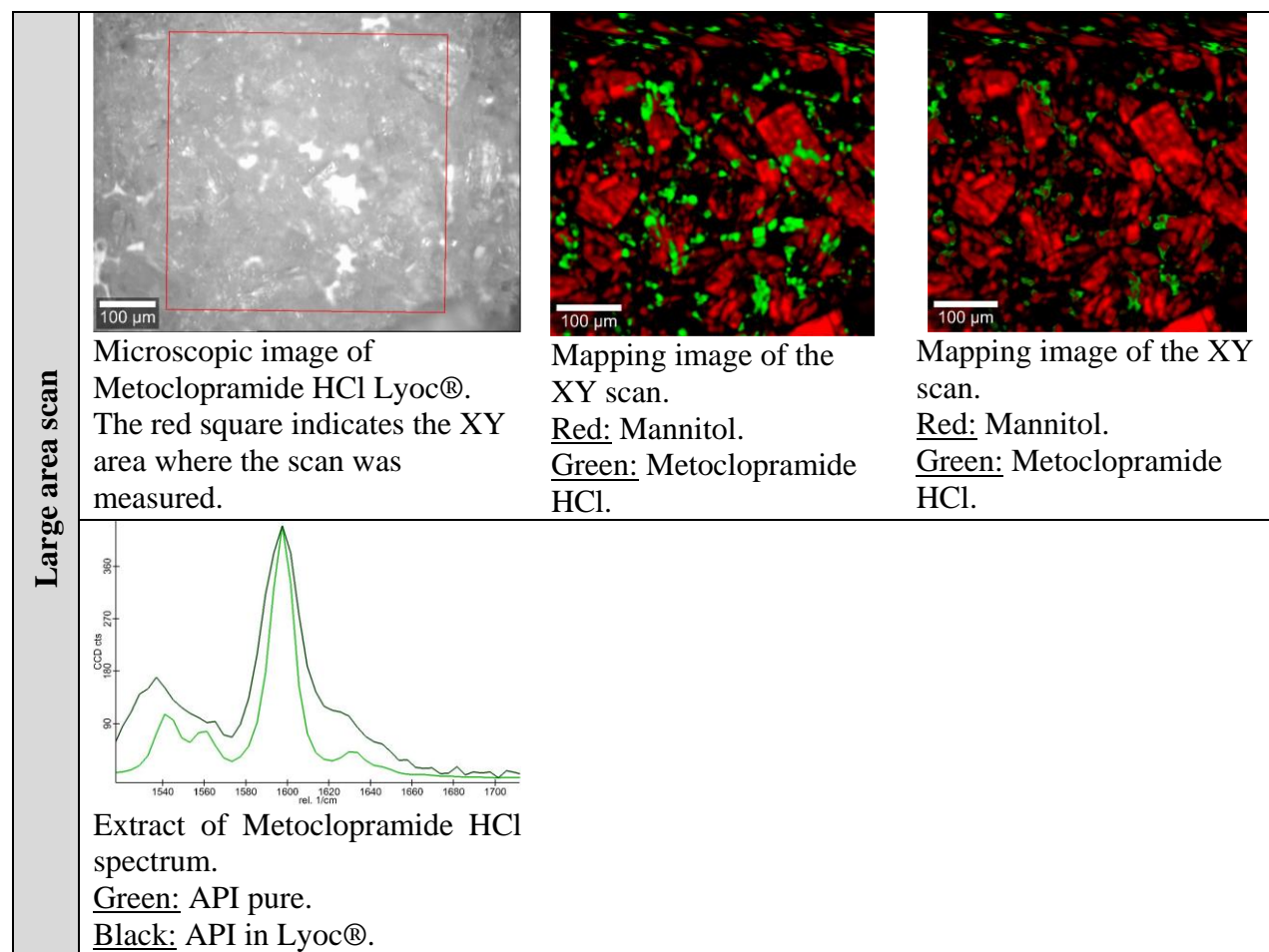


Figure 4-64: Light microscopy picture, Raman mapping and spectra of Metoclopramide HCl Lyoc® in a large scan area, plane XY.

Figure 4-64 represents the Raman mapping of a 500x500 μm area. The colored pictures were calculated with the spectra of mannitol and metoclopramide HCl. As dextran is present in a too low concentration in the Lyoc® formulation (i.e. 3,4 %) and due to its low Raman activity, it was not detectable. On the first mapping, the API is on the top, whereas on the second mapping, mannitol lies on the top. With those two mappings, it is thus possible to determine the areas where the API and mannitol solidified alone or in a close contact during the lyophilization process. The black areas present on the mapping is represented the porous structure of the Lyoc®.

By scanning a position where the API is present in the Lyoc® and by comparing the resulting spectrum with the spectrum of pure API, a peak broadening could be observed in the spectrum extracted from the Lyoc® at ca. 1600 cm^{-1} (see “Extract of Metoclopramide HCl spectrum” in Figure 4-64). The full width at half maximum was determined at 12 cm^{-1} for the API pure and 19 cm^{-1} for the API in Lyoc®. This kind of phenomenon is a typical case of amorphization of the substance. This observation matches perfectly the results obtained with XRPD. Any peak broadening was detected for mannitol, meaning that mannitol is present in a crystalline state, disproving the statement that the API could exist in a solid solution state. Indeed, if this was the case, mannitol would also be present in an amorphous state.

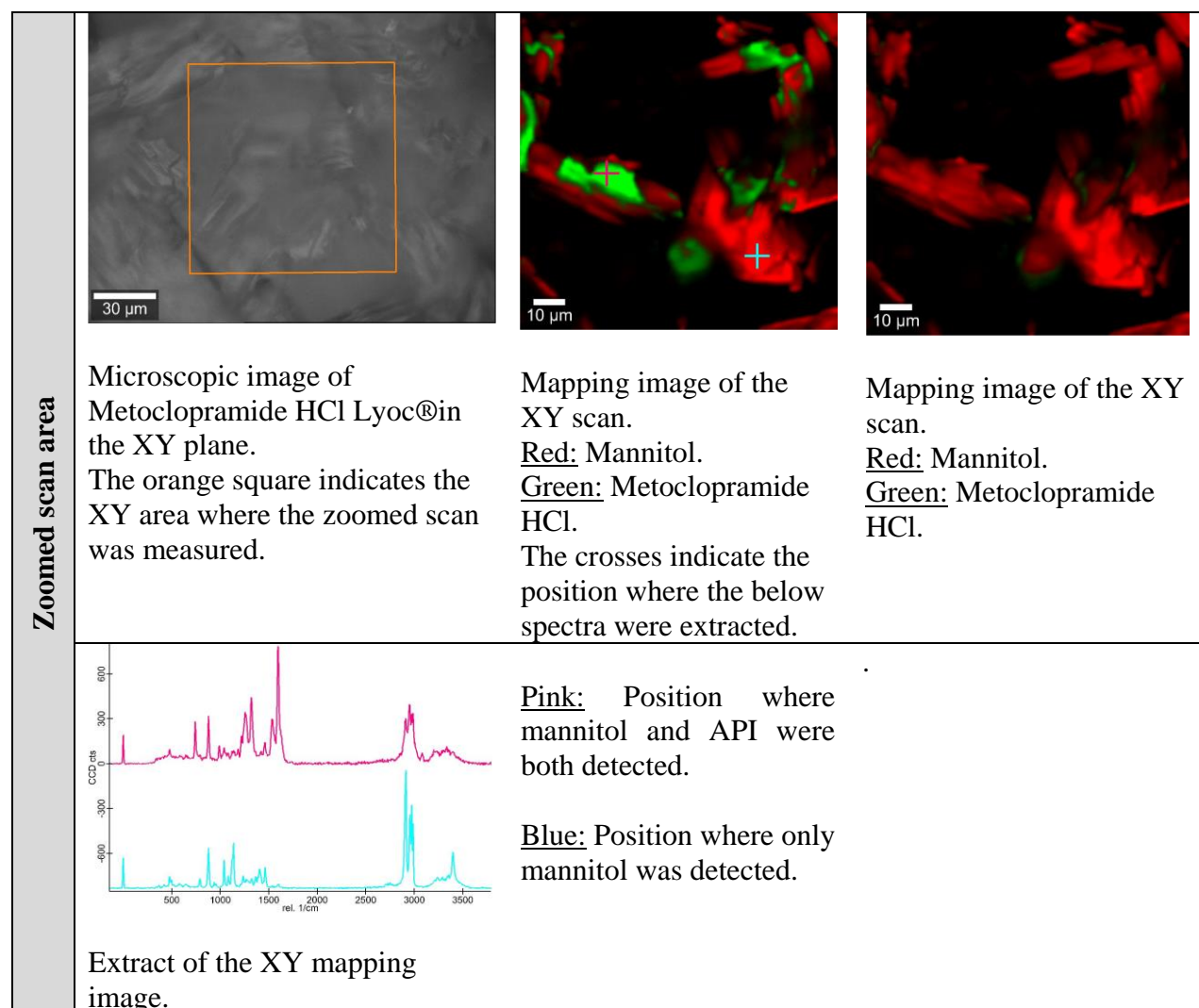


Figure 4-65: Light microscopy picture, Raman mapping and spectra of Metoclopramide HCl Lyoc® in a zoomed scan area, plane XY.

Figure 4-65 shows the Raman mapping of a 100x100 μm area. Mapping images were again constructed, with API on the top for the first colored picture and mannitol on the top for the second picture. Those two mappings show that the API is only solidifying in a close contact with mannitol, whereas mannitol is also able to solidify alone. This hypothesis was proved by extracting two different spectra: one where API and mannitol are both present on the same position and another one where only mannitol was detected. For the pink pattern, both spectra of mannitol and metoclopramide HCl are visible, whereas the blue one only shows the intact spectrum of pure mannitol. This could be supported by two explanations:

- Mannitol and metoclopramide HCl are either solidifying together, forming a mixed crystal,
- or metoclopramide HCl is solidifying on or underneath mannitol, in a very close position.

Depth profiling has to be performed in order to answer this question.

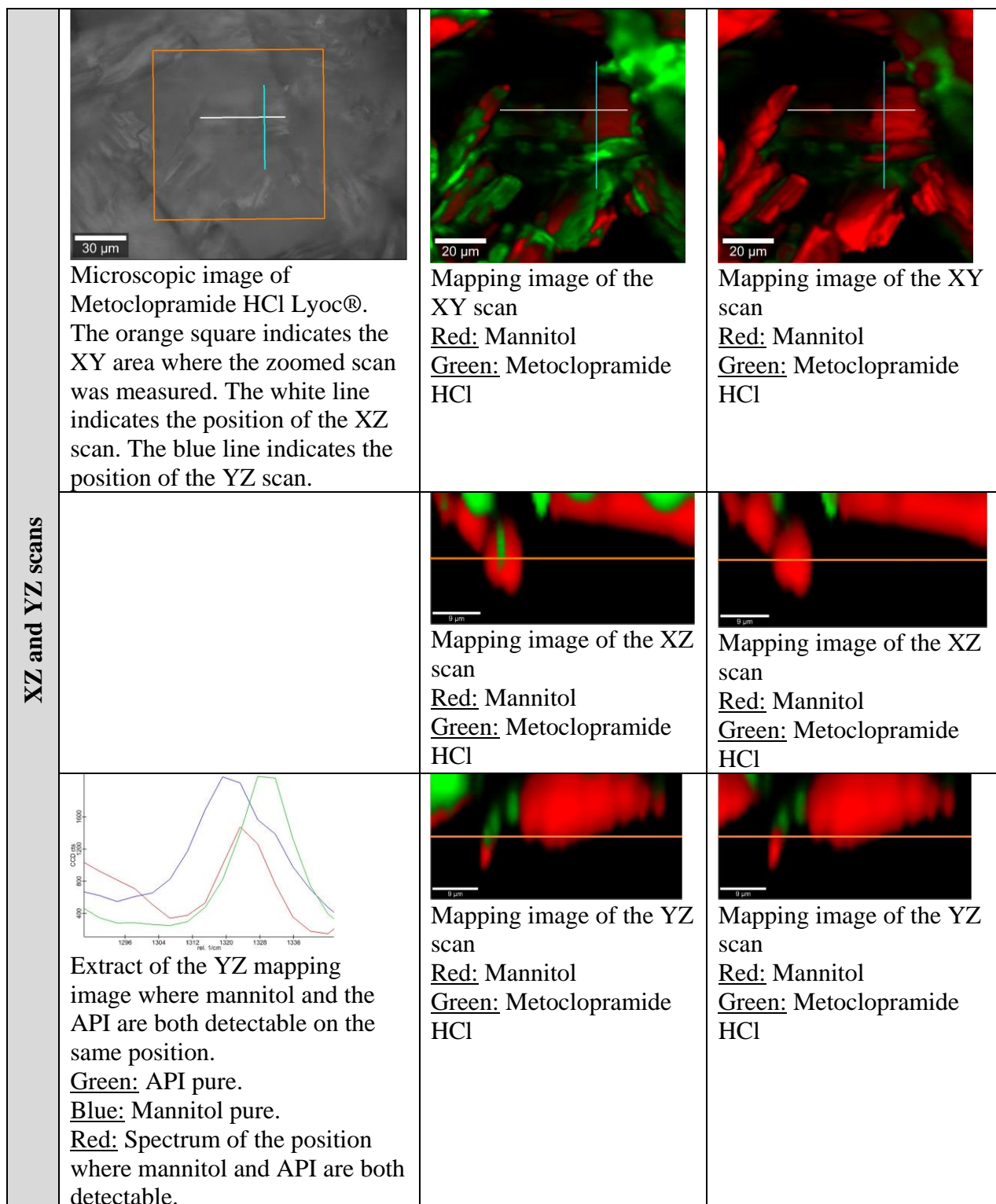


Figure 4-66: Light microscopy picture, Raman mapping and spectra of Metoclopramide HCl Lyoc® in a depth profile area, planes XZ and YZ.

Figure 4-66 is representing Raman mapping of depth profiles on the XY and YZ sections (50x25 μm area). Mapping images were again constructed, with API on the top for the first colored picture and mannitol on the top for the second picture. It could be clearly observed on both sections that the API is solidifying very close to mannitol. After extracting a spectrum on the YZ plan, where both mannitol and the API are detectable, the characteristic peak of metoclopramide HCl was shifted from ca. 1328 cm^{-1} for the pure API to 1320 cm^{-1} for the

lyophilized API. This shift could be explained by an existing interaction between the API and mannitol, which means that both substances are possibly interacting.

According to the Raman results, it could be stated from the large scan area that metoclopramide HCl is getting amorphous during the lyophilization process, detectable through the broadening of the pattern peak of metoclopramide HCl at ca. 1600 cm^{-1} . Moreover, the zoomed scan area could show that metoclopramide HCl may solidify really close to mannitol and that an interaction between mannitol and the API may exist.

4.3.1.2 Metamizol Sodium Lyocs®

The following formulations summarized in Table 4-34 were produced using metamizol Na as API, with a batch size of 150 g on dried substance.

Table 4-34: Composition of the tested formulations containing metamizol sodium.

Substance	mg / dose				
	Placebo	F1	F2	F3	F4
Batch Nr	150521	150475	150476	150485	150486
Metamizol sodium <i>SAP-Nr 17993</i>	0	50	100	110	120
Mannitol <i>SAP-Nr 245445</i>	715	665	615	605	695
Dextran <i>SAP-Nr 236561</i>	25	25	25	25	25
Water <i>SAP-Nr 14022</i>	550	550	550	550	550
Total	1290	1290	1290	1290	1290

For F1-F4, the API-water mixture was completely transparent, meaning that the Metamizol Na was completely solved in water. The Metamizol Na Lyocs® exploded beyond 120 mg API. The maximal API load is thus evaluated at 15 % on the dried mass of Lyocs®.

Table 4-35: IPC results of the tested formulations, $\pm\text{SD}$.

IPC results					
	Placebo	F1	F2	F3	F4
H [N], n=20	66 \pm 21	83 \pm 20	85 \pm 15	85 \pm 14	78 \pm 13
D.T [s], n=6	15 \pm 2	14 \pm 3	11 \pm 5	8 \pm 4	5 \pm 5

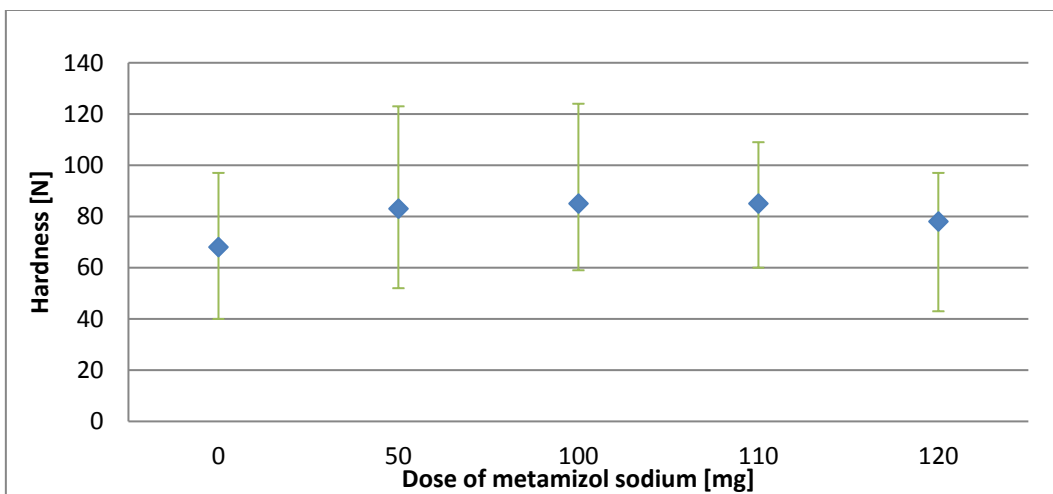


Figure 4-67: Hardness average with min and max values (n=20).

No significant influence of the quantity of metamizol Na in the formulation on the hardness of the resulting Lyocs® was noticed (see Figure 4-67). This means that the Lyocs® are losing their structure from a certain amount of metamizol Na (beyond 120 mg) within the Lyoc®, causing an explosion of the Lyoc® during the sublimation step. In the case of metamizol Na, the D.T is not suddenly decreasing (see Table 4-35), but it decreases step by step with increasing API in the formulation. This could mean that metamizol Na has more cohesion between the substances, maybe due to a partial amorphization of the API, unlike metoclopramide HCl where the amorphization was evaluated as fully.

Metamizol Na 100 mg Lyoc® and the respective raw materials of its formulation were firstly analyzed by means of DSC in order to evaluate the solid state of metamizol Na after lyophilization. Figure 4-68 represents the crystalline structure of Pearlitol® 110 C through the presence of a sharp melting peak at 167,93 °C (n=3). Figure 4-69 shows a sharp endothermic-exothermic peak 230 °C and 255 °C (n=3), which correspond to the deterioration of metamizol Na, probably by an oxidation-reduction reaction (Euro-OTC-Pharma, 2017; Fernandes et al., 1999). The first bright peak (between ca. 90 °C and 155 °C) could be due to the loss of water, as the metamizol Na is used as the monohydrate. This theory was confirmed by a TGA analysis (see Annex 6.2.2) where the loss of weight of water was determined. Figure 4-70 represents a superposition of the thermograms of Metamizol Na 100 mg Lyoc® (black), mannitol (red), and metamizol Na (green). The thermogram of the Lyoc® shows a loss of water (first bright peak at ca. 135 °C), followed by a melting peak. This melting peak could represent a change in mannitol polymorphism after lyophilization (Kim et al., 1998) as already explained in 4.3.1.1. Moreover, the lack of the melting peak of metamizol Na on the thermogram of the Lyoc® could be due to the entire amorphization of the substance during lyophilization. Both of those theories will be further investigated by means of a XRPD study.

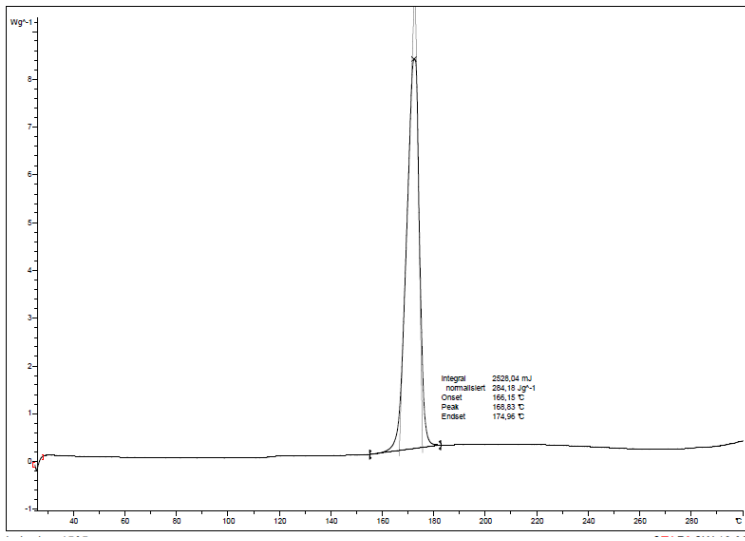


Figure 4-68: DSC thermogram of mannitol.

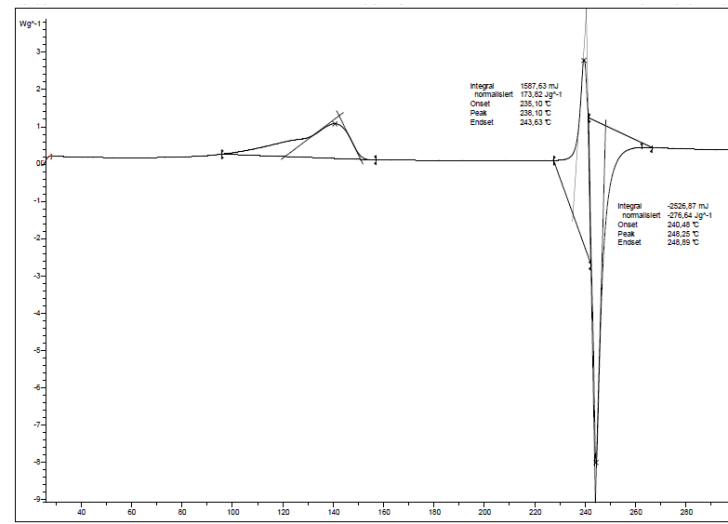


Figure 4-69: DSC thermogram of metamizol Na.

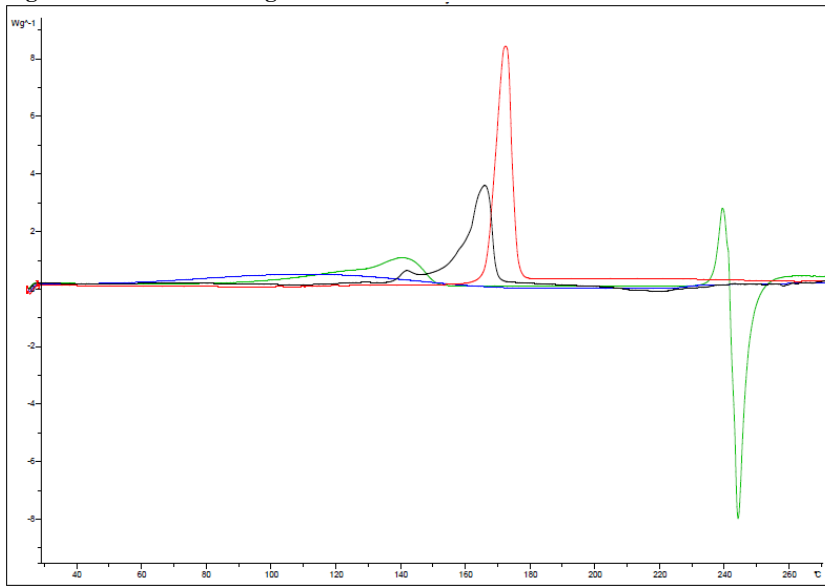


Figure 4-70: DSC thermogram of dextran (blue), mannitol (red), metamizol Na (green) and Metamizol Na 100 mg Lyoc® (black).

Metamizol Na and the Lyocs® formulations (placebo, F1, F2 and F4) were analyzed through XRPD (see Figure 4-71). The freeze-dried tablets were carefully milled and the resulting powder was disposed on the sample carrier.

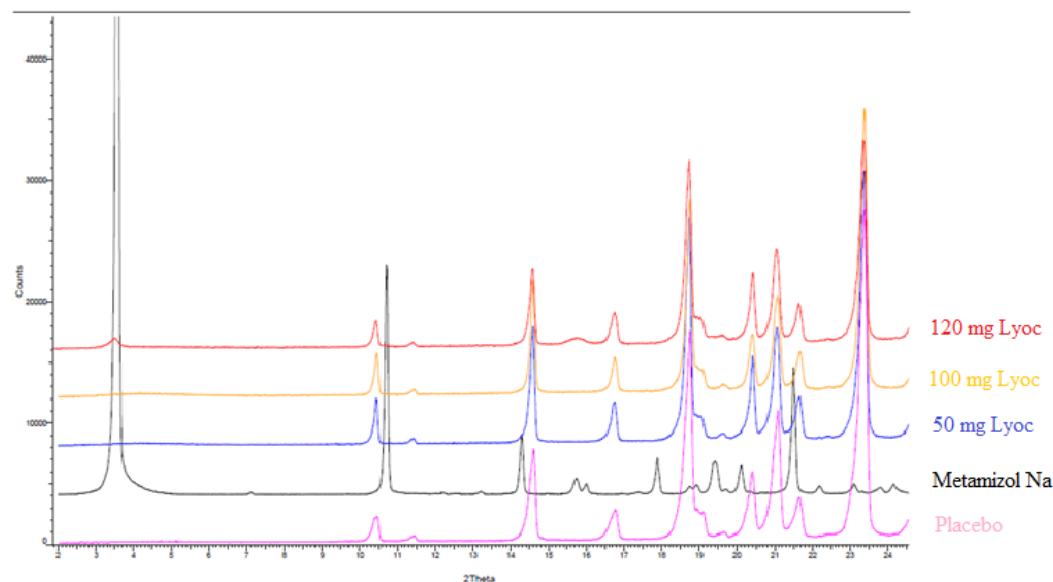


Figure 4-71: X-ray powder diffractogram overlay of metamizol sodium and of the freeze-dried formulations.

As shown in Figure 4-71, the diffractograms of Placebo, F1 and F2 are identical regarding the peak positions. F1 and F2 do not have any characteristic reflexes of metamizol Na. F4 shows two additional peaks (at 3,4 and 15,7°2-Theta) which are not related to the ones of the placebo pattern. Those both additional peaks (at 3,4 and 15,7°2-Theta) are corresponding to the characteristic reflexes of metamizol Na. The API could be thus postulated to be partly amorphous. Indeed, the crystalline part present in F1 and F2 could be under the detection limit, which could explain the absence of the characteristic reflexes of metamizol sodium in F1 and F2.

Figure 4-72 shows the Raman spectra of each pure substance measured with the conditions described in the Section 3.2.5.7. Since the Raman spectra of each compound are very different from each other (see Figure 4-72), the API distribution within the Lyocs® should be easily detectable.

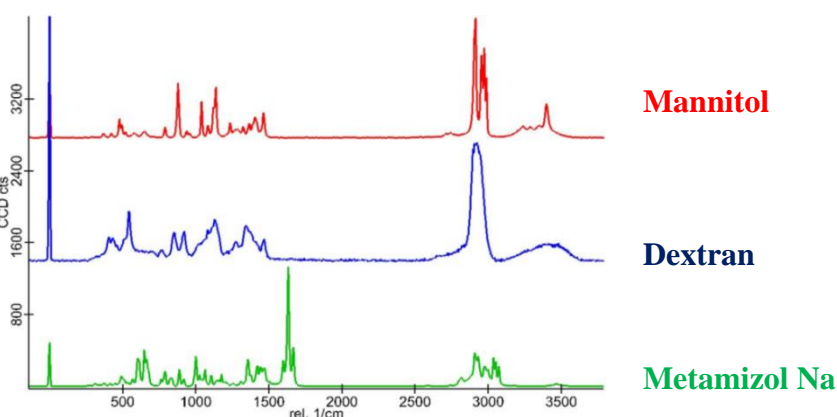


Figure 4-72: Raman spectra of mannitol, dextran and metamizol Na.

The same substances mapping analysis was performed as the one for Metoclopramide HCl Lyocs® through Raman microscopy. A horizontal and a vertical scan were conducted and the characteristic peaks of each substance were then registered and filtered in order to build up a color mapping representation of the Lyoc® surface. This analysis will thus determine at which position the substances can be observed and determine if the substances solidify alone or together, by further studying the obtained mapping picture.

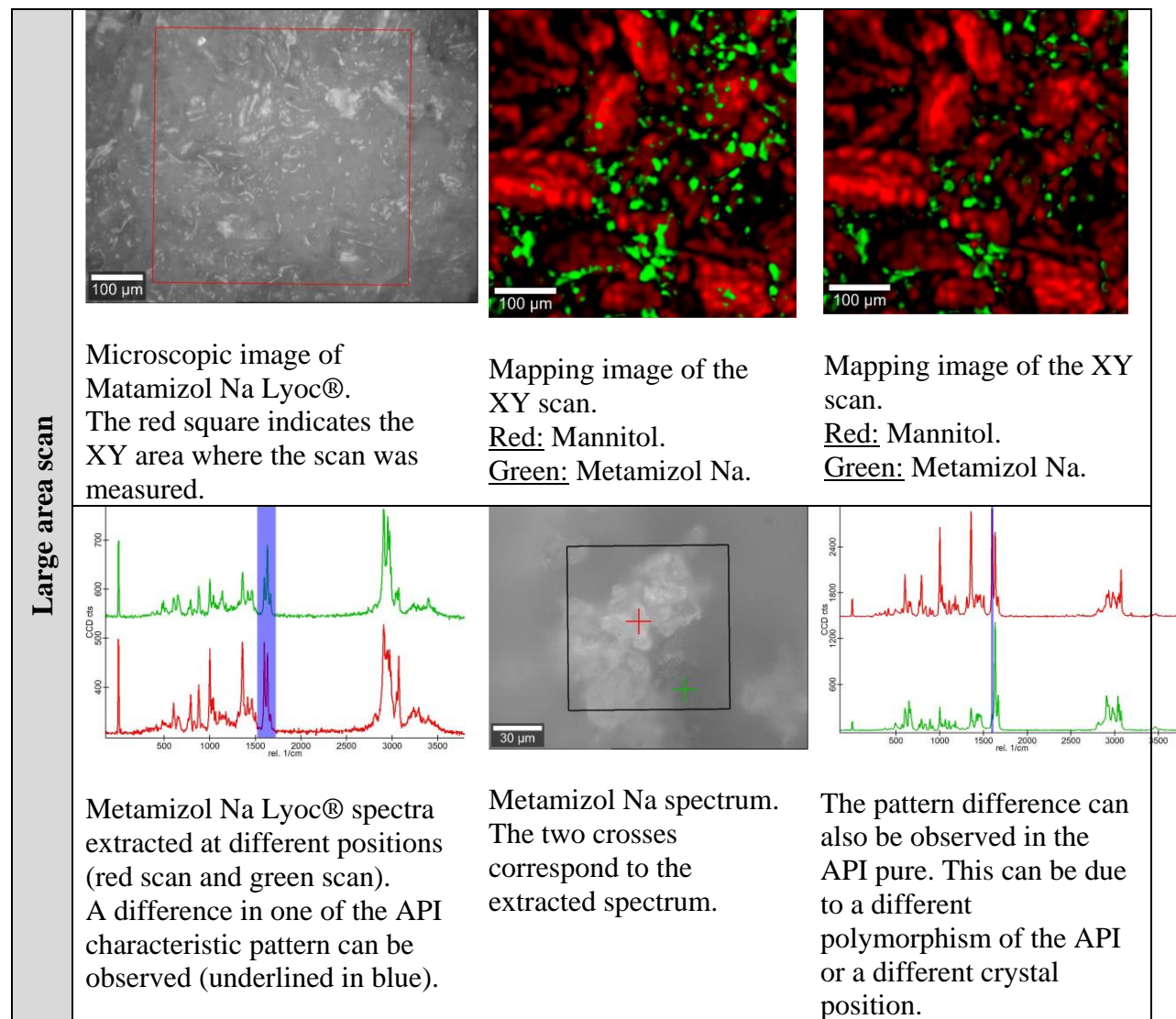


Figure 4-73: Light microscopy picture, Raman mapping and spectra of metamizol Na Lyoc® in a large scan area, plane XY.

Figure 4-73 represents the Raman mapping of a 500x500 µm area. The colored pictures were calculated with the spectra of mannitol and metamizol Na. As dextran is present in a too low concentration (3,4 %) and was actively low by Raman microscopy, it was not detectable. On the first mapping, the API lies on the top, whereas on the second mapping, mannitol lies on the top. With those two mappings, it is thus possible to determine the areas where the API and mannitol solidified alone or in a close contact during the lyophilization process. The black areas present on the mapping is represented the porous structure of the Lyoc®.

By scanning a position where the API is present in the Lyoc®, any peak broadening could be observed, meaning that the API is also present in a crystalline state. The amorphous state could

not be detected by Raman, maybe because its pattern is too inactive in comparison to the crystalline one. Another phenomenon could nevertheless be observed: the pattern of lyophilized metamizol Na showed a different peak intensity on the triplet peak at ca. 1600 cm^{-1} . After analyzing different positions of pure metamizol Na, this phenomenon could be also observed. The change of intensity within the peaks is not related to amorphization of metamizol Na during lyophilization, but is due to the orientation of the crystals within the sample. It could be concluded that for a same crystal having a different orientation, a different peak intensity is delivered.

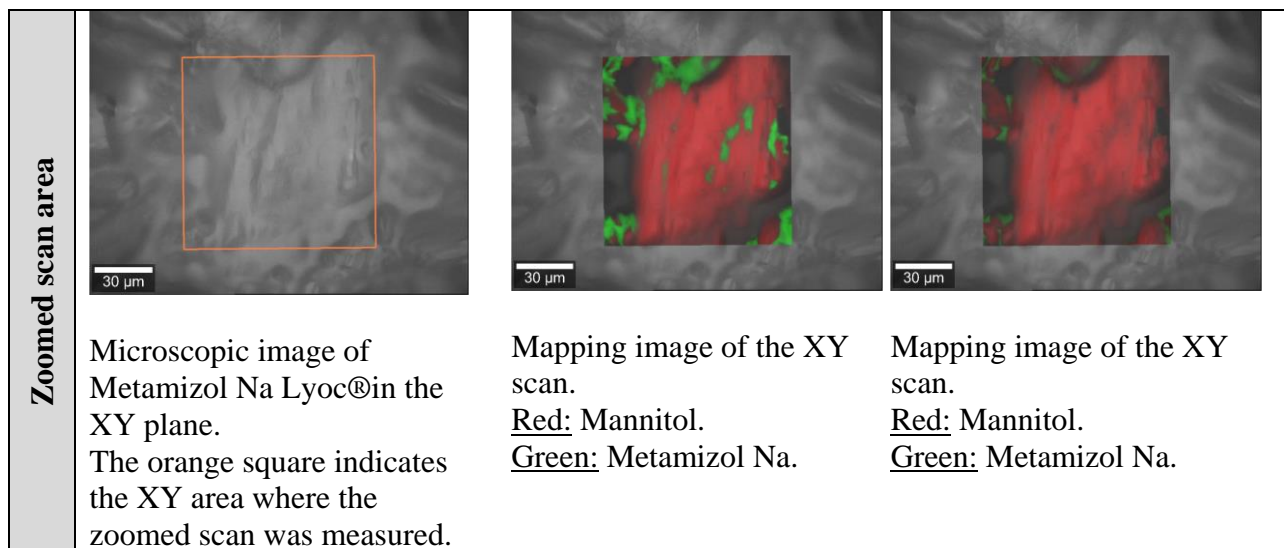


Figure 4-74: Light microscopy picture and Raman mapping of Metamizol Na Lyoc® in a zoomed scan area, plane XY.

The Figure 4-74 shows the Raman mapping of a $100\times 100\text{ }\mu\text{m}$ area. Mapping images were again constructed, with API on the top for the first colored picture and mannitol on the top for the second picture. Those two mappings show that the API is only solidifying in a close contact with mannitol, whereas mannitol is also able to solidify alone.

- Mannitol and metamizol Na are either solidifying together, forming a mixed crystal,
- or metamizol Na is solidifying on or underneath mannitol.

Depth profiles were performed in order to answer this question.

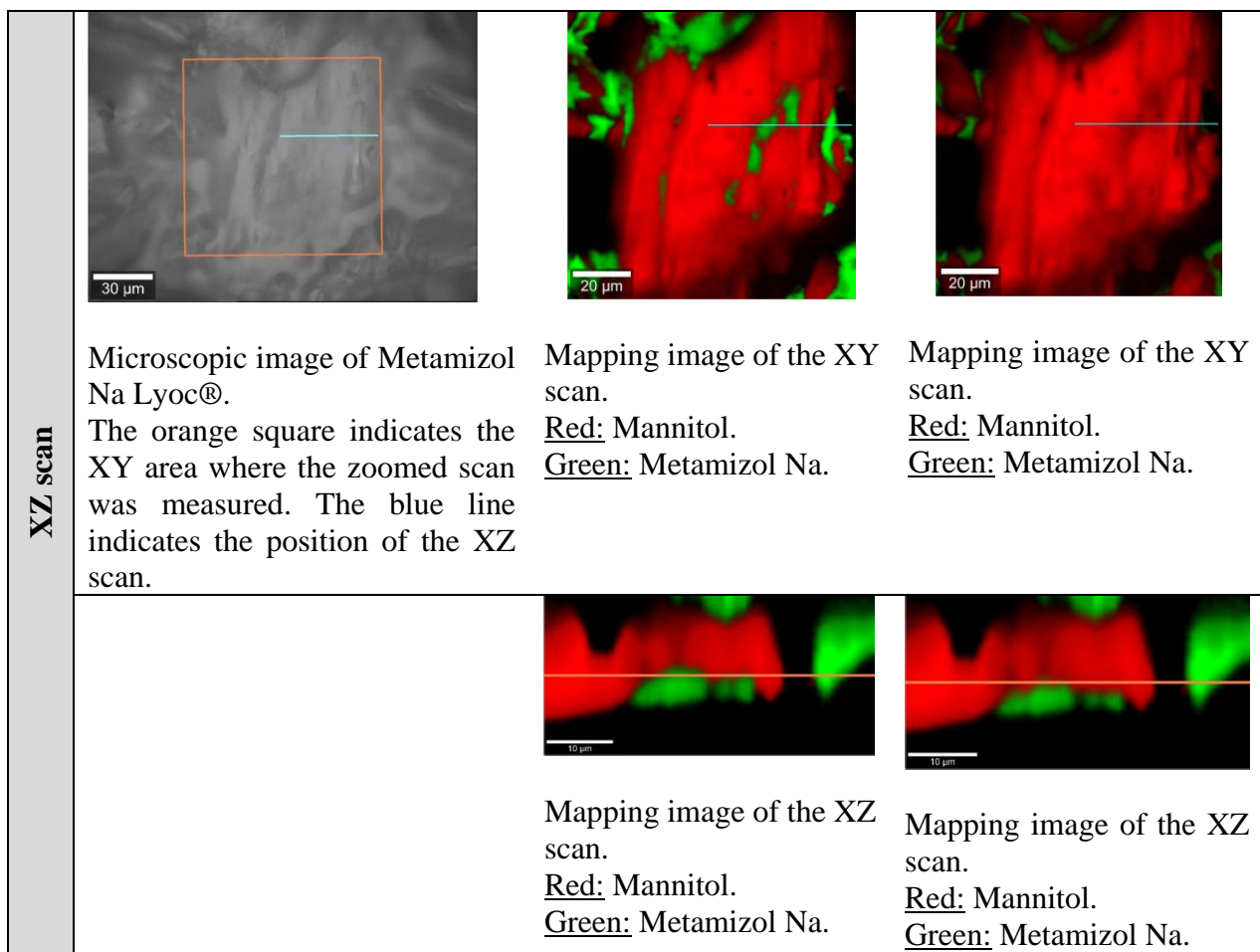


Figure 4-75: Light microscopy picture and Raman mapping of Metamizol Na Lyoc® in a depth profile area, plane XZ.

Figure 4-75 is showing Raman mapping of depth profiles on the XY and YZ sections (50x25 µm area). Mapping images were again constructed, with API on the top for the first colored picture and mannitol on the top for the second picture. It could be clearly observed on both sections that the API and mannitol are both solidifying alone.

According to the Raman results, it could be stated that metamizol Na is also present in crystalline state after lyophilization, and that it solidifies separately from mannitol.

The observation of crystalline API in the sample supports once again the results obtained by XRPD. Indeed, crystalline metamizol Na was also detectable at low intensity, meaning that the API is partly amorphous and crystalline. However, the amount of crystallized metamizole Na could not be exactly quantified in this complex mixture.

4.3.2 Study on Less-Water Soluble APIs

4.3.2.1 Paracetamol Lyocs®

The following formulations summarized in Table 4-36 were produced using paracetamol as API, with a batch size of 150 g on dried substance.

Table 4-36: Composition of the tested formulations containing paracetamol.

Substance	mg / dose			
	Placebo	F1	F2	F3
Batch Nr	150521	160065	160066	160067
Paracetamol	0	50	100	150
Mannitol	715	665	615	565
Dextran	25	25	25	25
Water	550	550	550	550
Total	1290	1290	1290	1290

The 3 formulations gave Lyocs® of good quality (see IPC results in Table 4-37). It can be noticed that the D.T stays quite constant for Placebo such as F1, F2, F3 ($15 \text{ s} < \text{D.T} < 17 \text{ s}$), showing that paracetamol does not play affect the Lyoc® morphology.

Table 4-37: IPC results of the tested formulations, $\pm \text{SD}$.

IPC results				
	Placebo	F1	F2	F3
H [N], n=20	66 \pm 21	66 \pm 20	44 \pm 6	57 \pm 7
D.T [s], n=6	15 \pm 2	15 \pm 2	17 \pm 2	16 \pm 2

Paracetamol 100 mg Lyoc® and the raw materials contained in its formulation were firstly analyzed by means of DSC in order to determine the solid state of paracetamol after lyophilization. Figure 4-76 represents the crystalline structure of Pearlitol® 110 C through the presence of a sharp melting peak at 167,93 °C (n=3). Figure 4-77 represents the crystalline structure of paracetamol through the presence of a sharp melting peak at 171,04 °C (n=3). Figure 4-78 represents a superposition of the thermograms of Paracetamol 100 mg Lyoc® (black), mannitol (red), and paracetamol (green). The thermogram of the Lyoc® shows a single melting peak at 163,15 °C (n=3). This melting peak is shifted, as it corresponds neither to the one of mannitol nor paracetamol. This peak shift can be explained through two hypotheses:

- either paracetamol is getting amorphous and mannitol polymorphism is changing after lyophilization,
- or paracetamol is interacted with mannitol during lyophilization.

These theories were further investigated by means of a XRPD measurement.

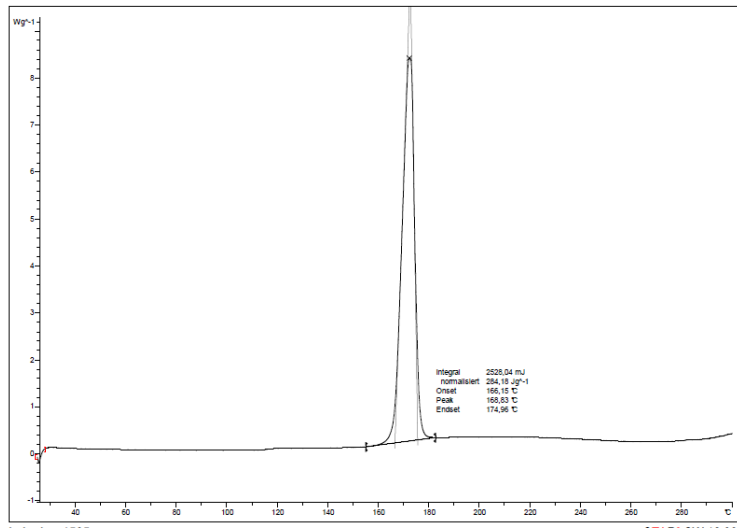


Figure 4-76: DSC thermogram of mannitol.

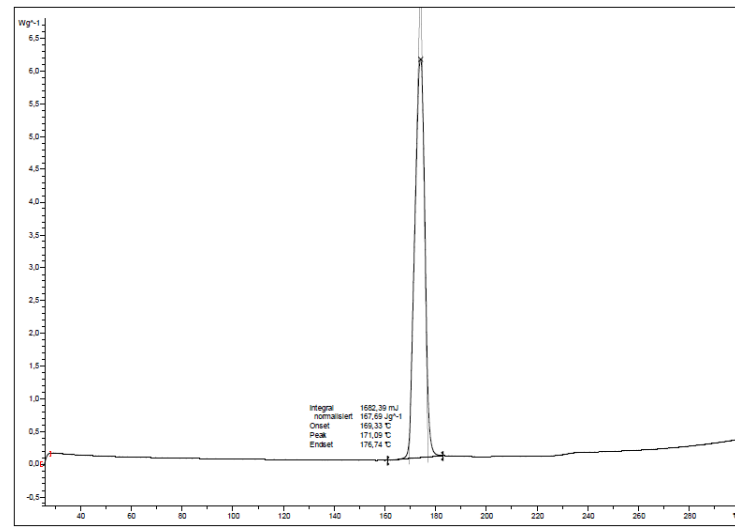


Figure 4-77: DSC thermogram of paracetamol.

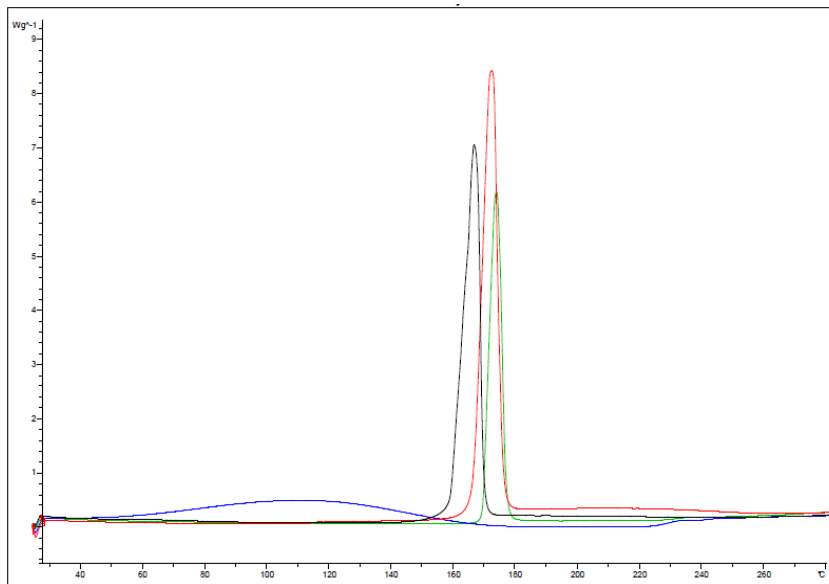


Figure 4-78: DSC thermogram of dextran (blue), mannitol (red), paracetamol (green) and Paracetamol 100 mg Lyoc® (black).

Paracetamol and the formulations Placebo, F1, F2 and F3 were analyzed through XRPD (see Figure 4-79). The freeze-dried tablets were carefully milled and the resulting powder was disposed on the sample carrier.

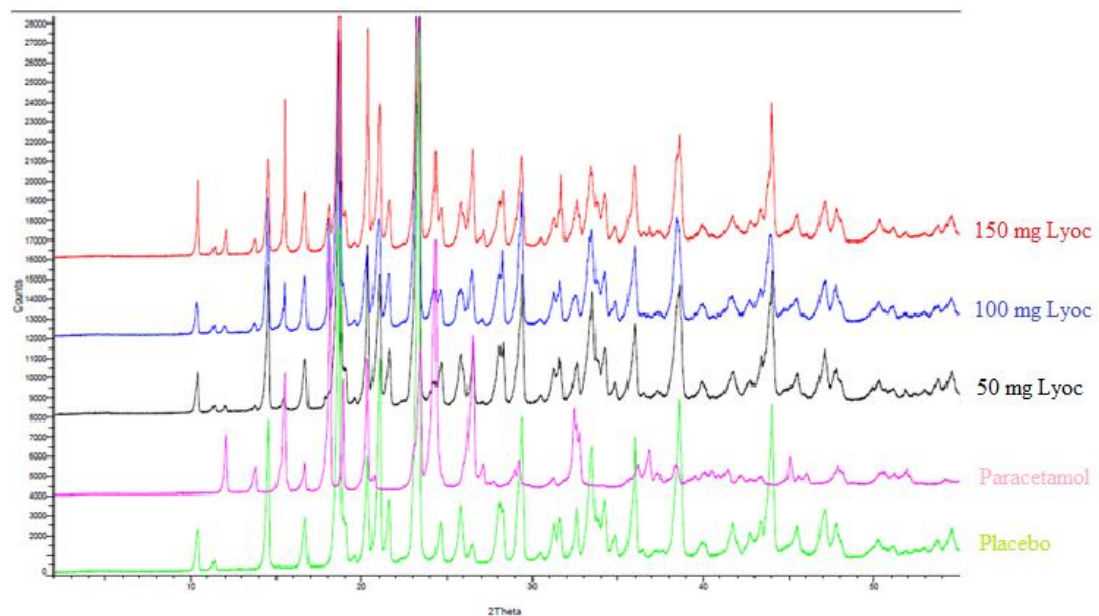


Figure 4-79: X-ray powder diffractogram overlay of paracetamol and of the freeze-dried formulations.

As shown on Figure 4-79, F1, F2 and F3 have identical diffractograms regarding to the peak positions. They present characteristic reflexes of paracetamol. Moreover, the increasing peak intensity of the characteristic reflexes of pure crystalline paracetamol (at 12 and 15,5°2-Theta for instance) from F1 to F3 reinforce the fact that paracetamol stays in a crystalline state after lyophilization. Indeed, the fact that the peak intensity increases from F1 to F3 proves that the proportion of crystalline paracetamol after lyophilization increases with its concentration.

4.3.2.2 Sildenafil Citrate Lyocs®

The following formulations summarized in Table 4-38 were produced using sildenafil citrate as API, with a batch size of 150 g on dried substance.

Table 4-38: Composition of the tested formulations containing sildenafil citrate.

Substance	mg / dose			
	Placebo	F1	F2	F3
Batch Nr	150521	150372	150373	150374
Sildenafil Citrate <i>SAP-Nr 115199</i>	0	50	100	150
Mannitol <i>SAP-Nr 245445</i>	715	665	615	565
Dextran <i>SAP-Nr 236561</i>	25	25	25	25
Water <i>SAP-Nr 14022</i>	550	550	550	550
Total	1290	1290	1290	1290

Table 4-39: IPC results of the tested formulations ±SD.

IPC results				
	Placebo	F1	F2	F3
H [N], n=20	66±21	65±11	61±8	62±8
D.T [s], n=6	15±2	15±4	16±2	15±2

The 3 formulations gave good Lyocs® quality (see IPC results in Table 4-39). The D.T of the placebo and the formulations containing API are similar, such as the H, meaning that the API does not have an influence on the Lyoc® quality/morphology. This could be due to the fact that the API may build up a crystalline structure, reinforcing the Lyoc® network in comparison to the Lyocs® of Section 4.3.1 containing water-soluble APIs.

Sildenafil Citrate 100 mg Lyoc® and the respective raw materials of its formulation were firstly analyzed by means of DSC in order to check the solid state of sildenafil citrate after lyophilization. Figure 4-80 represents the crystalline structure of Pearlitol® 110 C through the presence of a sharp melting peak at 167,93 °C (n=3). Figure 4-81 shows a 3-peak pattern of sildenafil citrate between 190 °C and 220 °C (n=3), where the first peak represents the crystalline structure of sildenafil citrate, followed by its decomposition. Figure 4-82 represents a superposition of the thermograms of Sildenafil Citrate 100 mg Lyoc® (black), mannitol (red), and sildenafil citrate (green). The thermogram of the Lyoc® shows a double melting peak of mannitol, meaning that mannitol presents other polymorphs after lyophilization. The attenuated 3-peak pattern of sildenafil citrate (due to the high concentration of mannitol in the formulation) is also present on the thermogram of the Lyoc® meaning that sildenafil stays crystalline after lyophilization. A double pic is observable at 168 °C (i.e the melting peak of mannitol), meaning that several polymorphic forms of mannitol are present in the Lyoc®, probably α and β (Kim et al., 1998) due to the slow freezing rate like explained in paragraph 4.3.1.1.

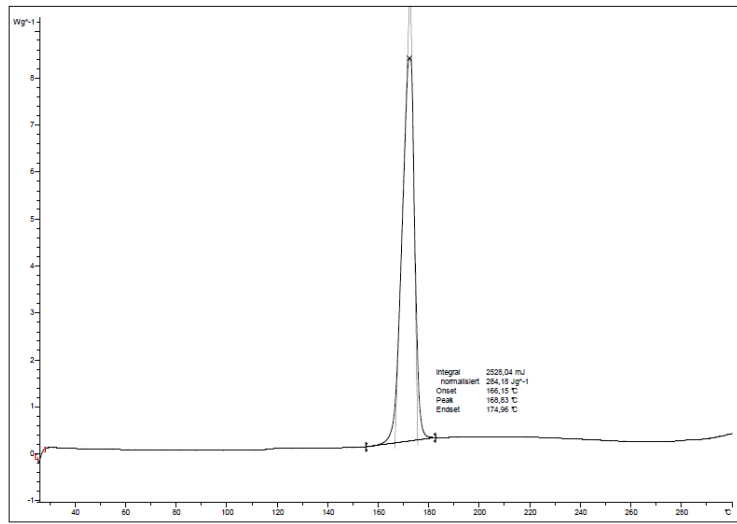


Figure 4-80: DSC thermogram of mannitol.

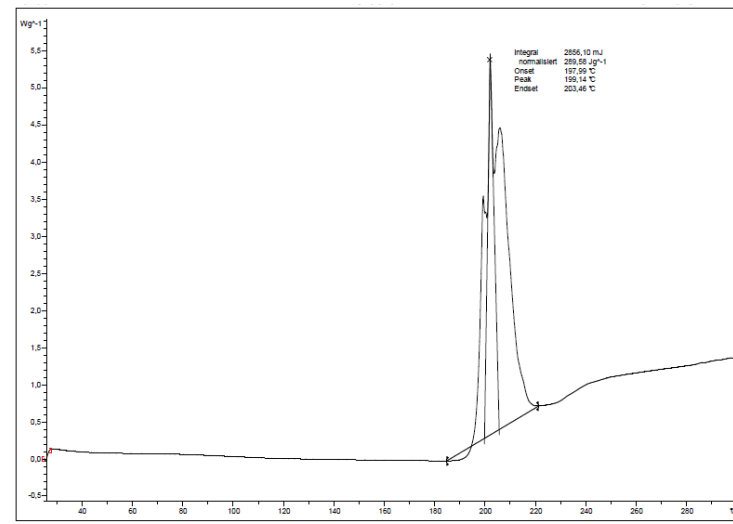


Figure 4-81: DSC thermogram of sildenafil citrate.

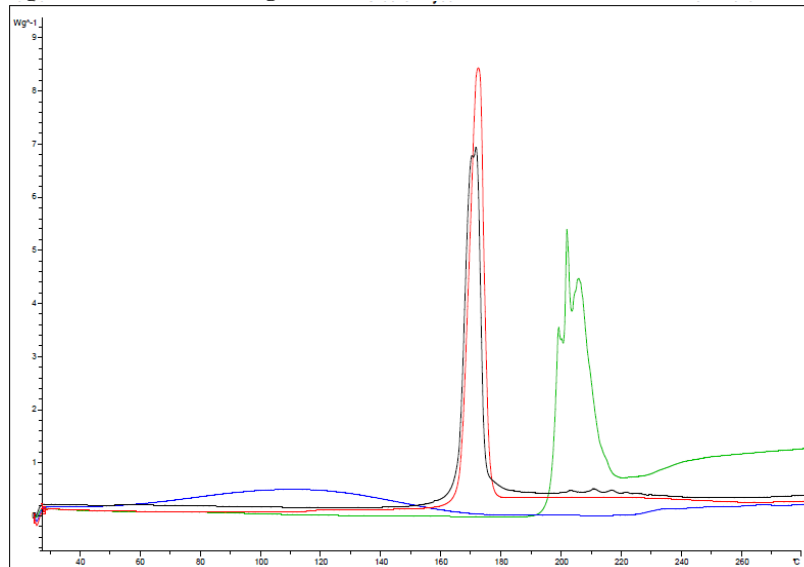


Figure 4-82: DSC thermogram of dextran (blue), mannitol (red), sildenafil citrate (green) and Sildenafil Citrate 100 mg Lyoc® (black).

Sildenafil citrate and the formulations Placebo, F1, F2 and F3 were analyzed through XRPD (see Figure 4-83). The freeze-dried tablets were carefully milled and the resulting powder was disposed on the sample carrier.

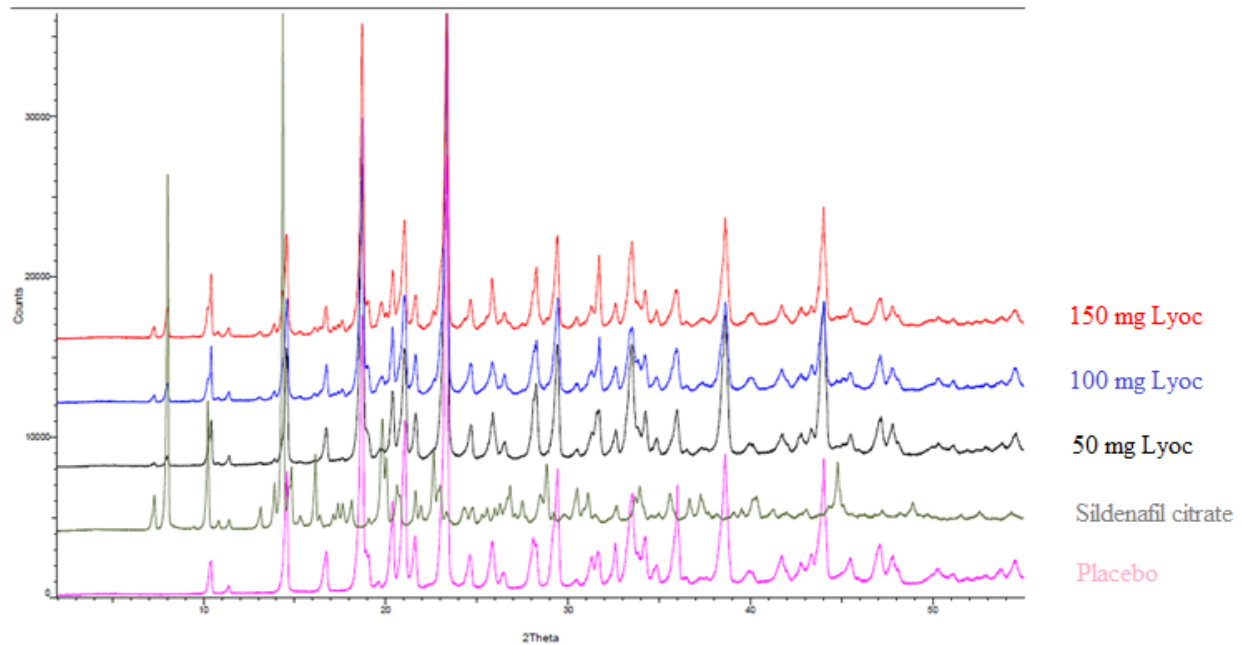


Figure 4-83: X-ray powder diffractogram overlay of sildenafil citrate and of the freeze-dried formulations.

As shown on Figure 4-83, F1, F2 and F3 have identical diffractograms regarding to the peak positions. They present characteristic reflexes of sildenafil citrate. Moreover, some concentration related differences could be detected in F1, F2 and F3 regarding the intensity of the characteristic reflexes of sildenafil citrate (at 7 and 14,5°2-Theta for instance). These signals are the proof of the presence of crystalline sildenafil citrate in those samples, meaning that sildenafil citrate stays in a crystalline state after lyophilization.

4.3.3 Microscopic Characteristics

The Lyocs® of both categories of API (i.e. water soluble and less-water soluble) were microscopically observed by means of SEM.

Cracks could be observed on the surface of the Lyocs® (see respectively Figure 4-84, 4-87, 4-90 and 4-93), which improve the penetration of saliva within the Lyocs®. Regarding the general morphology of the Lyocs®, a significant difference could be observed between water-soluble (see Figures 4-89 and 4-92) and less-water soluble APIs (see Figures 4-83 and 4-86). For Paracetamol 100 mg Lyoc® and Sildenafil 100 mg Lyocs® (i.e. less-water soluble APIs), a crystalline structure can be observed, unlike for Metamizol Na 100 mg Lyoc® and Metoclopramide HCl 100 mg Lyoc® (i.e. water soluble APIs), where the structure is more amorphous (the crystalline structure of mannitol is barely recognizable on Figures 4-91 and 4-94). A sharp and arranged structure is observable in the case of Paracetamol 100 mg Lyoc® and Sildenafil 100 mg Lyocs® (limited-water soluble APIs), which is comparable to a crystalline structure. Whereas the structure of Metamizol Na 100 mg Lyoc® and Metoclopramide HCl 100 mg Lyoc® present more air between the particles (see the black areas

in Figures 4-89 and 4-92) with amorphous/melted particles. This larger pore structure may be responsible of the quicker D.T of Metamizol Na 100 mg Lyoc® (11 s) and Metoclopramide HCl 100 mg Lyoc® (7 s) in comparison to Paracetamol 100 mg Lyoc® (17 s) and Sildenafil 100 mg Lyocs® (16 s), by allowing a higher penetration rate of saliva within the Lyocs®.

These microscopic results are confirmed by the XRPD measurements, where the less-water soluble APIs remained crystalline after lyophilization unlike the water-soluble APIs which turned into an amorphous state.

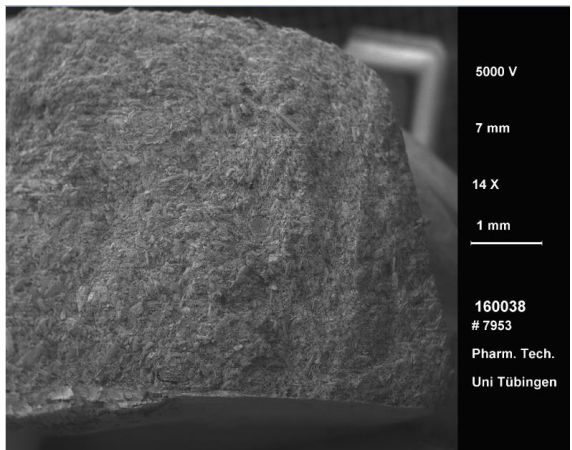


Figure 4-84: SEM picture of Paracetamol 100 mg Lyoc® (Entire structure), 14x magnification.

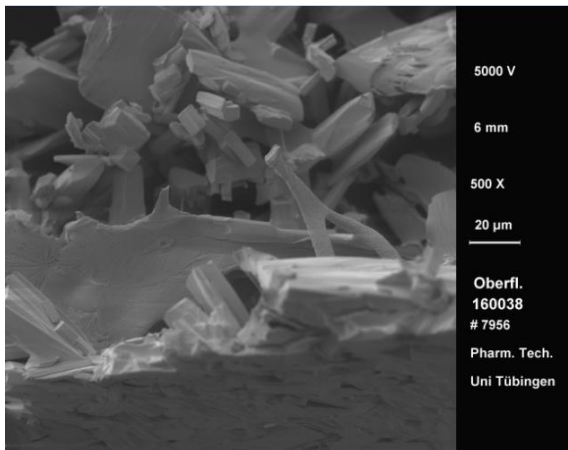


Figure 4-85: SEM picture of Paracetamol 100 mg Lyoc® (Surface), 500x magnification.

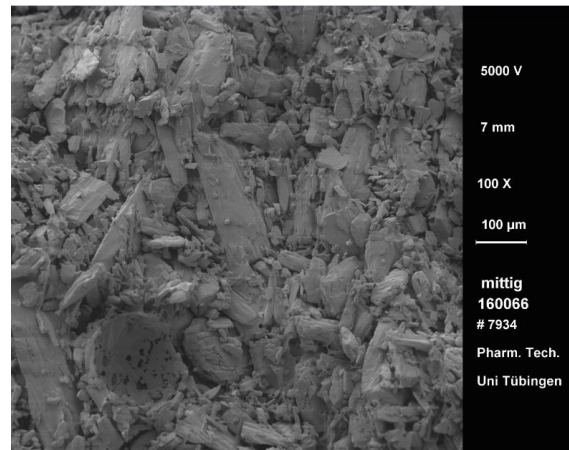


Figure 4-86: SEM picture of Paracetamol 100 mg Lyoc® (Center), 100x magnification.

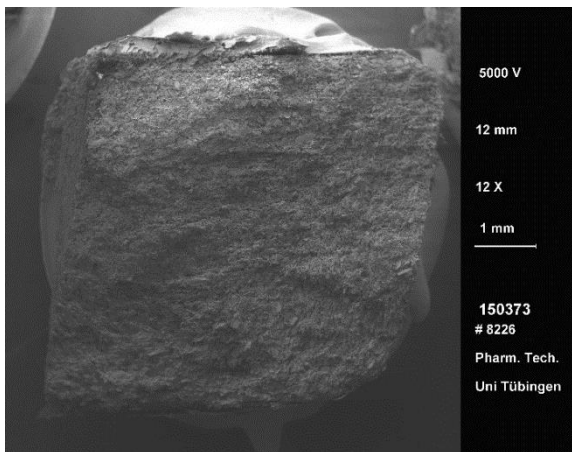


Figure 4-87: SEM picture of Sildenafil 100 mg Lyoc® (Entire structure), 12x magnification.

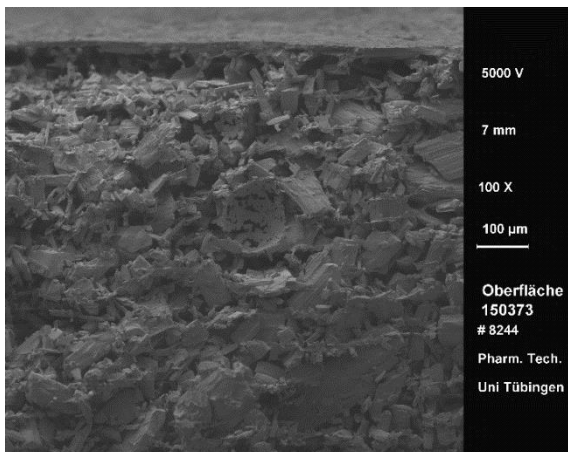


Figure 4-88: SEM picture of Sildenafil 100 mg Lyoc® (Surface), 100x magnification.

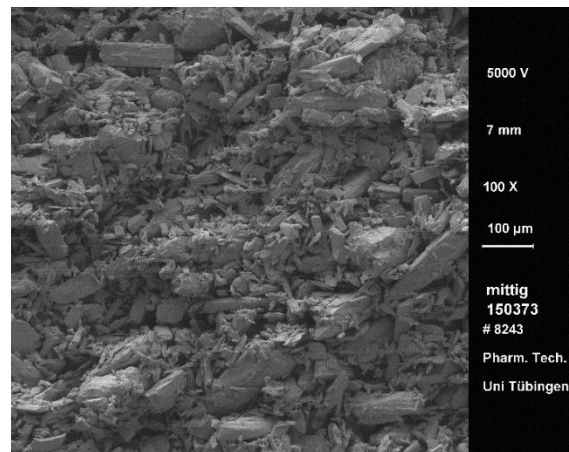


Figure 4-89: SEM picture of Sildenafil 100 mg Lyoc® (Center), 100x magnification.

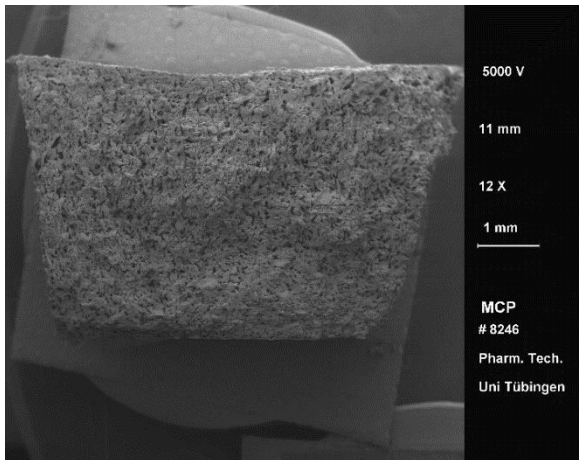


Figure 4-90: SEM picture of Metoclopramide HCl 100 mg Lyoc® (Entire structure), 12x magnification.

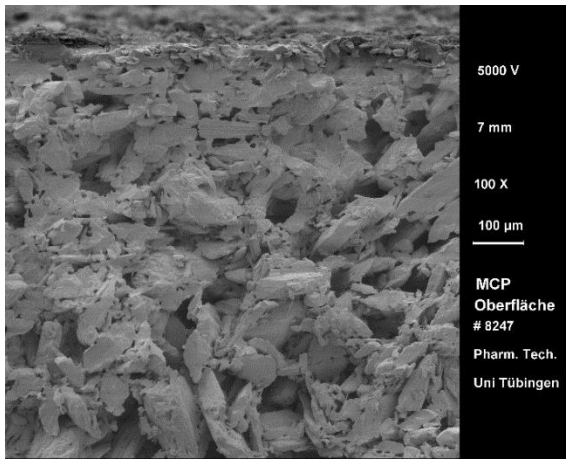


Figure 4-91: SEM picture of Metoclopramide HCl 100 mg Lyoc® (Surface), 100x magnification.

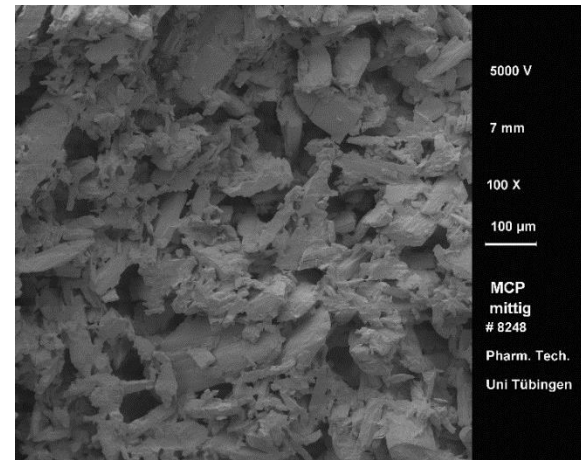


Figure 4-92: SEM picture of Metoclopramide HCl 100 mg Lyoc® (Center), 100x magnification.

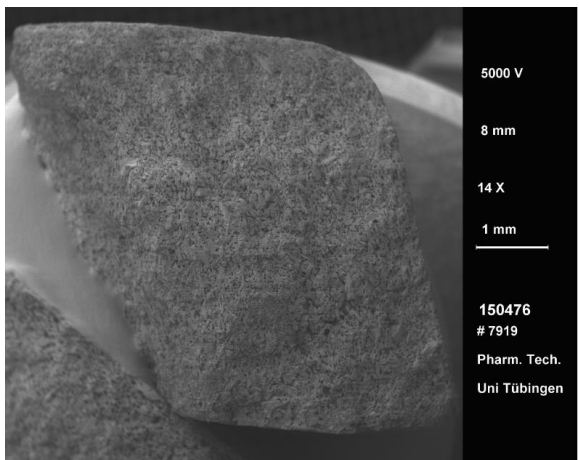


Figure 4-93: SEM picture of Metamizol Na 100 mg Lyoc® (Entire structure), 14x magnification.

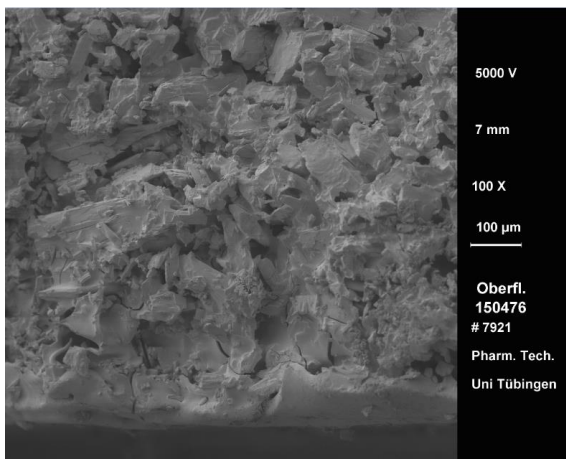


Figure 4-94: SEM picture of Metamizol Na 100 mg Lyoc® (Surface), 100x magnification.

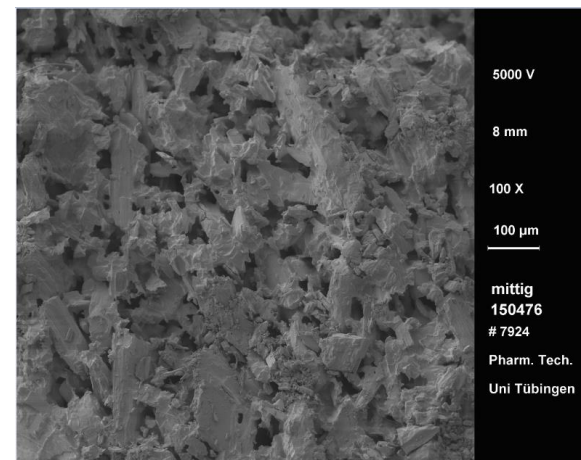


Figure 4-95: SEM picture of Metamizol Na 100 mg Lyoc® (Center), 100x magnification.

4.3.4 Conclusion

The solubility characteristics of APIs used within Lyocs® was further investigated. In the frame of this study, two crystalline soluble APIs (metoclopramide HCl monohydrate and metamizol Na) and two crystalline less-soluble APIs (paracetamol and sildenafil citrate) were used in order to identify their solid state after lyophilization.

For Lyocs® containing soluble APIs, XRPD and Raman mapping were conducted on the resulting Lyocs®, allowing the determination of the API solid state. Regarding the soluble APIs, they both get partially or completely amorphous during the lyophilization process. Due to this API amorphization, the cohesion within the Lyocs® was reduced, leading to an explosion of Lyocs® in the FD during the lyophilization. The loading limit of soluble API was estimated at 16 % of the total dried mass of the Lyoc®, meaning that above this percentage, no Lyocs® can be produced.

Regarding the less-soluble APIs, XRPD study was the best method to prove that both APIs stay crystalline after lyophilization, giving elegance to the Lyoc® structure.

4.4 Case Study: Development of Paracetamol 100 mg Lyocs®

The development of Paracetamol 100 mg Lyocs® formulation was investigated in this chapter. Paracetamol was selected for this formulation development study, since it is sparingly soluble in water, which matches perfectly the class of API used in the Lyoc® technology (see Section 4.3). Moreover, two doses of Paracetamol Lyocs® already exist on the market, namely 250 mg and 500 mg doses. Both marketed formulations contain Pearlitol® 110 C and dextran as excipients. That is why any compatibility study between paracetamol and the two previously named excipients needed to be performed to ensure the stability of the API in the formulation. The influence of mannitol grade on the IPC results, on the API release and on the API sedimentation during lyophilization was especially studied. In the second step, the lyophilization process was optimized with respect to process time in order to reduce the energy costs of the company. For this purpose, the critical quality attribute was defined to be the final moisture content of the final product.

4.4.1 Influence of Mannitol Grade

4.4.1.1 Tested Formulations

The placebo formulations of the Chapter 4.1.3.2.4 were used as a basis for the Paracetamol Lyoc® formulation. The quantity of paracetamol (i.e. 100 mg) replaced the corresponding quantity of mannitol. Paracetamol Lyocs® with Pearlitol® 160 C were not manufactured due to the gritty feeling in mouth observed in Section 4.1.3.2.4. The formulations are summarized below, in Table 4-40.

F1: Paracetamol 100 mg Lyocs® with Pearlitol® 25 C.

F2: Paracetamol 100 mg Lyocs® with Pearlitol® 50 C.

F3: Paracetamol 100 mg Lyocs® with Pearlitol® 110 C.

F4: Paracetamol 100 mg Lyocs® with a mixture of Pearlitol® 25 C and 160 C (1+1).

F5: Paracetamol 100 mg Lyocs® with a mixture of Pearlitol® 25 C and 160 C (3+1).

F6: Paracetamol 100 mg Lyocs® with a mixture of Pearlitol® 25 C and 160 C (1+3).

Table 4-40: Composition of the formulations tested.

Substance	mg / dose					
	F1	F2	F3	F4	F5	F6
Batch Nr	160284	160285	160283	160289	160290	160291
Paracetamol <i>SAP-Nr 251937</i>	100	100	100	100	100	100
Mannitol	615	615	615	-	-	-
Pearlitol® 25 C	-	-	-	307,5	410	205
Pearlitol® 160 C	-	-	-	307,5	205	410
Dextran <i>SAP-Nr 236561</i>	25	25	25	25	25	25
Water <i>SAP-Nr 14022</i>	550	550	550	550	550	550
Total	1290	1290	1290	1290	1290	1290

IPCs are summarized in Table 4-41.

Table 4-41: IPC results of the formulations F1-F6 \pm SD.

IPC results						
	F1	F2	F3	F4	F5	F6
η [mPa.s]	221	152	83	158	154	93
F	0,98	0,98	0,98	0,98	1	1
Sedimentation in FD	No	No	No	No	No	No
H [N], n=20	54 \pm 17	53 \pm 11	48 \pm 8	42 \pm 12	39 \pm 11	50 \pm 10
D.T [s], n=6	18 \pm 4	8 \pm 2	5 \pm 1	9 \pm 3	11 \pm 2	8 \pm 2
Appearance	Good visual aspect. Do not break during unpacking. Not powdery	Good visual aspect. Do not break during unpacking. Not powdery.	Good visual aspect. Do not break during unpacking. Not powdery.	Good visual aspect. Do not break during unpacking. Not powdery.	Good visual aspect. Do not break during unpacking. Not powdery.	Good visual aspect. Do not break during unpacking. Not powdery.

The IPCs obtained for each batch are very concluding (Table 4-41). As expected, D.T increases in the following order: F3 < F2 < F1. This is due to the particle size of mannitol (the smaller the particle size, the higher the cohesion within the Lyocs®). The same trend could be observed for the D.T of the formulations containing a mixture of Pearlitol® 25 C and

Pearlitol® 160 C. Indeed, D.T (F6) < D.T (F4) < D.T (F5). This result is coherent since the amount of Pearlitol® 25 in F6 is lower than in F4, which is itself also lower than in F5 (see Section 4.1.3.2.4 and the respective D.T results of F1, F2, F3). The visual aspect of the Lyocs® was the same for each formulation. The Lyocs® resulting from F1 to F6 were indeed all smooth, without visual defects, and were not powdery. The viscosity of F1 is like expected the highest one, due to the higher amount of small particle size of mannitol in the suspension. F2, F4 and F5 (where mannitol particle size is medium) have close viscosities between 152 and 158 mPa.s. The same phenomenon can be observed for F3 and F6, where mannitol particle size is the bigger. As previously seen in Section 4.1.3.2.4, when two suspensions of a constant mass, the one containing small particles has more particles in its system, increasing the interactions between the particles and thus leading to an increase in the viscosity. Any real trend (i.e. any significant difference) could be detected for H in function of mannitol particle size for F1 to F6. The results obtained in this section are fully comparable to the one of the respective placebos (see Section 4.1.3.2.4). Paracetamol only has a marginal effect on the resulting Lyocs®.

4.4.1.1 Microscopic Characteristic

The first picture of each Lyoc® (see Figures 4-96, 4-99, 4-102, 4-105, 4-107 and 4-111) shows their entire microscopically structure. They are quite homogeneous, except for F5 (see Figure 4-108), where agglomerates are observed. Those agglomerates could be due to a bad homogenization of the suspension during the mixing step, leading to remaining powder clumps in the suspension. A finer structure and a better homogeneity could be observed for F1 (Figure 4-96) and F4 (Figure 4-105) than F2 (Figure 4-99), F3 (Figure 4-102), F5 (Figure 4-108) and F6 (Figure 4-111). Air bubbles are also observable on Figures 4-96, 4-98, 4-99, 4-101, 4-104, 4-106, 4-108, 4-110, 4-111 and 4-113 (see red marks on each Figure), which could have been incorporated through a too intense mixing of the suspension. The incorporation of air bubbles in the formulation might be nevertheless avoided by mixing the suspension in a closed container and by applying a vacuum in order to degas the suspension. Moreover, it was also observed that the microscopically structure of the placebos (see Figures of Paragraph 4.1.3.2.5) are very similar to the formulations containing paracetamol, which means that the API does not interfere the microscopically structure of the Lyocs®.

By combining the microscopic analysis carried out by means of SEM with the IPC results (especially the D.T), it can be concluded that F2, F3, F4 and F6 are the most appropriated formulations. F4 and F6 could even bring a plus to the formulation, due to the cooling effect given through the Pearlitol® 25 C grade.

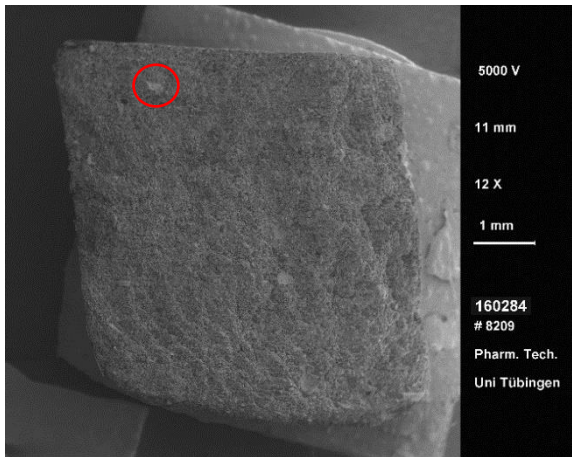


Figure 4-96: SEM picture of F1 (Entire structure),
12x magnification.

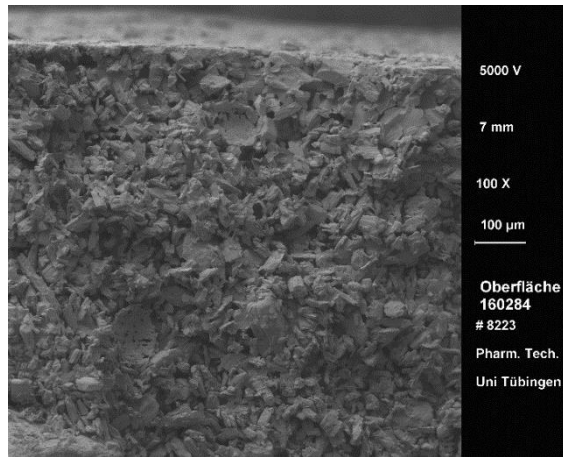


Figure 4-97: SEM picture of F1 (Surface),
100x magnification.

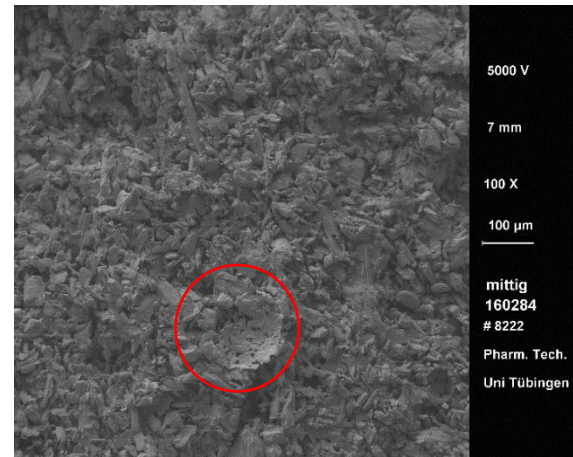


Figure 4-98: SEM picture of F1 (Center),
100x magnification.

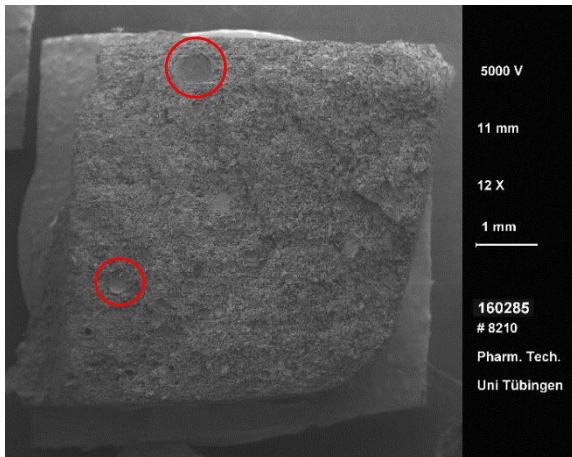


Figure 4-99: SEM picture of F2 (Entire structure),
12x magnification.

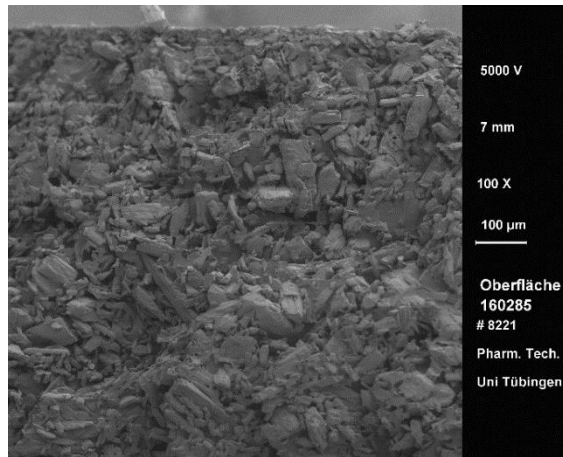


Figure 4-100: SEM picture of F2 (Surface),
100x magnification.



Figure 4-101: SEM picture of F2 (Center),
100x magnification.

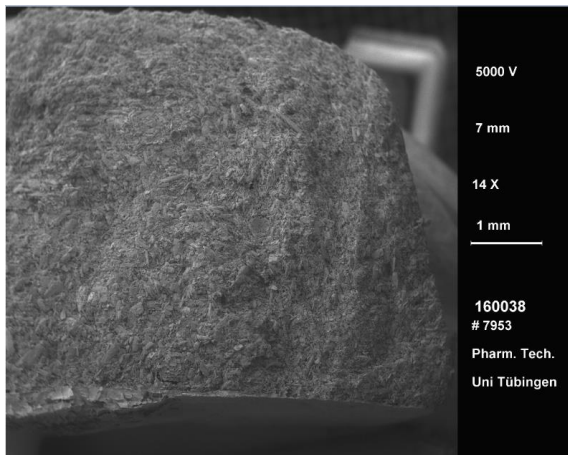


Figure 4-102: SEM picture of F3 (Entire structure),
12x magnification.

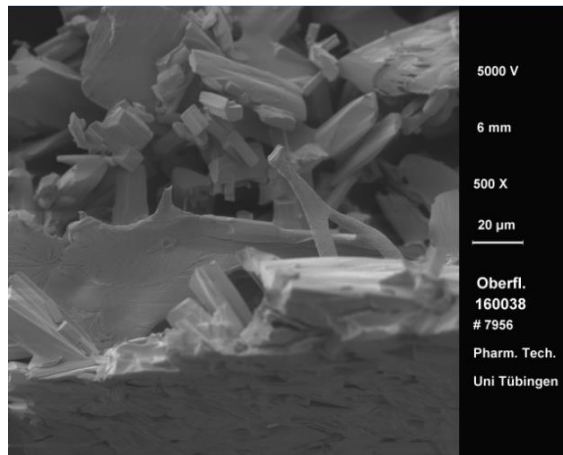


Figure 4-103: SEM picture of F3 (Surface),
500x magnification.

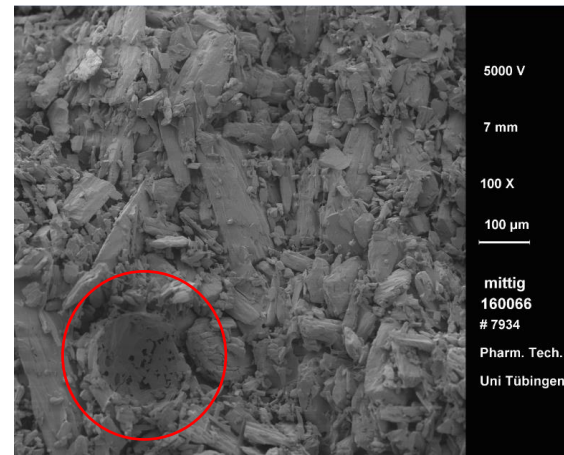


Figure 4-104: SEM picture of F3 (Center),
100x magnification.

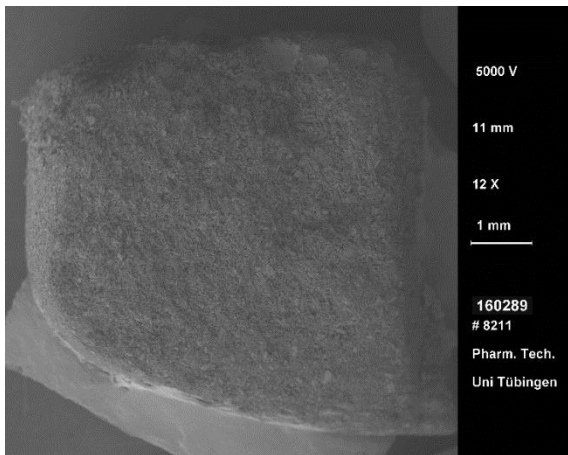


Figure 4-105: SEM picture of F4 (Entire structure),
12x magnification.



Figure 4-106: SEM picture of F4 (Surface),
100x magnification.

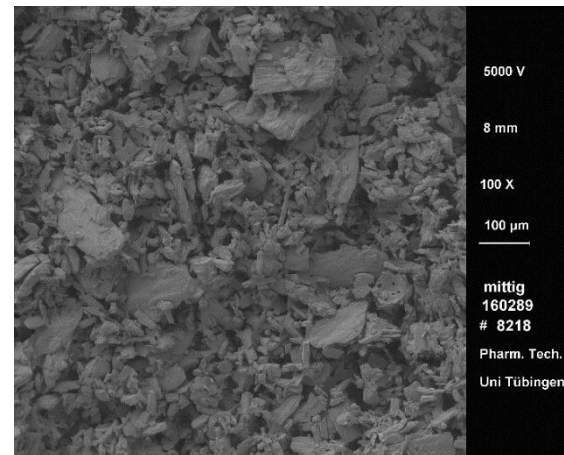


Figure 4-107: SEM picture of F4 (Center),
100x magnification.

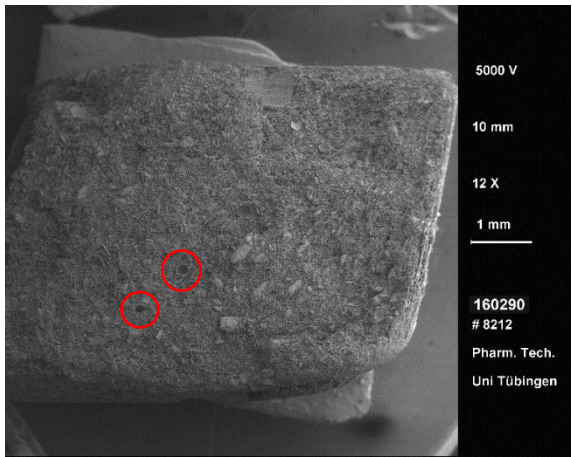


Figure 4-108: SEM picture of F5 (Entire structure),
12x magnification.

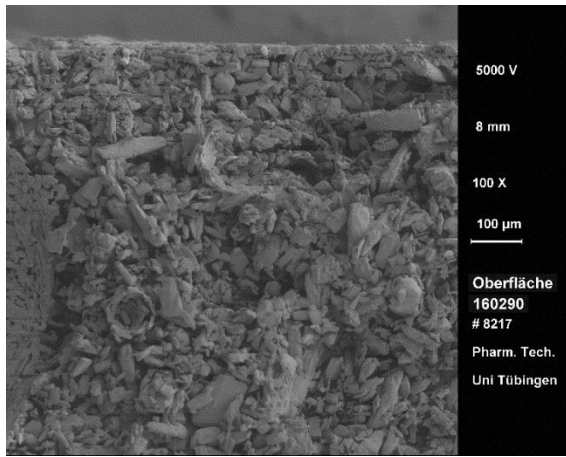


Figure 4-109: SEM picture of F5 (Surface),
100x magnification.

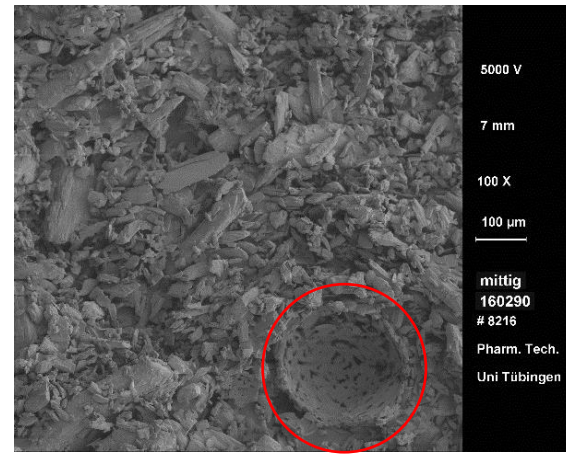


Figure 4-110: SEM picture of F5 (Center),
100x magnification.

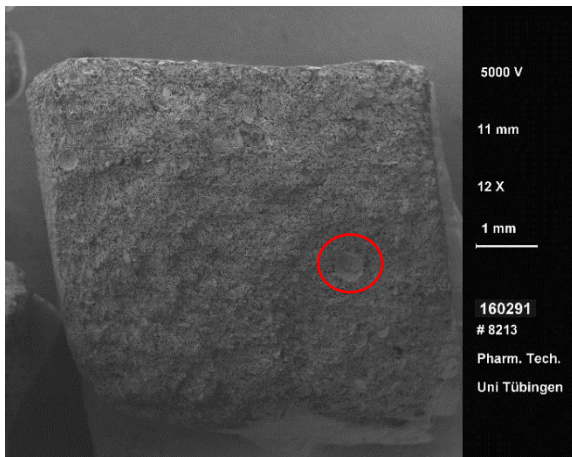


Figure 4-111: SEM picture of F6 (Entire structure),
12x magnification.

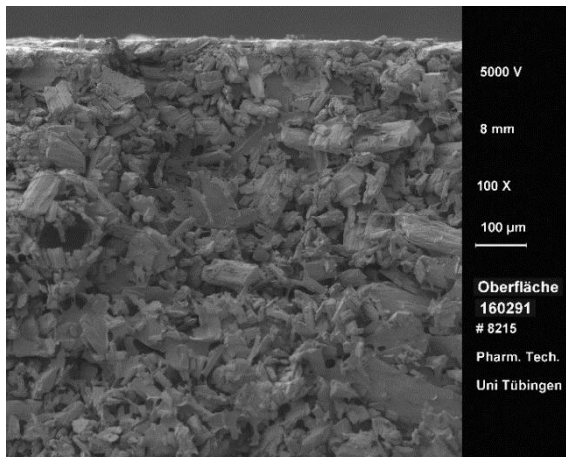


Figure 4-112: SEM picture of F6 (Surface),
100x magnification.

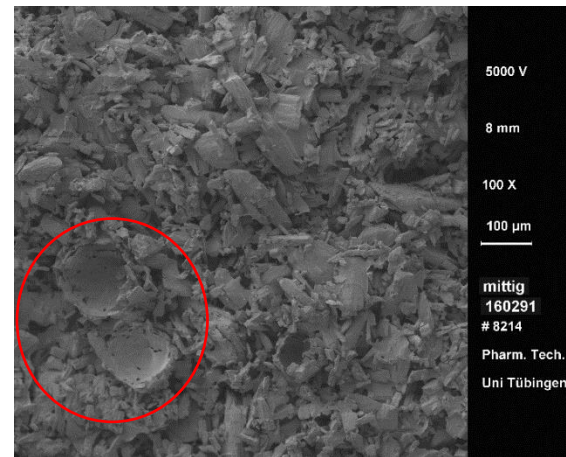


Figure 4-113: SEM picture of F6 (Center),
100x magnification.

4.4.1.1.2 Porosity of Lyocs®

Table 4-42 summarizes the porosity results of the Lyoc® formulations F1-F6. Those porosity results vary between 57 % and 59 %. The results obtained are consistent with the ones obtained to the respective placebo formulations (see Table 4-20)

The % error between the measured porosity and the calculated one is lower than 5 % for F1 and F4.

The % error of F2, F3, F5 and F6 is higher than 5 %, which could be explained by the presence of air bubbles in the Lyocs® (see Figures 4-99, 4-102, 4-108 and 4-111). Those air bubbles could have been incorporated in the formulation during the mixing step, due to a too high shear rate. The formula used to calculate the porosity of Lyocs® is still appropriated in order to quickly estimate the product porosity, even if a measurement might be more precise in the case of Lyocs®.

Table 4-42: Porosity measurements of the different placebo Lyocs® (n=5).

	Porosity measured [%]	Porosity calculated [%]	% error
F1	56,9	55,0	3,3
F2	58,2	55,0	5,5
F3	58,7	55,0	6,3
F4	56,8	55,0	3,2
F5	58,6	55,0	6,1
F6	58,5	55,0	6,0

4.4.1.2 API Release

The API release of the formulations F1-F6 was measured by means of UV-VIS spectroscopy according to the Ph.Eur. Paragraph 2.9.3, with a validated method of the Analytical Department of Teva Ulm. The measurement conditions are summarized in Annex (see Section 6.3). API release is a primordial test to complete in formulation development, as it determines the percentage of API that has been released from the dosage form and has dissolved in the dissolution medium during the test period. It can provide an estimation on the matrix which releases the API faster for same measurement conditions.

Table 4-43: Paracetamol release of F1-F3 (n=6).

F1				F2				F3				Paracetamol 1g Tablet			
Time [h:mm]	Average %	Min %	Max %	Time [h:mm]	Average %	Min %	Max %	Time [h:mm]	Average %	Min %	Max %	Time [h:mm]	Average %	Min %	Max %
0:00	0,00	0,00	0,00	0:00	0,00	0,00	0,00	0:00	0,00	0,00	0,00	0:00	0,00	0	0
0:05	74,93	60,48	89,96	0:05	73,70	65,16	83,73	0:05	80,66	64,44	98,59	0:05	59,40	37,65	72,60
0:10	91,95	82,27	98,90	0:10	91,57	82,33	99,19	0:10	91,77	79,99	97,77	0:10	87,39	85,34	91,99
0:15	96,83	93,23	100,11	0:15	96,47	92,19	99,26	0:15	95,70	89,49	98,15	0:15	91,88	86,43	96,36
0:20	98,25	97,09	100,09	0:20	97,42	96,15	98,95	0:20	96,86	93,79	98,12	0:20	95,14	90,00	98,24
0:30	98,54	97,14	100,09	0:30	97,59	96,53	98,96	0:30	97,00	94,02	98,69	0:30	97,03	92,26	100,51
0:45	98,47	97,13	100,05	0:45	97,61	96,60	98,96	0:45	96,93	94,00	98,35	0:45	98,11	95,16	101,31
1:00	98,50	97,23	100,03	1:00	97,63	96,61	99,02	1:00	96,98	93,95	98,65	1:00	98,64	96,55	101,60

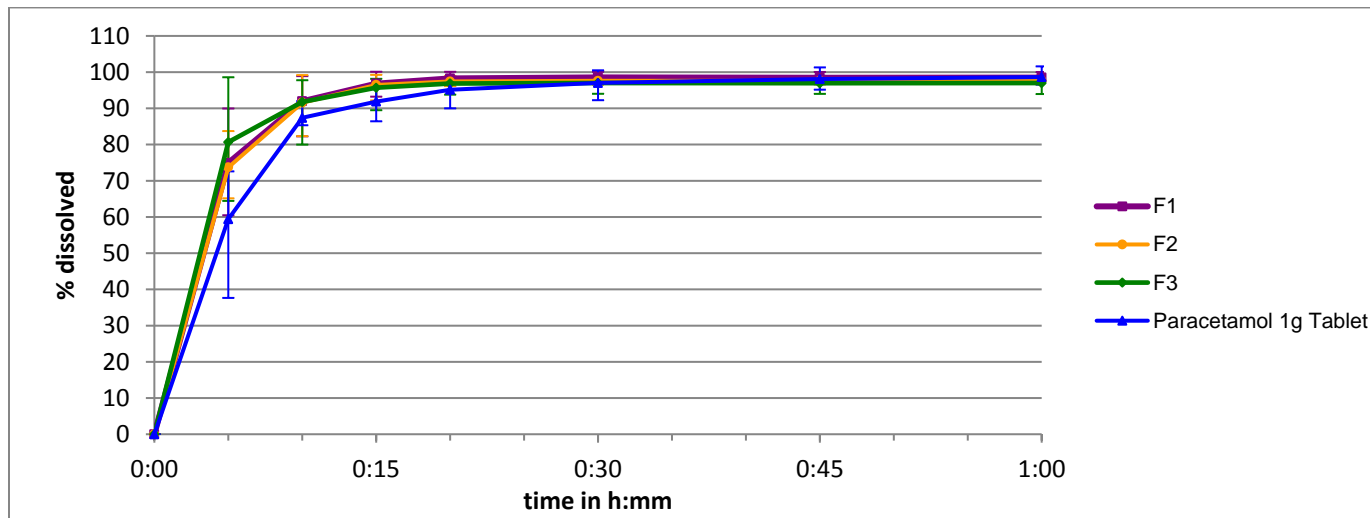


Figure 4-114: In-Vitro-Dissolution of Paracetamol 100 mg Lyoc® F1-F3 (n=6), Paddle / Buffer pH 5.8 / 900 mL / 50 rpm / GF 1µm / UV-Evaluation

Table 4-44: Paracetamol release of F4-F6 (n=6).

F4				F5				F6				Paracetamol 1g Tablet			
Time [h:mm]	Average %	Min %	Max %	Time [h:mm]	Average %	Min %	Max %	Time [h:mm]	Average %	Min %	Max %	Time [h:mm]	Average %	Min %	Max %
0:00	0,00	0,00	0,00	0:00	0,00	0,00	0,00	0:00	0,00	0,00	0,00	0:00	0,00	0	0
0:05	71,97	50,91	87,06	0:05	82,42	71,24	94,65	0:05	76,02	67,09	81,93	0:05	59,40	37,65	72,60
0:10	87,32	71,41	96,35	0:10	95,23	88,34	98,75	0:10	92,89	86,58	97,26	0:10	87,39	85,34	91,99
0:15	92,54	81,02	96,87	0:15	98,04	96,70	98,93	0:15	97,23	94,63	99,04	0:15	91,88	86,43	96,36
0:20	94,30	85,75	96,86	0:20	98,30	97,97	98,93	0:20	98,55	97,65	99,76	0:20	95,14	90,00	98,24
0:30	94,91	87,51	97,72	0:30	98,28	97,95	98,93	0:30	98,62	97,67	99,80	0:30	97,03	92,26	100,51
0:45	93,54	87,34	98,42	0:45	98,30	97,97	98,95	0:45	98,64	97,67	99,81	0:45	98,11	95,16	101,31
1:00	94,86	87,29	97,51	1:00	98,30	97,98	98,97	1:00	98,68	97,71	99,83	1:00	98,64	96,55	101,60

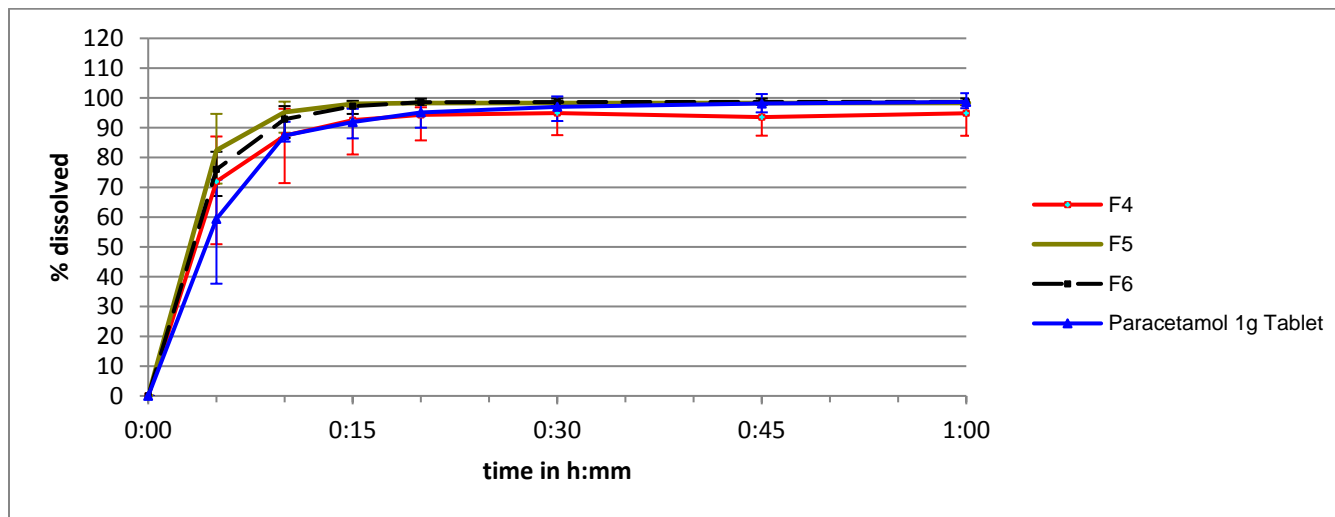


Figure 4-115: In-Vitro-Dissolution of Paracetamol 100 mg Lyoc® F4-F6 (n=6), Paddle / Buffer pH 5.8 / 900 mL / 50 rpm / GF 1µm / UV-Evaluation

Figure 4-114 shows that the API release is not influenced by the mannitol quality. Based on Table 4-43, between ca. 74 and 81 % of API is already released after 5 minutes from F1-F3, whereas only 59 % of API is released after 5 min from a conventional tablet. Ca. 96 % of API release is reached after 15 minutes for the Lyoc® formulations, whereas the normal tablet needs between 20 and 30 min to release this amount of API.

Figure 4-115 did not show any statistical difference of API release between those 3 formulations. Based on Table 4-44, between ca. 72 and 82 % of API is already released after 5 minutes from F4-F6, whereas 59 % of API is released after 5 min from a conventional tablet. Ca. 96 % of API release is reached after 15 minutes for the Lyoc® formulations, whereas the normal tablet needs between 20 and 30 min to release this amount of API.

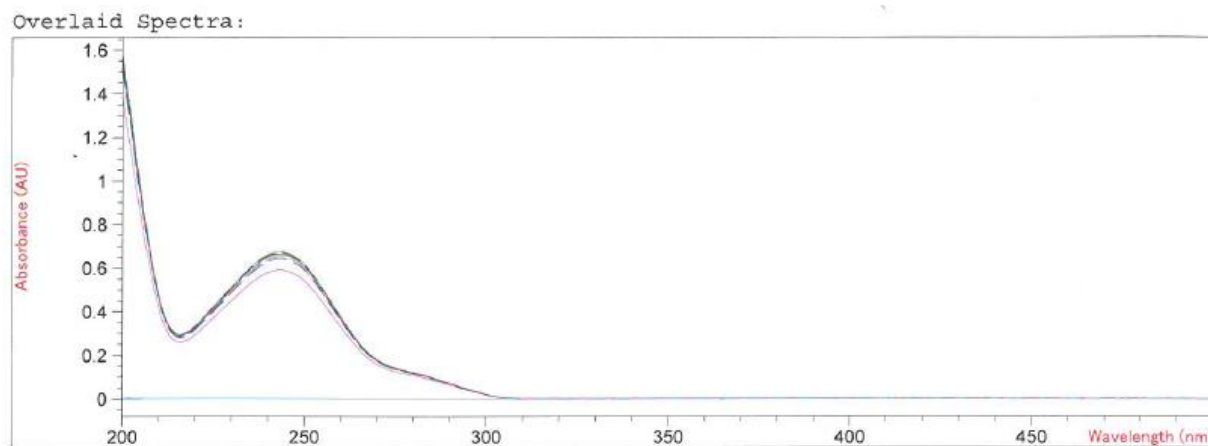
The Lyoc® formulations thus allow a much faster release, since ca. 15 % more of the API is released 5 minutes after the intake of the drug than the conventional tablet. Lyocs® could thus give the API faster available in the body than a conventional tablet. This could lead to a faster action of the drug in the organism.

A comparison of dissolution profile between the conventional tablet and the Lyocs® formulations (F1 to F6) was carried out by calculating both difference factor (f_1) and similarity factor (f_2). The results are summarized in Annex 6.3.2. It is to note that the f_2 factors of F3 and F5 are very close to 50, meaning that a faster API release could be expected for both formulations rather than conventional tablets. For F1, F2, F4 and F6, $f_1 < 15$ and $f_2 > 50$, meaning that their dissolution profile are similar to the one of conventional tablets. The performance of Paracetamol Lyocs® is thus equivalent to the one of conventional tablets. Nevertheless, Lyocs® provide to the patient a better treatment comfort due to an easier and more discreet treatment, since no water is needed for the intake of the drug and the ODT disintegrates itself in the patient's mouth.

4.4.1.3 Content of Uniformity

The content of uniformity of each batch was measured, in order to prove the homogeneity of API within the tablets. This test was made according to the Ph. Eur., paragraph 2.9.40 (EDQM, 2014f). The measurement conditions are summarized in Annex (see Section 6.4.1)

The statistical results such as the average content \bar{X} , the sample standard deviation s , the relative standard deviation RSD were thus determined.



#	Name	Abs<243nm>	#	Name	Abs<243nm>
1	Lösungsmittel	4.7684E-7	9	160283XXXT_3	0.66040
2	Placebo 160295	3.4332E-5	10	160283XXXT_4	0.66656
3	Placebo 160296	1.2112E-4	11	160283XXXT_5	0.65992
4	Placebo 160297	6.3419E-5	12	160283XXXT_6	0.66286
5	Standard 2	0.58871	13	160283XXXT_7	0.64920
6	Standard 1	0.67223	14	160283XXXT_8	0.65983
7	160283XXXT_1	0.65922	15	160283XXXT_9	0.66818
8	160283XXXT_2	0.65963	16	160283XXXT_10	0.64213

Figure 4-116: Absorption measurement of Placebo formulations, Reference solutions and F3.

As shown on the placebo curves in the Figure 4-116, the excipients do not have any absorption at 243 nm, meaning that the absorption at 243 nm is directly correlated with the API content in the LyoCs®, and is not influenced through the excipients.

Table 4-45: API content of LyoCs® with statistical values (n=10).

	F1	F2	F3	F4	F5	F6
\bar{X} [%]	97,12	98,60	97,41	94,32	101,64	105,35
s	2,94	4,18	1,15	8,55	1,24	0,68
RSD	3,03	4,24	1,18	9,06	1,22	0,65

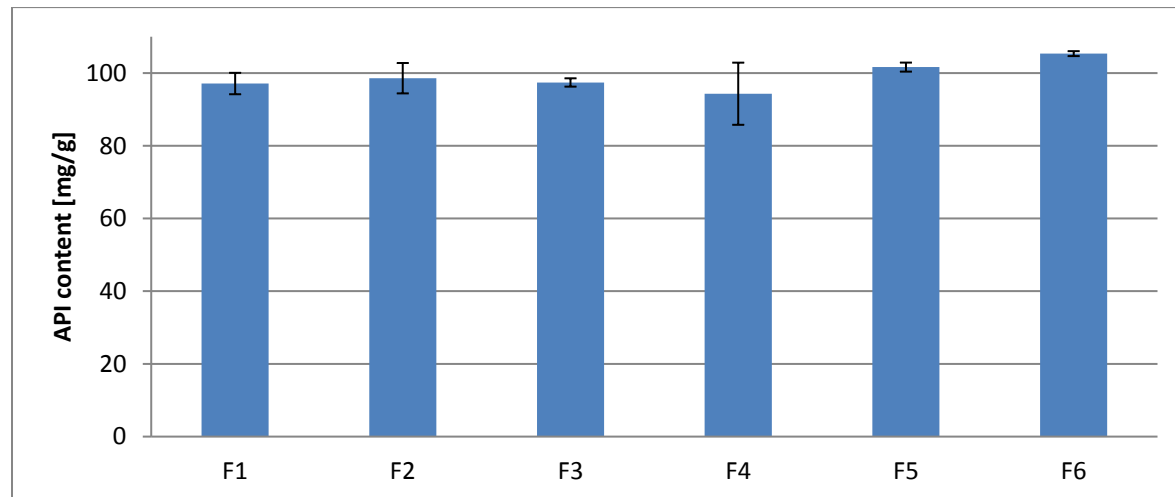


Figure 4-117: Content of uniformity in F1-F6 (n=10) ± SD.

The API content of F1, F2, F3 and F5 is good, as \bar{X} of those formulations stays in the interval $100 \pm 5\%$. Formulations having the bigger amount of Pearlitol® 160 C (i.e. F4 and F6) both have an API deviation greater than 5 %, meaning that the API homogeneity in those formulations is varying too much. The use of Pearlitol® 160C in proportion higher than 27,7 % on the dried mass of the formulation is thus not appropriate for the Lyoc® technology. This deviation could be the result of a bad mixture between the two different grades of mannitol. The higher inhomogeneity of F4 could also be seen in the API release curve (see Figure 4.115), where the error indicator interval was quite higher than the one of other formulations, as on Figure 4-117 where the standard deviation is clearly bigger than for the other formulations. Since the suspension of F4 had the same characteristics as the other formulations, the API inhomogeneity could be explained by a bad manufacturing process (e.g. air inclusion during the mixing step due to a too high mixing rate or bad pipetting).

A one-way ANOVA with a significance level $\alpha=0,05$ and a Tukey Post hoc statistical analysis were performed on the uniformity of content between all the groups F1 to F6. Based on the results summarized in Annex 6.4.2, a significant difference could be observed between [F1-F6], [F2-F6], [F3-F6], [F4-F6] and [F4-F5]. Indeed, the two main anomalies are observed for F4 (too low mean value and too high standard deviation) and F6 (too high mean value). Those two formulations are containing the highest concentration of Pearlitol® 160 C in the mannitol grade mixture (Pearlitol® 25 C + Pearlitol® 160 C). The following proposition could be established: when Pearlitol® 160 C is present in too big proportions in the mixture Pearlitol® 25 C + Pearlitol® 160 C, the mixture behavior with Pearlitol® 25 C may be bad, leading to an inhomogeneity of materials in the suspension. To confirm this hypothesis, the one-way ANOVA analysis should be carried out on 3 batches for each formulation and not 1. Unfortunately, due to lack of time and capacity, 3 batches per formulation could not be produced.

4.4.1.4 Study of Sedimentation Within The Pipette

The same analytical measurement system was used as in Chapter 4.4.1.3. F3 was produced with different pipette tip volumes, namely 10 mL, 25 mL and 50 mL in order to determine if sedimentation occurs within the pipette. 1 mL of suspension was poured in each blister cavity. For each pipette volume, 10 samples coming from the beginning of the pipetting and 10 samples coming from the end of the pipetting were randomly picked up.

Table 4-46: API content of Lyocs® with statistical values (n=10).

Batch Nr	10 mL pipette		25 mL pipette		50 mL pipette	
	Beginning	End	Beginning	End	Beginning	End
\bar{X} [%]	90,11	92,49	98,10	95,88	92,10	96,52
s	0,59	0,90	1,54	1,70	3,61	3,24
RSD	0,66	0,97	1,57	1,77	3,92	3,36

The standard deviation of the 3 pipette volumes increased from 10 mL pipette to 50 mL pipette. It can be concluded that the 10 mL pipette gives a more precise dosage ($0,59 < s < 0,90$) than

a 25 mL ($1,54 < s < 1,70$) and a 50 mL pipette ($3,24 < s < 3,61$). Nevertheless, the s value of the 25 mL is still acceptable to be used in the development step, since s lies below 3.5. In comparison to the 10 mL pipette, a 25 mL pipette gives a faster dispensing time and offers more comfort to the worker by reducing the number of suspension sampling.

The API content [%] \pm SD was schematically represented in Figure 4-118 in order to determine if sedimentation occurred within the pipette tip.

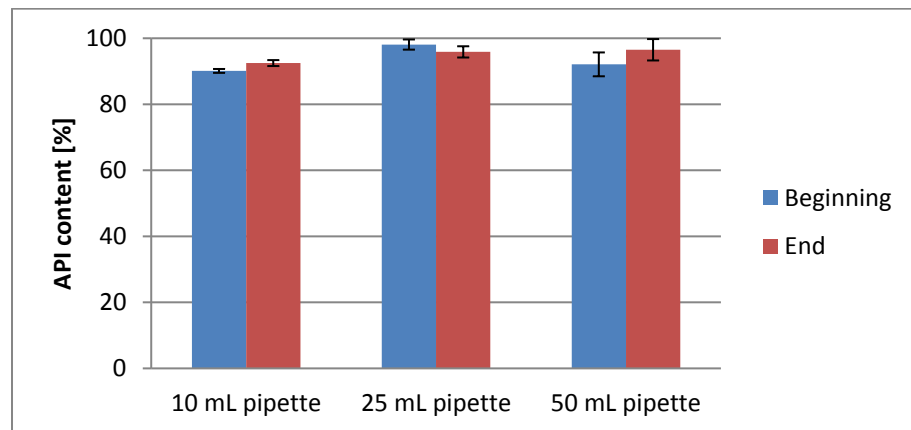


Figure 4-118: API content \pm SD of Lyocs® at the Beginning and the End of pipetting (n=10).

As shown on Figure 4-118, it could be supposed that the only statistical difference is observed for the 10 mL tip pipette, since the SD ranges for the beginning and the end of the pipetting are not overlapping. The SD ranges of the 25 mL and the one of the 50 mL are overlapping, which may mean that no statistical difference is observed between the API concentration at the beginning and at the end of the pipetting for those two pipette tips. A t-test analysis was carried on in the 3 pipette tips in order to study the statistical difference of API content between the beginning and the end of the pipetting step. Based on the results summarized in Annex 6.5.1, the calculated t-value is for the 3 cases above t-critical value, meaning that a statistical difference is observable for all the 3 pipette tips.

Figure 4-118 and the results summarized in Table 4-46 both show that the API content of the beginning of pipetting is lower than the end of pipetting for the 10 mL and 50 mL pipette tips. This phenomenon could be explained for the 10 mL pipette tip by the fact that the diameter of the dispensing hole of the 10 mL pipette tip (diameter = 0,8 mm) is the smaller than the one of 25 mL (diameter = 1,34 mm) and 50 mL (diameter = 1,92 mm) pipette tips. A possible reason for that can be that at the beginning of the pipetting, the API sticks to the pipette tip wall, giving a bad API repartition and disturbing the mean API value, as represented on Figure 4-119.

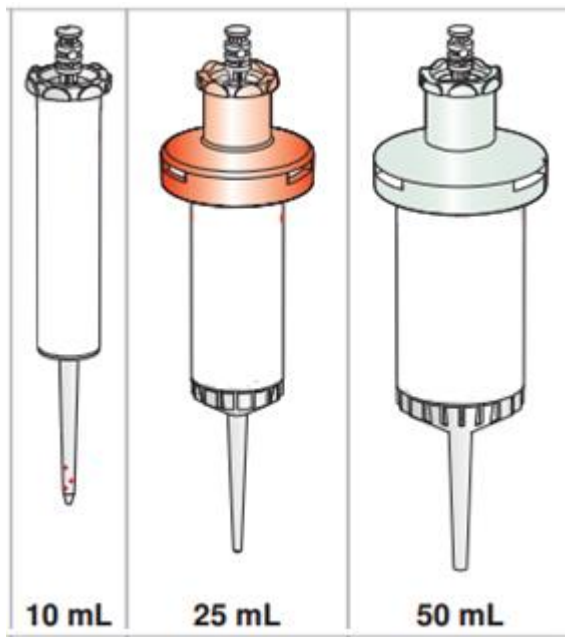


Figure 4-119: Fluid behaviour in the pipette tips, Red Particles = API.

For the 50 mL pipette tip, the lower API content at the beginning of the it could be due that

The 25 mL is thus the best suitable pipette for the Lyoc® technique as it has smaller SD than the 50 mL pipette.

4.4.1.5 Study of Sedimentation Within The Suspension Placed in The Blister Cavity

The sedimentation within the Lyocs® of the 6 formulations of the chapter 4.4.1.1 was studied as described in Chapter 3.2.5.10.2.

Table 4-47 summarizes the paracetamol content in mg/g per half Lyoc® \pm SD.

Table 4-47: API content [mg/g] in each half Lyoc® of the formulations F1-F6 (n=6) \pm SD, where “Bottom” corresponds to the half part in contact with the PVC cavity whereas “Top” corresponds to the half part in contact with the aluminum foil.

		F1	F2	F3	F4	F5	F6
API content	Bottom	158,17 \pm 3,0 3	158,76 \pm 4,7 8	157,92 \pm 3,5 5	159,07 \pm 4,6 9	158,80 \pm 5,6 2	159,13 \pm 5,4 8
	Top	153,89 \pm 5,0 9	154,19 \pm 3,9 7	152,91 \pm 3,0 2	151,70 \pm 3,8 7	153,23 \pm 4,4 2	154,54 \pm 5,2 7

A t-test analysis with a significance level $\alpha=0,05$ was conducted on the results of Table 4-47 in order to statistically conclude on the sedimentation of the API in the manufactured suspension during the lyophilization process. Indeed, this test allows to analyze the possible differences within the batch (i.e. interbatch variability) and the results are summarized in Annex (see Section 6.5.2).

Since the t-values of F1, F2, F5 and F6 is below t-critical, no statistical significant difference can be observed between the two half Lyocs® of those formulations. No significant sedimentation occurs during the lyophilization process for F1, F2, F5 and F6.

However, t-value (F3) and t-value (F4) are bigger than the critical value. That is why it can be concluded that for F3 and F4, there is a statistical difference between the half Lyocs®. Therefore, sedimentation occurs within those two samples.

It is to note that the particle size D₅₀ of Paracetamol is 150 µm.

This sedimentation occurring by can be due to the particle size of mannitol. F3 indeed contains Mannitol of 110 µm, whereas F4 contains 50% of Pearlitol® 25 C and 50 % of Pearlitol® 160 C. For F4, maybe the two grades are not mixing well together (as already underlined in Section 4.4.1.3) bringing an inhomogeneity within the Lyocs®. For F3, the lower particle size of Pearlitol® leads to faster sedimentation within the Lyocs® according to the Stock's law, which is why a significant sedimentation may occur in this sample.

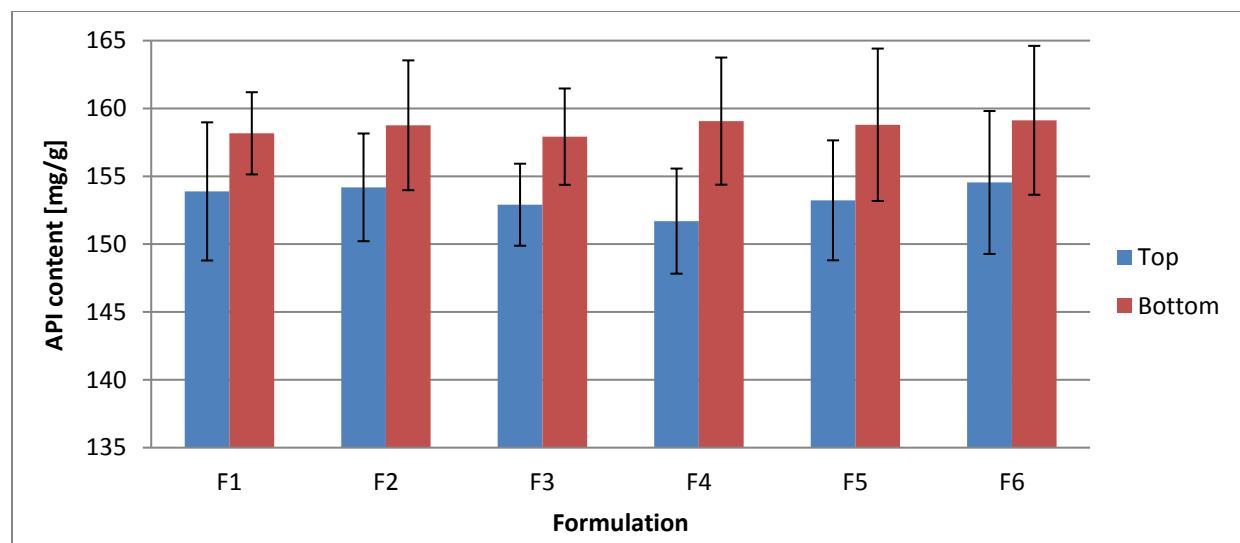


Figure 4-120: Representation of the API content [mg/g] of each half Lyoc® contained in F1-F6 ± SD (n=6).

After schematically representing the paracetamol content per half Lyoc® ± SD for F1-F6 (see Figure 4-120), a certain trend of API sedimentation within the Lyocs® can be observed, since a significant difference can be noticed for each formulation between the API content of the bottom and the top of each Lyoc®. It can thus be concluded at first sight, that sedimentation occurs thus whatever the mannitol grade, but a statistical difference between both Lyoc® halves could only be noticed for F3 and F4.

4.4.1.6 Conclusion

After having conducted an analytical study on Paracetamol 100 mg Lyocs®, it could be noticed that API release is quite independent of the mannitol grade. A faster onset of action could have been expected for the Lyocs® than the conventional tablets, possibly due to a faster D.T of Lyocs® in comparison to the one of conventional tablets. Nevertheless, the API release of Lyocs® was equivalent to the one of conventional tablets, as shown by the statistical analysis based on both f1 and f2 factors.

The Lyoc® formulations containing Pearlitol® 25 C, Pearlitol® 50 C, Pearlitol® 110 C and Pearlitol® 25 C/160 C (3+1) (i.e. F1, F2, F3 and F5) presented a more consistent API content than Lyoc® formulations with Pearlitol® 25 C/160 C (1+1) and (1+3) (i.e. F4 and F6). This could be explained by the too high concentration of Pearlitol® 160 C, which may cause a bad mixture between Pearlitol® 25 C and 160 C, causing an inhomogeneity in the suspension. This result should nevertheless be studied more in details, by increasing the number of tested samples (completion of 2 other batches, in order to have a significant ANOVA statistical study).

A sedimentation trend could also be observed between the top and the bottom of each Lyocs®, as the API content was significantly different between both Lyocs® part. This trend is also notable with small Mannitol particle size. The use of a viscosity enhancer (such as xanthan gum) could prevent this sedimentation issue within the suspension and thus, provide more homogeneous tablets.

4.4.2 Process Optimization

In order to reduce the time and energy costs of the process, a process optimization was done on F1, F2 and F3. The product quality was then checked through IPCs and through a moisture content measurement by means of LoD.

F1: Paracetamol 100 mg Lyocs® with Pearlitol® 25 C.

F2: Paracetamol 100 mg Lyocs® with Pearlitol® 50 C.

F3: Paracetamol 100 mg Lyocs® with Pearlitol® 110 C.

In the production scale, the suspension is dispensed in blisters and cooled down at -40°C in a refrigerating chamber during one hour before being dried in the FD. That is why no changes were made on the freezing step in this study, in order to stay the closest to the production conditions. The studied parameters were thus T_s, p and process time of primary drying and secondary drying.

4.4.2.1 Initial Process

Table 4-48 summarizes the initial manufacturing process. The total duration is set at 15:25, almost twice as much as in the production scale.

Table 4-48: Initial manufacturing process of Lyocs®.

Step	Time [hh:mm]	T [°C]	Vacuum [mbar]	T ramp [°C/min]
Loading	00:00	-40	1000	-
Freezing	02:15	-40	1000	-
P.D	00:35	-40	0,2	-
	01:35	45	0,2	0,89
	06:00	45	0,2	-
S.D	04:00	45	0,2	-
	00:30	25	0,2	0,67
	00:30	25	0,2	-
Total duration	15:25			

Figure 4-122 shows the monitoring process during the initial lyophilization cycle. The first observation that can be made is that the three products are behaving the same during the lyophilization cycle. Therefore, the mannitol grade does not seem to have any influence on the sublimation rate occurring in the product.

The process time lasts longer than the 8 hours predetermined from the production scale. Nevertheless, the freeze-dryer characteristics of the production are different, especially the maximum shelf temperature. The shelves can reach up to 80°C in the production compared to 45°C in our case. As this process is quite gentle for the Lyoc® technology, it can be used at first for each type of formulation.

The process will be optimized step by step, in order to see the influences of every change on the product. The first step to be changed is thus the freezing one. It can be seen that the freezing process could be shortened by one hour, as the product temperature does not evolve after 2 hours (see Figure 4-122). As the product is not sensitive to temperature (even with a high increase of T after the freezing step, the product is not deteriorated), the first increase of T ramp could also be increased without any influences on the product quality, accelerating the sublimation rate and so decreasing the process duration.

The “Eiskond” curve (see black line on Figure 4-122) represents the T_{cc} during the process. A peak can be observed at the beginning of the P.D (at $t=5:00$ hours) when P_c is decreasing, reflecting the brutal entrapment of water molecule present in the chamber (such as surrounding humidity added during the loading step, frost accumulated on the chamber wall, and beginning of sublimation) (Le Floch, 2008). T_{cc} is slightly decreasing at 13:00, meaning the end of the sublimation step and that no water molecules are being entrapped on the condenser anymore (Le Floch, 2008). This is confirmed with T_p , as it can be noticed on Figure 4-122 that when T_{cc} decreases, $T_p=T_s$ designating the end of the P.D step.

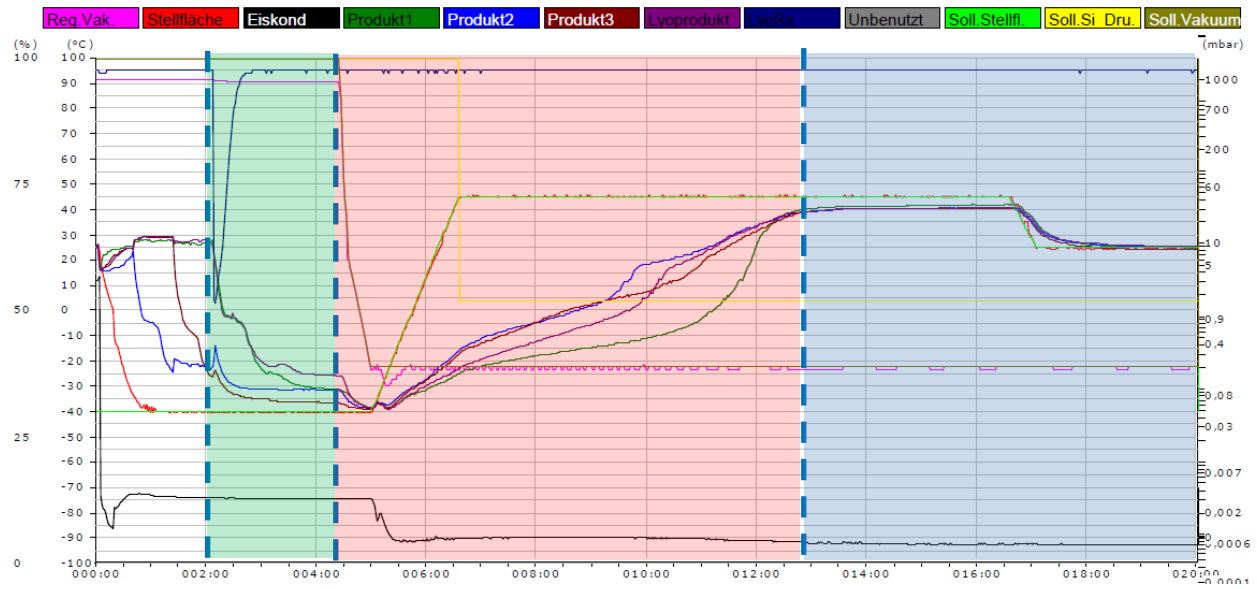


Figure 4-122: Temperature and pressure evolution during the initial lyophilization process, white=loading step, green=freezing step, red=P.D, blue=S.D.

A further evaluation can be done on the freezing step of Figure 4-122. A zoomed picture was created and represented on Figure 4-123. With Figure 4-123, two main characteristics can be determined, namely the ice formation where a plateau on the product temperature can be observed at -5°C , and the solidification point (at around -20°C) where the LyoRx curve does not change anymore as this sensor measures the electrical resistance present in the product (ChristMartin, 2015). The freezing step could thus be considerably decreased, at least 1 hour.

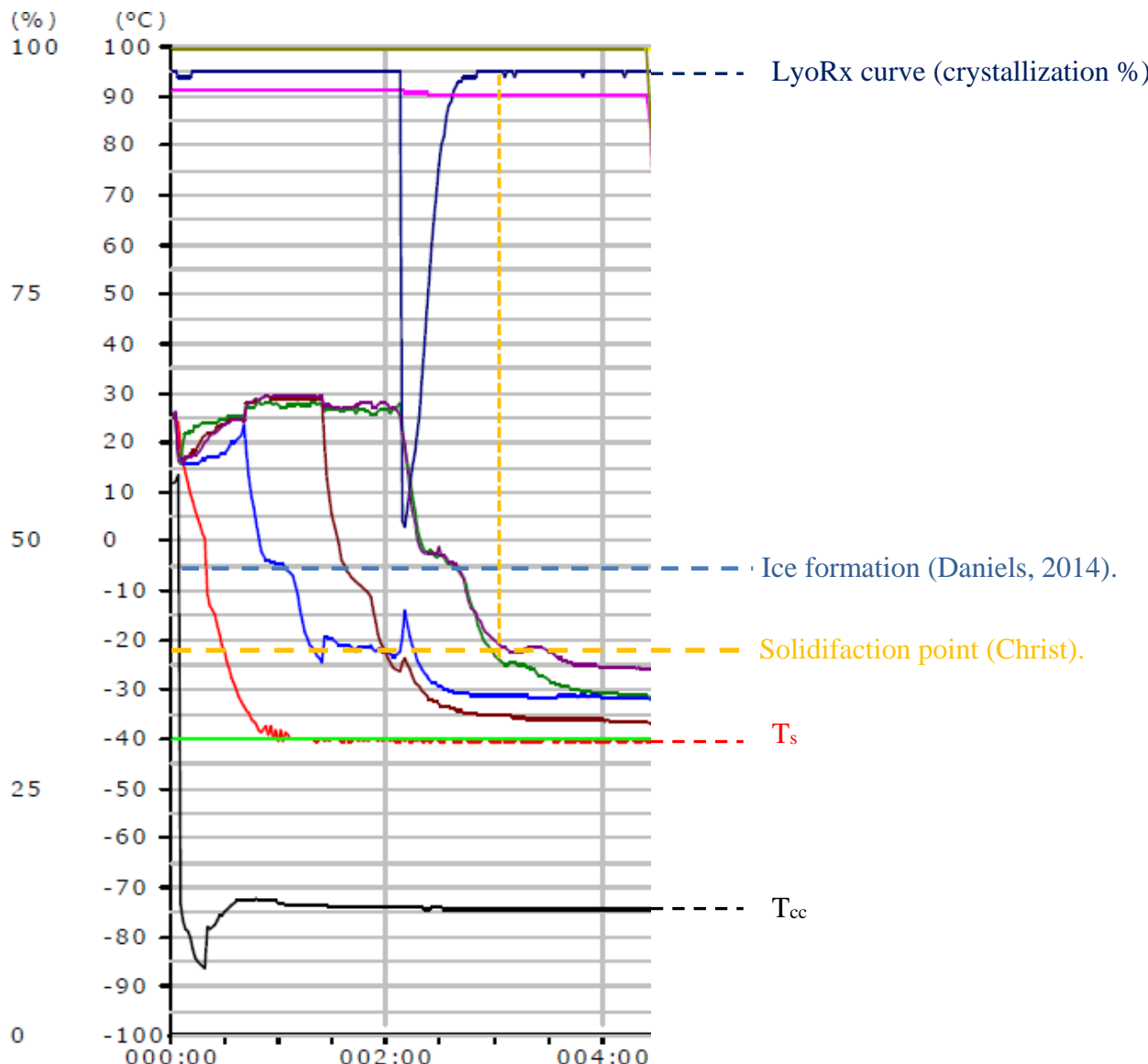


Figure 4-123: Representation of the zoomed zone of the freezing step in order to determine the Ice formation and the Solidification point of the product.

Table 4-49: IPC results of F1-F3 \pm SD.

IPC results			
	F1	F2	F3
Batch Nr	160284	160285	160283
LoD [%], n=2	0,41	0,44	0,43
H [N], n=20	54 \pm 17	53 \pm 11	48 \pm 8
D.T [s], n=6	18 \pm 4	8 \pm 2	5 \pm 1
Aspect	Good visual aspect. Do not break during unpacking. Not powdery.	Good visual aspect. Do not break during unpacking. Not powdery.	Good visual aspect. Do not break during unpacking. Not powdery.

The IPCs obtained with the initial process in Table 4-49 will be taken as reference for the optimization study. The LoD value will be carefully observed. It can be firstly noticed that whatever the mannitol grade, the LoD values are similar, meaning that the LoD is not influenced by structural aspects of Lyocs®.

4.4.2.2 Optimization 1

Table 4-50 summarizes the first optimization of the manufacturing process. The total duration is decreased down to 13:20 (2 hours less than the initial process). For this, as explained in Section 4.4.2.1, the freezing step was reduced from 2:15 to 1:00 and the T ramp at the beginning of the P.D was considerably accelerated from 1:35 to 00:45.

Table 4-50: First optimization of the manufacturing process of Lyocs®, the parameters which were changed are marked in green.

Step	Time [hh:mm]	T [°C]	Vacuum [mbar]	T ramp [°C/min]
Loading	00:00	-40	1000	-
Freezing	01:00	-40	1000	-
P.D	00:35	-40	0,2	-
	00:45	45	0,2	1,89
	06:00	45	0,2	-
S.D	04:00	45	0,2	-
	00:30	25	0,2	0,67
	00:30	25	0,2	-
Total duration	13:20			

Figure 4-124 shows the monitoring process during the first optimized lyophilization cycle. It can be seen that the freezing step was shortened correctly, as the beginning of the freezing plateau is still visible at the end of the freezing step. The T ramp increase at the beginning of P.D was divided by two, bringing no changes to the visual aspect of the product (no exploded Lyocs® were obtained, meaning that the Lyoc® products could bear the high T increase).

What role does the p exactly play? Indeed, the faster sublimation rate occurs when $P_{chamber} = \frac{P_{ice\ over\ the\ product}}{2}$. At the end of the freezing step, $T_p = -35^\circ\text{C}$, which corresponds to an ice pressure of 0,220 mbar (ChristMartin, 2015). P_c could be thus set at 0,110 mbar during the P.D. It can also be observed on Figure 4-124 that the end of the P.D is not reached at 10:30 (end of the red area), as $T_p \neq T_s$. The P.D should thus last until 12:00 in order to have $T_p=T_s$.

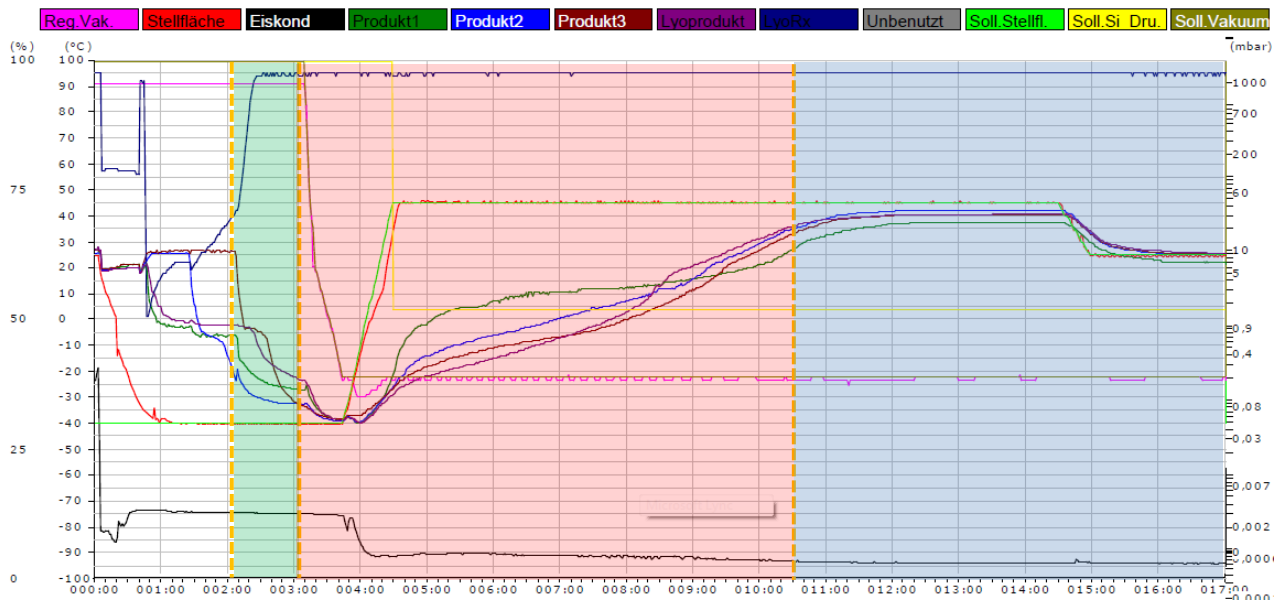


Figure 4-124: Temperature and pressure evolution during the first optimized lyophilization process, white=loading step, green=freezing step, red=P.D, blue=S.D.

Table 4-51: IPC results of F1-F3 \pm SD.

IPC results			
	F1	F2	F3
Batch Nr	160305	160306	160304
LoD [%], n=2	0,29	0,30	0,30
H [N], n=20	53 \pm 13	57 \pm 11	46 \pm 10
D.T [s], n=6	16 \pm 3	10 \pm 2	5 \pm 2
Aspect	Good visual aspect. Do not break during unpacking. Not powdery	Good visual aspect. Do not break during unpacking. Not powdery.	Good visual aspect. Do not break during unpacking. Not powdery.

Table 4-51 summarizes the IPC results of the Lyocs® resulting from optimization 1.

It can be noticed that the D.T and H stay approximately the same between the initial process (see table 4-49) and the first optimization process (see table 4-51). The lower LoD observed for the first optimization process ($LoD \approx 0,4\%$ for the products manufactured with the initial process, whereas $LoD \approx 0,3\%$ for the products manufactured with the first optimization process) could be explained by the fact that the higher T ramp of the beginning of P.D extracts more molecules of water, leading to a measurable decrease of the LoD.

4.4.2.3 Optimization 2

In the second optimization, the pressure in the chamber was decreased from 0,2 mbar to 0,11 mbar in order to see the influence of the pressure on the Lyocs®, as explained in paragraph 4.4.2.2. Table 4-52 summarizes the second optimization of the manufacturing process used. The entire process lasts 13:20.

Table 4-52: Second optimization of the manufacturing process of Lyocs®, the parameters which were changed are marked in green.

Step	Time [hh:mm]	T [°C]	Vacuum [mbar]	T ramp [°C/min]
Loading	00:00	-40	1000	-
Freezing	01:00	-40	1000	-
P.D	00:35	-40	0,11	-
	00:45	45	0,11	1,89
	06:00	45	0,11	-
S.D	04:00	45	0,11	-
	00:30	25	0,11	0,67
	00:30	25	0,11	-
Total Duration	13:20			

Figure 4-125 represents the lyophilization cycle of the second optimization. It looks like the frozen products need 7 hours to be completely sublimated, as T_p reaches the T_s 7 hours after the beginning of the T ramp increase (see Figure 4-125). In the case of optimization 1, T_p reaches the T_s 7:45 hours after the end of the T ramp increase (see Figure 4-125). Therefore, the decrease in pressure allowed shortening the process by another one hour. The long plateau observed at the beginning of the S.D (excess of over 3 hours) can also be shortened in order to decrease the cycle duration. This last change will be applied to finally optimize the process. Moreover, during the S.D, all the adsorbed molecules of water have to be removed by decreasing P_c down to 1 µbar. This P change will also be applied to the final optimized process.

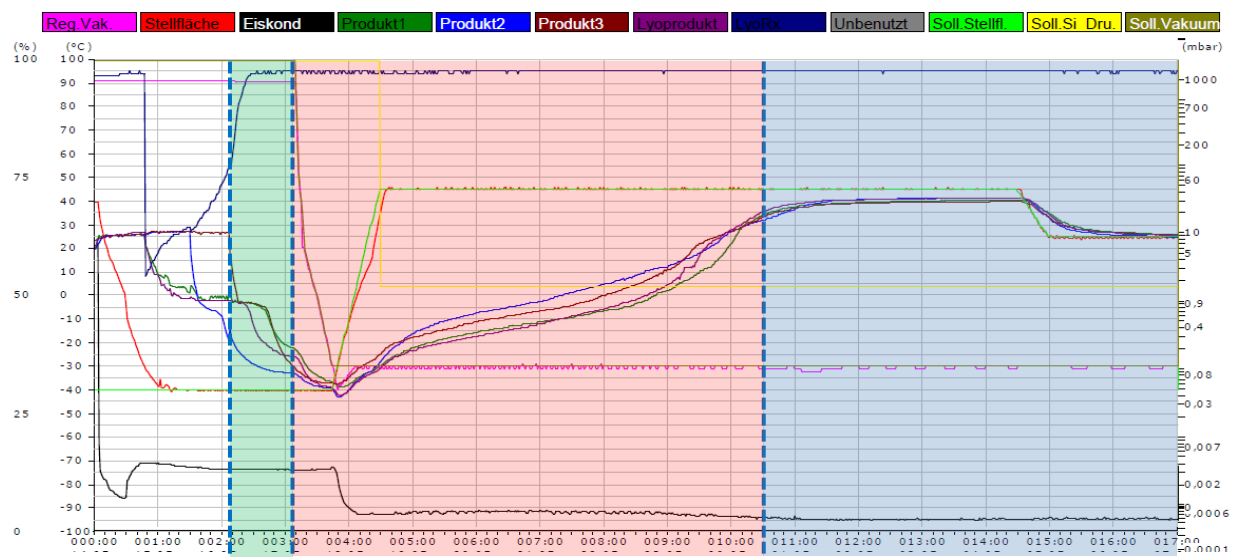


Figure 4-125: Temperature and pressure evolution during the second optimized lyophilization process, white=loading step, green=freezing step, red=P.D, blue=S.D.

Table 4-53: IPC results of F1-F2 ± SD.

IPC results			
	F1	F2	F3
Batch Nr	160308	160309	160307
LoD [%], n=2	0,30	0,33	0,30
H [N], n=20	69±13	56±11	49±8
D.T [s], n=6	20±6	13±5	5±1
Aspect	Good visual aspect. Do not break during unpacking. Not powdery	Good visual aspect. Do not break during unpacking. Not powdery.	Good visual aspect. Do not break during unpacking. Not powdery.

Table 4-53 summarizes the IPC results of the Lyocs® resulting from optimization 2.

The IPC results summarized in Table 4-53 are similar to the one of optimization 1 (see Table 4-51), meaning that the new parameters applied to this second optimized process do not have any negative impacts on the product quality. However, the lower P at the beginning of P.D in comparison with optimization 1, allowed to shorten the process (45 min shorter with P=0,11 mbar as with P=0,2 mbar).

4.4.2.4 Final Process Optimization

Table 4-54 summarizes the initial manufacturing process used. As explained in Section 4.4.2.3, the P.D was extended by 1 hour, in order to reach $T_p = T_s$. The long plateau between P.D and S.D was also clearly shortened by 3 hours in order to shorten the process time. The influence of P_c was also studied, by decreasing P_c from 0,11 to 0,001 mbar during the S.D in order to remove the adsorbed molecules of water. The final total duration is thus set at 11:50.

Table 4-54: Final optimization of the manufacturing process of Lyocs®, the parameters which were changed are marked in green.

Step	Time [hh:mm]	T [°C]	Vacuum [mbar]	T ramp [°C/min]
Loading	00:00	-40	1000	-
Freezing	01:00	-40	1000	-
P.D	00:35	-40	0,11	-
	00:45	45	0,11	1,89
	07:00	45	0,11	-
S.D	00:30	45	0,001 - Pressure rise test	-
	01:00	45	0,001	-
	00:30	25	0,001	0,67
	00:30	25	0,001	-
Total duration	11:50			

Figure 4-126 represents the lyophilization cycle of the ultimately finally optimized process. The process duration could be successfully shortened by 3:35. A pressure rise test was also performed at the end of the P.D (see decrease of P on the yellow curve of Figure 4-126). During this test, the valve separating the chamber and the condenser was closed, in order to ensure that the product was completely dried. As shown in the Figure 4-126, P_c did not increase during this pressure rise test, meaning that the P.D is finished and that the product is correctly dried. Moreover, the decrease of P_c from 0,11 to 0,001 mbar during S.D shows a slight decrease of T_{cc} at 12:00. This shows that no adsorbed water molecules are being entrapped on the condenser anymore (Le Floch, 2008).

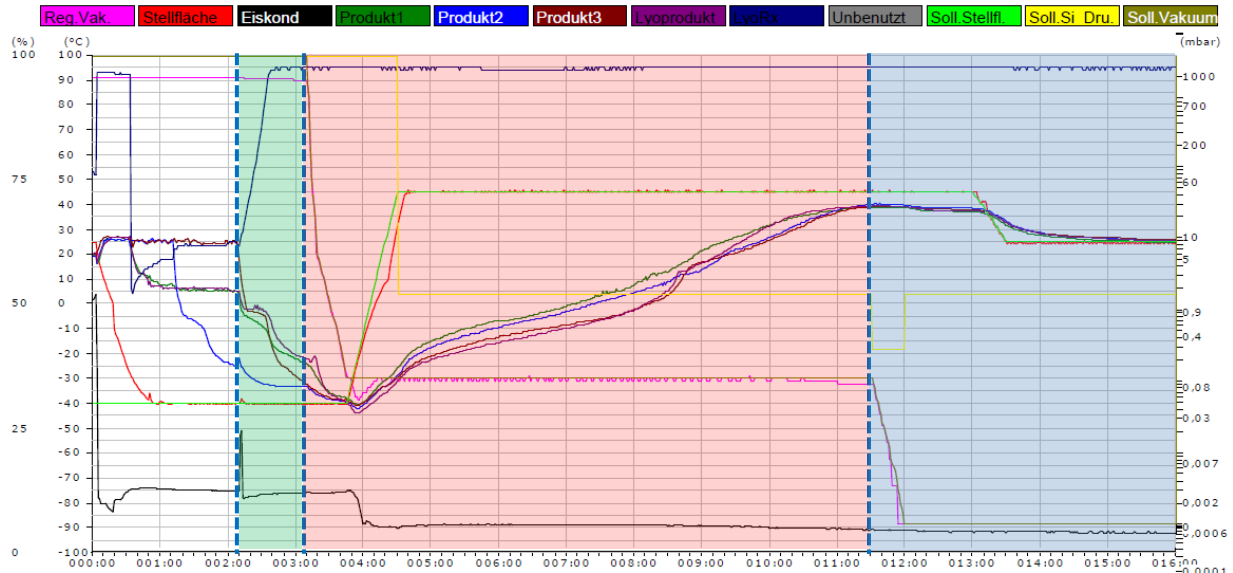


Figure 4-126: Temperature and pressure evolution during the final optimized lyophilization process, white=loading step, green=freezing step, red=P.D, blue=S.D.

Table 4-55: IPC results of F1-F3 ± SD.

IPC results			
	F1	F2	F3
Batch Nr	160311	160312	160310
LoD [%], n=2	0,33	0,31	0,30
H [N], n=20	55±14	55±12	45±10
D.T [s], n=6	15±4	10±2	6±1
Aspect	Good visual aspect. Do not break during unpacking. Not powdery	Good visual aspect. Do not break during unpacking. Not powdery.	Good visual aspect. Do not break during unpacking. Not powdery.

The IPC results summarized in Table 4-55 are similar to the one of optimization 1 (see Table 4-51) and optimization 2 (see Table 4-53), meaning that the new parameters applied to this final process do not have any negative impact on the product quality.

The lyophilization process was thus completed successfully, as the process time was reduced from 15:25 to 11:50, without any significant changes in the product quality.

4.4.2.5 Conclusion

The D.T and the LoD of the 3 products manufactured with the different processes are very similar, such as the H and the visual aspect of the product. It means that the process duration could successfully be shortened from 15:30 to 11:50 without any influences on the product quality. The characteristics of the T_s of the laboratory scale freeze-dryer and the production machine are very different. Indeed, $T_{s \max}$ of the development machine is maximum 45°C, whereas $T_{s \max}$ of the production machine is 80°C, allowing to impose higher T during the primary drying step, which decreases a lot the process duration through a faster sublimation rate. This T characteristic will have to be taken into considerations later on, when scale-up studies are performed on the process. Indeed, a pilot scale-equipment with a larger production capacity than in the lab scale has to be used in order to produce 1/10 of the total production. This pilot scale instrument can have characteristics that are more closely to the production scale than the lab scale could. This is especially the case for the T_s characteristics. A further study can then be carried out in detail in order to evaluate the influence of higher T_s on the product quality, in order to attempt to reach the 8 hours of process duration of the production.

5 Summary

The goal of this doctoral thesis was to characterize and optimize the formulation of lyophilized ODTs, by using more specifically the patented Lyoc® technology. ODTs have several advantages in comparison to conventional tablets, since they allow the patient to have a convenient administration (no need of water, discreet treatment, does not leave any residue in the mouth after administration). This dosage form is thus adapted for patients who have swallowing difficulties (such as pediatric use, geriatric use, and patients suffering from dysphagia), and might be particularly advantageous for the treatment of psychiatric patients.

A Lyoc® formulation is based on a suspension system containing mainly a diluent, a binder, API, and water which is subsequently lyophilized.

Using a lyophilization technology in the manufacturing of ODTs presents the advantage of rapidly disintegrating solid dosage forms. However, it is more expensive than the manufacturing of conventional tablets. Not only is the formulation of Lyoc® hard to develop and optimize, but the process optimization of the multiple critical parameters is also complex to complete.

In this thesis, firstly an excipient screening was performed in order to limit the possible usable excipients in the formulation of Lyocs® and their range of use. This study showed that crystalline mannitol with a particle size lower than 160 µm was the most appropriate diluent due to:

- its good ability to crystallize during the freezing step,
- its sweetening properties and cooling effect,
- its ability to allow fast sublimation leading to a high water loss at the beginning of the drying process.

Mixing the two mannitol grades Pearlitol® 25 C ($D_{50} = 25 \mu\text{m}$) and 160 C ($D_{50} = 160 \mu\text{m}$), also brought convincing improvements to the formulation concerning the suspension properties and the taste of the resulting Lyocs®.

Regarding binders, diverse water-soluble polymers were found to be appropriate for the Lyoc® technology, namely dextran, dextlates, and povidone with a maximum ratio of Diluent/Binder up to 90 %/10 % w/w of the dried mass in lyophilized tablets. Beyond 10 %, the lyophilized tablets are too hard because of the cohesion caused by the binding agent within the particles, leading to an unacceptable high disintegration time.

Further optimization of base formulations consisting of Mannitol as diluent and either Hypromellose or dextran as binder was performed by means of a DoE study. This served to investigate if the high multi-variable system could be successfully optimized by using a tailor-made design (“Custom Design” tool in the JMP® software). Indeed, the amount of diluent, binder and water had to be optimally determined in order to obtain optimum physical properties of the product (i.e. F, viscosity, D.T, H). Despite the multiple responses, the large

factors variability and the broad range of IPCs, an optimum could be identified for both placebo systems.

A further issue was to study the influence of the API solubility used in Lyoc® formulation. In the context of this study, two crystalline very soluble APIs (metoclopramide HCl monohydrate and metamizol Na) and two crystalline sparingly or slightly soluble APIs (paracetamol and sildenafil citrate) were used to identify the solid state of the API after lyophilization. XRPD and Raman mapping were conducted on the resulting Lyocs®, allowing the determination of the solid state. Regarding the very soluble APIs, both remain partially or completely amorphous after the lyophilization process. Due to this API amorphization, Lyocs® tend to lose their structures during the lyophilization process. The loading limit of soluble API was estimated at 16 % of the total dried mass of the Lyoc®. Regarding the less-soluble APIs, XRPD study proved that both APIs recrystallize during lyophilization. This crystallinity imparts elegance to the Lyoc® structure.

Finally, a systematic study was undertaken on Paracetamol Lyocs®. First, the influence of the mannitol grade on the IPC results, on the API release and on the API sedimentation during lyophilization was specifically studied. In the second step, the lyophilization process was optimized with respect to the required processing time.

By combining microscopic analysis with the IPC results (especially D.T), it can be concluded that Paracetamol 100 mg Lyocs® with Pearlitol® 25 C, 50 C, 110 C, 25 C / 160 C (3+1) are an adequate option for the Lyocs® formulations.

The Paracetamol release was independent of the used mannitol grade. A faster onset of action might be expected for the Lyocs® (ca. 96 % of API release is reached after 15 minutes) compared to conventional tablets (ca. 90 % of API release is reached after 15 minutes), due to a shorter disintegration time of Lyocs® in comparison to the conventional tablets, and therefore a faster release of API out of the Lyoc® matrix. Nevertheless, the calculation of the difference factor (f_1) and the similarity factor (f_2) showed that Lyocs® and conventional tablets have both similar dissolution profiles, since $f_1 < 15$ and $f_2 > 50$ for all formulations. However, the f_2 factor of Paracetamol 100 mg Lyoc® with Pearlitol® 100 C and of Paracetamol 100 mg Lyoc® with a mixture of Pearlitol® 25 C and 160 C (3+1) were very close to 50, meaning that a faster API release could be expected for these formulations in comparison to the conventional tablets.

Based on IPC and API release results, the most appropriate formulations are therefore Paracetamol 100 mg Lyocs® with Pearlitol® 100 C and with Pearlitol® 25 C / 160 C (3+1). The mixture of Pearlitol® 25 C with 160 C showed an additional benefit due to the cooling effect related to Pearlitol® 25 C.

Independent from the used grade of mannitol, sedimentation occurred in the suspension after dispensing and before the freezing step. This resulted in significantly different API contents in the top and bottom parts of the Lyocs®. The use of a viscosity enhancer (such as xanthan gum) should prevent this sedimentation issue within the suspension and thus, provide homogeneous tablets.

Regarding the process optimization, no significant differences in the freeze-drying behavior of the formulations using the several mannitol grades were detected (no collapsed Lyocs® were obtained).

The initial lyophilization process which lasted 15:25 h could be reduced by 3.5 h with the same lab scale equipment, thanks to a faster T ramp during P.D and a lower P_c during P.D and S.D without generating a negative impact on the product quality.

To conclude, the following main points summarized in Table 5-1 need to be carefully studied during the development steps of freeze-dried tablets.

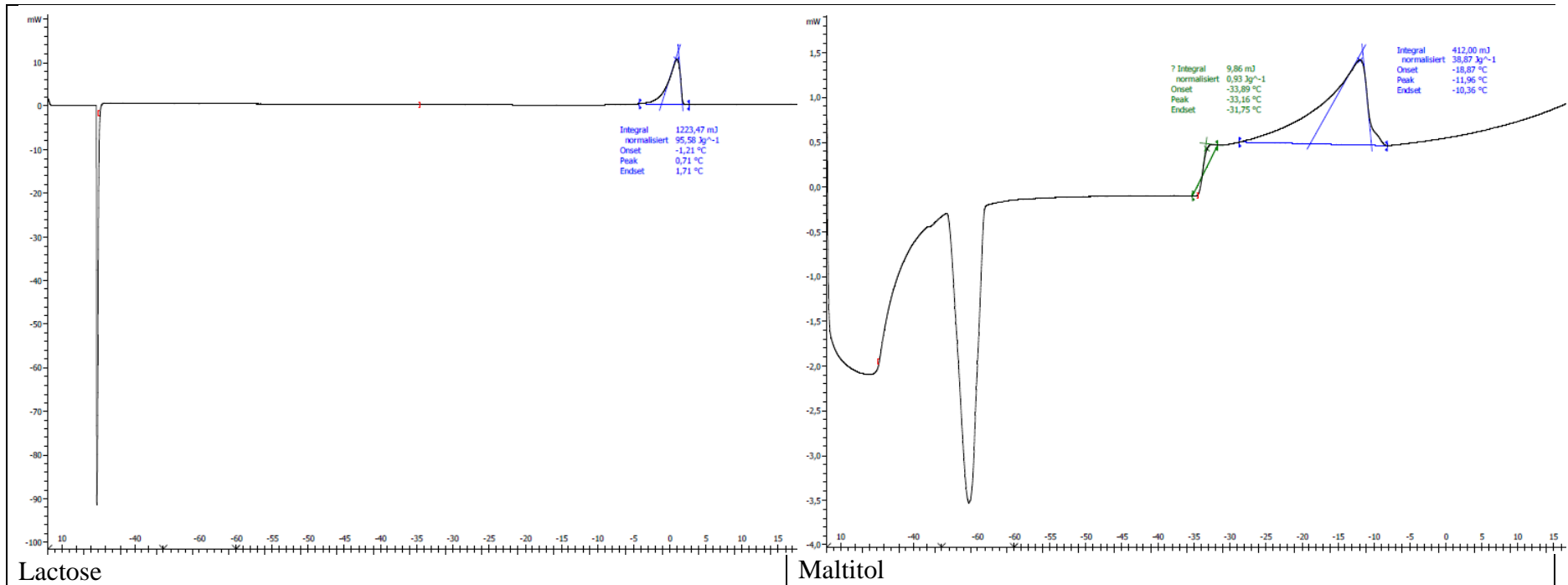
Table 5-1: Summary of formulation and process parameters to take into consideration during galenic and process development.

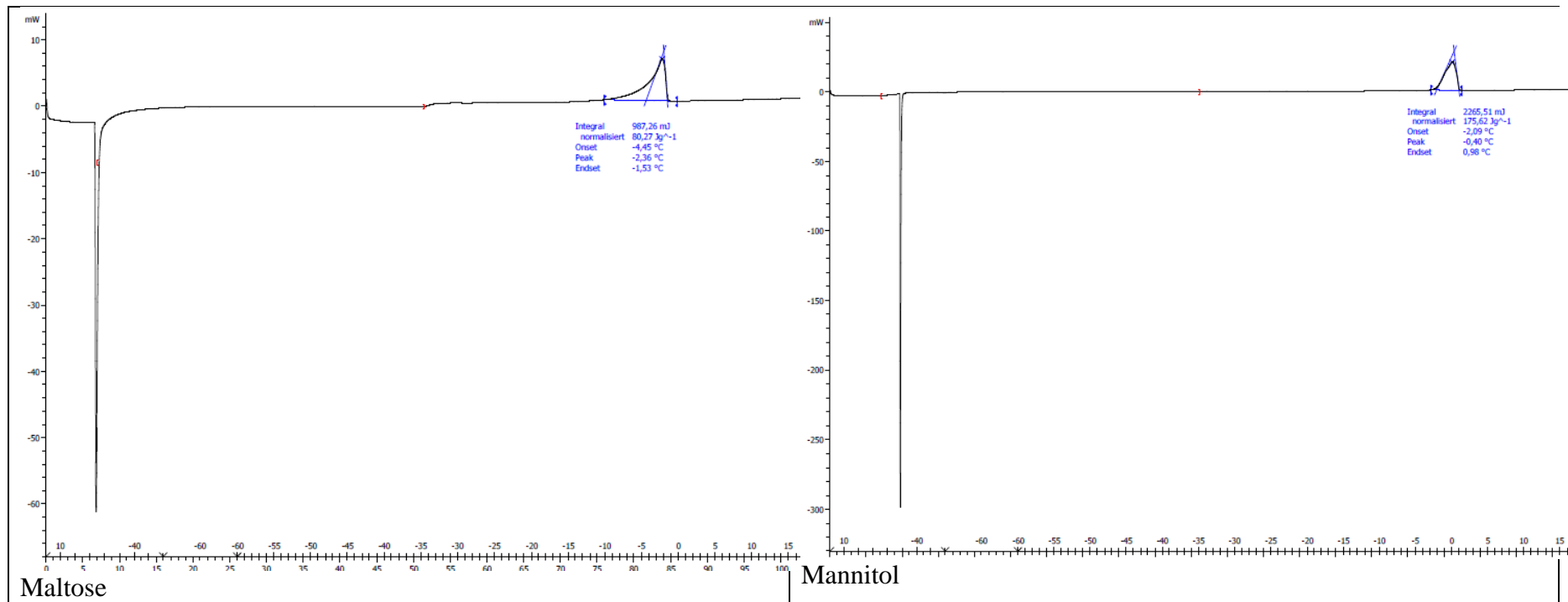
Formulation	Process
Collapse temperature of the suspension is of paramount importance and has to be determined (by means of DSC) for suspension characterization and for process optimization.	Influence of critical process parameters (P_c , T_s) on the product quality should be evaluated preferably by means of a Quality by Design (QbD) approach.
Viscosity and degree of sedimentation needs to be carefully studied in order to allow pipetting and to avoid sedimentation in the FD.	Scale-up activities on dispensing are necessary in order to determine the influence of suspension viscosity on the suspension dispersion.
Study on API solubility and on API load within Lyocs® need to be performed. XRPD characterization on Lyocs® may be helpful to determine the solid state of API after lyophilization.	Scale-up activities on freeze-dried process should be performed in order to optimize and shorten the process duration.
Combination of Pearlitol® 25 C and 160 C grades brings a cooling effect to the drug product → advantageous for bitter APIs.	

6 Annex

6.1 DSC Measurements

6.1.1 DSC Measurements of Diluent/Water Suspensions





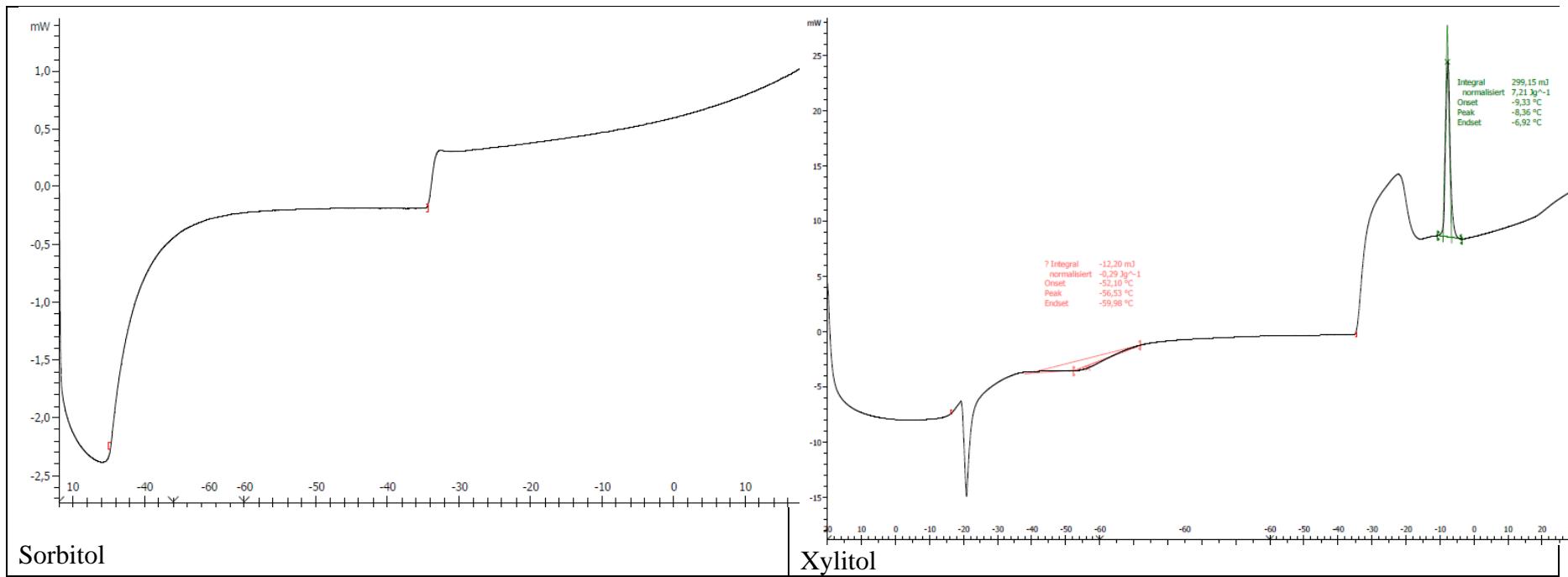


Figure 6-1: DSC thermogram of Diluent/Water suspensions.

6.1.2 DSC Measurements of Mannitol/Binder Suspensions

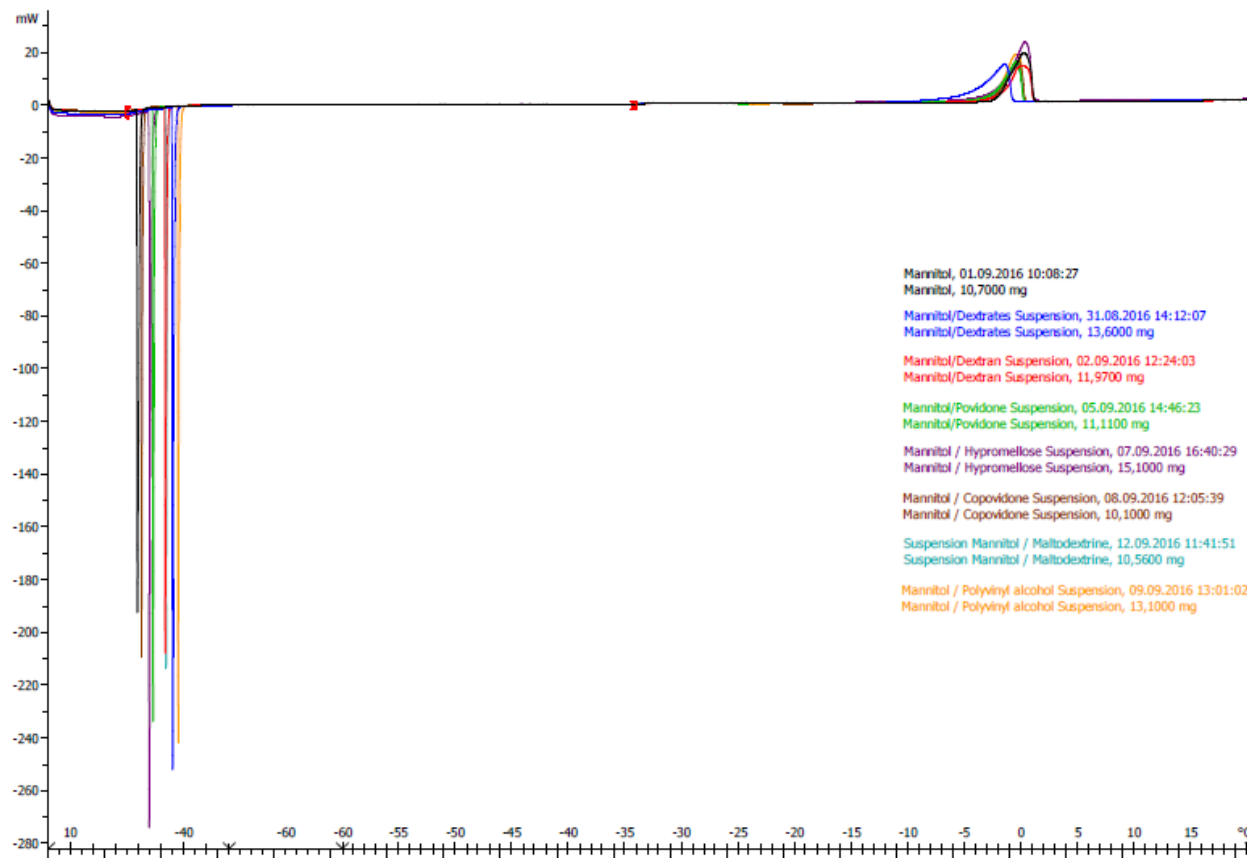


Figure 6-2: DSC thermogram of the suspensions Mannitol/Binder.

6.2 TGA Measurements

6.2.1 Metoclopramide HCl

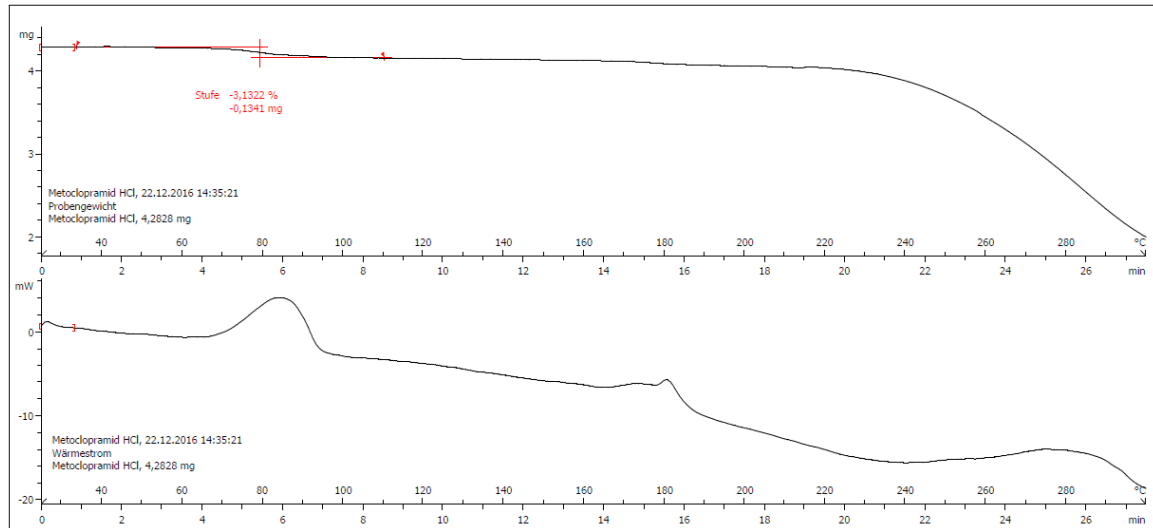
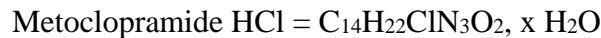


Figure 6-3: TGA thermogram of Metoclopramide HCl.



$$M(\text{C}_{14}\text{H}_{22}\text{ClN}_3\text{O}_2) = 299 \text{ g/mol}$$

$$M(\text{H}_2\text{O}) = 18 \text{ g/mol}$$

The mass loss notable between 60 °C and 100 °C of 3,1 % :

$$\frac{M(\text{H}_2\text{O})}{M(\text{C}_{14}\text{H}_{22}\text{ClN}_3\text{O}_2) + M(\text{H}_2\text{O})} = \frac{18}{299+18} = 5,68 \% \xrightarrow{\frac{5,68\%}{2}} 2,84 \% \text{, corresponding to a half molecule of water } \rightarrow x=1/2.$$

6.2.2 Metamizol Na

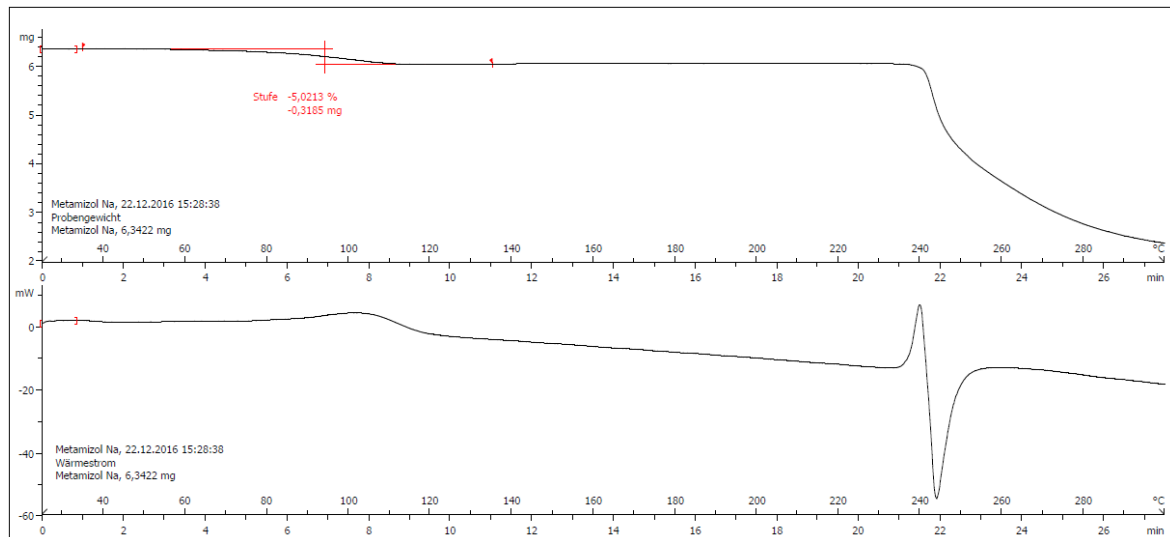
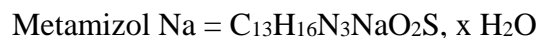


Figure 6-4: TGA thermogram of Metamizol Na.



$$M(\text{C}_{13}\text{H}_{16}\text{N}_3\text{NaO}_2\text{S}) = 333 \text{ g/mol}$$

$$M(\text{H}_2\text{O}) = 18 \text{ g/mol}$$

The mass loss notable between 80 °C and 120 °C of 5,0 % :

$$\frac{M(\text{H}_2\text{O})}{M(\text{C}_{13}\text{H}_{16}\text{N}_3\text{NaO}_2\text{S})+M(\text{H}_2\text{O})} = \frac{18}{333+18} = 5,1 \% \text{, corresponding to a half molecule of water.}$$

The API used is thus a monohydrate → x=1

6.3 API Release

6.3.1 Measurement

The choice of the size of the quartz cell was made by measuring the absorbance (A) of two reference solutions containing different concentrations C of pure paracetamol (i.e. $C_{\text{Ref } 1}=111,56 \text{ mg/L}$ and $C_{\text{Ref } 2}=56,05 \text{ mg/L}$). Ref 1 will set the size of the cell and Ref 2 will play the role of measurement verification by calculating the standard comparison value (SV), where $\pm 2 \%$ is allowed.

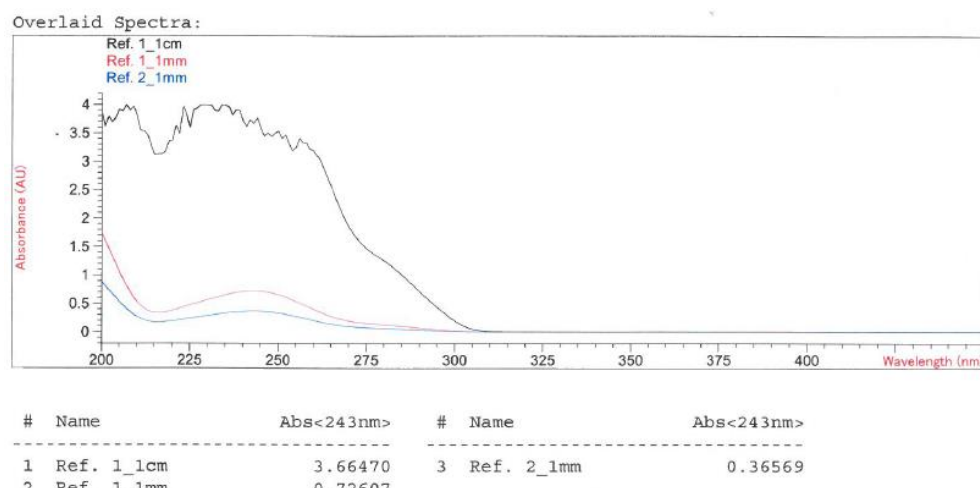


Figure 6-5: Absorbance of Ref 1 and Ref 2 with a 1 cm cuvette and a 1 mm cuvette

According to the Beer-Lambert equation, A has to be below 1. On Figure 6-5, the absorption curve of the 1 cm quartz cell is too high, meaning that the cell size needs to be lowered. $A_{\lambda_{\text{max}}}$ of Ref 1 with the 1 mm cuvette is 0,72607 which is below 1. $A_{\lambda_{\text{max}}}$ of the Ref 2 with the 1 mm cuvette equals 0,36569.

$$SV = \frac{A_{\text{Ref } 2} C_{\text{Ref } 1}}{A_{\text{Ref } 1} C_{\text{Ref } 2}} 100 = 100,2 \% < 2 \%.$$

The measurement method is thus approved and a 1 mm quartz cell is used for the measurement of the API release. As shown on the Figure 6-5, the maximum wavelength (λ) of paracetamol is at 243 nm. That is why the measuring λ is set at 243 nm.

The A was then converted into % of API released using the formula:

$$\text{Paracetamol dissolved (\%)} = \frac{A_{Tst} C_{Ref} V_1 100\%}{A_{Ref} V_{Ref} G}$$

- A_{Tst} = Absorption of the test solution at λ_{max} (i.e. 243 ± 2 nm)
 C_{Ref} = Concentration of paracetamol (mg) in the reference solution
 V_1 = Volume (mL) of test batch
 A_{Ref} = Absorption of the reference at λ_{max} (i.e. 243 ± 2 nm)
 V_{Ref} = Volume (mL) of reference solution
 G = Content of paracetamol (mg/tablet)

6.3.2 Dissolution Profile Comparison

	f_1	f_2
F1	4.81	82.80
F2	4.37	60.89
F3	5.43	53.65
F4	3.92	63.29
F5	6.69	50.84
F6	5.27	57.32

6.4 Content of Uniformity

6.4.1 Measurement conditions

The measurement conditions such as λ_{max} , the sample concentration and the size of the cell were firstly determined by means of a preliminary test. 1 tablet was firstly dissolved in 50 mL of solvent (i.e. $C_{solution} = 2$ mg/mL). According to the Beer-Lambert equation, the absorbance A has to be below 1. $A_{\lambda_{max}}$ of the 0,2 mm cuvette is 2,50, which is too high. $A_{\lambda_{max}}$ of the 0,1 mm cuvette is 1,27.

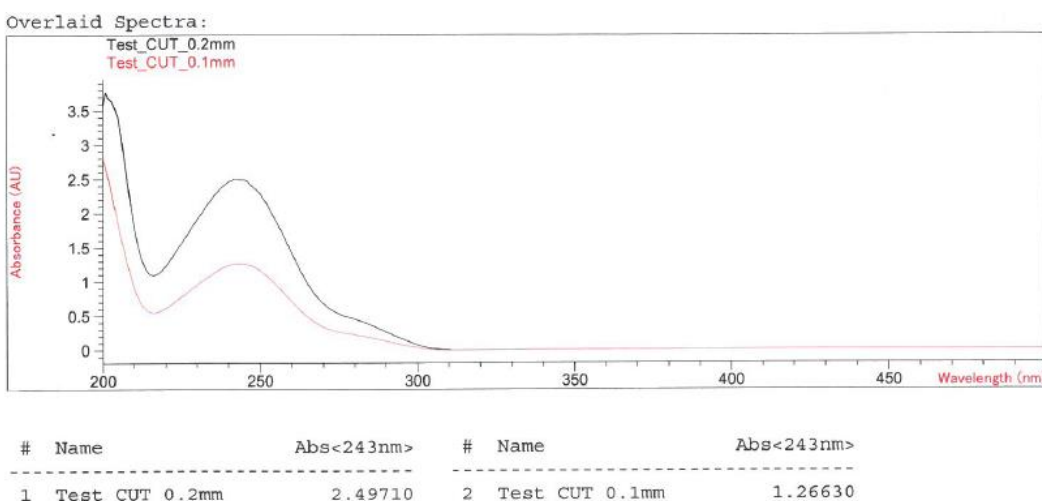


Figure 6-6: Absorption measurement for the choice of the cuvette size.

That is why the system of measurement is set as:

- 10 tablets were randomly picked up in each batch and each tablet was separately dissolved in 100 mL of the solvent, i.e. $C_{\text{solution}} = 1 \text{ mg/mL}$,
- 0,1 mm cuvette,
- $\lambda_{\text{measurement}} = [200-500]$.

Two standard solutions with different concentration of pure paracetamol were also measured ($C_{\text{Ref1}} = 0,99 \text{ mg/mL}$, and $C_{\text{Ref2}} = 0,87 \text{ mg/mL}$), in order to calculate the concentration of the samples from the A value with the following formula:

$$\text{Paracetamol content (mg/mL)} = \frac{C_{\text{Ref1}} A_{\text{Tst}}}{A_{\text{Ref1}}}$$

A linearity study was also carried out, to ensure that the measurements are within the linearity area. For this step, the absorbance of 8 parent solutions of paracetamol with concentrations ranging from 0,20 mg/mL to 2 mg/mL were measured (see Figure 6.7).

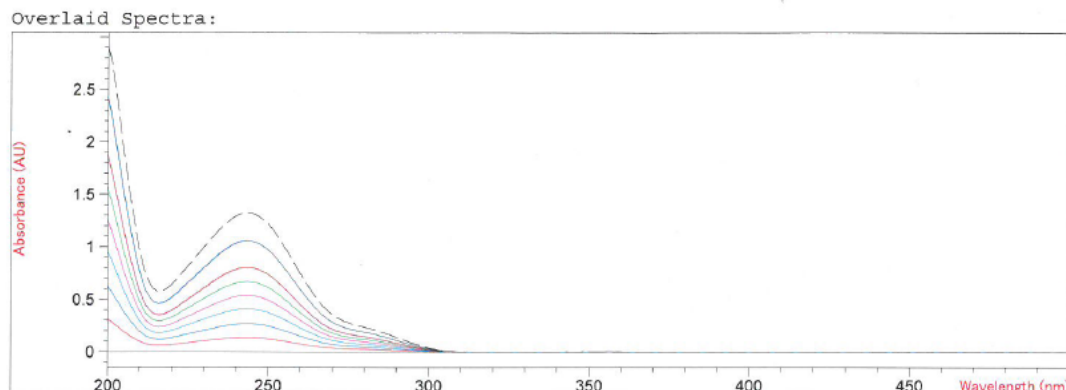


Figure 6-7: Absorption measurement of the solvent and of the parent solution having different concentrations.

As shown on Figure 6-8, $R^2=0,9999$ which means that all Paracetamol concentration between 0,20 mg/mL to 2 mg/mL is within the linear area.

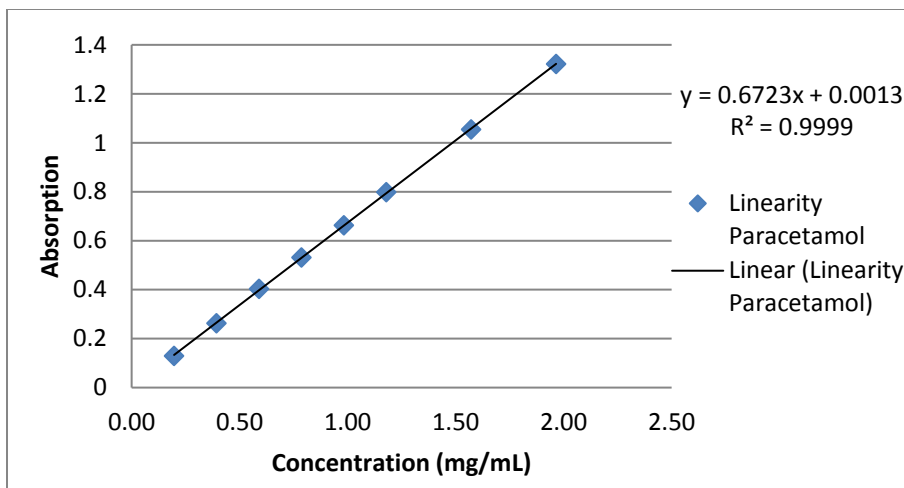


Figure 6-8: Linearity range of the measurement method.

6.4.2 Statistical Analysis

A one-way ANOVA with a significance level $\alpha=0,05$ and a Tukey Post hoc were performed in order to study the statistical difference of content of uniformity between the 6 formulations F1 to F6.

Anova: Single Factor

SUMMARY

Groups	Count	Sum	Arith. Mean	Variance
F1	10	971,202556	97,1202556	8,659769279
F2	10	985,9546705	98,59546705	17,47546405
F3	10	974,1390779	97,41390779	1,313036403
F4	10	943,2125779	94,32125779	73,09354891
F5	10	1016,437991	101,6437991	1,537917813
F6	10	1053,528631	105,3528631	0,463464134

ANOVA

Source of Variation	Square Sum (SS)	Degrees of Freedom (df)	Mean Square sum (MS)	Test Value (F)	P-Value	F crit.
Between Groups	754,1856317	5	150,8371263	8,825770532	3,602E-06	2,38606986
Within Groups	922,8888053	54	17,09053343			
Total	1677,074437	59				

P-value << α , that is why a difference of content of uniformity can be statistically noticed between the 6 formulations F1 to F6. In order to detect between which groups exactly a statistical difference exists, a Tukey post hoc test was carried out.

Honest Significant Difference (HSD)	$q_\alpha /(\text{MSE}/n)^{1/2}$	5.4384
Multiplier	q_α read in the table "Critical Values for the Tukey Q Test"	4.16
Mean Squared Error (MSE)	SS/df (within groups)	17.09053
N	Count	10

The difference between the arithmetical means of each batch was then calculated.

	F1	F2	F3	F4	F5	F6
F1		-1,48	-0,29	2,8	-4,55	-8,23
F2			1,19	4,28	-3,07	-6,75
F3				3,09	-4,26	-7,94
F4					-7,35	-11,03
F5						-3,68
F6						

As the absolute value of the yellow marked values is above HSD, it can be concluded that there is a statistical difference in the content of uniformity between F1-F6, F2-F6, F3-F6, F4-F6 and F4-F5.

6.5 Sedimentation Study

6.5.1 Sedimentation Within The Pipette

Formulation	t-value	Critical t-value	Conclusion
10 mL pipette	7.000		t-value > critical t-value, hence significant difference between the beginning and the end of pipetting.
25 mL pipette	3.061	2,101 Read in the t-table (SanJoséStateUniversity, 2007).	t-value > critical t-value, hence significant difference between the beginning and the end of pipetting.
50 mL pipette	2,890		t-value > critical t-value, hence significant difference between the beginning and the end of pipetting.

6.5.2 Sedimentation Within The Lyocs®

Formulation	t-value	Critical t-value	Conclusion
F1	1,771		t-value < critical t-value, hence no significant difference between the top and the bottom of the Lyoc®.
F2	1,802	2,228 Read in the t-table (SanJoséState University, 2007).	t-value < critical t-value, hence no significant difference between the top and the bottom of the Lyoc®.
F3	2,635		t-value > critical t-value, hence significant difference between the top and the bottom of the Lyoc®.
F4	2,970		t-value > critical t-value, hence significant difference between the top and the bottom of the Lyoc®.
F5	1,909		t-value < critical t-value, hence no significant difference between the top and the bottom of the Lyoc®.
F6	1,476		t-value < critical t-value, hence no significant difference between the top and the bottom of the Lyoc®.

7 Bibliography

- Abdul-Fattah, A. M., Truong, V. L.** (2010). Drying Process Methods for Biopharmaceutical Products: An Overview. Formulation and Process Development Strategies for Manufacturing Biopharmaceuticals, John Wiley & Sons, Inc., 705-738.
- Amar, I., Mansour, O., et al.** (2015). "Orally Disintegration Tablets – Patient Friendly Tablets." International Journal of Pharmaceutical Sciences Review and Research 32(1): 135-142.
- AntonPaar** Tips and Tricks from Joe Flow Cones, Plates and Cylinders: Spoilt for Choice, Anton Paar.
- Awotwe-Otoo, D., Khan, M. A.** (2015). Lyophilization of Biologics: An FDA Perspective. Lyophilized Biologics and Vaccines: Modality-Based Approaches, Springer-Verlag New York.
- AzbilTelstar** (2015). Freeze Dryer Supervision and Maintenance. Training at TEVA-ratioharm, Blaubeuren.
- Barley, J.** (2016). "Basic Principles of Freeze Drying." Retrieved 5th September, 2016, from <http://www.spscientific.com/freeze-drying-lyophilization-basics/>.
- Bhambere, D., A. Gaidhani, K., et al.** (2015). "LYOPHILIZATION / FREEZE DRYING – A REVIEW." World Journal of Pharmaceutical Research 4(8): 516-543.
- Blonde, P.** (1974). Method of preparation of pharmaceutical products. Orsymonde. USA, Google Patents. US 3855712 A.
- Caelo.** (2015). "Metamizol-Natrium, API." Retrieved 4th August, 2016, from https://www.google.de/url?sa=t&rct=j&q=&esrc=s&source=web&cd=7&cad=rja&uact=8&ved=0ahUKEwiE1-S91ajOAhVGC8AKHQaCArIQFghSMAY&url=http%3A%2F%2Fwww.caelo.de%2Fgetfile.html%3Ftype%3Dsdb_en%26cntry%3Den%26num%3D2486&usg=AFQjCNHvNeoidpItzd4yznuvq5r02PUNqw.
- Catalent** (2013). Oral Drug Delivery Guide, Catalent Institute.
- CDER** (1997). Guidance for Industry - Dissolution Testing of Immediate Release Solid Oral Dosage Forms.
- CDER** (2008). Guidance for Industry - Orally Disintegrating Tablets, Food and Drug Administration.
- Cephalon** (2009). Spasfon Lyoc 160 mg, Oral Lyophilisate, Cephalon.
- Chang, B. S., Patro, S. Y.** (2004). Freeze-Drying Process Development for Proteins Pharmaceuticals. Lyophilization of Biopharmaceuticals, American Association of Pharmaceutical Scientists, 1, 113-133.
- ChristMartin** (2015). Smart Freeze-Drying - Basic principles, optimum procedures and applications, Christ Martin.
- Daniels, R.** (2014). Grundlagen der Lyophilisation. APV Basics Seminar: Lyophilisation, Darmstadt.
- Doctissimo.** (2015). "Guide des Médicaments." Retrieved 24th May, 2016, from http://www.doctissimo.fr/asp/medicaments/medicaments_loupe.htm.
- Dulieu, C., Durfee, S., et al.** (2010). Lyophilized pharmaceutical compositions and methods of making and using same. Cephalon. USA, Google Patents. US 20100080829 A1.
- Dutch, S.** (2001). "Ice Structure." Retrieved 2nd October, 2016, from <https://www.uwgb.edu/dutchs/Petrology/Ice%20Structure.HTM>.
- EDQM** (2014a). Disintegration of Tablets. European Pharmacopoeia 8.0, 285-286.
- EDQM** (2014b). Loss on Drying. European Pharmacopoeia 8.0, 52.

- EDQM** (2014c). Paracetamol. European Pharmacopoeia8.0, 2963-2964.
- EDQM** (2014d). Resistance to Crushing. European Pharmacopoeia8.0.
- EDQM** (2014e). Tablets. European Pharmacopoeia8.0, 809-812.
- EDQM** (2014f). Uniformity of Dosage Units. European Pharmacopoeia8.0, 358.
- EMEA** (2010). Guideline On The Investigation Of Bioequivalence, Committee For Medicinal Products For Human Use, 20-21.
- Euro-OTC-Pharma** (2017). Sicherheitsdatenblatt Metamizol-Natrium-Monohydrat.
- Faqi, A. S.** (2013). ADME in Drug Discovery A Comprehensive Guide to Toxicology in Preclinical Drug Development, Academic Press, 3-30.
- FDA**. (2014). "GUIDE TO INSPECTIONS OF LYOPHILIZATION OF PARENTERALS." Retrieved 16th September, 2016, from <http://www.fda.gov/ICECI/Inspections/InspectionGuides/ucm074909.htm>.
- Felton, L. A.** (2013). Remington - Essentials of Pharmaceutics, Pharmaceutical Press.
- Fernandes, N. S., Carvalho, F. M. A. d., et al.** (1999). "Thermal decomposition of some chemotherapeutic substances." Journal of the Brazilian Chemical Society 10(6): 459-462.
- Fissore, D., Pisano, R., et al.** (2011). "On the Methods Based on the Pressure Rise Test for Monitoring a Freeze-Drying Process." Drying Technology 29: 73-90.
- Fletcher, J., Hill, A.** Making the Connection - Particle Size, Size Distribution and Rheology, Malvern Instruments Ltd.
- Fu, Y., Yang, S., et al.** (2004). "Orally fast disintegrating tablets: developments, technologies, taste-masking and clinical studies." Crit Rev Ther Drug Carrier Syst 21(6): 433-476.
- Fulzele, S., Moe, D., et al.** (2012). "Lyoc (Lyophilized Wafer): An orally disintegrating tablet technology." Drug Development & Delivery 12: 51-57.
- Galan, M.** (2010). Monitoring and Control of Industrial Freeze-Drying Operations: the Challenge of Implementing Quality-by-Design (QbD). Freeze-Drying/Lyophilization of Pharmaceutical and Biological Products, Third Edition, informa healthcare: 19, 441-459.
- Gole, D. J., Levinson, R. S., et al.** (1993). Preparation of pharmaceutical and other matrix systems by solid-state dissolution. USA, Google Patents. US 5215756 A.
- Gryczke, A.** (2012). "Solid Dispersions by Hot-Melt Extrusion - The advantages and disadvantages of hot-melt extrusion in solid dispersion formulations." Pharmaceutical Technology Europe 24(9).
- Hatley, R. H. M., Franks, F., et al.** (1996). "Stabilization of a pharmaceutical drug substance by freeze-drying: A case study." Drug Stability 1: 73-85.
- HermesPharma** (2014). Survey Reveals Widespread Prevalence of Difficulties in Swallowing Tablets: Conventional tablets may no longer be the go-to solution., Pharmaceutical Technology Editors
- Hidehisa, K.** (2013). Characterizations of Functions of Biological Materials Having Controlling-Ability Against Ice Crystal Growth. Advanced Topics on Crystal Growth, InTech: 5, 90-119.
- Jennings, T. A.** (2008a). The Freezing Process. Lyophilization: Introduction and Basic Principles, informa healthcare: 7, 261-282.
- Jennings, T. A.** (2008b). The Importance of Process Water. Lyophilization: Introduction and Basic Principles, informa healthcare: 3, 59-82.
- Jennings, T. A.** (2008c). Introduction. Lyophilization: Introduction and Basic Principles, informa healthcare: 1, 1-14.
- Jennings, T. A.** (2008d). Lyophilization: Introduction and Basic Principles, Jennings, Thomas A.
- Jennings, T. A.** (2008e). Phase Changes. Lyophilization: Introduction and Basic Principles, informa healthcare: 4, 83-92.

- Jennings, T. A.** (2008f). Product Formulation. Lyophilization: Introduction and Basic Principles, informa healthcare: 2, 15-58.
- Jennings, T. A.** (2008g). Thermal Analytical Methods. Lyophilization: Introduction and Basic Principles, informa healthcare: 6, 109-260.
- Jennings, T. A.** (2008h). The Thermal Properties of Formulations. Lyophilization: Introduction and Basic Principles, informa healthcare: 5, 93-108.
- Jeong, S. H., Lee, J., et al.** (2010). Fast Disintegrating Tablets. Oral Controlled Release Formulation Design and Drug Delivery, John Wiley & Sons, Inc., 155-167.
- Kearney, P.** (2002). The Zydus Oral Fast-Dissolving Dosage Form. Modified-Release Drug Delivery Technology, Marcel Dekker, Inc., 191-201.
- Kim, A. I., Akers, M. J., et al.** (1998). "The physical state of mannitol after freeze-drying: Effects of mannitol concentration, freezing rate, and a noncrystallizing cosolute." Journal of Pharmaceutical Sciences 87(8): 931-935.
- Kimura, S., Uchida, S., et al.** (2015). "Effect of granule properties on rough mouth feel and palatability of orally disintegrating tablets." International Journal of Pharmaceutics 484(1): 156-162.
- Kumare, S.** (2008). "Orally Disintegrating Tablet." Retrieved August 30th, 2015, from <http://www.pharmainfo.net/reviews/orally-disintegrating-tablet-rapid-disintegration-sweet-taste-and-target-release-profile>.
- Labconco** (2010). A Guide To Freeze-Drying for the Laboratory.
- Le Floch, L.** (2008). Facteurs pouvant influencer la durée d'un cycle de lyophilisation, Cephalon.
- Le, J.** (2014a). "Merck Manuals - Drug Absorption." Retrieved 30th May, 2016, from <http://www.merckmanuals.com/professional/clinical-pharmacology/pharmacokinetics/drug-absorption>.
- Le, J.** (2014b). "Merck Manuals - Drug Distribution to Tissues." Retrieved 1st June, 2016, from <http://www.merckmanuals.com/professional/clinical-pharmacology/pharmacokinetics/drug-distribution-to-tissues>.
- Le, J.** (2014c). "Merck Manuals - Drug Excretion." Retrieved 2nd June, 2016, from <http://www.merckmanuals.com/professional/clinical-pharmacology/pharmacokinetics/drug-excretion>.
- Le, J.** (2014d). "Merck Manuals - Overview of Pharmacokinetics." Retrieved 30th May, 2016, from <http://www.merckmanuals.com/professional/clinical-pharmacology/pharmacokinetics/overview-of-pharmacokinetics>.
- Lipp, R.** (2013). "Major Advances in Oral Drug Delivery over the Past 15 Years." American Pharmaceutical Review 16(1).
- Lunter, D. J.** (2016). Raman-mikroskopische Untersuchung von Metoclopramid-Tabletten mit Mannitol und Dextran, Pharmazeutische Universität Tübingen.
- McLaughlin, R., Banbury, S., et al.** (2009). "Orally Disintegrating Tablets: The Effect of Recent FDA Guidance on ODT Technologies and Applications." Pharmaceutical Technology 18(5).
- Mezger, T.** (2012). Fließverhalten und Viskosität Das Rheologie Handbuch: Für Anwender von Rotations- und Oszillations-Rheometern, Vincentz Network GmbH & Company KG: 2, 23-34.
- MillrockTechnology, I.** (2009). "Freeze Drying / Lyophilization Info Online - Definitions." Retrieved September 16th, 2016, from <http://freezedryinginfo.com/Definitions.html>.
- Milton, N.** (2010). Pharmaceutical Freeze Drying: The Lyophilization Process. Product Development, E. L. a. C.

- Mogoșanu, G. D., Grumezescu, A. M.** (2015). Pharmaceutical Natural Polymers: Structure and Chemistry. Handbook of Polymers for Pharmaceutical Technologies, John Wiley & Sons, Inc.: 16, 477-519.
- Nail, S. L., Jiang, S., et al.** (2002). Fundamentals of Freeze-Drying. Development and Manufacture of Protein Pharmaceuticals, Springer US, 14: 5, 281-360.
- Nguyen, T. T.** (2011). Oral lyophilised compositions. Cephalon. Europe, Google Patents. EP 2359812 A1.
- Ölmez, S. S., Vural, I.** (2009). "Advantages and quality control of orally disintegrating tablets." FABAD Journal of Pharmaceutical Sciences 34: 167-172.
- Pahl, M., Gleißle, W., et al.** (1991). Suspensionsrheologie. Praktische Rheologie der Kunststoffe und Elastomere, VDI-Verlag: 14, 391-412.
- Parkash, V., Maan, S., et al.** (2011). "Fast disintegrating tablets: Opportunity in drug delivery system." Journal of Advanced Pharmaceutical Technology & Research 2(4): 223-235.
- Pavlik, M.** (2011). The dependence of suspension viscosity on particle size, shear rate and solvent viscosity. Master of Science, DePaul University.
- Pelkonen, O., Ahokas, J.** (2009). Pharmacokinetics: How Does The Body Handle Drugs? . Pharmacology EOLSS Publishers Co Ltd 1: 7, 148-164.
- Pfister, W. R., Ghosh, T. K.** (2010a). Intraoral Delivery System: An Overview, Current Status, and Future Trends. Drug Delivery to the Oral Cavity - Molecules to Market. London, informa healthcare, 145: 1, 1-40.
- Pfister, W. R., Ghosh, T. K.** (2010b). Quick-Dispensing Oral Drug Delivery Systems. Drug Delivery to the Oral Cavity - Molecules to Market. London, informa healthcare, 145, 261-289.
- Pharmacosmos.** (2016). "Pharmaceutical Quality Dextran." Retrieved 9th August, 2016, from <http://www.dextran.net/application-areas/vaccines.aspx>.
- Pikal, M.** (2010). Freeze-Drying, University of Connecticut, School of Pharmacy.
- Pikal, M., Nail, S. L.** (2014). Freeze-Drying Short Course. KelCon. Germany.
- Reihbandt, T.** (2016). Some Common Methods Used to Detect the End of Primary Drying Millrock Technology.
- Remmler, T.** (2015). Understanding the Link Between Particle Properties and Rheology of Suspensions. TestXpo Fachmesse für Prüftechnik, Ulm.
- ResearchMethodsKnowledgeBase.** (2006). "The T-Test." Retrieved 20th September, 2016, from http://www.socialresearchmethods.net/kb/stat_t.php.
- Ronis, D.** (2001). "Thermodynamic Stability: Free Energy and Chemical Equilibrium." Retrieved 2nd October, 2016, from http://ronispc.chem.mcgill.ca/ronis/chem213/free_energy.pdf.
- Roquette** (2006). PEARLITOL(R) mannitol for pharmaceutical applications.
- Roquette.** (2012). "NEOSORB Sorbitol Powder." Retrieved 4th August, 2016, from <http://www.roquette-pharma.com/brochures/09/visio.html>.
- Roquette.** (2016). "Product Finder." Retrieved 29th September, 2016, from <https://www.roquette.com/product-finder-pharma>.
- Rowe, R. C., Sheskey, P. J., et al.** (2009). Handbook of Pharmaceutical Excipients – 6th Edition, Pharmaceutical Press.
- Sadikoglu, H., Ozdemir, M., et al.** (2006). "Freeze-Drying of Pharmaceutical Products: Research and Development Needs." Drying Technology 24(7): 849-861.
- Sakai, J. B.** (2008). Pharmacokinetics: The Absorption, Distribution and Excretion of Drugs. Practical Pharmacology for the Pharmacy Technician, Lippincott Williams and Wilkins 3, 27-40.
- SanJoséStateUniversity.** (2007). "t-table." Retrieved 21st September, 2016, from <http://www.sjsu.edu/faculty/gerstman/StatPrimer/t-table.pdf>.

- Sattar, S., Shakeel Ahmed, M., et al.** (2004). "Inert Medication Ingredients Causing Nonadherence Due to Religious Beliefs." *Annals of Pharmacotherapy* 38: 621-624.
- Schubert, O.** (2014). *Beispiele für Lyophilisate aus dem pharmazeutische Bereich*. APV basics: Lyophilisation, Darmstadt.
- Seager, H.** (1998). "Drug-delivery Products and the Zydis Fast-dissolving Dosage Form." *Journal of Pharmacy and Pharmacology* 50(4): 375-382.
- Selleckchem.** (2013). "Metoclopramide HCl." Retrieved 4th August, 2016, from <http://www.selleckchem.com/products/metoclopramide-hcl.html>.
- Sharma, K., Pfister, W. R., et al.** (2010). Quick-Dispersing Oral Drug Delivery Systems. *Drug Delivery to the Oral Cavity: Molecules to Market*, informa healthcare, 145: 11, 261-289.
- Shon, M.,Mather, L.** (2012). The Importance of Controlling Nucleation Temperature during the Freeze Step., SP Scientific
- Siow, C. R. S., Wan Sia Heng, P., et al.** (2016). "Application of freeze-drying in the development of oral drug delivery systems." *Expert Opinion on Drug Delivery* 13(11): 1595-1608.
- Srivastava, S. K., Verma, R., et al.** (2014). "Orally Disintegrating Tablets; a Dosage Form That Extends the Market Exclusivity and Patent Protection." *World Journal of Pharmacy and Pharmaceutical Sciences* 3(7): 526-546.
- Sunu.** (2013). "Drug Excretion - Slide Share." Retrieved 2nd June, 2016, from <http://de.slideshare.net/suniu/drug-excretion>.
- Swarbrick, J., Rubino, J. T., et al.** (2014). Coarse Dispersions. *Essentials of Pharmaceutics*, Remington, 41: 21, 371-392.
- Tang, X.,Pikal, M. J.** (2004). "Design of Freeze-Drying Processes for Pharmaceuticals: Practical Advice." *Pharmaceutical Research* 21(2): 191-200.
- TechnologyCatalysts** (2008). Orally Disintegrating Tablet and Film Technology - 5th Edition, Technology Catalysts.
- TechnologyCatalysts** (2010). Orally Disintegrating Tablet and Film Technology - 6th Edition, Technology Catalysts.
- TEVA-ratiopharm** (2010). CTD Report of Paracetamol Tablets. Ulm, TEVA-ratiopharm.
- TEVA-ratiopharm** (2012). CTD Report of Sildenafil Effervescent Tablets. Ulm, TEVA-ratiopharm.
- Travers, R.,Grother, L.** (2013). Quick Thinking: Fast Dissolve Formulations, Catalent Pharma Solutions.
- Triantafillopoulos, N.** (1988). Measurement of Fluid Rheology and Interpretation of Rheograms. 2.
- Umasankar, K.** (2014). "DRUG DISTRIBUTION." Retrieved 1st June, 2016, from <http://de.slideshare.net/UmasankarKrishnamaraju/drug-distribution-40685564>.
- UnitedNations** (2015). World Population Ageing Report 2015 - Population Division. New York, Department of Economic and Social Affairs United Nations.
- Vissamsetti, B., Payne, M., et al.** (2012). "Inadvertent prescription of gelatin-containing oral medication: its acceptability to patients." *Postgraduate Medical Journal* 88(1043): 499-502.
- Wang, B.,Pikal, M.** (2012). "Stabilization of lyophilized pharmaceuticals by process optimization: Challenges and opportunities." *ResearchGate* 15(1).
- Wright, T.** (2015). "Solid Dosage Manufacturing Trends." *Contract Pharma*.